UNIVERSITY OF CALIFORNIA, SAN DIEGO

Interannual-to-Decadal Changes in Phytoplankton Phenology, Fish Spawning Habitat, and Larval Fish Phenology

A dissertation submitted in partial satisfaction of the

requirements for the degree Doctor of Philosophy

in

Oceanography

by

Rebecca G. Asch

Committee in charge:

David Checkley, Chair
Dan Cayan
Phil Hastings
Tony Koslow
Sam McClatchie
Mark Ohman
Jonathan Shurin

2013

The Dissertation of Rebecca G. Asch is approved, and it is acceptable in quality and form for publication on microfilm and electronically:

_____

_____

_____

_____

_____

_____

_____

Chair

University of California, San Diego

2013

DEDICATION

To my grandparents, Mollie Asch, Murray Asch, Herta Illes, and Zoltan Illes, in honor of their love, support, bravery, practical advise, and *joie de vivre*.

TABLE OF CONTENTS

LIST OF FIGURES

CHAPTER 1 FIGURES

CHAPTER 1 SUPPLEMENTAL FIGURES

LIST OF TABLES

CHAPTER 3 TABLES

ACKNOWLEDGMENTS

This research was funded by California Sea Grant Project R/FISH-210, the NOAA Nancy Foster Scholar Program, NSF IGERT Grant No. 0333444, the U.S. Integrated Ocean Observing System Grant No. NA17RJ1231, and the San Diego ARCS Foundation. This research was also associated with the California Current Ecosystem Long Term Ecological Research (LTER) site, which is supported by NSF. I am greatly indebted to the many scientists and crewmembers who collected and processed data from CalCOFI cruises.

Chapter 1, in full, is currently being prepared for submission for publication of the material. The dissertation author was the primary investigator and author of this material.

Chapter 1 acknowledgments: Karen Baker, Noelle Bowlin, and Susie Jacobson provided helpful, initial guidance on use of CalCOFI ichthyoplankton data. I acknowledge the Program for Climate Model Diagnosis and Intercomparison (PCMDI), the WCRP's Working Group on Coupled Modeling (WGCM), and the individual modeling groups who contributed to the development of the CMIP3 multi-model dataset. Support for developing the CMIP3 dataset was provided by the Office of Science in the U.S. Department of Energy. David Checkley, Dan Cayan, Phil Hastings, Tony Koslow, Sam McClatchie, Sung-Hyun Nam, Mark Ohman, and Jon Shurin provided useful suggestions at various stages of this research, which contributed to improving this manuscript.

Chapter 2, in full, is a reprint of the material as it appears in: Asch, R.G. and D.M. Checkley, Jr. 2013. Dynamic height: A key variable for identifying the spawning habitat

of small pelagic fishes. *Deep-Sea Research I* 71: 79-91. The dissertation author was the primary investigator and author of this paper.

Chapter 2 acknowledgments: Jennifer Rodgers-Wolgast provided assistance with calculating the dynamic height relative to 500 m at shallow stations. I appreciate guidance from Nanyc Lo, Ed Weber, and Juan Zwolinski regarding spatial autocorrelation. Mati Kahru offered helpful advice about how to delineate the extent of eddies. Suggestions from Dan Cayan, Peter Franks, Tony Koslow, Martin Lindegren, Sam McClatchie, Mark Ohman, M. Priede, Ryan Rykaczewski, and two anonymous reviewers also improved this manuscript.

Chapter 3, in part, is currently being prepared for submission for publication of the material. The dissertation author was the primary investigator and author of this material. Matthew C. Long will be a co-author of this publication.

Chapter 3 acknowledgments: The methods used to identify phenological transition points were developed as part of a Nancy Foster Scholar research collaboration with the Environmental Research Division (ERD) of the NOAA's Southwest Fisheries Science Center (SWFSC). Discussions with Steven Bograd, Frank Schwing, Isaac Schroeder, and Ricardo Lemos provided many helpful suggestions and insights during this research collaboration. David Checkley, Dan Cayan, Mark Ohman, Sam McClatchie, and Tony Koslow reviewed an earlier draft of this manuscript and provided a number of helpful suggestions.

Lastly, I would like to thank my family and partner for supporting me throughout the years as I worked on completing my dissertation. Special thanks goes to Michael Peto, Clare Asch, Robert Asch, and Marc Asch.

VITA

2000	Bachelor of Arts, Smith College
2000-2002	Environmental Scientist, Center for Coastal Monitoring and Assessment, National Oceanic and Atmospheric Administration
2006	Master of Science, University of Rhode Island
2006-2007	John A. Knauss Marine Policy Fellow, Climate Program Office, National Oceanic and Atmospheric Administration
2013	Doctor of Philosophy, University of California, San Diego

PUBLICATIONS

Turgeon, D.D. and R.G. Asch. 2002. National summary. In: The State of Coral Reef Ecosystems of the United States and Pacific Freely Associated States: 2002. National Oceanic and Atmospheric Administration/National Ocean Service/National Centers for Coastal Ocean Science, Silver Spring, MD. 265 p. http://coastalscience.noaa.gov/documents/status_coralreef.pdf

Asch, R.G. and D.D. Turgeon. 2003. Detection of gaps in the spatial coverage of coral reef monitoring projects in the U.S. Caribbean and Gulf of Mexico. *Journal of Tropical Biology* 51 (Supl. 4): 127-140.

Asch, R.G. 2006. A Photographic Analysis of Bottom Fishing Disturbance and Microhabitat Associations among the Colonial Epifauna of Georges Bank. Master's Thesis. University of Rhode Island, Narragansett, RI. 265 p.

Bullard, S.G., G. Lambert, M.R. Carman, J. Byrnes, R.B. Whitlatch, G. Ruiz, R.J. Miller, L. Harris, P.C. Valentine, J.S. Collie, J. Pederson, D.C. McNaught, A.N. Cohen, R.G. Asch, J. Dijkstra and K. Heinonen. 2007. The colonial ascidian *Didemnum* sp.: current distribution, basic biology, and potential threat to marine communities of the northeast and west coasts of North America. *Journal of Experimental Marine Biology and Ecology* 342(1): 99-108.

Valentine, P.C., J.S. Collie, R.N. Reid, R.G. Asch, V.G. Guida and D.S. Blackwood. 2007. The occurrence of the colonial ascidian *Didemnum* sp. on Georges Bank gravel habitat — ecological observations and potential effects on groundfish and scallop fisheries. *Journal of Experimental Marine Biology and Ecology* 342(1): 179-181.

Asch, R.G. and J.S. Collie. 2008. The role of bottom fishing and ecological succession in structuring the benthic megafaunal community. *Fishery Bulletin* 106: 438-456.

Checkley, Jr., D.M., A.G. Dickson, M. Takahashi, J.A. Radich, N. Eisenkolb and R. Asch. 2009. Elevated CO_2 enhances otolith growth in young fish. *Science* 324: 1683.

Davison, P. and R.G. Asch. 2011. Plastic ingestion by mesopelagic fishes in the North Pacific Subtropical Gyre. *Marine Ecology Progress Series* 432: 173-180.

Asch, R. 2013. Student perspectives: phenology in the California Current Ecosystem: CalCOFI and beyond. p. 211-213. In: Regional Fisheries Oceanography of the California Current System. The CalCOFI Program. S. McClatchie. Springer, New York, NY.

Asch, R.G. and D.M. Checkley, Jr. 2013. Dynamic height: A key variable for identifying the spawning habitat of small pelagic fishes. *Deep-Sea Research Part I* 71: 79-91.

ABSTRACT OF THE DISSERTATION

Interannual-to-Decadal Changes in Phytoplankton Phenology, Fish Spawning Habitat, and Larval Fish Phenology

by

Rebecca G. Asch

Doctor of Philosophy in Oceanography

University of California, San Diego, 2013

Professor David Checkley, Chair

Phenology is the study of seasonal, biological events and how they are influenced by climate. Climate change has prompted an earlier arrival of spring in numerous ecosystems. It is uncertain whether such changes are occurring in coastal upwelling ecosystems, because these regions are subject to decadal climate oscillations and regional

climate models predict later seasonal upwelling. To answer this question, chapter 1 investigated decadal changes in the phenology of 43 larval fish species in southern California. The first principal component of this dataset showed a progression towards the earlier appearance of larvae, although 18% of phenological events exhibited seasonal delays. These changes were best explained by a secular trend towards earlier warming of surface waters. Species with earlier phenology were characterized by an offshore, epipelagic distribution, while fishes with delayed phenology were more likely reside in coastal, demersal habitats.

Chapter 2 focused on improving understanding of how oceanic factors affect fish spawning habitat. Spawning habitat models can be applied to examine variations in fish phenology. Using data from spring cruises conducted between 1998-2004, dynamic height was investigated as a variable affecting the spawning habitat of anchovy, sardine, and jack mackerel. The greatest probability of encountering anchovy, sardine, and jack mackerel eggs occurred at dynamic heights of 79–83 cm, 84–89 cm, and 89–99 cm, respectively. Dynamic height explained more variance than any other variable (*e.g.*, temperature, salinity, chlorophyll, zooplankton volume, geographic currents, eddies) in models of sardine and anchovy spawning habitat.

Chapter 3 examined variations in phytoplankton phenology across the North Pacific using a hindcast of the Community Earth System Model 1.0 (CESM1) forced with atmospheric observations. Comparisons with SeaWiFS chlorophyll indicated that CESM1 could simulate mean dates of phytoplankton bloom initiation with as much skill as it could predict mean bloom magnitude. The first principal component for each of five phenological metrics (bloom initiation, midpoint, termination, duration, and magnitude)

was either correlated with the Multivariate ENSO Index or displayed a long-term trend. Compared to terrestrial ecosystems, long-term trends in phytoplankton phenology were noteworthy due to their rapid rate of change and greater prevalence of delayed phenology.

INTRODUCTION – A HISTORICAL OVERVIEW OF THE STUDY OF PHENOLOGY

Phenology refers to the study of recurring, biological events and the effects of climatic and meteorological conditions on those events. The term phenology is derived from the ancient Greek word "phainesthai", which means "to appear." The word was originally coined in 1853 by Charles Morren, a Belgian botanist, who first used the term "phenology" in a scientific paper describing an exceptionally warm winter where plants flowered for a second time in a year (Demarée and Rutishauser, 2009). Despite the 19th century origin of the word phenology, this scientific discipline has much older historical roots reflecting the fact that successful agriculture required accurate knowledge of the seasonal cycle of plants, livestock, and agricultural pests. In fact, Aldo Leopold once quipped that the first "paper" on phenology was the Book of Solomon in the Old Testament, which contains the following verse:

> For, lo, the winter is past,
> The rain is over and gone;
> The flowers appear on the earth;
> The time of the singing of birds is come
> And the voice of the turtle is heard in our land.
> (Solomon, 2:12, quoted in Leopold and Jones, 1947)

The oldest known calendar of phenological events was developed in China in the 11th century B.C. (Yoshino, 2004). This calendar divides the year into 24 periods called *jiequi*, which were further subdivided into a set of five-day periods called *hou*. Each *hou* corresponded to a particular phenological event or agricultural activity (Yoshino, 2004).

Similarly, the date of the first flowering of cherry trees has been recorded on an annual basis in Kyoto, Japan since the 9th century (Aono and Kazui, 2008). This 732-year record of cherry tree phenology has been used to reconstruct spring temperatures in Japan prior to the beginning of instrumental records. In France, Switzerland, and Germany, records of the date of the first wine grape harvest each year have been officially registered by parishes and municipalities, with some records extending as far back as 1221 (Pfister, 1988). Using a reconstruction of spring-summer temperatures based on grape harvest phenology from Burgundy, France, Chuine *et al*. (2004) determined that the 2003 heat wave in Europe was unprecedented in this time series that began in 1370.

The first scientific network of sites dedicated to monitoring phenology was developed by Carolus Linnaeus in 1750. This network recorded the timing of first flowering, leafing, fruiting, and leaf fall at 18 sites across Sweden. Linnaeus also published a methodological guide for studying phenology and encouraged students to write dissertations about phenology in several Nordic countries (Terhivuo *et al.*, 2009).

The history of British phenology extends back to 1789 when two important phenological treatises were published. During this year, Gilbert White, England's first ecologist, published *The Natural History and Antiquities of Selbourne*, which contains notes describing the phenology of > 400 plant and animal species that White studied over a 25-year period. Also in 1789, the British Royal Society published a manuscript by Robert Marsham, a British landowner, whose family monitored 27 biological indicators of spring on their property over the course of seven generations. The Marsham time series covers the period between 1736-1947, with a few gaps in this record (Sparks and Carey, 1995). A recent re-analysis of the Marsham dataset revealed that the phenology of

plants was more closely correlated with local temperature than the phenology of animals, reflecting the migratory behavior of many of the animal species monitored by the Marsham family (Sparks and Carey, 1995).

A second historical, phenological dataset, recently been rediscovered and reanalyzed, was developed by the American philosopher and writer Henry David Thoreau. Between 1852-1858, Thoreau recorded the first flowering dates of > 500 taxa in Concord, Massachusetts. Thoreau had intended to publish a manuscript on this work, as well as an accompanying calendar of phenological events, but he died of tuberculosis before this project was completed. The area surveyed by Thoreau was studied between 2004-2006 by Miller-Rushing and Primack (2008). Since Thoreau's lifetime, temperatures in Concord had warmed by 2.4° C. This change in temperature corresponded to a mean advancement of phenological events by 7 days (Miller-Rushing and Primack, 2008). A companion study by Willis *et al*. (2008) noted that plant species that did not adjust their phenology to changing climatic conditions were more likely to have become locally extinct in Concord.

Another well known American naturalist and philosopher who made extensive phenological observations was Aldo Leopold. Between 1935-1945, Leopold investigated 328 phenological events at two field sites, one of which was located near his home in Sauk County, Wisconsin. The other field site was located at the University of Wisconsin—Madison, where Leopold worked. In 1947, Leopold published a monograph describing his phenological investigations (Leopold and Jones, 1947). In addition to documenting phenological patterns observed in central Wisconsin, this monograph outlines the characteristics of species that make them ideal candidates for inclusion in

phenological monitoring programs, discusses common sources of error in phenological studies, and introduces a new type of graph for visualizing variations in phenology. Leopold and Jones (1947) also presented the results of a set of "natural experiments" where they compared years with contrasting seasonal temperature and precipitation patterns in order to distinguish between the effects of these two climatic factors on plant phenology. To the best of my knowledge, this paper also represents the first study of decadal variations in phenology, since Leopold and Jones (1947) compared their work with a set of observations made at the Wisconsin College of Agriculture in the early 1880s. Due to warmer temperatures in February through May during the 1935-1945 period, Leopold and Jones (1947) observed that phenological events occurred two weeks earlier than they had in the 1880s. Aldo Leopold's daughter, Nina Leopold Bradley, continued to make phenological observations in the area surrounding her family home between 1976-1998. An analysis of this time series published in 1999 documented that 17 of 55 phenological events occurred significantly earlier in the year at the end of the time series due to warming temperatures (Bradley *et al.*, 1999).

Like terrestrial phenology, the study of seasonality in the ocean also has a long history, although these two disciplines developed along separate paths with relatively little interaction between each other. As a result, the term "phenology" is not used frequently in the literature on biological oceanography even when seasonal patterns are described. Victor Henson, the German scientist who first coined the term "plankton", conducted the first study of seasonality among pelagic organisms (Mills, 1989). Between 1883-1886, Henson and his colleagues conducted 34 cruises off Kiel, Germany on a roughly monthly basis to study the seasonal cycle of phytoplankton abundance. A spring

peak in diatom abundance and an autumn maximum in dinoflagellate concentration were noted. However, Henson believed that these seasonal maxima reflected sampling error, because he had assumed that the seasonal cycle in the ocean would be analogous to that on land (Mills, 1989). Franz Schütt, a German oceanographer who collected many of these seasonal plankton samples on behalf of Henson, did recognize the seasonal pattern associated with spring and fall plankton blooms and wrote about this in a book entitled *Analytische Plankton-Studien* (Mills, 1989). Schütt also described the seasonal succession of different phytoplankton species, stating, "…with just as absolute certainty as the cherries bloom before the sunflowers, so *Skeletonemas* arrive at their yearly peak earlier than the *Ceratiums*" (Schütt, 1892 quoted in Mills, 1989).

Another prodigious effort to sample seasonal patterns of plankton abundance was undertaken by Sir William Herdman and his colleagues who collected macroplankton samples six days a week between 1907-1921 off the Isle of Man in the Irish Sea. Johnstone *et al*. (1924) published a book based on this work that was mainly intended to serve as a guide to plankton identification in the Irish Sea. However, this book also included graphs and tables documenting the monthly abundance of 38 plankton taxa over the 14-year period of this study. Like Schütt, Johnstone *et al.* (1924) described the seasonal succession of plankton species in detail. However, unlike their predecessors, Johnstone *et al*. (1924) also emphasized interannual variability in phenology, noting, for example, that peaks in the diatom *Chaetoceros* would occur in March during some years and in May during other years. Johnstone *et al.* (1924) expressed an interest in correlating interannual variations in plankton abundance and phenology with hydrographic

conditions, but they were unable to pursue this research due to a lack of concurrent sampling of physical oceanographic conditions around the Isle of Man.

Ultimately, the modern theory of how phytoplankton seasonality is influenced by oceanographic and meteorological conditions was developed by Harald Sverdrup. However, Sverdrup's work was influenced by a number of predecessors, most notably H.H. Gran who developed the idea of compensation depth and Gordon Riley who recognized that phytoplankton growth is often inversely proportional to mixed layer depth (MLD) (Mills, 1989). Sverdrup (1953) developed the critical depth hypothesis to explain the timing of the spring phytoplankton bloom that is typically observed each year in temperate areas of the ocean. The critical depth is defined as the location where depth-integrated primary production is equal to depth-integrated community respiration. Respiration rates were assumed by Sverdrup to be constant throughout the water column, whereas photosynthesis decreases exponentially with depth due to light limitation. As a result, critical depth is a function of solar irradiance and the transparency of the water column. Sverdrup (1953) argued that a phytoplankton bloom cannot occur when the MLD exceeds the critical depth since depth-integrated respiration will be greater than primary production. Such conditions exist in winter when MLD reaches its seasonal maximum. As winter ends, the MLD shoals due to increased stratification reflecting surface warming of the water column and/or decreases in salinity due to melting of snow and sea ice. At the same time, the critical depth becomes deeper as solar irradiance increases in the spring. Sverdrup (1953) tested this hypothesis using field data collected in 1949 aboard Weather Ship "M" in the Norwegian Sea. He found that the critical depth increased from 30-40 m in March to approximately 300 m in May. MLD shoaled below

the critical depth in late April. By mid-May, copepod abundance had increased so that phytoplankton growth was suppressed by heavy grazing (Sverdrup, 1953). Sverdrup's critical depth hypothesis is still cited as the predominant explanation for spring blooms in temperate ocean ecosystems, although, in the last three years, alternative hypotheses have been proposed to explain observations of increased phytoplankton growth prior to the shoaling of MLD (Behrenfeld, 2010; Taylor and Ferrari, 2011; Mahadevan *et al*., 2012).

In the field of fisheries oceanography, interest in seasonal cycles stemmed from the development of the match-mismatch hypothesis by David Cushing in 1974. This hypothesis seeks to explain how order-of-magnitude variations in fish recruitment are connected to fluctuations in ocean climate (Cushing, 1974). Cushing observed that populations of sockeye salmon, Atlantic herring, and plaice had seasonal peaks in spawning that varied between years with less than a 1-week standard deviation. These spawning peaks typically coincided with the time of the spring bloom, but the bloom exhibited more interannual variability in its seasonal occurrence. Cushing proposed that, when there was a seasonal mismatch between plankton production and fish egg and larval production, this would result in poor feeding conditions for larval fishes and would increase their mortality due to starvation (Cushing, 1974). The reduced survival of larvae would then lead to lower recruitment once this year class grew to a size where it would be susceptible to the capture by fisheries. Support for the mismatch hypothesis has been provided by research on a variety of commercially important fishes, including Atlantic cod (Beaugrand *et al.*, 2003), haddock (Platt *et al.*, 2003), and coho salmon (Chittenden *et al.*, 2010). However, it is also widely recognized that, while mismatches often result in poor recruitment, seasonal matches between phytoplankton blooms and larval production

do not guarantee high recruitment given that recruitment is controlled by a number of oceanographic variables that influence fishes throughout several life history stages (Houde, 2008). In studies of terrestrial phenology, seasonal mismatches between predator and prey species, as well as between plants and pollinators, have been documented (Durant *et al*., 2007), although many of these terrestrial studies fail to recognize and cite that the extensive and older marine ecological literature on the match-mismatch hypothesis (*e.g*., Visser *et al.*, 1998).

In both marine and terrestrial ecosystems, climate change has led to a renewed interest in phenology given that warming temperatures are expected to lead to the earlier occurrence of spring conditions. Noting this point, Miller-Rushing and Primack (2008) declared, "Of [the] biological responses to climate change, changes in the timing of phenological events are the most widely reported and probably the most easily detectable." In terrestrial habitats, several meta-analyses have confirmed that spring phenological events are indeed responding to climate change by occurring earlier in the year (Parmesan and Yohe, 2003; Root *et al*., 2003; Parmesan, 2007; Cleland *et al.*, 2012; Cook *et al.*, 2012; Wolkovich *et al.*, 2012). However, a number of gaps exist in these meta-analyses due to the fact that they mainly analyzed data from temperate Northern Hemisphere ecosystems, often excluded fall and winter phenological events, and included relatively little data from marine ecosystems and arid, terrestrial habitats.

Eastern Boundary Current upwelling systems may experience shifts in phenology due to climate change that differ from those observed in terrestrial ecosystems, because regional climate models have predicted a delayed onset of seasonal upwelling. This issue was first examined by Snyder *et al*. (2003) in a model of the California Current

Ecosystem (CCE) that investigated the effects of a doubling of atmospheric CO_2 on wind-driven upwelling. This model simulation suggested that upwelling is likely to decrease during April-May and increase during July-October in the northern CCE, resulting in a one-month delay in the spring transition. A more complex regional climate model, which accounted for positive feedbacks due to changes in land cover, confirmed these results for the northern CCE, but predicted that the southern CCE would experience an increase in early-season upwelling and a decrease in peak and late-season upwelling (Diffenbaugh *et al.*, 2004). This could cause an advance in the seasonal cycle of southern CCE upwelling, as well as potentially dampen its seasonal pattern.

The predictions of these regional climate models also seem to be echoed in the unusual upwelling patterns observed in the northern CCE in 2005. During this year, the spring transition did not occur until May 24, over a month later than normal, while the initiation of substantial upwelling was delayed two months (Kosro *et al.*, 2006; Barth *et al.*, 2007). These events were accompanied by a positive 2° C anomaly in nearshore waters off central Oregon, a 50% decrease in surf-zone chlorophyll, and a 30% reduction in spring nitrate (Barth *et al.*, 2007). A northward shift in the jet stream's position caused stronger-than-average upwelling to begin in mid-July, such that by September cumulative upwelling reached the climatological mean. This shift in the seasonal pattern of upwelling affected all trophic levels. The zooplankton assemblage between northern California and British Columbia was characterized by reduced abundance of fauna with a northern biogeographic affinity and a shift in the life cycles of some species to earlier in the year (Mackas *et al.*, 2006). Fish assemblages responded with increases in the abundance of offshore species, such as ocean sunfish, Pacific pomfret, opah, and

yellowtail (Brodeur *et al.*, 2006). Many southern fish species shifted their distribution northward. For example, larvae of Pacific hake and jack mackerel were found off Oregon and British Columbia. These species typically spawn in the Southern California Bight (SCB), so this represents a ~1,000-km shift in distribution (Brodeur *et al.*, 2006). Similarly, sardine and anchovy were captured as far north as Southeast Alaska. The unusual events of 2005 induced delays in the timing of the reproduction and recruitment of mussels and barnacles (Barth *et al.*, 2007). Breeding success of Cassin's auklet was severely disrupted by reduced krill abundance resulting from delayed upwelling (Sydeman *et al.* 2006).

The research presented in this dissertation is primarily focused on identifying long-term changes and interannual-to-decadal variations in the phenology of phytoplankton and fishes found in the North Pacific. In Chapter 1, biological and physical oceanographic data collected by California Cooperative Ocean Fisheries Investigations (CalCOFI) are used to investigate changes in larval fish phenology between 1951-2008. I analyzed this dataset on a decadal basis since quarterly CalCOFI surveys were often conducted during different months in successive years. Through decadal averaging, I was able to generate a monthly time series of larval fish concentration for 43 species. In addition to examining long-term trends in larval fish phenology, this chapter also investigates whether local oceanic variables (*e.g.*, sea surface temperature, coastal upwelling, mesozooplankton displacement volume) and basin-scale climate oscillations (*e.g.*, El Niño-Southern Oscillation, Pacific Decadal Oscillation, North Pacific Gyre Oscillation) affect fish phenology. The chapter concludes with an

examination of what ecological characteristics of fishes are associated with phenological sensitivity to climate change.

Chapter 1 principally focused on assemblage-wide changes in fish phenology because decadal averaging reduced the amount of phenological data available for each species (*e.g.*, one estimate of fish phenology per decade per species). In contrast, Chapter 2 took a more species-specific approach examining interannual variations in the spawning habitat of three small pelagic fishes (*e.g.*, *Sardinops sagax*, *Engraulis mordax*, and *Trachurus symmetricus*). The spatial distribution of fish spawning habitat was compared to variations in dynamic height during spring CalCOFI cruises between 1998-2004. Dynamic height was hypothesized to influence the location of spawning habitat, because it is related fluctuations in temperature, salinity, primary and secondary production, and geostrophic current flow. These are all oceanic variables that have been previously shown to affect the distribution of the spawning habitat of small pelagic fishes (Lluch-Belda *et al*., 1991; Checkley *et al.*, 2000; Lynn, 2003; Reiss *et al*., 2008; Weber and McClatchie, 2010; Zwolinski *et al*., 2011). Generalized linear models were used to assess how much variance in fish spawning habitat could be explained by each of these oceanic variables. An improved understanding of the relationship between oceanic variables and spawning habitat can contribute to the investigation of fish phenology since oceanic variables are monitored on a more routine basis than fishes by remote sensing and *in situ* measurements by gliders. Habitat models can then be applied to examine the phenology of spawning habitat availability based on the higher temporal resolution data on oceanic variables.

Since chlorophyll concentration has only been monitored regularly in the CCE since 1984, Chapter 1 did not directly evaluate whether there have been changes in phytoplankton phenology that could produce mismatches with the timing of fish spawning. To explore this question in greater depth, variations in phytoplankton phenology were investigated in Chapter 3 using a hindcast of the ocean component of the Community Earth System Model 1.0 (CESM1) that was forced with atmospheric observations made between 1961-2007. The 1° spatial resolution of the current generation of global climate models, such as CESM1, is too coarse to characterize physical processes associated with coastal upwelling, resulting in the overestimation of SST in Eastern Boundary Current upwelling systems (Wang *et al.*, 2010; Stock *et al*., 2011). As a result, the examination of phytoplankton phenology with CESM1 focused on a larger spatial scale, investigating variations in the timing of phytoplankton blooms throughout the North Pacific. Chapter 3 first validates whether CESM1 can accurately assess phytoplankton phenology through a comparison with remotely sensed SeaWiFS chlorophyll. This chapter then examines whether phytoplankton phenology across different regions of the North Pacific was correlated with interannual-to-decadal climate oscillations or exhibited a long-term, phenological trend.

References

Aono, Y. and K. Kazui. 2008. Phenological data series of cherry tree flowering in Kyoto, Japan, and its application to reconstruction of springtime temperatures since the 9th century. *International Journal of Climatology* 28: 905-914.

Barth, J.A., B.A. Menge, J. Lubchenco, F. Chan, J.M. Bane, A.R. Kirincich, M.A. McManus, K.J. Nielsen, S. D. Pierce and L. Washburn. 2007. Delayed upwelling alters nearshore coastal ocean ecosystems in the northern California current. *Proceedings of the National Academy of Sciences* 104(10): 3719-3724.

Beaugrand, G., K.M. Brander, J.A. Lindley, S. Souissi and P.C. Reid. 2003. Plankton effect on cod recruitment in the North Sea. *Nature* 426: 661-664.

Behrenfeld, M.J. 2010. Abandoning Sverdrup's critical depth hypothesis on phytoplankton blooms. *Ecology* 91(4): 977-989.

Bradley, N.L., A.C. Leopold, J. Ross and W. Huffaker. 1999. Phenological changes reflect climate change in Wisconsin. *Proceedings of the National Academy of Sciences* 96: 9701-9704.

Brodeur, R.D., S. Ralston, R.L. Emmett, M. Trudel, T.D. Auth and A.J. Phillips. 2006. Anomalous pelagic nekton abundance, distribution, and apparent recruitment in the northern California Current in 2004 and 2005. *Geophysical Research Letters* 33, L22S08, doi:10.1029/2006GL026614.

Checkley, D.M., Jr., R.C. Dotson, and D.A. Griffith. 2000. Continuous, underway sampling of eggs of Pacific sardine (*Sardinops sagax*) and northern anchovy (*Engraulis mordax*) in spring 1996 and 1997 off southern and central California. *Deep-Sea Research II* 47: 1139-1155.

Chittenden, C.M., J.A. Jensen, D. Ewart, S. Anderson, S. Balfry, E. Downey, A. Eaves, S. Saksida, B. Smith, S. Vincent, D. Welch and R.S. McKinley. 2010. Recent salmon declines: result of lost feeding opportunities due to bad timing? *Plos One* 5(8), doi:10.1371/journal.pone.0012423.

Chuine, I, P. Yiou, N. Viovy, B. Seguin, V. Daux and E. Le Roy Ladurie. 2004. Grape ripening as a past climate indicator. *Nature* 432: 289-290.

Cleland, E.E., J.M. Allen, T.M. Crimmins, J.A. Dunne, S. Pau, S.E. Travers, E.S. Zavaleta and E.M. Wolkovich. 2012. Phenological tracking enables positive species responses to climate change. *Ecology* 93(8): 1765-1771.

Cook, B.I., E.M. Wolkovich and C. Parmesan. 2012. Divergent responses to spring and winter warming drive community level flowering trends. *Proceedings of the National Academy of Sciences* 109(23): 9000-9005.

Cushing, D.H. 1974. The natural regulation of fish populations. p. 399-412. In Sea Fisheries Research. F.R.H. Jones (ed). John Wiley & Sons, New York, NY.

Demarée, G.R and T. Rutishauser. 2009. Origins of the word "phenology." *Eos* 90(34): 4.

Diffenbaugh, N.S., M.A. Snyder and L.C. Sloan. 2004. Could CO_2-induced land-cover feedbacks alter near-shore upwelling regimes? *Proceedings of the National Academy of Sciences* 101(1): 27-32.

Durant, J.M., D.O. Hjermann, G. Ottersen and N.C. Stenseth. 2007. Climate and the match or mismatch between predator requirements and resource availability. *Climate Research* 33: 271-283.

Houde, E.D. 2008. Emerging from Hjort's shadow. *Journal of the Northwest Atlantic Fishery Science* 41: 53-70.

Johnstone, J., A. Scott and H.C. Chadwick. 1924. The Marine Plankton. The University Press of Liverpool, London, UK. 194 p.

Kosro, P.M., W.T. Peterson, B.M. Hickey, R.K. Shearman, and S.D. Pierce. 2006. Physical versus biological spring transition: 2005. *Geophysical Research Letters* 33, L22S03, doi:10.1029/2006GL027072.

Leopold, A. and S.E. Jones. 1947. A phenological record for Sauk and Dane Counties, Wisconsin, 1935-1945. *Ecological Monographs* 17(1): 81-122.

Lluch-Belda, D., D.B. Lluch-Cota, S. Hernandez-Vazquez, C.A. Salinas-Zavala and R.A. Schwartlose. 1991. Sardine and anchovy spawning as related to temperature and upwelling in the California current System. *California Cooperative Oceanic Fisheries Investigations Reports* 32: 105-111.

Lynn, R. 2003. Variability in the spawning habitat of Pacific sardine (*Sardinops sagax*) off southern and central California. *Fisheries Oceanography* 12(6): 541-553.

Mackas, D.L., W.T. Peterson, M.D. Ohman and B.E. Lavaniegos. 2006. Zooplankton anomalies in the California Current system before and during the warm ocean conditions of 2005. *Geophysical Research Letters* 33, L22S07, doi:10.1029/2006GL02730.

Mahadevan, A., E. D'Asaro, C. Lee and M.J. Perry. 2012. Eddy-driven stratification initiates North Atlantic spring phytoplankton blooms. *Science* 337: 54-58.

Miller-Rushing, A.J. and R.B. Primack. 2008. Global warming and flowering times in Thoreau's Concord: a community perspective. *Ecology* 89(2): 332-341.

Mills, E.L. 1989. Biological Oceanography. An Early History, 1870-1960. Cornell University Press, Ithaca, NY. 378 p.

Parmesan, C. and G. Yohe. 2003. A globally coherent fingerprint of climate change impacts across natural systems. *Nature* 421: 37-42.

Parmesan, C. 2007. Influences of species, latitudes and methodologies on estimates of phenological response to global warming. *Global Change Biology* 13: 1860-1872.

Pfister, C. 1988. Variations in the spring-summer climate of central Europe from the High Middle Ages to 1850. p. 57-82. In Long and Short Term Variability of Climate. H. Wanner and U. Siegenthaler (eds). Springer-Verlag, Berlin.

Platt, T., C. Fuentes-Yaco and K.T. Frank. 2003. Spring algal bloom and larval fish survival. *Nature* 423: 398-399.

Reiss, C.S., D.M. Checkley, Jr and S.J. Bograd. 2008. Remotely sensed spawning habitat of Pacific sardine (*Sardinops sagax*) and Northern anchovy (*Engraulis mordax*) within the California Current. *Fisheries Oceanography* 17(2): 126-136.

Root, T.L., J.T. Price, K.R. Hall, S.H. Schneider, C. Rosenweig and J.A. Pounds. 2003. Fingerprints of global warming on wild animals and plants. *Nature* 421(2): 57-60.

Snyder, M.A., L.C. Sloan, N.S. Diffenbaugh and J.L. Bell. 2003. Future climate change and upwelling in the California Current. *Geophysical Research Letters* 30(15), 1823, doi:10.1029/2003GL017647.

Sparks, T.H. and P.D. Carey. 1995. The responses of species to climate over two centuries: an analysis of the Marsham phenological record, 1736-1947. *Journal of Ecology* 83: 321-329.

Stock, C.A., M.A. Alexander, N.A. Bond, K.M. Brander, W.W.L. Cheung, E.N. Curchitser, T.L. Delworth, J.P. Dunne, S.M. Griffies, M.A. Haltuch, J.A. Hare, A.B. Hollowed, P. Lehodey, S.A. Levin, J.S. Link, K.A. Rose, R.R. Rykaczewski, J.L. Sarmiento, R.J. Stouffer, F.B. Schwing, G.A. Vecchi and F.E. Werner. 2011. On the use of IPCC-class models to assess the impact of climate on Living Marine Resources. *Progress in Oceanography* 88: 1-27.

Sverdrup, H.U. 1953. On conditions for the vernal blooming of phytoplankton. *Journal du Conseil International pour l'Exploration de la Mer* 18: 287-295.

Sydeman, W.J., R.W. Bradley, P. Warzybok, C.L. Abraham, J. Jahncke, K.D. Hyrenbach, V. Kousky, J.M. Hipfner and M.D. Ohman. 2006. Planktivorous auklet *Ptychoramphus aleuticus* responses to ocean climate, 2005: Unusual atmospheric blocking? *Geophysical Research Letters* 33, L22S09, doi:10.1029/2006GL026736.

Taylor, J.R. and R. Ferrari. 2011. Shutdown of turbulent convection as a new criterion for the onset of spring phytoplankton blooms. *Limnology and Oceanography* 56(6): 2293-2307.

Terhivuo, J., E. Kubin and J. Karhu. 2009. Phenological observation since the days of Linné in Finland. *Italian Journal of Agrometeorology* 1: 45-49.

Visser, M.E., A.J. van Noordwijk, J.M. Tinbergen and C.M. Lessells. 1998. Warmer springs leads to mistimed reproduction in great tits (*Parus major*). *Proceedings of the Royal Society, London B* 265: 1867-1870.

Wang, M., J.E. Overland and N.A. Bond. 2010. Climate projections for selected large marine ecosystems. *Journal of Marine Systems* 79: 258-266.

Weber, E.D. and S. McClatchie. 2010. Predictive models of northern anchovy *Engraulis mordax* and Pacific sardine *Sardinops sagax* spawning habitat in the California Current. *Marine Ecology Progress Series* 406: 251-263.

Willis, C.G., B. Ruhfel, R.B. Primack, A.J. Miller-Rushing and C.C. Davis. 2008. Phylogenetic patterns of species loss in Thoreau's woods are driven by climate change. *Proceedings of the National Academy Sciences* 105(44): 17029-17033.

Wolkovich, E.M., B.I. Cook, J.M. Allen, T.M. Crimmins, J.L. Betancourt, S.E. Travers, S. Pau, J. Regetz, T.J. Davies, N.J.B. Kraft, T.R. Ault, K. Bolmgren, S.J. Mazer, G.J. McCabe, B.J. McGill, C. Parmesan, N. Salamin, MD. Schwartz and E.E. Cleland. 2012. Warming experiments underpredict plant phenological responses to climate change. *Nature* 485: 494-497.

Yoshino, M. 2004. Development of phenological recognition and phenology in ancient China. *Japanese Journal of Biometeorology* 41: 141–154.

Zwolinski, J.P., R.L. Emmett and D.A. Demer. 2011. Predicting habitat to optimize sampling of Pacific sardine (*Sardinops sagax*). *ICES Journal of Marine Science* 68(5): 867-879.

CHAPTER 1. CLIMATE CHANGE AND DECADAL SHIFTS IN THE PHENOLOGY OF LARVAL FISHES IN THE CALIFORNIA CURRENT ECOSYSTEM

Abstract

Climate change has prompted an earlier arrival of spring in numerous ecosystems. It is uncertain whether such changes are occurring in Eastern Boundary Current upwelling ecosystems, because these regions are subject to decadal climate oscillations and regional climate models predict seasonal delays in upwelling. To answer this question, the phenology of 43 species of larval fishes was investigated between 1951-2008 in southern California. The first principal component of this dataset showed a progression towards the earlier appearance of larvae. 39% of phenological events indicated increasingly early peaks in larval abundance, while 18% exhibited delayed phenology. These changes were best explained by a secular trend towards earlier warming of surface waters rather than by decadal climate cycles, such as the Pacific Decadal Oscillation and the North Pacific Gyre Oscillation. Species displayed similar changes in phenology at both the decadal scale and the interannual scale associated with El Niño. Species with earlier phenology were characterized by an offshore, epipelagic distribution, while species with delayed phenology were more likely reside in coastal, demersal habitats. Earlier spawning was correlated solely with changes in sea surface temperature (SST). A combination of SST and upwelling were responsible for delays in fish phenology. Since species with earlier phenology were not changing their seasonal abundance synchronously with upwelling and mesozooplankton, they may be increasingly subject to mismatches with their prey in the future. Among species with no long-term phenological trends, a contraction in the length of their spawning season was detected, which could increase recruitment variability.

1. Introduction

Phenology is the study of seasonal, biological processes and how they are influenced by climate and weather. Since warmer temperatures are frequently associated with earlier phenological events, changes in phenology are common indicators of the effects of climate change on ecological communities (Parmesan and Yohe, 2003; Root et *al*., 2003; Menzel *et al*., 2006; Parmesan, 2007). Meta-analysis has showed that phenological events have advanced at a rate of 2.8 ± 0.4 SE days decade^{-1} relative to historical baselines (Parmesan, 2007). Among species for which phenological changes were detected, >80% of these shifts occurred in a direction consistent with climate change (Parmesan and Yohe, 2003; Root et *al*., 2003).

Despite the inclusion of hundreds of species in meta-analyses examining climate change effects on phenology, gaps in knowledge persist because most long-term studies of phenology have monitored spring events affecting terrestrial species residing in temperate habitats in the northern hemisphere (Root et *al*., 2003; Parmesan, 2007). Marine species are particularly underrepresented in these meta-analyses (Richardson and Poloczanska, 2008). For example, one meta-analysis examined the phenology of 694 species of which only one exclusively resides in marine habitats (Root et *al*., 2003). Underrepresentation of marine species is problematic not only due to their ecological importance, but also because recent studies suggest shifts in phenology may occur more rapidly in marine environments than terrestrial ecosystems (Edwards and Richardson, 2004; Burrows *et al*., 2011). Compared to other marine organisms, there is a longer history of studying the phenology of teleost fishes, since the seasonal coincidence

between phytoplankton blooms and fish spawning can affect recruitment to commercial fisheries (Cushing, 1974; Cushing, 1990; Stenseth and Mysterud, 2002; Durant *et al.*, 2007). Nevertheless, little research has investigated the impact of anthropogenic climate change on fish phenology and, with a few exceptions (Greve *et al.*, 2005; Genner *et al*., 2010), studies have been limited to a small set of commercially fished species. To address this issue, this study investigated the influence of local and basin-scale climatic and oceanic factors on the phenology of 43 fish species whose larval abundance has been monitored off southern California since 1951.

In the California Current Ecosystem (CCE), wind-driven upwelling is one of the predominant physical processes regulating the seasonal cycle of primary and secondary productivity. The seasonal onset of upwelling, referred to as the "spring transition", is associated with the commencement of southward, alongshore winds that induce offshore Ekman transport of coastal waters (Huyer *et al*., 1979). This coincides with a decrease in coastal sea surface temperature (SST) by 1.5-4°C, the development of a nearshore, southward oceanic jet, and an increase in fluorescence indicative of elevated primary production in the coastal zone (Lynn *et al*., 2003). In the central and northern CCE (>35° N), upwelling intensifies through summer until wind direction reverses in the fall. In the southern CCE (<35° N), upwelling is observed in all seasons, but its intensity diminishes in fall and winter (Snyder *et al.*, 2003; Henson and Thomas, 2007). One area less affected by seasonal upwelling dynamics is the Southern California Bight (SCB), which is located south of Point Conception (Fig. S1.1; Chelton *et al*., 1982; Schwing and Mendelssohn, 1997; Mantyla *et al*., 2008). Seasonal primary production in the SCB is influenced by the shoaling of isopycnals associated with cyclonic circulation and winter convection, which

both transport nutrients to surface waters (Mantyla *et al*., 2008). This leads to a spring maximum in chlorophyll concentration occurring between March and May (Hayward and Venrick, 1998; Mantyla *et al*., 2008; Kim *et al.*, 2009). The peak in phytoplankton is followed by a summer maximum in mesozooplankton abundance between May and July (Chelton *et al*., 1982; McGowan *et al.*, 2003). Fishes spawn in the southern CCE year round, although most species exhibit distinct seasonal patterns of larval abundance (Moser *et al*., 2001).

There is increasing evidence that seasonal cycles of temperature, sea surface height (SSH), and chlorophyll concentration may not be stationary in the CCE (Mendelssohn *et* al., 2004; Venegas *et al*., 2008). Empirical observations and regional climate models suggest that climate change is leading to intensification of upwelling during spring and/or summer months, but not other seasons (Bakun, 1990; Schwing and Mendelssohn, 1997; Snyder *et al*., 2003; Diffenbaugh *et al*., 2004). A model simulation that doubled atmospheric CO_2 indicated that upwelling off northern California is likely to increase during July-October, but decrease in April-May, resulting in a one-month delay in the spring transition (Snyder *et al*., 2003). When feedbacks due to changes in land cover were accounted for, similar results were obtained for the northern CCE, but model predictions suggested that the southern CCE would experience an increase in early-season upwelling and a decrease in peak and late-season upwelling (Diffenbaugh *et al*., 2004). This could cause an advance in the seasonal cycle of southern CCE upwelling, as well as potentially dampen its seasonal amplitude. Empirical observations of ocean temperature and the Bakun upwelling index validate these model results indicating delays in the onset and peak of upwelling, particularly in the northern CCE (Mendelssohn *et al*.,

2004; Bograd *et al.*, 2009). In accordance with model predictions of earlier upwelling in the southern CCE, phytoplankton blooms were observed 1-2 months earlier in the late 1990s in this region compared to previous years (Kim *et al*., 2009).

In addition to anthropogenic climate change, oceanography in the CCE is affected by climate oscillations with interannual-to-decadal periods, including El Niño-Southern Oscillation (ENSO), the Pacific Decadal Oscillation (PDO), and the North Pacific Gyre Oscillation (NPGO). El Niño is frequently accompanied by delays in seasonal upwelling (Schwing *et al*., 2006; Bograd *et al.*, 2009), although lower frequency climate oscillations, such as the PDO, do not have as pronounced of an effect on upwelling seasonality (McGowan *et al.*, 2003; Bograd *et al.*, 2009). Due to delayed and reduced upwelling, El Niño can be associated with later spring phytoplankton blooms, although this effect varies between regions and has not been observed in all years (Henson and Thomas, 2007; Yoo *et al*., 2008). While little research has been conducted in the CCE investigating PDO effects on phytoplankton bloom timing, this climate oscillation influences phytoplankton phenology elsewhere in the North Pacific (Sasaoka *et al*., 2011; Chiba *et al.*, 2012). Among zooplankton in the southern CCE, the 1977 change from a negative to positive PDO conditions coincided with a two-month shift towards earlier maximum displacement volume of zooplankton (McGowan *et al.*, 2003), as well as the earlier occurrence of the copepod *Neocalanus plumchrus* (Mackas *et al*., 2007). At the next trophic level, climate oscillations are known to influence the phenology of two fish species in the CCE. Earlier than usual spawning of northern anchovy (*Engraulis mordax*) was observed during the 1983 El Niño (Brodeur *et al.*, 1985). Similarly, early spawning migrations of chinook salmon (*Oncorhynchus tshawytscha*) are weakly correlated with

warm PDO anomalies (Keefer *et al*., 2008). The physiological mechanism responsible for these changes in phenology likely reflects the fact that warmer temperatures promote rapid gonadal development among fishes, leading to earlier spawning (Ware and Tanasichuk, 1989; Hutchings and Myers, 1994; Lange and Greve, 1997; Gillet and Quétin, 2006). The NPGO is a recently defined climate oscillation based on the second mode of variability of SSH in the Northeast Pacific (Di Lorenzo *et al*., 2008). In the southern CCE, the NPGO is more closely correlated to variations in salinity, nutrients, and chlorophyll than the PDO. Whether this mode of climate variability has an impact on the phenology of marine organisms is a subject yet to be investigated.

The match-mismatch hypothesis provides a mechanism explaining how climate-induced changes in fish and plankton phenology could potentially alter the abundance of fish stocks (Cushing, 1974; Cushing, 1990). This hypothesis proposes that fishes spawn during peak seasonal plankton production, which increases the likelihood that their larvae will encounter sufficient prey. However, due to interannual variability in the timing of plankton production and fish spawning, these events do not always coincide. During such "mismatches", first-feeding larvae may experience increased vulnerability to starvation or slower growth, which can heighten susceptibility to predation (Houde, 1987; Anderson, 1988). Poor larval survival can result in reduced recruitment and decreased fishery landings in subsequent years. While many other processes during the early life history of fishes influence recruitment (Houde, 2008), variations between in plankton phenology can result in order-of-magnitude changes in the recruitment and survival of commercially important fishes (Beaugrand *et al*., 2003; Logerwell *et al.*, 2003; Platt *et al.*, 2003).

Climate change could increase phenological mismatches through two mechanisms. First, certain seasonal cues, such as solar insolation and day length, will not be affected by global warming, whereas other seasonal processes will likely exhibit distinct rates of change (*e.g*., surface vs. bottom temperatures) (Mackas *et al.*, 2007; Koeller *et al.*, 2009). Since predators and prey may use different environmental factors as signals to initiate seasonal behaviors, this can lead to a higher frequency of mismatches if these indicators become decoupled (Durant *et al*., 2007; Mackas *et al.*, 2007). Second, individual species inevitably have distinct climate sensitivities that result in differing rates of phenological response to climate change. These differences can lead to non-linear responses where even small changes in climate can unbalance established patterns of synchrony (Durant *et al*., 2007).

To investigate whether climate change and variability may be leading to increased mismatches between larval fishes and their prey, this study examined decadal changes in the phenology of 43 species of fish larvae off California. Other objectives of this study were to: 1) determine whether such changes were correlated with variations in regional climate indices and the seasonality of SST, coastal upwelling, and zooplankton abundance; 2) assess which life history characteristics of fishes are linked to changes in phenology, and; 3) forecast 21st century changes in fish phenology based on predicted changes in seasonal SST and upwelling. Several hypotheses can be proposed regarding how fish phenology has changed since 1951, when ichthyoplankton surveys began in the southern CCE:

- H_0: The phenology of larval fishes will remain constant regardless of variations in seasonal oceanographic conditions. This would be expected if photoperiod were the predominant factor affecting fish phenology (de Vlaming, 1972).
- H_{A1}: Fish larvae will uniformly occur earlier during periods with warmer temperature, reflecting earlier spawning. This could arise due to accelerated oocyte growth under warmer temperatures (Ware and Tanasichuk, 1989; Hutchings and Myers, 1994; Lange and Greve, 1997; Gillet and Quétin, 2006) or the tendency of spawning to track phytoplankton blooms, which have occurred earlier in the southern CCE in recent years (Kim *et al*., 2009).
- H_{A2}: Spring-spawning fishes will exhibit earlier larval phenology during periods with warmer temperatures, while fall-spawning species will exhibit delayed phenology, reflecting a later onset of cooler, fall conditions.
- H_{A3}: Delays in upwelling will lead to later spawning and occurrence of larvae.
- H_{A4}: The phenology of larval fishes will display interannual-to-decadal variability synchronous with climate oscillations, such as ENSO, PDO, and/or NPGO.

2. Results

2.1. Detection of Phenology Trends

Surveys of fish larvae were conducted between 1951-2008 on a monthly-to-quarterly basis (with some gaps between 1967-1983) by the California Cooperative Oceanic Fisheries Investigations (CalCOFI) (Fig. S1.1; Kramer *et al*., 1972; Hewitt,

1988). Monthly abundance of 43 fish species was calculated by decadally averaging data from quarterly surveys conducted in different months in successive years. This dampened the influence of interannual variability, while highlighting decadal changes. Since eight species exhibited two peaks in larval abundance each year, a total of 51 phenophases (*e.g.*, phenological events) were examined (Table S1.1). Changes in phenology were detected based on the central tendency (CT) of seasonal larvae occurrence each decade (Edwards and Richardson, 2004; Genner *et al*., 2010; Jansen and Gislason, 2011). Since calculating CT relative to decadal means led to a small sample size for each phenophase ($n = 6$) and reduced statistical power, this study did not focus on species-level changes in phenology. Instead, each phenophase was treated as a replicate for examining assemblage-wide patterns. Variations in CT were treated as a proxy for spawning time, since CalCOFI mainly collects young, pre-flexion larvae (Methot, 1983; Koslow *et al*., 2011) and the egg stage of many species lasts 2-4 days at temperatures in the southern CCE (Zwiefel and Lasker, 1976). Depending on the species and temperature, flexion occurs between 3-25 days post-hatch (Zwiefel and Lasker, 1976; Moser, 1996; Love *et al.*, 2002).

The first principal component of this dataset, which accounted for 32.6% of its variance, indicated that larvae are progressively appearing earlier in the year (Fig. 1.1). Similarly, linear regression of CT anomalies (calculated relative to the multi-decadal mean) versus year showed that on average fishes have advanced their phenology by 7.2 days since the initiation of the CalCOFI time series ($Y = 9.3305 – 0.0047X$, $F = 6.5$, d.f. = 288, $p < 0.05$). CT anomalies suggested that this trend is mainly due to changes over the last two decades (Fig. S1.2c).

Since divergent trends among species would not be evident when examining assemblage means, most ensuing analyses were performed on three groups of phenophases that shared similar decadal patterns. This categorization was based on the correlation between the CT of each phenophase and time, where phenophases with a correlation coefficient $r \geq 0.5$ were classified as having later phenology, $r \leq -0.5$ indicated earlier phenology, and intermediate values corresponded to phenophases with no long-term, linear changes. Twenty phenophases fell into the earlier phenology group; 9 were classified as exhibiting later phenology, and; 22 did not show a trend (Table S1.1). Regressions of CT anomalies versus decade for each group demonstrated that changes were statistically significant for earlier and later groups (earlier species: $Y = 38.6701 - 0.0195X$, $F = 80.1$, d.f. = 108, $p < 0.001$; later species: $Y = -31.9468 + 0.0161X$, $F = 36.9$, d.f. = 50, $p < 0.001$). Among species with earlier phenology, the rate of phenological change varied between -2.8 to -12.4 days decade^{-1}, with a mean of -6.4 days decade^{-1} (Fig. 1.2a). Commercially fished species with earlier phenology included jack mackerel (*Trachurus symmetricus*), Pacific hake (*Merluccius productus*), Pacific mackerel (*Scomber japonicus*), and three rockfishes (*Sebastes aurora*, *S. diploproa*, and *S. jordani*).

Species with later phenology shifted their spawning times at a slightly slower rate (mean: 5.1 days decade^{-1}; range: 3.0-7.2 days decade^{-1}) than the earlier phenology group (Fig. 1.2c). The time series of CT anomalies for later species showed an abrupt shift between the 1970s and 1980s (Fig. S1.2i). Species with later phenology targeted by commercial fisheries included chilipepper (*Sebastes goodei*) and the spring phenophase of California halibut (*Paralichthys californicus*). The 90% confidence intervals of

changes in CT were estimated to be ±2.8-3.1 days decade^{-1} based on a Monte Carlo simulation of modeled larvae with generic characteristics (Supplemental Information [SI] text, Table S1.2). These confidence intervals corresponded closely to the minimum rate of change observed among species in the earlier and later phenology groups.

For species with no long-term trend in phenology, the histogram showing rates of change was centered at 0 days decade^{-1} (Fig. 1.2b). However, some species in this group, such as *Sardinops sagax*, exhibited large, non-linear fluctuations in spawning times. Other commercially important species in this group were northern anchovy (*E. mordax*), California halibut (*P. californicus*, summer phenophase), Pacific sanddab (*Citharichthys sordidus*, both phenophases), English sole (*Parophrys vetulus*), and bocaccio (*Sebastes paucispinis*).

In addition to shifts in phenology, changes in the seasonal duration of peak larval abundance were also examined. This metric remained constant throughout this time series for fishes with earlier and later phenology ($F \leq 1.4$, $p \geq 0.25$). However, among species with no long-term trends in phenology, season duration contracted by 22 days since the 1950s (Fig. 1.3; $Y = 30.9781 - 0.0147X$, $F = 4.1$, d.f. = 126, $p < 0.05$). This result should be viewed with some caution due to the low capacity to detect changes in the duration of peak larval abundance given the frequency of CalCOFI sampling (SI text, Fig. S1.3b, Table S1.3).

2.2. Relationships between Phenology, Climate, Oceanic Conditions, and Ecological Traits

Fish phenology changed markedly during El Niño events, but the direction of these changes depended on phenology group. For species that exhibited a shift towards earlier phenology at the decadal scale, El Niño was also associated with earlier occurrence of larvae (Fig. 1.4a). Based on a Kruskal-Wallis test, this was significant at $p < 0.05$ ($X^2 = 7.5$, d.f. = 2,57). This suggested that fishes in this group reacted similarly to warming at the interannual scale associated with ENSO and the decadal scale. In contrast, species in the two other phenology groups experienced significant delays in spawning during El Niño (Fig. 1.4b-c; species without a linear trend: $F_{2,63} = 6.3$, $p < 0.01$; later species: $F_{2,24} = 5.3$, $p < 0.05$).

Attributing changes in phenology to the PDO is complicated by the fact that CalCOFI started during a negative, cold PDO period that persisted through 1976 and was followed by a positive, warm PDO phase continuing through 1998. Prior to 1998, the signal of anthropogenic climate change and warming related to the PDO were confounded. The return of negative PDO conditions in 1999 allowed for clearer distinction between these potential influences on phenology (Stewart *et al*., 2005). If the PDO was responsible for changes in phenology, then the timing of larval occurrence during recent, negative PDO years should be similar to that observed during the earlier, negative PDO. To examine this, ANOVAs were performed comparing fish phenology during the first negative PDO phase (1951-1976), the second negative PDO phase (1999-2002 and 2007-2008), and the warm PDO phase (1977-1998) (Fig. 1.4d-f). These ANOVAs indicated that there were significant changes in phenology across these periods for both species with long-term delays and advances in phenology (earlier species: $F_{2,57} = 21.5$, $p < 0.001$; later species: $F_{2,24} = 11.4$, $p < 0.001$). No significant effects were

observed for species without linear trends in phenology ($F_{2,63} = 0.1$, $p = 0.88$). For advancing species, Tukey-Kramer multiple comparison tests revealed that these differences were due to changes in phenology between the recent, negative PDO and all previous years (Fig. 1.4d). Phenology during the first, negative PDO differed from all subsequent periods among species with later phenology (Fig. 1.4f). In neither case were the first and second negative PDO periods similar to each other, suggesting that trends in phenology could be better attributed to secular warming than the PDO.

A similar analysis was conducted to evaluate whether fish phenology was influenced by negative, neutral, or positive NPGO conditions. ANOVAs examining this were not significant for any phenology group (Fig. S1.4). Again, this confirmed that assemblage-wide changes in phenology were more indicative of long-term trends than decadal climate oscillations.

To further investigate what factors were responsible for changes in fish phenology, the effects of three locally measured oceanic variables (*e.g.*, CalCOFI SST, CalCOFI mesozooplankton displacement volume, and the Bakun upwelling index) were examined. CT anomalies of these variables were calculated and regressed against time to assess decadal changes in seasonal patterns. Changes in SST CT indicated that ocean temperatures are now warming 25.9 days earlier than in the 1950s (Fig. 1.5a; $Y = 33.7200 - 0.0170X$, $F = 11.0$, d.f. = 4, $p < 0.05$). Upwelling did not exhibit a significant trend in decadal phenology (Fig. S1.5a; $F = 1.2$, d.f. = 4, $p = 0.34$), although peak upwelling during the 1980s and 2000s occurred slightly later than at the start of the time series. The CT of zooplankton volume was characterized by delayed phenology in the 1970s and early phenology in the 1980s (Fig. S1.5b), possibly reflecting changes related to the 1977

PDO shift (McGowan *et al*., 2003). The CT of zooplankton volume was close to zero in other decades, with no long-term trend ($F = 1.0$, d.f. = 4, $p = 0.30$).

Species in the earlier phenology group displayed a significant, positive correlation with SST CT (Fig. 1.5b), but were not influenced by upwelling or zooplankton volume (data not shown). Species whose phenology was delayed since the 1950s spawned later when the onset of upwelling also occurred later (Fig. 1.5d). In addition, this phenology group was inversely correlated with SST CT, such that fishes spawned earlier in years when seasonal temperatures remained cool for a longer time (Fig. 1.5c). CT anomalies for species with no long-term trends in phenology were not correlated with any oceanic variables ($|r| \leq 0.08$, d.f. = 130, $p \geq 0.35$).

Next, this study investigated whether species that displayed phenological changes shared certain ecological traits. The characteristics examined included the six most common taxonomic orders, season of maximal larval abundance, the amplitude of each species' seasonal cycle, trophic level, habitat of adult fishes, cross-shore distribution of larvae, biogeographic affinity (*e.g.*, warm-water, cool-water, or widespread distribution), frequency of larval occurrence during surveys, fishing status, changes in abundance of unfished species, and historical shifts in species range (Table S1.1). One of the most important characteristics associated with changes in phenology was whether a species used epipelagic, mesopelagic, or demersal habitats as an adult. Epipelagic species were more likely to exhibit earlier spawning, whereas as demersal fishes were more likely to show delayed phenology (Fig. 1.6b; $F_{2,48} = 3.4$, $p < 0.05$). The cross-shore distribution of larvae was a second habitat-related characteristic that affected phenology. Larvae in coastal areas were more likely to exhibit delayed phenology than species in coastal-

oceanic habitats, although this result was only marginally significant at $p = 0.07$ (Fig. 1.6c; $F_{2,48} = 2.8$). There is some overlap between these two habitat categories, since most demersal fishes surveyed by CalCOFI occurred in coastal habitats, while epipelagic and mesopelagic species were frequently found in coastal-oceanic and oceanic habitats, respectively. In addition, phenology was significantly affected by taxonomy (Fig 1.6a; $F_{5,39} = 2.9$, $p < 0.05$). Flatfishes in the order Pleuroniformes tended to display later phenology. Stomiiformes, an order including bristlemouths, hatchetfishes, and dragonfishes, were the group most likely to show earlier phenology. Shifts towards earlier spawning were especially common among the most frequently occurring species (Fig. 1.6d). One final characteristic of the earlier phenology group was that they were more likely to undergo range shifts in response to changes in climatic and oceanic conditions (Hsieh *et al.*, 2008; Hsieh *et al.*, 2009; one-tailed binomial test: $n = 16$, $p < 0.05$). No other ecological characteristics had a statistically significant relationship with phenology.

2.3. Projections of 21st-Century Changes in Phenology

The Intergovernmental Panel on Climate Change (IPCC) A1B scenario was used to forecast future changes in fish phenology. This is a medium-range emissions scenario, where atmospheric CO_2 stabilizes at 720 ppm (IPCC, 2007). Projections were based on the empirical relationship between species with earlier phenology and SST and the relationships between species with delayed phenology, SST, and upwelling. Changes in mean phenology between 2000-2009 and 2090-2099 were forecasted using outputs from

12 IPCC models. Models unanimously projected that SST would continue to warm earlier in the year through the 21st century. Predicted changes in SST CT between the 2000s and 2090s ranged between -1.5 and -18.0 days (mean = -10.5 days). In contrast, model outputs indicated high uncertainty in future changes in upwelling seasonality in the southern CCE, with 15 model runs predicting earlier upwelling and 11 runs predicting later upwelling. Mean change in upwelling CT between 2000-2009 and 2090-2099 was -3.9 days, with a range of -18.9 to 11.8 days. Projections for species with earlier phenology indicated that fishes would advance their phenology by -9.0 days on average relative to current conditions (Fig. S1.6a; range: -0.8 to -15.8 days). Due to inconsistencies between models when forecasting changes in upwelling CT, projections suggested that species with later phenology may spawn anywhere between 29.2 days earlier to 28.1 days later compared to current conditions (Fig. S1.6b; mean = -1.8 days).

3. Discussion

3.1. Evaluation of Hypotheses.

The null hypothesis (H_0) stated that larval fish phenology would remain nearly constant through time if photoperiod were the primary factor affecting the timing of reproduction. Photoperiod may influence fish phenology either through physiological processes associated with gonadal development (de Vlaming, 1972) or mediated through food web effects, since the timing of diatom spore germination and growth and copepod diapause are regulated by photoperiod among some species (Greve, 2003; Ji *et al.*, 2010).

The current study provides equivocal support for this null hypothesis since 57% of fish phenophases showed decadal trends in phenology. Furthermore, even species in the phenology group with no long-term trend exhibited interannual variations in larval occurrence associated with El Niño (Fig. 1.4b), indicating that their phenology was not as steadfast as suggested by H_0. Also, some species in this phenology group, such as *S. sagax*, displayed large interdecadal fluctuations in phenology that were non-linear.

Before evaluating alternative hypotheses, it is important to examine whether phenological trends could be due to variations in the intensity of CalCOFI sampling. During periods of greater sampling effort, there is a higher likelihood of detecting precocious individuals who spawn early even if no change in the mean distribution of spawning occurred (Leopold and Jones, 1947; Miller-Rushing *et al.*, 2008). CalCOFI survey effort was greatest in the 1950s when 3,952 ichthyoplankton samples were collected in the southern CCE. Effort dropped during the 1960s and 1970s, such that 1,614 samples were collected during the latter decade. Following the resumption of annual sampling in 1984, between 2,228 and 2,651 samples per decade were collected. As a result, trends in phenology cannot be attributed to a linear increase or decrease in sampling effort. Similarly, the increasingly standardized timing of cruises, which led to gaps in monthly sampling during the 2000s, did not have a major effect on the first principal component of this dataset nor the three phenology groups (Fig. S1.2, SI text).

H_{A1} proposed that earlier occurrence of larvae would be observed during periods with warm temperatures. Support for H_{A1} was provided by the positive correlation between SST CT and species with earlier phenology (Fig. 1.5b). Similar relationships between temperature and fish phenology were identified among ichthyoplankton in the

North Sea and English Channel (Greve *et al.*, 2005; Genner *et al.*, 2010). However, these studies considered a much smaller area (1-3 sites) and their time series were not long enough to differentiate between the effects of global warming and climate oscillations. Other studies of fish phenology have linked the gonadal maturation of individual species to cumulative temperature often measured in degree days (Ware and Tanasichuk, 1989; Hutchings and Myers, 1994; Lange and Greve, 1997; Gillet and Quétin, 2006), providing a physiological mechanism that may explain the relationships observed here. Alternatively, the effect of SST CT on larval phenology could reflect temperature-induced changes in the duration of the egg and larval stages among poikilotherms. While a shortened duration of these life history stages under warmer temperatures could be partially responsible for phenological advances, it is unlikely that changes in stage duration alone could result in the observed rates of 3-12 days decade^{-1} of phenological change. This is because the egg stage of many fishes only lasts 2-4 days at temperatures in the southern CCE (Zwiefel and Lasker, 1976). Also, larger, late-stage larvae that would be more affected by changes in stage duration were rare in CalCOFI samples (Hewitt, 1980).

In addition to direct physiological effects, the influence of temperature on phenology may be mediated through other oceanic and biological processes. For example, temperature can affect swimming speed during seasonal migrations, which can in turn impact travel time required to reach spawning grounds (Jansen and Gislason, 2011). Similarly, temperature can alter the migratory routes used by fishes in estuarine and shelf habitats, leading to changes in spawning phenology (Hutchings and Myers, 1994; Genner *et al*., 2010). Among anadromous species and fishes that spawn in river

plumes, temperature effects on spawning time may reflect the fact that earlier river flow has been documented throughout the western USA due to earlier snow melt (Stewart *et al*., 2005; Kaltenberg *et al.*, 2010; Moody and Pitcher, 2010). Lastly, temperature could affect fish phenology by altering the seasonal availability of prey, which could influence spawning time (Carscadden *et al.*, 1997).

Two hypotheses were proposed to explain delays in fish phenology. H_{A2} suggested that fishes spawning in fall may exhibit delayed phenology if climate change leads to an extended period of warm summer temperatures, whereas H_{A3} asserted that delayed phenology would result from a later onset of upwelling. This study provided scant support for H_{A2}, because the season of maximal larval abundance did not have a significant effect on fish phenology. Only two of the nine phenophases with delayed phenology were fall-spawning fishes. While a long-term trend in upwelling seasonality was not observed (Fig. S1.5a), species with delayed phenology showed a positive correlation with upwelling CT (Fig. 1.5d), providing support for H_{A3}. Upwelling could affect fish phenology through two mechanisms, with one mechanism primarily operating among species who spawn during winter and the second affecting spring and summer spawners. Among the coastal, demersal fishes that were more likely to show delayed phenology (Fig. 1.6b-c), it is imperative to develop life history strategies that minimize advection of larvae into unsuitable, offshore habitats. Since upwelling results in cross-shore transport, many coastal fishes spawn during winter when upwelling is minimal to increase retention (Parrish *et al*., 1981). The phenology of these species may be positively correlated with the timing of upwelling to maintain their reproductive activity in synchrony with the winter lull in upwelling. For species whose larvae are most abundant

in spring and summer, upwelling likely affects phenology through its impact of primary and secondary production, which in turn increases prey availability. While this effect on fish phenology has not been previously documented, the breeding phenology of seabirds in the CCE is similarly influenced by winter preconditioning where small pulses of winter upwelling extend the season of high biological productivity (Abraham and Sydeman 2004; Schroeder *et al.*, 2009; Black *et al.*, 2011).

H_{A4} proposed that, in lieu of long-term trends, interannual-to-decadal variations in phenology associated with basin-scale climate cycles would be observed. While ENSO was related to significant fluctuations in fish phenology, the PDO and NPGO did not have clear-cut effects (Fig. 1.4). This finding may initially seem surprising since the PDO and NPGO affect the abundance and geographic distribution of several species considered here (Moser *et al*., 2001; Koslow *et al*., 2011; Hsieh *et al.*, 2008; Hsieh *et al.*, 2009; Koslow *et al.*, 2013). However, time series of CCE ocean temperature (a key factor controlling fish phenology) indicate that, although there have been PDO-like oscillations in the magnitude of this variable, there was also a concurrent, secular shift in the phase of its seasonal cycle relative to a 1950s baseline (Fig. 1.5a; Mendelssohn *et al.*, 2004). This long-term phase shift may explain why the seasonality of larval fishes is less sensitive to the PDO. This result may be part of a more generalized pattern, since the PDO has a weak effect on the phenology of spring chinook salmon (*O. tshawytscha*) (Keefer *et al.*, 2008; Anderson and Beer, 2009), a species whose abundance is strongly influenced by this climate cycle (Mantua *et al.*, 1997).

3.2. Rates of Current and Future Phenological Change

In the southern CCE, fishes that spawn earlier during warm conditions advanced their phenology at a mean rate of 6.4 days decade^{-1}, while species whose phenology was influenced by upwelling experienced mean delays of 5.1 days decade^{-1}. Since this region warmed by 1.3° C between 1949-2000 (Di Lorenzo *et al.*, 2005), this translated into a mean temperature sensitivity of 24.6 days per °C for the earlier phenophases (range: 10.8-47.7 days per °C) and 19.6 days per °C for later phenophases (range: 11.5-27.7 days per °C). When examining all phenology groups jointly using absolute values of phenological change, a mean of 4.3 ± 3.0 S.D. days decade^{-1} or 16.7 ± 11.4 S.D. days per °C was obtained. These rates were comparable to results from other studies of the phenology of marine and freshwater fishes and meroplankton (Edwards and Richardson, 2004; Gillet and Quétin, 2006; Genner *et al*., 2010; Frederiksen *et al*., 2011; Jansen and Gislason, 2011), but much faster than phenological rates from terrestrial ecosystems (Sparks *et al.*, 2000; Parmesan and Yohe, 2003; Menzel *et al.*, 2006; Parmesan, 2007; Miller-Rushing and Primack, 2008; Wolkovich *et al.*, 2012). Although a sensitivity analysis suggested that this study may have limited power to detect shifts smaller than ~3 days decade^{-1} (Table S1.2, SI text), it is unlikely that the phenological rates calculated here were biased fast since center of gravity metrics, such as CT, are usually conservative and estimate slower rates than examining the start date of phenological events (Miller-Rushing *et al.*, 2008; Ji *et al.*, 2010). Instead, the rapid changes observed in this and other marine systems were more likely due to the smaller amplitude of the seasonal temperature changes in marine habitats. This weak seasonal gradient implies that marine species need to undergo large phenological shifts to ensure that temperature-sensitive

activities continue to occur at a constant temperature (Burrows *et al.*, 2011). Furthermore, the high fecundity and dispersal capacity of fishes may allow them to adapt more rapidly than terrestrial organisms to changing conditions (Richardson and Poloczanska, 2008).

Another way in which these results differed from most terrestrial studies was that a lower percentage of phenophases responded to warming by occurring earlier. In the southern CCE, 39% of phenophases advanced their phenology. In contrast, >60% of species have responded to warming temperatures by advancing their phenology in most terrestrial systems (Parmesan and Yohe, 2003; Menzel *et al.*, 2006; Miller-Rushing and Primack, 2008; Wolkovich *et al.*, 2012), as well as in some marine and aquatic systems (Greve *et al.*, 2005; Thackeray *et al.*, 2010). Studies of the changing geographic distribution of fishes in the southern CCE also showed that slightly less than half of the species were responsive to climate forcing (Hsieh *et al.*, 2008; Hsieh *et al.*, 2009). This suggests that the large percentage of non-responsive species may be characteristic of the southern CCE and possibly other Eastern Boundary Currents (EBCs). This may be due to weak seasonality in EBCs, their high proportion of mesopelagic fishes that may be less exposed to variations in upper ocean climate (Koslow *et al.*, 2011; Koslow *et al*., 2013), or opposing trends in SST and upwelling seasonality.

Future projections indicated that fishes in the earlier phenology group would advance their phenology at a mean rate of -1.0 days decade^{-1} (range: 0.1-1.8 days decade^{-1}), which is slower than their current rate of change. For the later phenology group, predictions were highly variable between model runs (Fig. S1.6). Both the varying projections for delayed species and the slower rate of predicted change for the advancing species may be related to the relatively low spatial resolution (≥1°) of most IPCC general

circulation models (GCMs). This resolution limits the ability of models to represent fine-scale oceanographic dynamics associated with coastal upwelling (Wang *et al.*, 2010; Stock *et al.*, 2011). As a result, most GCMs overestimate temperatures in EBCs (Stock *et al.*, 2011). Overestimation of current temperatures could potentially lead to an underestimation of future changes in temperature and phenology in these regions. Also, the limited resolution of GCMs is likely related to the high variability between modeled upwelling rates observed here and in Wang *et al.* (2010). This suggests that future predictions of fish phenology may be improved by either using regional climate models or the next generation of IPCC models, some of which will have resolutions as low 0.1° x 0.1°. Nevertheless, the accuracy of such projections may still be limited if there are non-linear thresholds beyond which fishes are no longer able to adapt to changing conditions by altering their phenology (Sparks *et al.*, 2000; Stenseth and Mysterud, 2002).

3.3. Implications for Fisheries Management and Marine Ecology

Species with earlier phenology were influenced by variations in the seasonality of SST, but not upwelling or zooplankton volume. The diverging phenological trajectories of zooplankton and this phenology group suggests that climate change may lead to an increasing frequency of mismatches between trophic levels. Increased mismatches are less likely to occur among the other phenology groups, given the lack of a long-term trend in zooplankton phenology and the fact that the delayed phenology group tracked upwelling CT, another proxy for lower trophic level productivity. During the early life history of fishes, mismatches can result in decreased foraging efficiency, slower growth,

starvation, increased vulnerability to predators, and lower survival (Platt *et al.*, 2003; Abraham and Sydeman, 2004; Durant *et al*., 2007; Sullivan *et al.*, 2007; Chittenden *et al*., 2010). These impacts may eventually lead to poor recruitment, declines in abundance, and even local extinctions (Beaugrand *et al*., 2003; Philippart *et al*., 2003; Sullivan *et al.*, 2007; Burkle *et al.*, 2013). At times, mismatches between fishes and zooplankton can be transmitted up the food web to higher trophic levels (Frederiksen *et al.*, 2011). Nevertheless, zooplankton volume is a bulk measure of a myriad of species, including both predators and prey of larval fishes. Phenological monitoring of individual zooplankton species is needed to confirm whether mismatches between larval fishes and their prey are truly becoming more frequent.

Species that did not exhibit long-term trends in phenology may also be vulnerable to global warming due to their reduced capacity to adapt to changing conditions. One indication of this is that the duration of the peak period of larval abundance appears to have contracted among these species (Fig. 1.3). A shorter spawning season increases the likelihood that in some years there will be little-to-no temporal overlap between larvae and environmental conditions conducive to growth and survival. As a result, contracted spawning periods are often accompanied by greater recruitment variability (Mertz and Myers, 1994). Climate-induced range contraction of species has been linked to reduced genetic diversity (Rubidge *et al*., 2012). It is possible that phenological contractions could have similar effects on genetic diversity. In addition, a lack of adaptive phenological change in some species has been associated with declining abundance (Willis *et al.*, 2008; Cleland *et al.*, 2012).

These factors suggest that phenological plasticity may be a useful metric for predicting which species may benefit from or be impaired by climate change (Cleland *et al.*, 2012). Further evidence of this comes from the fact that fishes with earlier spawning were more likely to shift their range in response to climatic variations (Hsieh *et al.*, 2008; Hsieh *et al.*, 2009), suggesting a link between these two modes of adapting to climate change. Commonalities between species in each phenology group may prove useful for discerning how species yet to be studied will react to climate change. Characteristics that affected phenology were habitats used by larvae and adults, taxonomy, and relative abundance (Fig. 1.6). Habitat not only influenced phenology, but is also a major factor affecting synchronous variations in fish abundance in the CCE (Koslow *et al.*, 2013). Epipelagic species using coastal-oceanic habitats were the group most likely to exhibit earlier spawning. Their phenological plasticity may reflect the fact that many of these species are batch spawners that can reproduce as frequently as once a week (Hunter and Goldbert, 1980). These species also live in the upper water column where they are exposed to larger changes in climate. Lastly, epipelagic species typically have short life spans allowing for possible genetic adaptation to changing conditions. Other studies of climate change effects on fishes have indicated that pelagic species possess heightened climate sensitivity (Murawski, 1993; Cheung *et al.*, 2009).

While taxonomic order was indicated as a species characteristic that influenced phenology, the importance of this characteristic is uncertain given that habitat use co-varies across taxonomic groups. In addition, different species in the same genera (*e.g., Sebastes*), as well as different phenophases of the same species, were often classified as belonging to separate phenology groups (Table S1.1). Terrestrial studies have produced

divergent results regarding whether phylogenetic relatedness affects phenological plasticity (Willis *et al.*, 2008; Cleland *et al.*, 2012).

Frequency of occurrence in CalCOFI samples was the third species trait related to phenological change (Fig. 1.6d). While this could potentially reflect difficulties in detecting trends among rarer species, this seems unlikely given that even the least frequently occurring species in this analysis was sampled 185 times. A more likely explanation is that abundant species in this region are adapted to large natural, interannual-to-decadal variations in climate in the CCE, such that they have developed behavioral strategies that allow them to shift phenology in response to changing temperatures. This responsiveness to natural variability may ensure that these species will exhibit greater flexibility in adapting to secular trends in climate.

Current and future changes in fish phenology will require that fishery managers implement precautionary and adaptive management approaches. Management activities that may be affected by changing phenology include: 1) seasonal fishing closures designed to protect sensitive life stages or maintain sustainable escapement, 2) stock assessment surveys timed to coincide with seasonal migrations or the occurrence of a key life history stage (*e.g.*, daily egg production method surveys), and; 3) optimizing the release time of hatchery reared fish for stock enhancement (Chittenden *et al.*, 2010; Kaltenberg *et al.*, 2010). Monitoring long-term changes in phenology and periodically adjusting the timing of seasonal closures, surveys, and hatchery releases will be important for ensuring that management tactics remain effective. In cases where fish phenology is linked to cumulative, seasonal changes in temperature or other variables, it may be possible to develop short-term, operational forecasts to predict when a fishery should

open or when a stock assessment survey should occur (Anderson and Beer, 2009; Greve *et al.*, 2004). In cases where climate change leads to increased phenological mismatches and resulting recruitment failure, the carrying capacity of an ecosystem may be reduced, necessitating changes to harvest guidelines. Longer rebuilding times of depleted stocks may also be needed if mismatches lead to prolonged periods of poor recruitment (Holt and Punt, 2009).

In conclusion, long-term, secular changes in the spawning phenology of fishes were apparent in the CCE even though this region is strongly influenced by decadal climate oscillations. Among species whose phenology has become earlier since the 1950s, the mean rate of change was 6.4 days decade^{-1}. This rate was much faster than rates from many terrestrial ecosystems, but was comparable to phenological studies of other marine organisms, indicating that climate change may lead to a rapid reorganization of seasonal patterns in marine communities. In contrast to other ecosystems, both sustained advances and delays in phenology were observed in the CCE, reflecting the opposing influences of temperature and upwelling on phenology. Similar changes are likely to occur in other EBCs if global warming alters the seasonal intensity of upwelling. Among species with no long-term shifts in phenology, a shortened seasonal peak in larval abundance could lead to heightened recruitment variability. Since zooplankton phenology did not change in synchrony with fishes that are spawning earlier, these species may be subject to increased mismatches with their prey.

4. Materials and Methods

Ichthyoplankton samples were collected by CalCOFI along six transects (*i.e.*, lines 76.7-93.3), which extended offshore of California between San Diego (33.0° N) and north of Point Conception (35.1° N). During each cruise, 66 stations were typically surveyed with oblique tows of bongo or ring nets (Fig. S1.1). Kramer *et al*. (1972) describes methods used to catch, preserve, and identify ichthyoplankton. Throughout this time series, two modifications were made to sampling methods. First, tow depth was increased from 140 m to 210 m in 1969. This was accompanied by a change from using a net with 550-µm silk mesh to a nylon net with a 505-µm mesh. Second, the 1.0-m ring net initially used to sample ichthyoplankton was replaced with a 0.71-m bongo net in 1977 (Ohman and Smith, 1995). While slightly more larvae >6.75 mm TL were caught with the bongo net, large larvae made up such a small fraction of total abundance that there was not a significant difference between the number of larvae captured by the two nets (Hewitt, 1980). The change in tow depth also had a minimal effect on abundance because most larvae resided at depths <125 m (Ahlstrom, 1959; Koslow *et al.*, 2013). Data were averaged decadally to develop a monthly time series.

Only taxa identified to species level were included in this analysis to avoid confounding changes in species composition with shifts in phenology (Edwards and Richardson, 2004). Cumulative rank occurrence of ichthyoplankton taxa sampled between 1951-1998 was used to select species for inclusion in this study. The 90th percentile of the cumulative rank occurrence curve included 43 species, which were examined here. Due to improvements over time in identifying larval fishes, some taxa were not consistently identified during the first two decades of CalCOFI. As a result, insufficient data were available to analyze three species during the 1950s (*Argyropelecus*

sladeni, *Lestidiops ringens*, and *Oxyjulis californica*) and an additional three species during both the 1950s and 1960s (*Cyclothone signata*, *Danaphos oculatus*, and *Melamphaes lugubris*). Three criteria were used to determine whether a species with several seasonal peaks in abundance should be classified as having multiple phenophases. First, peaks in abundance must be separated by ≥3 months. Second, the amplitude of each peak must be >50% of the annual range in larval abundance. Third, the dip in abundance between peaks must encompass >35% of the annual range. Mean seasonal abundance from the full time series was used to evaluate these criteria.

CT was used as the main measure of phenology in this study because it accounted for data collected during all seasons, can be calculated from a time series with a monthly resolution, and is a conservative metric that is unlikely to overestimate the rate of phenological change (Ji *et al.*, 2010). The CT of each phenophase was calculated with the formula (Edwards and Richardson, 2004):

$$CT = \sum_{i=1}^{12} (m_i * a_i) / \sum_{i=1}^{12} a_i,$$

where a_i was mean abundance of larvae in month m_i, such that i = 1, 2, …12 denoted January, February, ... December. For species with two phenophases, each year was divided into two six-month periods (typically January-June and July-December) for which the CT was computed. For species whose abundance increased between December and January, the CT was calculated so that i = 1 referred to the month when the seasonal rise in abundance started. Phenological anomalies were calculated relative to the mean of the CTs from the six decades examined. This ensured that each decade was weighted equally regardless of whether fish abundance was high or low. An anomaly of 1 indicated

a 1-month change in phenology. To convert monthly anomalies into daily values, they were multiplied by 30.44. The duration of peak larval abundance was used as a second metric to examine changes in fish phenology. This was defined as the number of months when mean abundance of larvae was ≥70% of its annual maximum.

All statistical analyses were conducted in MATLAB (MathWorks, Inc., Natick, MA, USA). Two approaches were applied to examine assemblage-wide trends in phenology. First, a linear regression was performed in which decadal CT anomalies of all phenophases were regressed against year. The slope of this regression was used to estimate the mean rate of change in days decade^{-1}. For all statistical tests, $p < 0.05$ was considered significant, while $p < 0.10$ was classified as marginally significant. Principal components analysis (PCA) was employed as a second method for assessing assemblage-wide changes. The CT of each phenophase was normalized by its mean and standard deviation to give equal weight to all phenophases in the PCA (Clarke and Warwick, 2001). Species with missing data from the 1950s and 1960s were excluded from this analysis, so that the correlation matrix for the PCA would be complete.

Phenophases were classified into three groups based on correlations between CT and year. Phenophases with $r \leq -0.5$ were categorized as exhibiting earlier phenology; correlations between -0.5 and 0.5 indicated no long-term, linear changes, and; phenophases with $r \geq 0.5$ were classified as displaying later phenology. Note that $|r| \geq 0.5$ does not correspond to a specific threshold of statistical significance, but is instead intended to provide a liberal indication of the direction of phenological change. As was done for the assemblage-wide mean, the slope of regressions between CT anomalies and year were used to estimate rates of change for phenophases in each group. Regression

was also used to investigate changes in the duration of peak larval abundance. Based on the regressions, the mean and standard error of changes in CT and season duration were calculated for phenology groups. Monte Carlo simulation was used to determine confidence intervals for long-term changes in CT and the duration of peak larval abundance (SI text, Fig. S1.3, Tables S1.2-S1.3). The SI text and Fig. S1.2 also include an evaluation of potential bias due to missing data from May, September, and December during the 2000s.

This study examined how three basin-scale climate oscillations, three local oceanic variables, and 11 ecological characteristics affected the phenology of larval fishes. Details of each analysis are described in the SI text. Climate indices (*e.g.*, ENSO, PDO, NPGO) were partitioned into a set of three categorical variables for use in ANOVA. Lilliefors' test, Bartlett's test, and plots of residuals were used to ascertain whether the ANOVA assumptions of normality, homoscedasticity, and independence of residuals were met (Sokal and Rohlf, 1995). If an ANOVA indicated a significant climate effect, Tukey-Kramer multiple comparison tests were employed *post-hoc* to determine which climate phases exhibited significant phenological differences. The CT of local oceanic variables (*e.g.*, SST, zooplankton volume, coastal upwelling) was calculated on a decadal basis for the years 1951-2008 to identify long-term trends and fluctuations in the seasonality of these variables. Linear regressions were performed to investigate the relationship between the CT of oceanic variables and the CT of fishes in each phenology group. The effects of ecological characteristics on fish phenology were either evaluated with linear regression or ANOVA depending on whether each independent variable was categorical or continuous.

Projections of 21st century changes in phenology were based on a multi-model dataset developed during phase 3 of the World Climate Research Programme's (WCRP's) Coupled Model Intercomparison Project (CMIP3) (http://www-pcmdi.llnl.gov/ipcc/about_ipcc.php). Of the 25 models included in CMIP3, 12 were selected for examination due to their ability to replicate the spatial signature of the PDO with a correlation of $r \geq 0.7$ (Wang *et al*., 2010). Data on SST and coastal upwelling derived from meridional wind speed were extracted from CMIP3 to serve as predictors of changes in fish phenology. Monthly SST and meridional wind speed from the A1B scenario were examined during 2000-2009 and 2090-2099 and averaged over 30-35° N and 117-125° W. Projections of seasonal upwelling were unaffected by whether winds were extracted from this area or solely the area west of Point Conception, where upwelling is maximal off southern California (Mantyla *et al.*, 2008). To calculate the volume of offshore Ekman transport (Q_x), wind stress (τ) was first computed with the formula: $\tau_y = \rho_{air}\, C_d\, v^2$, where v is meridional wind speed at an atmospheric pressure of 100 kPa, ρ_{air} is the density of air, and C_d is a drag coefficient (1.2×10^{-3}) (Trenberth *et al.*, 1989; Stewart, 2004). Q_x was calculated from the equation: $Q_x = \tau_y * (\rho f)^{-1}$, where ρ is the density of seawater and f is the Coriolis parameter (Pond and Pickard, 1995). A mean surface water density of 1,024.5 kg m^{-3} and an f of $7.83 * 10^{-5}$ s^{-1} (based on a mean latitude of 32.5° N) were assumed for the CalCOFI region. Q_x was multiplied by 100 since the Bakun upwelling index examined Ekman transport over 100 m of coastline (Bakun, 1973). The CT of SST and upwelling were calculated from decadally averaged CMIP3 data for the 2000s and 2090s. The linear regression between SST CT and species with earlier phenology (Fig. 1.5b) was used to predict the extent of phenological changes

between these decades. For species with delayed phenology, a multiple regression using the CT of SST and the Bakun upwelling index as independent variables was developed from CalCOFI data. The resulting regression equation was $Y = -0.0092 - 0.5503X_1 + 1.7836X_2$, where Y was the CT anomalies of species with delayed phenology, X_1 was SST CT, and X_2 was the upwelling CT ($F = 13.2$, d.f. = 49, $p < 0.001$). This formula was then applied to forecast changes in the CT of delayed species between the 2000s and 2090s with CMIP3 data.

5. Acknowledgments

This research was funded by California Sea Grant Project R/FISH-210. Additional support was received from the NOAA Nancy Foster Scholar Program, NSF IGERT Grant No. 0333444, and the San Diego ARCS Foundation. This research was also associated with the California Current Ecosystem Long Term Ecological Research (LTER) site, which is supported by NSF. I am especially indebted to the many scientists who collected and processed data from CalCOFI cruises. K. Baker, N. Bowlin, and S. Jacobson provided helpful, initial guidance on use of CalCOFI ichthyoplankton data. I acknowledge the Program for Climate Model Diagnosis and Intercomparison (PCMDI), the WCRP's Working Group on Coupled Modeling (WGCM), and the individual modeling groups who contributed to the development of the CMIP3 multi-model dataset. Support for developing the CMIP3 dataset was provided by the Office of Science in the U.S. Department of Energy. D. Checkley, D. Cayan, P. Hastings, T. Koslow, S.

McClatchie, S.H. Nam, M. Ohman, and J. Shurin provided useful suggestions at various stages of this research, which contributed to improving this manuscript.

This chapter, in full, is currently being prepared for submission for publication of the material. The dissertation author was the primary investigator and author of this material.

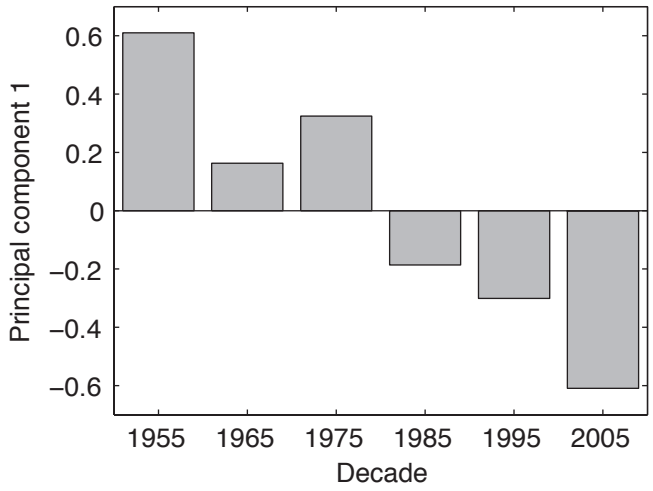

Figure 1.1. First principal component of the central tendency of larval fishes. Positive values of eigenvectors on the y-axis indicate later occurrence of larvae, where negative values indicate earlier occurrence.

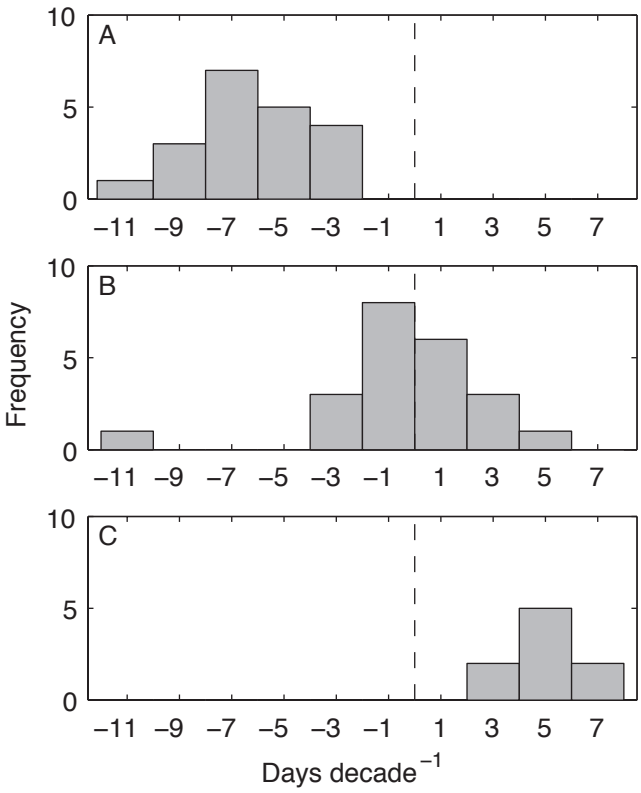

Figure 1.2. Histograms showing the rate of phenological change in days decade^{-1} among species with phenophases displaying (A) earlier phenology (n = 20); (B) no long-term, linear change in phenology (n = 22), and; (C) later phenology (n = 9).

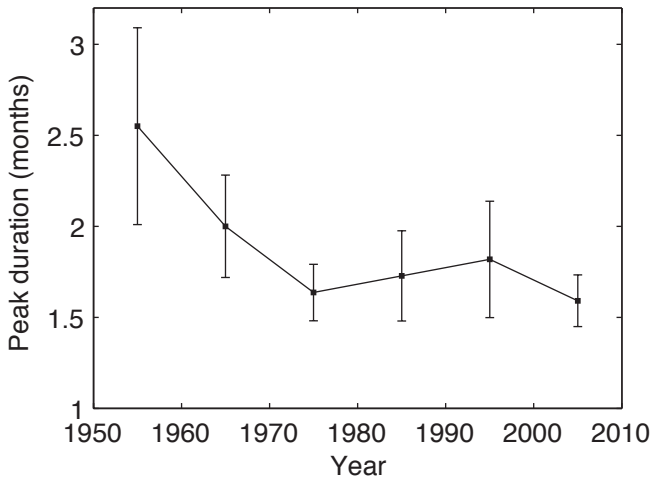

Figure 1.3. Decadal changes in the duration of peak larval abundance for species that did not exhibit long-term, linear changes in phenology based on central tendency. The duration of peak larval abundance was estimated as the number of months when larval abundance ≥70% of its annual maximum. Standard errors are shown. n = 128.

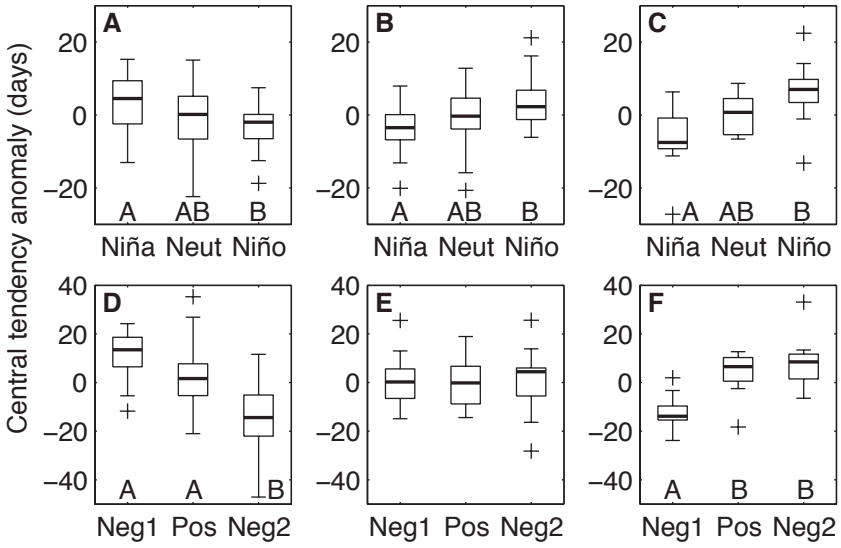

Figure 1.4. Effects of El Niño-Southern Oscillation (A-C) and Pacific Decadal Oscillation (PDO; D-F) on species displaying earlier phenology (left column; $n = 60$), no long-term, linear change in phenology (middle column; $n = 66$), and later phenology (right column; $n = 27$). In each box plot, the darkened line indicates the median; boxes show the inter-quartile range; whiskers indicate the expected extent of 99% of the data for a Gaussian distribution, and; crosses show outliers. Two outliers fall outside the range displayed in A. Capital letters below boxes indicate means that differ significantly at $p < 0.05$ based on Tukey-Kramer multiple comparison tests. (A-C) Duration of El Niño, neutral (Neut), and La Niña conditions is based on the Oceanic Niño Index. (D-F) Neg1 – Cold-phase PDO between 1951-1976; Pos – Warm-phase PDO from 1977-1998; Neg2 – Cold-phase PDO during 1999-2002 and 2007-2008.

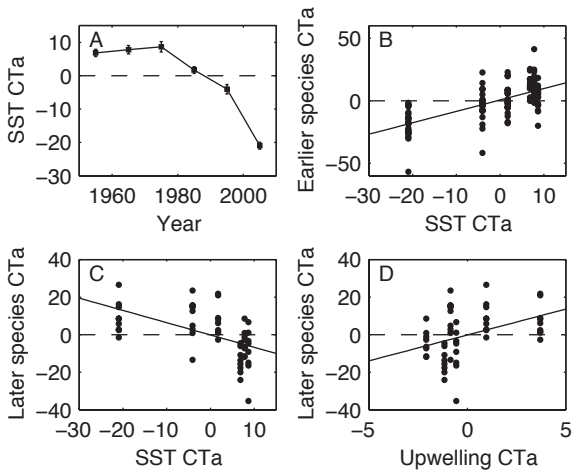

Figure 1.5. Responses of the phenology of larval fishes to changes in the central tendency (CT) of sea surface temperature (SST) and the Bakun upwelling index at 33° N and 119° W. Units of all CT anomalies (CTa) are days. (A) Decadal changes in SST CT. Standard errors from bootstrap analysis are shown. (B) Relationship between SST CT and species with earlier phenology. Regression line: $Y = 0.0201 + 0.9122X$, $F = 75.3$, $p < 0.001$, $n = 120$. (C) Relationship between SST CT and species with later phenology. Regression line: $Y = -0.0064 – 0.6544X$, $F = 20.1$, $p < 0.001$, $n = 57$. (D) Relationship between upwelling CT and species with later phenology. Regression line: $Y = -0.0061 + 2.7568X$, $F = 10.1$, $p < 0.01$, $n = 57$.

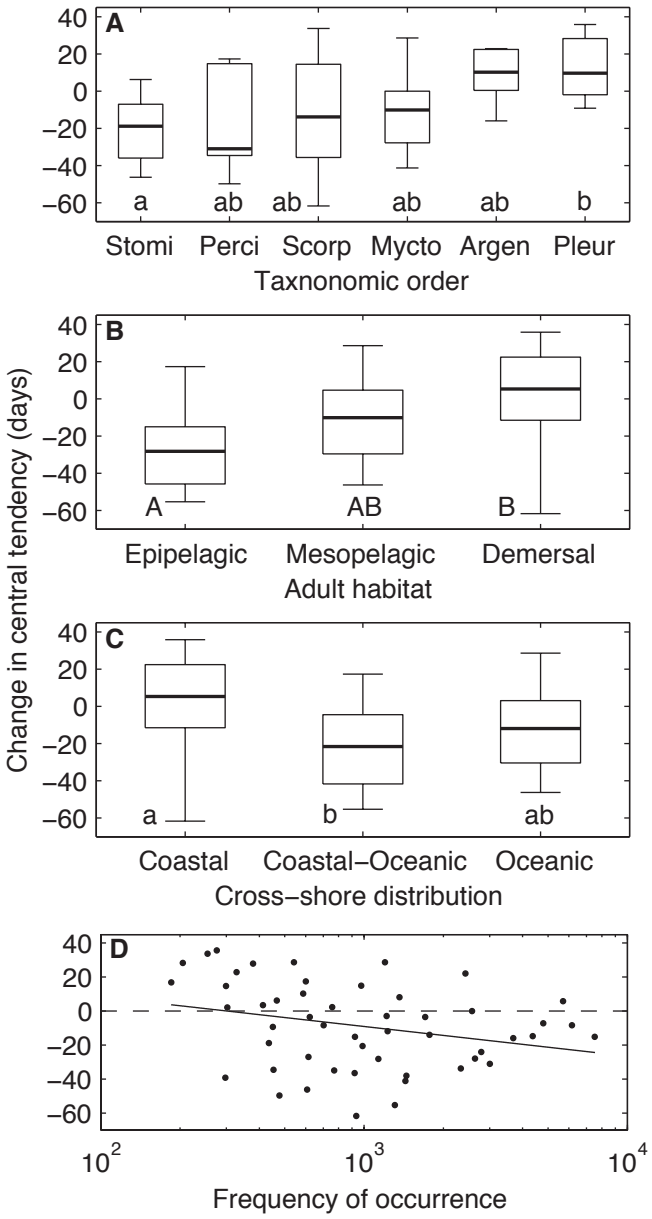

Figure 1.6. Species characteristics that exhibited a significant influence on changes in larval fish phenology: (A) taxonomic order (n = 45); (B) adult habitat (n = 51); (C) cross-shore distribution (n = 51), and; (D) frequency of larval occurrence in samples from California Cooperative Oceanic Fisheries Investigations (n = 51). Box plots are the same as in Figure 1.4. Lower case letters below boxes indicate means that differ at $p < 0.1$ based on Tukey-Kramer multiple comparison tests. (A) Orders: Stomi – Stomiiformes; Perci – Perciformes; Scorp – Scorpaeniformes; Mycto – Myctophiformes; Argen – Argentiniformes; Pleur – Pleuronectiformes. (D) Regression line: $Y = 43.2874 – 17.4528*\log_{10}(X)$, $F = 4.4$, $p < 0.05$.

CHAPTER 1 APPENDIX:

SUPPLEMENTAL INFORMATION FOR THE MANUSCRIPT *CLIMATE CHANGE AND DECADAL SHIFTS IN THE PHENOLOGY OF LARVAL FISHES IN THE CALIFORNIA CURRENT ECOSYSTEM*

S1. Precision of Estimates of Phenological Change and Evaluation of Bias due to Gaps in Sampling

A sensitivity analysis based on Monte Carlo simulation was conducted to quantify observation error related to noise from variations in larval abundance and the sparse, seasonal sampling resolution of California Cooperative Oceanic Fisheries Investigations (CalCOFI). First, the seasonal distribution of a simulated larval species was modeled with a Gaussian curve where June 15 was initially the mean date of larval occurrence and there was a 1-month standard deviation. This implied that 95% of larvae would be observed within ± 2 months of the mean. The Gaussian curve was multiplied by 10 to more realistically approximate larval abundance in the CalCOFI region. Variations in larval abundance that could affect the calculation of seasonal central tendency (CT) were stochastically generated from a coefficient of variation (C.V.) ranging between 0.05–0.60. Twelve C.V.'s separated by 0.05 intervals were used. This range was selected based on the empirical C.V. of monthly larval abundance for representative species sampled by CalCOFI (*e.g.*, *Argentina sialis*, *Engraulis mordax*, *Lipolagus ochotensis*, *Scomber japonicus*, *Tetragonurus cuvieri*). Next, shifts in phenology at rates of 0-12 days decade^{-1} were simulated over six decadal time steps. For each time step, the CT was calculated from monthly mean values extracted from the underlying continuous, Gaussian distribution. This process was repeated 1,000 times for each C.V. and rate of phenological change. The 90% and 95% confidence intervals of CT were calculated based on these simulated values to assess the precision of this estimate of phenological change.

The median CT from the Monte Carlo simulations accurately estimated the underlying changes in the Gaussian curve across all C.V.'s tested (Fig. S1.3a). For the largest C.V. considered, the 90% and 95% confidence intervals of CT always fell within ±2.8-3.1 and ±3.3-3.6 days decade^{-1}, respectively, of the simulated change in phenology (Table S1.2). The 90% confidence intervals corresponded closely to the minimum rate of change observed among species categorized as displaying earlier or later phenology (Fig. 1.2). This confirmed that, despite the coarse, seasonal sampling resolution of CalCOFI, this study was able to obtain reliable estimates of which species exhibited shifts in phenology.

A second Monte Carlo simulation was performed to assess how precisely changes in phenophase duration could be estimated. Here the mean of the underlying Gaussian curve was kept constant, but the standard deviation was varied between 1.5 and 1 months, corresponding to an approximately 2-month contraction in the period when 95% of larvae would be observed. For each decadal time step of the simulation, the number of months when larval abundance was ≥70% of its maximum was calculated to determine how well this metric was able to approximate changes in the underlying standard deviation. Decadal trends in the 70% metric were then estimated with linear regression across the six time steps for a simulated assemblage of 20 species. All other steps in this simulation were the same as those described above for the Monte Carlo simulation performed on CT.

The 70% metric used to approximate the duration of peak larval abundance consistently underestimated simulated changes in phenophase duration (Fig. S1.3b, Table S1.3). This was particularly true when larger C.V.'s were considered. The 70% metric

was also unable to detect significant changes in phenophase duration if the C.V. of simulated larval fish abundance was larger than 0.3 (Table S1.3). Conversely, the 90% and 95% confidence intervals for season duration were only significantly different from zero and contained the simulated rate of change when the C.V. was small (i.e., C.V. = 0.05) and the underlying change was large (i.e., ≥8 days decade^{-1}). This limited capacity to detect simulated changes may reflect a need for higher resolution, temporal sampling. Consequently, the observed change in season duration for the phenology group with no long-term trends (Fig. 1.3) should be viewed with caution. The underestimation of changes detected with the 70% metric may imply that this phenology group has actually undergone a much larger contraction in season duration. It is possible that other phenology groups may have experienced undetected shifts in phenophase duration since the 70% metric has a low capacity to detect significant changes.

A second potential source of error stemmed from the fact that no CalCOFI surveys were conducted in May, September, or December during the 2000s. This could skew estimates of CT from this decade and bias inter-decadal trends. To evaluate this bias, I recalculated CT after removing these months from the entire time series so that all decades would have an identical monthly distribution of data. The first principal component of this new dataset accounted for 29.9% of variance and continued to show a progression towards earlier phenology (Fig. S1.2b). However, phenological advancement was no longer evident when examining the mean CT for all 43 species (Fig. S1.2d). For the three phenology groups, decadal trends in CT were extremely similar regardless of whether the missing months were included or excluded from the analysis, indicating resiliency to this potential source of bias (Fig. S1.2e-j). In addition to being able to detect

divergent trends obscured by the mean, this is another reason why this analysis principally focused on the three phenology groups when investigating long-term, ecological changes.

Measurements of CalCOFI sea surface temperature (SST) and mesozooplankton displacement volume were also unavailable during May, September, and December in the 2000s. Again, these months were removed from the time series in its entirety and CT was recalculated to detect potential biases resulting from gaps in sampling. Figure 1.5 only presents results where there was consistency between the full and partial time series in terms of the significance of environmental effects on fish phenology.

S2. Relationships between Phenology, Climate, Oceanic Conditions, and Ecological Traits

The effects of three basin-scale climate oscillations (*e.g.*, ENSO, PDO, NPGO) and three local environmental variables (*e.g.*, SST, zooplankton volume, coastal upwelling) on fish phenology were examined. ENSO events were characterized with the Oceanic Niño Index (ONI) produced by the National Centers for Environmental Prediction (http://www.cpc.ncep.noaa.gov/products/analysis_monitoring/ensostuff/ensoyears.shtml). This index was selected because it defines the onset and termination of El Niño and La Niña on a monthly basis. The PDO index was obtained from the Joint Institute for the Study of the Atmosphere and Ocean (Mantua *et al*., 1997; http://jisao.washington.edu/pdo/PDO.latest). The NPGO index was developed and made available by Emanuele Di Lorenzo at the Georgia Institute of Technology (Di Lorenzo *et*

al., 2008; http://www.o3d.org/npgo/npgo.php). SST and mesozooplankton displacement volume were measured at CalCOFI stations where ichthyoplankton samples were collected. Gelatinous organisms with biovolumes >5 cm^3 were excluded from measurements of zooplankton volume (Kramer *et al*., 1972). Zooplankton volume from 1969-1977 was multiplied by a correction factor of 1.366 to account for changes in net type and tow depth (Ohman and Smith, 1995). The monthly Bakun upwelling index from 33° N and 119° W was obtained from the Environmental Research Division at the Southwest Fisheries Science Center (Bakun, 1973; http://www.pfeg.noaa.gov/products/pfel/modeled/indices/upwelling/upwelling.html). This index estimates offshore Ekman volume transport based on atmospheric pressure fields. At 33° N and 119° W, the Bakun upwelling index overestimates offshore transport due to a discontinuity in the atmospheric pressure gradient related to the presence of coastal mountains (Bakun, 1973). Nevertheless, this index is still correlated with upwelling measured with the QuikSCAT scatterometer (r = 0.6; Pérez-Brunius *et al.*, 2007). Also, the CT of QuikSCAT upwelling over the CalCOFI region during the 2000s fell within the 95% confidence interval of the Bakun upwelling index CT from this decade (Fig. S1.5).

Each climate index was partitioned into three categorical variables for use in ANOVA. The ONI was divided into La Niña, El Niño, and neutral periods. PDO categories included: 1) a negative PDO between 1951-1976; 2) a positive PDO between 1977-1998, and; 3) a second, negative PDO in 1999-2002 and 2007-2008 (Peterson, 2009). The years 2003-2006 were excluded since there were insufficient data to construct a monthly time series of larvae during this second, positive PDO. Positive, neutral, and negative NPGO periods were defined on a monthly basis according to whether this index

had a value ≥ 0.5, between 0.5 and -0.5, or ≤ -0.5, respectively. These thresholds were selected so that there were an approximately equal number of months in each NPGO category. For each climate index, CT anomalies were calculated for fish phenophases. Initially, crossed, two-way ANOVAs were performed using climate index and phenology group as independent variables. Since significant interactions were observed between most phenology groups and climate indices, separate one-way ANOVAs were performed to evaluate climate effects on each phenology group. Lilliefors' test, Bartlett's test, and plots of residuals were used to ascertain whether the assumptions of normality, homoscedasticity, and independence of residuals were met (Sokal and Rohlf, 1995). Lilliefors' test indicated that the assumption of normality was violated for the ANOVA examining ENSO effects on the earlier phenology group. As a result, a non-parametric Kruskall-Wallis test was performed in lieu of ANOVA. If an ANOVA or Kruskall-Wallis test revealed a significant climate effect, Tukey-Kramer multiple comparison tests were employed *post-hoc* to determine which climate phases exhibited significant phenological differences. The effects of the PDO and NPGO on individual species were also examined over time lags of 0 and 1 year. However, this analysis is not presented since results were not significant for any species after applying corrections for multiple hypothesis testing (Benjamini and Hochberg, 1995).

SST, zooplankton volume, and the Bakun upwelling index were selected as the local, environmental variables to be examined due to known interannual-to-decadal variations in their seasonality (McGowan *et al.*, 2003; Mendelssohn *et al.*, 2004; Venegas *et al.*, 2008; Bograd *et al.*, 2013; Liu and Peterson, 2010) and their potential to affect fish phenology through physiological and trophic pathways. The CT of these variables was

calculated decadally for years between 1951-2008. Unlike upwelling and larval fish abundance, measurements of SST and zooplankton volume never approached zero during any month of the year. This weakened the weighting of these variables by month when calculating the CT, resulting in a CT skewed towards the middle of the year. To increase the influence of monthly weights, the minimum monthly mean value (*e.g.*, 13° C for SST and 38 cm^3 per 1,000 m^3 of seawater strained for zooplankton volume) was subtracted from the decadally averaged time series prior to calculating the CT. After computing the CT of each variable, its standard error was estimated with a bootstrap approach (Efron and Tibshirani, 1993). Linear regressions were performed to investigate changes in the CT of environmental variables over time. A second set of regressions examined the relationship between the CT of environmental variables and the CT of fishes in each phenology group.

Seven characteristics of species related to their phylogeny, ecology, and fishery status were evaluated with ANOVA to assess whether they affected rates of phenological change. These characteristics included taxonomic order, season of maximal larval abundance, trophic level, habitat use by adult fishes, cross-shore distribution, biogeographic affinity, and fishing status. Table S1.1 describes classification of fishes with respect to these characteristics. Trophic level was divided into three categories (*e.g.*, ≤3.1, 3.1-3.5, and >3.5) for use in ANOVA. Initially, the mesopelagic category of habitats used by adult fishes was farther subdivided into vertically migrating and non-migratory mesopelagic species. These classifications were later merged since no significant difference was observed between migratory and non-migratory mesopelagic fishes in terms of phenological changes. The ANOVA examining taxonomic order only

evaluated orders for which there were data available on at least five phenophases. In the ANOVA on the season of maximal abundance, winter included December-February, spring encompassed March-May, summer covered June-August, and fall comprised September-November. Again, Lilliefors' test of normality, Bartlett's test of homogeneity of variances, and plots of residuals were used to verify that ANOVA assumptions were met. Since only two categorical variables were used to assess fishing status and these categories had unequal variances, a Behrens-Fisher test was used in lieu of ANOVA (Sokal and Rohlf, 1995). Tukey-Kramer multiple comparison tests were conducted *post-hoc* to evaluate which categories in ANOVAs were significantly different.

Four additional species characteristics that could not be easily reduced to categorical variables for inclusion in ANOVA were also examined. Research on terrestrial ecosystems has suggested that species that shift their phenology to track changing conditions often have higher reproductive output and faster growth, leading to increased abundance (Willis *et al.*, 2008; Cleland *et al.*, 2012). To evaluate whether phenological shifts were more common among abundant species, the $\log_{10}$ transformed frequency of larval occurrence during CalCOFI surveys was regressed against changes in CT. Since fishing also affects abundance, a second test only examined unfished species. This test assessed whether long-term trends in fish phenology were linked to changes in larval abundance. The mean decadal abundance of each unfished phenophase was regressed against time. The slope of the regressions was used to calculate a mean rate of changes in abundance and a 95% confidence interval for each phenology group to determine if any group exhibited a significant long-term decline or increase in the abundance of its constituent species.

The amplitude of a species' seasonal cycle of abundance is another ecological trait that may affect its likelihood to undergo a shift in phenology. This is especially relevant since some mesopelagic species (*e.g.*, *Danaphos oculatus*, *Diogenichthys atlanticus*) exhibited weak seasonality and their larvae were present year round in the southern CCE. To test the hypothesis that species with a small amplitude of seasonal abundance will be less likely to display phenological shifts in either direction, the $\log_e (x+1)$ transformed, mean amplitude of seasonal abundance was regressed against the absolute value of changes in the CT of larval fishes.

Lastly, this study explored whether species that underwent shifts in phenology were more likely to change their geographic range in response to fluctuating climatic conditions. This was accomplished through a comparison with Hsieh et al. (2008, 2009), who investigated climate-related shifts in the distribution of 35 of the species examined here (Table S1.1). One-tailed binomial tests were used to evaluate whether there was a >50% probability that species in each phenology group exhibited a range shift.

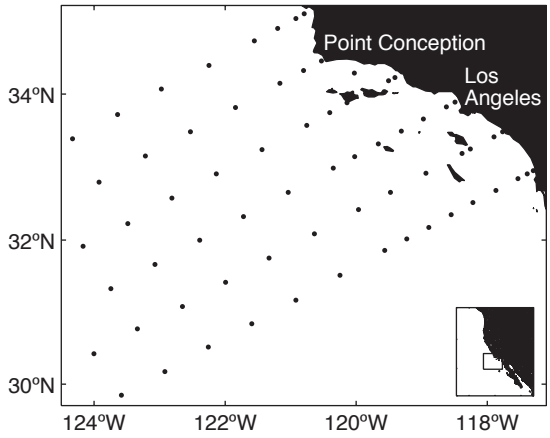

Figure S1.1. Sites where larval fish abundance was sampled. The rectangular box in the inset map shows the location of the study region relative to the West Coast of North America.

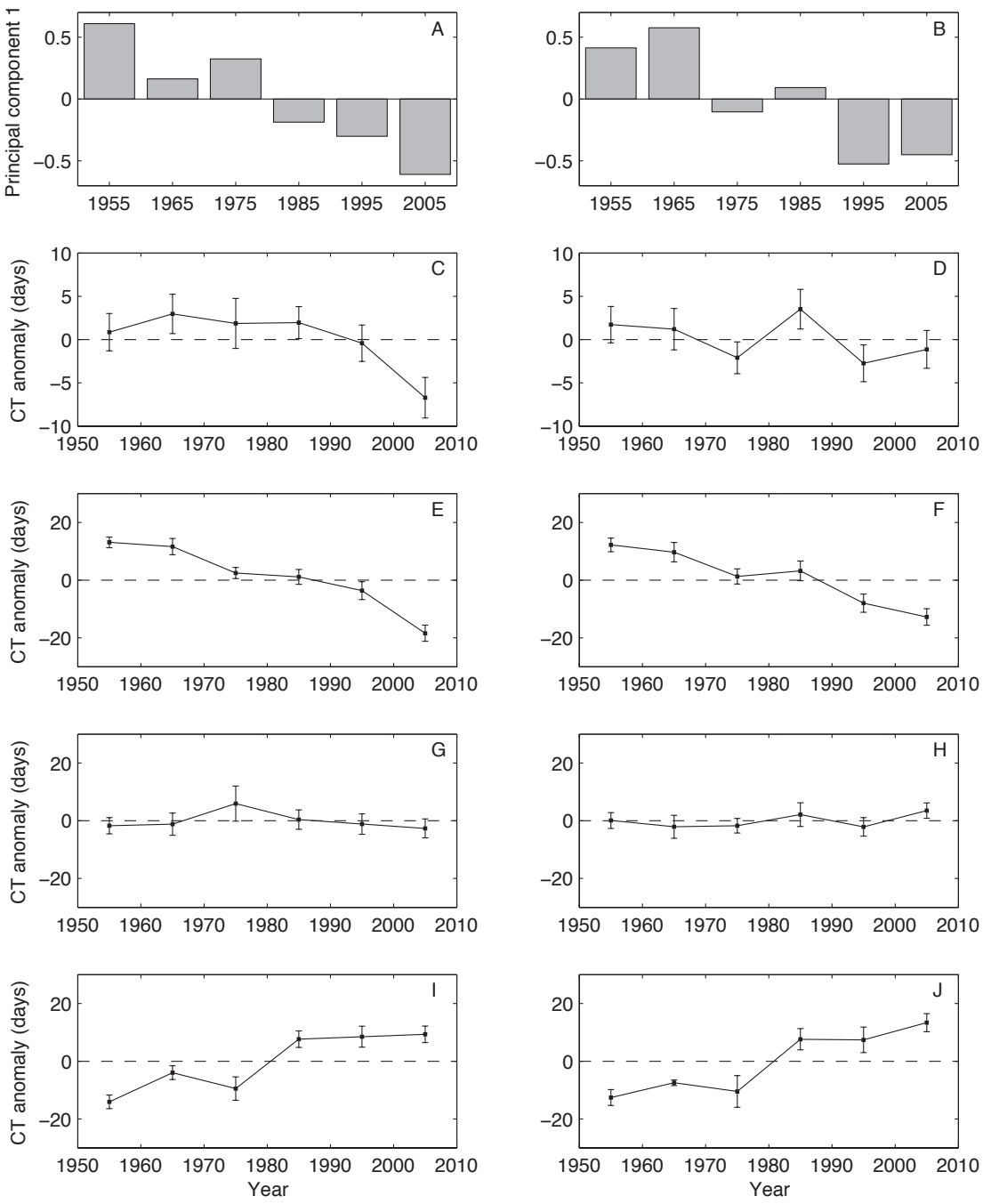

Figure S1.2. Decadal trends in the central tendency (CT) of larval fishes based on the full dataset (left column) and a partial dataset where May, September, and December were removed (right column). The partial dataset was used to examine any biases due to lack of sampling during these months in the 2000s. (A-B) Eigenvectors for each decade from the first principal component of the CT of larval fishes. Decadal means and standard errors of the CT of all fish species (C-D; $n = 290$), species with earlier phenology (E-F; $n = 110$), species with no long-term, linear trend in phenology (G-H; $n = 128$), and species with later phenology (I-J; $n = 52$).

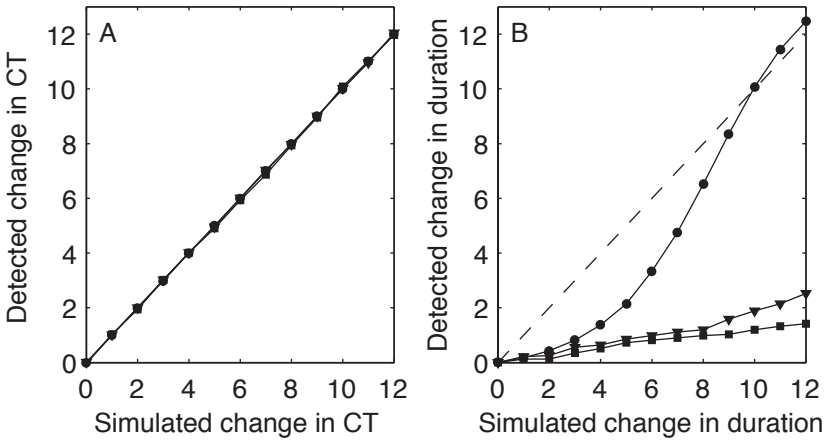

Figure S1.3. Median values of detected and simulated changes in (A) central tendency (CT) and the (B) duration of larval occurrence. Units on the x- and y-axes are days decade^{-1}. Medians were generated from 1,000 Monte Carlo simulations each for rates of phenological change between 0-12 days decade^{-1}. Results are shown for coefficients of variance of 0.05 (black circles), 0.30 (inverted, black triangles), and 0.60 (black squares). The dotted line shows a 1:1 relationship between simulated and detected changes. Note that these lines overlap in (A).

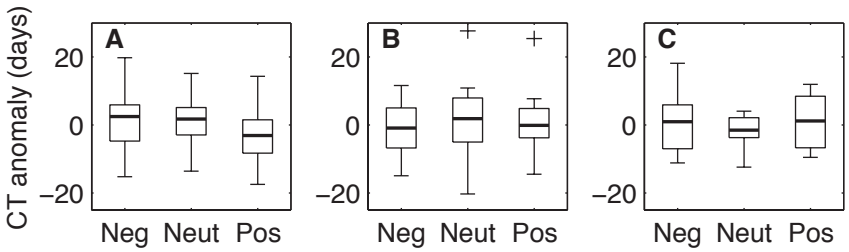

Figure S1.4. Effects of the North Pacific Gyre Oscillation (NPGO) on the seasonal central tendency (CT) of fish species displaying earlier phenology (A; $n = 60$), no long-term, linear change in phenology (B; $n = 66$), and later phenology (C; $n = 27$). In each box plot, the darkened line indicates the median; boxes show the inter-quartile range; whiskers indicate the expected extent of 99% of the data for a Gaussian distribution, and; crosses show outliers. Neg – NPGO index ≤ -0.5; Neut – NPGO index between -0.5 and 0.5; Pos – NPGO index ≥ 0.5. ANOVA results for earlier species: $F_{2,57} = 1.6$, $p = 0.22$; species without a linear trend: $F_{2,63} = 0.2$, $p = 0.81$; later species: $F_{2,24} = 0.5$, $p = 0.61$.

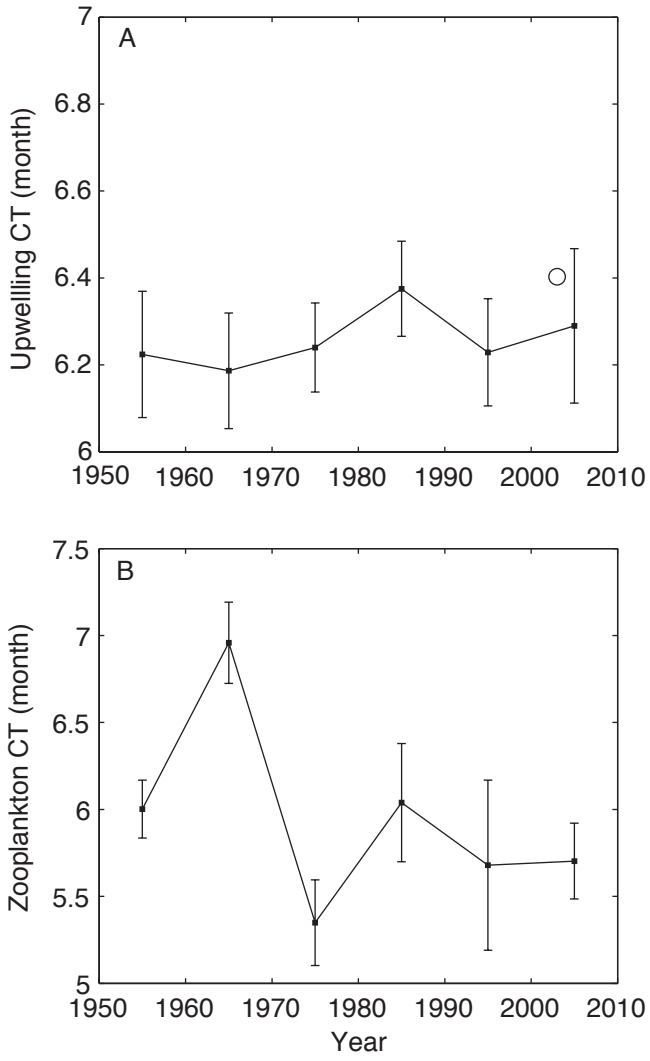

Figure S1.5. Decadal changes in the central tendency (CT) of the Bakun upwelling index at 33° N and 119° W (A) and zooplankton volume from California Cooperative Oceanic Fisheries Investigations (CalCOFI; B). 95% confidence intervals from bootstrap analysis are shown. The white circle in (A) denotes the decadal CT of upwelling velocity within the CalCOFI area based on data from the QuikSCAT scatterometer.

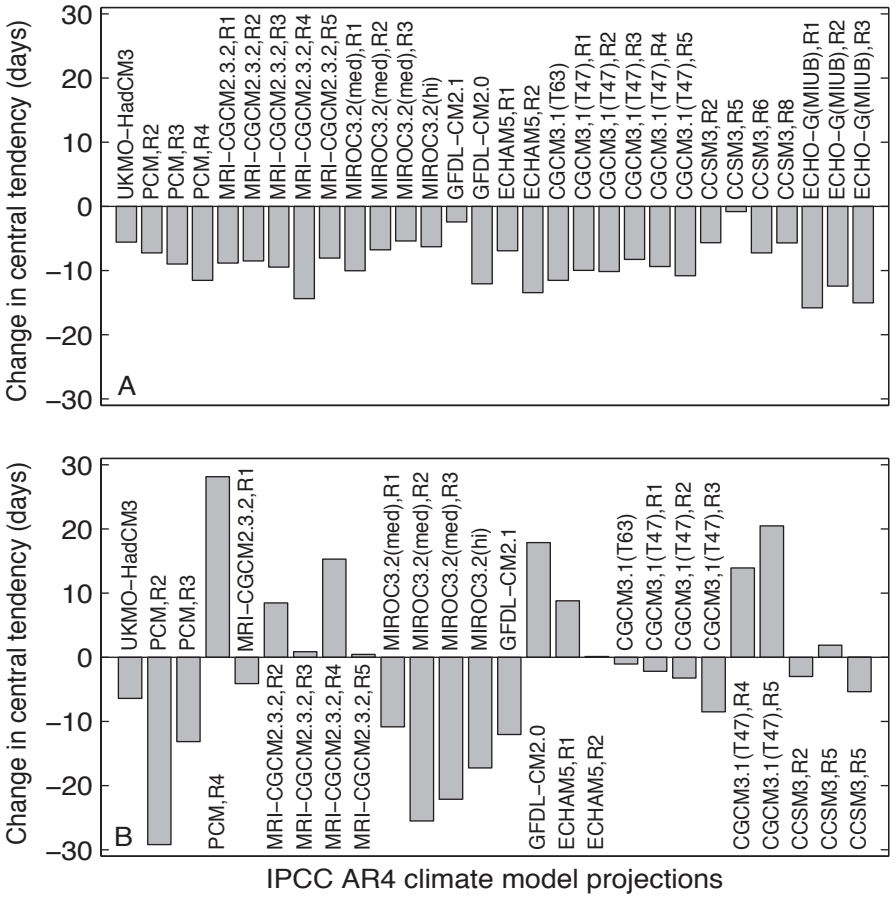

Figure S1.6. Projected changes in the phenology of larval fishes between 2000-2009 and 2090-2099 based on climate models from the Intergovernmental Panel of Climate Change Fourth Assessment Report (IPCC AR4). All predictions are for IPCC scenario A1B. Abbreviated IPCC names for each model are shown. (A) Species whose phenology became earlier during the 20th century. (B) Species whose phenology became later during the 20th century.

Table S1.1. Species characteristics tested to determine their effect on decadal shifts in larval phenology. Month of maximum larval abundance for each phenophase is based on mean seasonal patterns for the entire time series. Pearson correlation coefficients *r* from regressions between central tendency anomalies and decade are shown. Species were divided into phenology groups, such that $r \geq 0.5$ indicated a shift towards later phenology; $r \leq -0.5$ indicated earlier phenology, and; $-0.5 < r < 0.5$ indicated no long-term, linear change in phenology. $n = 6$. For species with two phenophases, separate correlation coefficients are included for each seasonal peak in larval abundance.

Species	Month(s) of maximum larval abundance	Adult habitat	Cross-shore distribution[1]	Biogeographic affinity	Adult trophic level	Fishing status[2]	Climate-related changes in distribution	*r*
Clueiformes								
Engraulidae								
Engraulis mordax	March	Epipelagic	Coastal-Oceanic	Wide distribution[1, 3]	3.0[4, 5]	Fished	Yes[3]	-0.39
Clupeidae								
Sardinops sagax	April	Epipelagic	Coastal-Oceanic	Warm-water[3]	2.7[4, 5, 6]	Fished	Yes[3]	-0.31
Argentiniformes								
Argentinidae								
Argentina sialis	March	Demersal	Coastal	Wide distribution[3]	3.1[4, 5]	Unfished	Yes[3]	0.26
Microstomatidae								
Bathylagus pacificus	March	Mesopelagic	Oceanic	Cool-water[7]	3.3[4]	Unfished	No[7]	0.84
Bathylagus wesethi	July	Mesopelagic	Oceanic	Cool-water[7]	3.2[6]	Unfished	No[7]	0.62
Leuroglossus stilbius	March	Mesopelagic	Coastal-Oceanic	Wide distribution[3]	3.3[4, 5]	Unfished	Yes[3]	0.23
Lipolagus ochotensis	March	Mesopelagic	Oceanic	Cool-water[7]	3.4[4]	Unfished	Yes[7]	-0.75
Stomiiformes								
Gonostomatidae								
Cyclothone signata	March September	Mesopelagic	Oceanic	Warm-water[7]	3.0[4]	Unfished	Yes[7]	-0.27 -0.64

Table S1.1 (continued)

Species	Month(s) of maximum larval abundance	Adult habitat	Cross-shore distribution[1]	Biogeographic affinity	Adult trophic level	Fishing status[2]	Climate-related changes in distribution	*r*
Sternoptychidae								
Argyropelecus sladeni	March	Mesopelagic	Oceanic	Wide distribution[7]	3.1[4]	Unfished	Yes[7]	-0.66
	November							-0.62
Danaphos oculatus	November	Mesopelagic	Oceanic	Wide distribution[8]	3.0[4]	Unfished	N/A	-0.76
Phosichthyidae								
Vinciguerria lucetia	August	Mesopelagic	Oceanic	Warm-water[7]	3.0[4]	Unfished	Yes[7]	-0.53
Stomiidae								
Chauliodus macouni	August	Mesopelagic	Oceanic	Cool-water[7]	4.1[4]	Unfished	Yes[7]	-0.11
Idiacanthus antrostomus	August	Mesopelagic	Oceanic	Wide distribution[7]	3.8[4]	Unfished	No[7]	-0.44
Stomias atriventer	March	Mesopelagic	Oceanic	Warm-water[7]	4.0[4]	Unfished	No[7]	0.22
Aulopiformes								
Paralepididae								
Lestidiops ringens	August	Mesopelagic	Oceanic	Wide distribution[8]	4.1[4]	Unfished	N/A	-0.65
Myctophiformes								
Myctophidae								
Ceratoscopelus townsendi	August	Mesopelagic	Oceanic	Wide distribution[7]	3.5[4]	Unfished	No[7]	-0.07
Diogenichthys atlanticus	April	Mesopelagic	Oceanic	Warm-water[7]	3.1[4]	Unfished	No[7]	-0.70
	September							0.51
Nannobrachium regale	July	Mesopelagic	Oceanic	Wide distribution[8]	3.2[4]	Unfished	N/A	0.10
Nannobrachium ritteri	March	Mesopelagic	Oceanic	Wide distribution[7]	3.4[4]	Unfished	Yes[7]	-0.87

Table S1.1 (continued)

Species	Month(s) of maximum larval abundance	Adult habitat	Cross-shore distribution[1]	Biogeographic affinity	Adult trophic level	Fishing status[2]	Climate-related changes in distribution	*r*
Protomyctophum crockeri	January	Mesopelagic	Oceanic	Cool-water[7]	3.2[6]	Unfished	Yes[7]	-0.25
Stenobrachius leucopsarus	March	Mesopelagic	Oceanic	Cool-water[7]	3.6[4]	Unfished	Yes[7]	-0.30
Symbolophorus californiensis	April	Mesopelagic	Oceanic	Cool-water[7]	3.1[4]	Unfished	Yes[7]	-0.90
	July							-0.62
Tarletonbeania crenularis	March	Mesopelagic	Oceanic	Cool-water[7]	3.1[4]	Unfished	Yes[7]	-0.47
	June							0.68
Triphoturus mexicanus	September	Mesopelagic	Oceanic	Warm-water[7]	3.3[4]	Unfished	Yes[7]	-0.94
Gadiformes								
Merlucciidae								
Merluccius productus	February	Epipelagic	Coastal-Oceanic	Wide distribution[1]	3.8[4, 5, 6]	Fished	Yes[3]	-0.66
Stephanoberyciformes								
Melamphaidae								
Melamphaes lugubris	March	Mesopelagic	Oceanic	Warm-water[7]	3.2[6]	Unfished	Yes[7]	0.06
	September							0.53
Scorpaeniformes								
Scorpaenidae								
Sebastes aurora	May	Demersal	Coastal	Cool-water[1, 3]	3.3[6]	Fished	Yes[3]	-0.83
Sebastes diploproa	October	Demersal	Coastal	Cool-water[1]	3.3[6]	Fished	N/A	-0.78
Sebastes goodei	February	Demersal	Coastal	Cool-water[1]	3.5[4]	Fished	N/A	0.58
Sebastes jordani	February	Demersal	Coastal	Cool-water[1, 3]	3.2[4, 5]	Fished	No[3]	-0.51
Sebastes paucispinis	January	Demersal	Coastal	Cool-water[1, 3]	3.5[4, 5]	Fished	No[3]	0.29

Table S1.1 (continued)

Species	Month(s) of maximum larval abundance	Adult habitat	Cross-shore distribution[1]	Biogeographic affinity	Adult trophic level	Fishing status[2]	Climate-related changes in distribution	*r*
Perciformes								
Carangidae								
Trachurus symmetricus	June	Epipelagic	Coastal-Oceanic	Wide distribution[1, 3]	3.7[4, 5]	Fished	No[3]	-0.87
Pomacentridae								
Chromis punctipinnis	August	Demersal	Coastal	Warm-water[1, 3]	2.7[4, 5]	Unfished	Yes[3]	0.55
Labridae								
Oxyjulis californica	August	Demersal	Coastal	Cool-water[1]	3.1[4]	Unfished	N/A	-0.75
Scombridae								
Scomber japonicus	May	Epipelagic	Coastal-Oceanic	Warm-water[3]	3.4[4, 5]	Fished	Yes[3]	-0.64
Centrolophidae								
Icichthys lockingtoni	June	Epipelagic	Coastal-Oceanic	Wide distribution[3]	3.7[4, 5]	Unfished	No[3]	-0.64
Tetragonuridae								
Tetragonurus cuvieri	October	Epipelagic	Coastal-Oceanic	Cool-water[1, 3]	3.8[4, 5]	Unfished	No[3]	0.28
Pleuronectiformes								
Paralichthyidae								
Citharichthys sordidus	February October	Demersal	Coastal	Cool-water[1]	3.4[4]	Fished	N/A	0.08 0.50
Citharichthys stigmaeus	October	Demersal	Coastal	Cool-water[1]	3.4[4]	Unfished	N/A	-0.005
Paralichthys californicus	March July	Demersal	Coastal	Warm-water[3, 7]	4.5[4, 5]	Fished	Yes[3]	0.92 0.34

Table S1.1 (continued)

Species	Month(s) of maximum larval abundance	Adult habitat	Cross-shore distribution[1]	Biogeographic affinity	Adult trophic level	Fishing status[2]	Climate-related changes in distribution	*r*
Pleuronectidae								
Lyopsetta exilis	April	Demersal	Coastal	Cool-water[1, 3]	3.5[4, 5]	Unfished	No[3]	-0.12
Parophrys vetulus	March	Demersal	Coastal	Cool-water[1]	3.3[4, 5, 6]	Fished	Yes[3]	-0.25
Pleuronichthys verticalis	March	Demersal	Coastal	Warm-water[3]	3.1[4]	Unfished	No[3]	0.87

[1] Hsieh *et al.* (2005)
[2] Lowther (2011)
[3] Hsieh *et al.* (2008)
[4] Source: www.fishbase.com
[5] Hsieh *et al.* (2006)
[6] Field *et al.* (2006)
[7] Hsieh *et al.* (2009)
[8] Moser *et al.* (2001)

Table S1.2. 95% confidence intervals for detecting simulated changes in the mean date of larval fish abundance. Changes in simulated fish phenology were estimated based on central tendency (CT). Confidence intervals were generated from 1,000 Monte Carlo simulations each for fishes whose abundance varied according to 12 sets of coefficients of variance and 13 rates of phenological change.

		Simulated phenological change (days decade^{-1})				
		0	1	2	3	4
Coefficient of variation	0.05	-0.3 - 0.3	0.7 - 1.3	1.7 - 2.3	2.7 - 3.3	3.7 - 4.3
	0.10	-0.5 - 0.5	0.5 - 1.5	1.5 - 2.5	2.4 - 3.6	3.5 - 4.5
	0.15	-0.8 - 0.7	0.3 - 1.8	1.2 - 2.8	2.2 - 3.7	3.2 - 4.8
	0.20	-1.0 - 1.1	-0.1 - 2.1	0.9 - 3.1	1.9 - 4.1	3.0 - 5.1
	0.25	-1.3 - 1.4	-0.3 - 2.2	0.7 - 3.4	1.6 - 4.3	2.6 - 5.4
	0.30	-1.6 - 1.7	-0.7 - 2.6	0.4 - 3.5	1.4 - 4.6	2.4 - 5.6
	0.35	-2.0 - 1.9	-0.9 - 2.9	-0.1 - 3.9	1.1 - 5.0	2.1 - 5.9
	0.40	-2.1 - 2.4	-1.3 - 3.2	-0.1 - 4.5	0.8 - 5.2	1.9 - 6.2
	0.45	-2.6 - 2.4	-1.6 - 3.5	-0.6 - 4.4	0.5 - 5.4	1.3 - 6.7
	0.50	-2.6 - 3.0	-2.0 - 3.8	-0.7 - 4.9	0.2 - 5.9	1.1 - 6.8
	0.55	-3.2 - 3.3	-2.0 - 4.1	-1.0 - 5.2	0.2 - 6.6	1.1 - 7.2
	0.60	-3.4 - 3.3	-2.3 - 4.5	-1.5 - 5.3	-0.2 - 6.6	0.5 - 7.4

		Simulated phenological change (days decade^{-1})				
		5	6	7	8	9
Coefficient of variation	0.05	4.7 - 5.3	5.8 - 6.2	6.7 - 7.3	7.7 - 8.3	8.7 - 9.3
	0.10	4.5 - 5.5	5.5 - 6.5	6.5 - 7.5	7.4 - 8.5	8.5 - 9.5
	0.15	4.2 - 5.8	5.1 - 6.8	6.2 - 7.8	7.2 - 8.8	8.2 - 9.8
	0.20	3.9 - 6.0	4.8 - 7.1	5.9 - 8.1	6.9 - 9.1	8.0 - 10.0
	0.25	3.5 - 6.4	4.7 - 7.4	5.7 - 8.4	6.7 - 9.4	7.6 - 10.2
	0.30	3.5 - 6.5	4.3 - 7.6	5.3 - 8.6	6.4 - 9.6	7.3 - 10.6
	0.35	3.0 - 7.1	4.0 - 7.8	5.2 - 8.9	6.1 - 9.9	7.2 - 10.9
	0.40	2.8 - 7.5	3.9 - 8.2	4.8 - 9.3	5.6 - 10.2	6.6 - 11.4
	0.45	2.4 - 7.6	3.3 - 8.3	4.6 - 9.8	5.6 - 10.5	6.4 - 11.6
	0.50	2.3 - 7.8	3.3 - 8.9	4.1 - 9.9	4.9 - 11.0	6.3 - 11.7
	0.55	1.9 - 8.0	3.1 - 9.4	3.7 - 10.1	4.5 - 11.1	5.8 - 12.1
	0.60	1.6 - 8.5	2.6 - 9.7	3.5 - 10.5	4.6 - 11.3	5.8 - 12.3

Table S1.2 (continued)

		Simulated phenological change (days decade^{-1})		
		10	11	12
Coefficient of variation	0.05	9.8 - 10.3	10.7 - 11.3	11.7 - 12.3
	0.10	9.5 - 10.5	10.5 - 11.5	11.4 - 12.5
	0.15	9.2 - 10.8	10.2 - 11.8	11.2 - 12.9
	0.20	8.9 - 11.0	9.9 - 12.1	11.0 - 13.0
	0.25	8.5 - 11.3	9.6 - 12.3	10.6 - 13.4
	0.30	8.3 - 11.6	9.3 - 12.8	10.4 - 13.8
	0.35	8.1 - 11.9	8.9 - 13.0	10.1 - 14.0
	0.40	7.8 - 12.1	8.8 - 13.1	9.8 - 14.2
	0.45	7.6 - 12.7	8.5 - 13.6	9.5 - 14.5
	0.50	7.0 - 12.9	8.3 - 13.9	9.2 - 15.0
	0.55	6.7 - 13.0	7.9 - 14.1	8.8 - 15.0
	0.60	6.5 - 13.5	7.7 - 14.5	8.5 - 15.3

Table S1.3. 95% confidence intervals for detecting simulated changes in the season duration of peak larval abundance. Changes in simulated season duration were estimated with the same method as in Figure 1.3. Confidence intervals were generated from 1,000 Monte Carlo simulations each for an assemblage of 20 simulated fish species whose abundance varied based on 12 sets of coefficients of variance and 13 rates of change in season duration.

		Simulated change in season duration (days decade^{-1})				
		0	1	2	3	4
Coefficient of variation	0.05	-0.8 - 0.8	-0.7 - 1.2	-0.5 - 1.5	-0.3 - 2.1	0.2 - 2.8
	0.10	-1.9 - 1.8	-1.7 - 2.1	-1.4 - 2.6	-1.1 - 3.2	-0.6 - 3.4
	0.15	-2.2 - 2.2	-2.1 - 2.4	-1.8 - 2.7	-1.5 - 3.1	-1.2 - 3.5
	0.20	-2.4 - 2.4	-2.3 - 2.6	-2.2 - 2.7	-1.8 - 3.2	-1.6 - 3.0
	0.25	-2.5 - 2.3	-2.4 - 2.5	-2.1 - 2.7	-1.7 - 2.8	-1.9 - 3.3
	0.30	-2.3 - 2.4	-2.4 - 2.9	-2.1 - 2.9	-1.9 - 2.9	-2.0 - 3.1
	0.35	-2.7 - 2.4	-2.3 - 2.7	-2.2 - 2.7	-1.9 - 3.2	-1.9 - 3.2
	0.40	-2.5 - 2.7	-2.4 - 2.4	-2.4 - 2.9	-2.0 - 2.8	-1.8 - 3.2
	0.45	-2.5 - 2.4	-2.4 - 2.7	-2.3 - 2.9	-2.1 - 2.8	-1.9 - 3.0
	0.50	-2.8 - 2.6	-2.2 - 2.6	-2.2 - 2.6	-2.1 - 2.7	-1.8 - 2.8
	0.55	-2.4 - 2.5	-2.5 - 2.5	-2.1 - 2.6	-2.1 - 2.8	-1.8 - 2.8
	0.60	-2.5 - 2.5	-2.2 - 2.6	-2.1 - 2.7	-1.9 - 2.7	-1.9 - 2.8

		Simulated change in season duration (days decade^{-1})				
		5	6	7	8	9
Coefficient of variation	0.05	0.8 - 3.8	1.7 - 5.0	3.1 - 6.7	4.3 - 8.3	6.4 - 10.0
	0.10	-0.1 - 4.4	0.6 - 4.9	1.3 - 5.8	2.1 - 6.6	2.9 - 7.6
	0.15	-0.6 - 3.8	-0.5 - 4.4	0.1 - 4.7	0.7 - 5.4	1.2 - 6.0
	0.20	-1.4 - 3.5	-1.2 - 3.6	-0.5 - 4.0	-0.3 - 4.7	0.1 - 4.8
	0.25	-1.6 - 3.4	-1.4 - 3.7	-0.9 - 3.7	-0.8 - 3.9	-0.5 - 4.4
	0.30	-1.6 - 3.2	-1.5 - 3.4	-1.3 - 3.6	-1.2 - 3.7	-0.8 - 3.8
	0.35	-1.8 - 3.1	-1.6 - 3.5	-1.3 - 3.2	-1.3 - 3.6	-1.1 - 3.9
	0.40	-1.7 - 3.0	-1.6 - 3.4	-1.4 - 3.4	-1.4 - 3.6	-1.2 - 3.6
	0.45	-1.6 - 3.0	-1.7 - 3.2	-1.4 - 3.3	-1.2 - 3.6	-1.0 - 3.6
	0.50	-1.7 - 3.0	-1.8 - 3.0	-1.5 - 3.2	-1.4 - 3.6	-1.2 - 3.6
	0.55	-1.7 - 3.3	-1.5 - 2.9	-1.3 - 3.2	-1.2 - 3.5	-1.2 - 3.6
	0.60	-1.7 - 3.0	-1.5 - 3.0	-1.4 - 3.3	-1.1 - 3.4	-1.2 - 3.3

Table S1.3 (continued)

		Simulated change in season duration (days decade^{-1})		
		10	11	12
Coefficient of variation	0.05	8.4 - 11.5	10.1 - 12.7	11.2 - 13.4
	0.10	4.1 - 8.5	5.3 - 9.4	6.3 - 10.2
	0.15	2.1 - 6.8	2.7 - 7.4	3.4 - 8.0
	0.20	0.7 - 5.3	1.3 - 5.8	1.6 - 6.3
	0.25	-0.3 - 4.5	0.1 - 5.1	0.7 - 5.4
	0.30	-0.6 - 4.1	-0.2 - 4.5	0.2 - 5.0
	0.35	-0.8 - 4.2	-0.4 - 4.2	-0.3 - 4.5
	0.40	-0.9 - 3.6	-0.9 - 4.1	-0.7 - 4.1
	0.45	-1.1 - 3.6	-1.0 - 3.8	-0.6 - 4.0
	0.50	-1.0 - 3.6	-0.7 - 3.8	-0.8 - 3.9
	0.55	-1.0 - 3.5	-0.8 - 3.6	-0.8 - 3.5
	0.60	-1.0 - 3.5	-1.0 - 3.4	-0.7 - 3.5

References

Abraham, C.L. and W.J. Sydeman. 2004. Ocean climate, euphausiids and auklet nesting: inter-annual trends and variation in phenology, diet and growth of a planktivorous seabird, *Ptychoramphus aleuticus*. *Marine Ecology Progress Series* 274: 235-250.

Ahlstrom, E.H. 1959. Vertical distribution of pelagic fish eggs and larvae off California and Baja California. *Fishery Bulletin* 60: 107-146.

Anderson, J.T. 1988. A review of size dependent survival during pre-recruit stages of fishes in relation to recruitment. *Journal of Northwest Atlantic Fishery Science* 8: 55-66.

Anderson, J.J. and W.N. Beer. 2009. Oceanic, riverine, and genetic influences on spring Chinook salmon migration timing. *Ecological Applications* 19(8): 1989-2003.

Bakun, A. 1973. Coastal Upwelling Indices, West Coast of North America, 1946-71. NOAA Technical Report, NMFS SSRF-671. National Marine Fisheries Service, Seattle, WA. 103 p.

Bakun, A. 1990. Global climate change and intensification of coastal ocean upwelling. *Science* 247: 198-201.

Beaugrand, G., K.M. Brander, J.A. Lindley, S. Souissi and P.C. Reid. 2003. Plankton effect on cod recruitment in the North Sea. *Nature* 426: 661-664.

Benjamini, Y. and Y. Hochberg. 1995. Controlling the false discovery rate: a practical and powerful approach to multiple testing. *Journal of the Royal Statistical Society. Series B (Methodological)* 57(1): 289-300.

Black, B.A., I.D. Schroeder, W.J. Sydeman, S.J. Bograd, B.K. Wells and F.B. Schwing. 2011. Winter and summer upwelling modes and their biological importance in the California Current Ecosystem. *Global Change Biology* 17: 2536-2545.

Bograd, S.J., I. Schroeder, N. Sarkar, X. Qiu, W.J. Sydeman and F.B. Schwing. 2009. Phenology of coastal upwelling in the California Current. *Geophysical Research Letters* 36, L01602, doi:10.1029/2008GL035933.

Brodeur, R.D., D.M. Gadomski, W.G. Pearcy, H.P. Batchelder and C.B. Miller. 1985. Abundance and distribution of ichthyoplankton in the upwelling zone off Oregon during anomalous El Niño conditions. *Estuarine, Coastal and Shelf Science* 21: 365-378.

Burkle, L.A., J.C. Marlin and T.M. Knight. 2013. Plant-pollinator interactions over 120 years: loss of species, co-occurrence, and function. *Science* 339: 1611-1615.

Burrows, M.T., D.S. Schoeman, L.B. Buckley, P. Moore, E.S. Poloczanska, K.M. Brander, C. Brown, J.F. Bruno, C.M. Duarte, B.S. Halpern, J. Holding, C.V. Kappel, W. Kiessling, M.I. O'Connor, J.M. Pandolfi, C. Parmesan, F.B. Schwing, W.J. Sydeman and A.J. Richardson. 2011. The pace of shifting climate in marine and terrestrial ecosystems. *Science* 234: 652-655.

Carscadden, J., B.S. Nakashima and K.T. Frank. 1997. Effects of fish length and temperature on the timing of peak spawning in capelin (*Mallotus villosus*). *Canadian Journal of Fisheries and Aquatic Sciences* 54: 781-787.

Chelton, D.B., P.A. Bernal and J.A. McGowan. 1982. Large-scale interannual physical and biological interaction in the California Current. *Journal of Marine Research* 40(4): 1095-1126.

Cheung, W.W. L., V.W.Y. Lam, J.L. Sarmiento, K. Kearney, R. Watson and D. Pauly. 2009. Projecting global marine biodiversity impacts under climate change scenarios. *Fish and Fisheries* 10: 235-251.

Chiba, S., S. Batten, K. Sasaoka, Y. Sasai and H. Sugisaki. 2012. Influence of Pacific Decadal Oscillation on phytoplankton phenology and community structure in the western North Pacific. *Geophysical Research Letters* 39, L15603, doi:10.1029.2012GL052912.

Chittenden, C.M., J.A. Jensen, D. Ewart, S. Anderson, S. Balfry, E. Downey, A. Eaves, S. Saksida, B. Smith, S. Vincent, D. Welch and R.S. McKinley. 2010. Recent salmon declines: result of lost feeding opportunities due to bad timing? *Plos One*, 5(8), e12423, doi:10.1371/journal.pone.0012423.

Clarke, K.R. and R.M. Warwick. 2001. Change in Marine Communities: An Approach to Statistical Analysis and Interpretation, 2nd ed. PRIMER-E, Plymouth, UK. 172 p.

Cleland, E.E., J.M. Allen, T.M. Crimmins, J.A. Dunne, S. Pau, S.E. Travers, E.S. Zavaleta and E.M. Wolkovich. 2012. Phenological tracking enables positive species responses to climate change. *Ecology* 93(8): 1765-1771.

Cushing, D.H. 1974. The natural regulation of fish populations. p. 399-412. In Sea Fisheries Research. F.R.H. Jones (ed). John Wiley & Sons, New York, NY.

Cushing, D.H. 1990. Plankton production and year-class strength in fish populations: an update of the match/mismatch hypothesis. *Advances in Marine Biology* 26: 249-293.

de Vlaming, V.L. 1972. Environmental control of teleost reproductive cycles: a brief review. *Journal of Fish Biology* 4: 131-140.

Diffenbaugh, N.S., M.A. Snyder and L.C. Sloan. 2004. Could CO_2-induced land-cover feedbacks alter near-shore upwelling regimes? *Proceedings of the National Academy of Sciences* 101(1): 27-32.

Di Lorenzo, E., A.J. Miller, N. Schneider and J.C. McWilliams. 2005. The warming of the California Current System: Dynamics and Ecosystem Implications. *Journal of Physical Oceanography* 35: 336-362.

Di Lorenzo, E., N. Schneider, K.M. Cobb, P.J.S. Franks, K. Chhak, A.J. Miller, J.C. McWilliams, S.J. Bograd, H. Arango, E. Curchitser, T.M. Powell and P. Rivière. 2008. North Pacific Gyre Oscillation links ocean climate and ecosystem change. *Geophysical Research Letters*, 35, L08607, doi:10.1029/2007GL032838.

Durant, J.M., D.O. Hjermann, G. Ottersen and N.C. Stenseth. 2007. Climate and the match or mismatch between predator requirements and resource availability. *Climate Research* 33: 271-283.

Edwards, M. and A.J. Richardson. 2004. Impact of climate change on marine pelagic phenology and trophic mismatch. *Nature* 430: 881-884.

Efron, B. and R.J. Tibshirani. 1993. An Introduction to the Bootstrap. Chapman & Hall/CRC, Boca Raton, FL. 436 p.

Field, J.C., R.C. Francis and K. Aydin. 2006. Top-down modeling and bottom-up dynamics: linking a fisheries-based ecosystem model with climate hypotheses in the Northern California Current. *Progress in Oceanography* 68: 238-270.

Frederiksen, M., D.A. Elston, M. Edwards, A.D. Mann and S. Wanless. 2011. Mechanisms of long-term decline in size of lesser sandeels in the North Sea explored using a growth and phenology model. *Marine Ecology Progress Series* 432: 137-147.

Genner, M.J., N.C. Halliday, S.D. Simpson, A.J. Southward, S.J. Hawkins and D.W. Sims. 2010. Temperature-driven phenological changes within a marine larval fish assemblage. *Journal of Plankton Research* 32(5): 699-708.

Gillet, C. and P. Quétin. 2006. Effect of temperature change on the reproductive cycle of roach in Lake Geneva from 1983 to 2001. *Journal of Fish Biology* 69: 518-534.

Greve, W. 2003. Aquatic plants and animals. p. 285-403. In Phenology: An Integrative Environmental Science. M.D. Schwartz (ed.). Kluwer Academic Publishers, Boston, MA.

Greve, W., F. Reiners, J. Nast and S. Hoffman. 2004. Helgoland Roads meso- and macrozooplankton time-series 1974 to 2004: lessons from 30 years of single spot,

high frequency sampling at the only off-shore island of the North Sea. *Helgoland Marine Research* 58: 274-288.

Greve, W., S. Prinage, H. Zidowitz, J. Nast and F. Reiners. 2005. On the phenology of North Sea ichthyoplankton. *ICES Journal of Marine Science* 62: 1216-1223.

Hayward, T.L. and E.L. Venrick. 1998. Nearsurface pattern in the California Current: coupling between physical and biological structure. *Deep-Sea Res Part II* 45: 1617-1638.

Henson, S.A. and A.C. Thomas. 2007. Interannual variability in timing of bloom initiation in the California Current System. *Journal of Geophysical Research* 112, C08007, doi:/10.1029/2006JC003960.

Hewitt, R. 1980. Distributional Atlas of Fish Larvae in the California Current Region: Northern Anchovy, *Engraulis mordax* (Girard), 1966-1979. California Cooperative Oceanic Fisheries Investigations Atlas 28. National Marine Fisheries Service, Southwest Fisheries Science Center, La Jolla, CA. 101 p. Available at http://www.calcofi.org/publications/atlases/CalCOFI_Atlas_28.pdf. Accessed February 7, 2013.

Hewitt, R.P. 1988. Historical review of the oceanographic approach to fishery research. *California Cooperative Oceanic Fisheries Investigations Reports* 29: 27-41.

Holt, C.A. and N. Mantua. 2009. Defining spring transition: regional indices for the California Current System. *Marine Ecology Progress Series* 393: 285-299.

Houde, E.D. 1987. Fish early life dynamics and recruitment variability. *American Fisheries Society Symposium* 2: 17-29.

Houde, E.D. 2008. Emerging from Hjort's shadow. *Journal of Northwest Atlantic Fishery Science* 41: 53-70.

Hsieh, C.H., C. Reiss, W. Watson, M.J. Allen, J.R. Hunter, R.N. Lea, R.H. Ronsenblatt, P.E. Smith and G. Sugihara. 2005. A comparison of long-term trends and variability in populations of larvae of exploited and unexploited fishes in the Southern California region: A community approach. *Progress in Oceanography* 67: 160-185.

Hsieh, C.H., C.S. Reiss, J.R. Hunter, J.R. Beddington, R.M. May and G. Sugihara. 2006. Fishing elevates variability in the abundance of exploited species. *Nature* 443: 859-862.

Hsieh, C.H., C.S. Reiss, R.P. Hewitt and G. Sugihara. 2008. Spatial analysis shows that fishing enhances the climatic sensitivity of marine fishes. *Canadian Journal of Fisheries and Aquatic Sciences* 65: 947-961.

Hsieh, C.H., H.J. Kim, W. Watson, E. Di Lorenzo and G. Sugihara. 2009. Climate-driven changes in abundance and distribution of larvae of oceanic fishes in the southern California region. *Global Change Biology* 15: 2137-2152.

Hunter, J.R. and S.R. Goldberg. 1980. Spawning incidence and batch fecundity in northern anchovy, *Engraulis mordax. Fishery Bulletin* 77(3): 641-652.

Hutchings, J.A. and R.A. Myers. 1994. Timing of cod reproduction: interannual variability and the influence of temperature. *Marine Ecology Progress Series* 108: 21-31.

Huyer, A., J.C. Sobey and R.L. Smith. 1979. The spring transition in currents over the Oregon continental shelf. *Journal of Geophysical Research* 84(C11): 6995-7011.

IPCC. 2007. Climate Change 2007: The Physical Science Basis. Contribution of Working Group I to the Fourth Assessment Report of the Intergovernmental Panel on Climate Change. S. Solomon, D. Qin, M. Manning, Z. Chen, M. Marquis, K.B. Averyt, M. Tignor and H.L. Miller (eds.). Cambridge University Press, Cambridge, UK. 996 p.

Jansen, T. and H. Gislason. 2011. Temperature affects the timing of spawning and migration of North Sea mackerel. *Continental Shelf Research* 31: 64-72.

Ji, R., M. Edwards, D.L. Mackas, J.A. Runge and A.C. Thomas. 2010. Marine plankton phenology and life history in a changing climate: current research and future directions. *Journal of Plankton Research* 32(10): 1355-1368.

Kaltenberg, A.M., R.L. Emmett and K.J. Benoit-Bird. 2010. Timing of forage fish seasonal appearance in the Columbia River plume and link to ocean conditions. *Marine Ecology Progress Series* 419: 171-184.

Keefer, M.L., C.A. Peery and C.C. Caudill 2008. Migration timing of Columbia River spring chinook salmon: Effects of temperature, river discharge, and ocean environment. *Transactions of the American Fisheries Society* 137: 1120-1133.

Kim, H.-J., A.J. Miller, J. McGowan and M.L. Carter. 2009. Coastal phytoplankton blooms in the Southern California Bight. *Progress in Oceanography* 82: 137-147.

Koeller, P., C. Fuentes-Yaco, S. Sathyendranath, A. Richards, P. Ouellet, D. Orr, U. Skúladóttir, K. Wieland, L. Savard and M. Aschan. 2009. Basin-scale coherence in phenology of shrimps and phytoplankton in the North Atlantic Ocean. *Science* 324: 791-793.

Koslow, J.A., R. Goericke, A. Lara-Lopez and W. Watson. 2011. Impact of declining intermediate-water oxygen on deepwater fishes in the California Current. *Marine Ecology Progress Series* 436: 207-218.

Koslow, J.A. R. Goericke and W. Watson. 2013. Fish assemblages in the Southern California Current: relationships with climate, 1951-2008. *Fisheries Oceanography* 22: 207-219.

Kramer, D., M.J. Kalin, E.G. Stevens, J.R. Thrailkill and J.R. Zweifel. 1972. Collecting and Processing Data on Fish Eggs and Larvae in the California Current Region. NOAA Technical Report NMFS CIRC-370. National Marine Fisheries Service, Seattle, WA. 38 p. Available at http://spo.nmfs.noaa.gov/Circulars/CIRC370.pdf. Accessed January 15, 2013.

Lange, U. and W. Greve. 1997. Does temperature influence the spawning time, recruitment and distribution of flatfish via its influence on the rate of gonadal maturation? *Deutsche Hydrographische Zeitschrift* 49(2): 251-263.

Leopold, A. and S.E. Jones. 1947. A phenological record for Sauk and Dane Counties, Wisconsin, 1935-1945. *Ecological Monographs* 17(1): 81-122.

Liu, H. and W.T. Peterson. 2010. Seasonal and inter-annual variations in the abundance and biomass of *Neocalanus plumchrus* in continental slope waters off Oregon. *Fisheries Oceanography* 19(5): 354-369.

Logerwell, E.A., N. Mantua, P.W. Lawson, R.C. Francis and V.N. Agostini. 2003. Tracking environmental processes in the coastal zone for understanding and predicting Oregon coho (*Oncorhynchus kisutch*) marine survival. *Fisheries Oceanography* 12(6): 554-568.

Love, M.S., M. Yoklavich and L. Thorsteinson. 2002. The Rockfishes of the Northeast Pacific. University of California Press, Los Angeles, CA. 404 p.

Lowther, A. 2011. Fisheries of the United States 2010. National Marine Fisheries Service, Office of Science and Technology, Silver Spring, MD. 103 p. Available at http://www.st.nmfs.noaa.gov/st1/fus/fus10/FUS_2010.pdf. Accessed on January 15, 2013.

Lynn, R.J., S.J. Bograd, T.K. Chereskin and A. Huyer. 2003. Seasonal renewal of the California Current: the spring transition off California. *Journal of Geophysical Research* 108(C8), 3279, doi:10.1029/2003JC001787.

Mackas, D.L., S. Batten and M. Trudel. 2007. Effects on zooplankton of a warmer ocean: Recent evidence from the Northeast Pacific. *Progress in Oceanography* 75: 223-252.

Mantua N.J., S.R. Hare, Y. Zhang, J.M. Wallace and R.C. Francis. 1997. A Pacific decadal climate oscillation with impacts on salmon. *Bulletin of the American Meteorological Society* 78: 1069-1079.

Mantyla, A.W., S.J. Bograd and E.L. Venrick. 2008. Patterns and controls of chlorophyll-a and primary productivity cycles in the Southern California Bight. *Journal of Marine Systems* 73: 48-60.

McGowan, J.A., S.J. Bograd, R.J. Lynn and A.J. Miller. 2003. The biological response to the 1977 regime shift in the California Current. *Deep-Sea Research II* 50: 2567-2582.

Mendelssohn, R., F.B. Schwing and S.J. Bograd. 2004. Nonstationary seasonality of upper ocean temperature in the California Current. *Journal of Geophysical Research* 109, C10015, doi:10.1029/2004JC002330.

Menzel, A., T.H. Sparks, N. Estrella, E. Koch, A. Aasa, R. Ahas, K. Alm-Kübler, P. Bissolli, O. Braslavská, A. Briede, F.M. Chmielewski, Z. Crepinsek, Y. Curnel, A. Dahl, C. Defila, A. Donnelly, Y. Filella, K. Jatczak, F. Måge, A. Mestre, O. Nordli, J. Peñuelas, P. Pirinen, V. Remišová, H. Scheifinger, M. Striz, A. Susnik, A.J.H. van Vliet, F.-E. Wielgolaski, S. Zach and A. Zust. 2006. European phenological response to climate change matches the warming pattern. *Global Change Biology* 12: 1969-1976.

Mertz, G. and R.A. Myers. 1994. Match/mismatch predictions of spawning duration versus recruitment variability. *Fisheries Oceanography* 3(4): 236-245.

Methot, R.D. 1983. Seasonal variation in survival of larval northern anchovy, *Engraulis mordax*, estimated from the age distribution of juveniles. *Fishery Bulletin* 81(4): 741-750.

Miller-Rushing, A.J. and R.B. Primack. 2008. Global warming and flowering times in Thoreau's Concord: a community perspective. *Ecology* 89(2): 332-341.

Miller-Rushing, A.J., D.W. Inouye and R.B. Primack. 2008. How well do first flowering dates measure plant responses to climate change? The effects of population size and sampling frequency. *Journal of Ecology* 96: 1289-1296.

Moody, M.F. and T.J. Pitcher. 2010. Eulachon (*Thaleichthys pacificus*): Past and Present. Fisheries Centre Research Reports 18(2). The Fisheries Centre, University of British Columbia, Vancouver, BC. 197 p.

Moser, H.G. 1996. The Early Stages of Fishes in the California Current Region. California Cooperative Oceanic Fisheries Investigations Atlas 33 Allen Press, Inc., Lawrence, KS. 1505 p.

Moser, H.G., R.L. Charter, P.E. Smith, D.A. Ambrose, W. Watson, S.R. Charter and E.M. Sandknop. 2001. Distributional Atlas of Fish Larvae and Eggs in the Southern California Bight Region: 1951-1998. California Cooperative Oceanic Fisheries Investigations Atlas 34. National Marine Fisheries Service, Southwest Fisheries Science Center, La Jolla, CA. 166 p. Available at http://www.calcofi.org/publications/atlases/CalCOFI_Atlas_34.pdf. Accessed January 15, 2013.

Murawski, S.A. 1993. Climate change and marine fish distributions: Forecasting from historical analogy. *Transactions of the American Fisheries Society* 122: 647-658.

Ohman, M.D. and P.E. Smith. 1995. A comparison of zooplankton sampling methods in the CalCOFI time series. *California Cooperative Oceanic Fisheries Investigations Reports* 36: 153-158.

Parmesan, C. 2007. Influences of species, latitudes and methodologies on estimates of phenological response to global warming. *Global Change Biology* 13: 1860-1872.

Parmesan, C. and G. Yohe. 2003. A globally coherent fingerprint of climate change impacts across natural systems. *Nature* 421: 37-42.

Parrish, R.H., C.S. Nelson and A. Bakun. 1981. Transport mechanisms and reproductive success of fishes in the California Current. *Biological Oceanography* 1(2): 175-203.

Pérez-Brunius, P., M. López, A. Parés-Sierra and J. Pineda. 2007. Comparison of upwelling indices off Baja California derived from three different wind data sources. *California Cooperative Oceanic Fisheries Investigations Reports* 48: 204-214.

Peterson, W.T. 2009. Copepod species richness as an indicator of long-term changes in the coastal ecosystem of the northern California Current. *California Cooperative Oceanic Fisheries Investigations Reports* 50: 73-81.

Philippart, C.J.M., H.M. van Aken, J.J. Beukema, O.G. Bos, G.C. Cadée and R. Dekker. 2003. Climate-related changes in recruitment of the bivalve *Macoma balthica. Limnology and Oceanography* 48(6): 2171-2185.

Platt, T., C. Fuentes-Yaco and K.T. Frank. 2003. Spring algal bloom and larval fish survival. *Nature* 423: 398-399.

Pond, S. and G.L. Pickard. 1995. Introductory Dynamic Oceanography, 2nd ed. Butterworth Heinemann, Oxford, UK.329 p.

Richardson, A.J. and E.S. Poloczanska. 2008. Under-resourced, under threat. *Science* 320: 1294-1295.

Root, T.L., J.T. Price, K.R. Hall, S.H. Schneider, C. Rosenweig and J.A. Pounds. 2003. Fingerprints of global warming on wild animals and plants. *Nature* 421(2): 57-60.

Rubidge, E.M., J.L. Patton, M. Lim, A.C. Burton, J.S. Brashares and C. Moritz. 2012. Climate-induced range contraction drives genetic erosion in an alpine mammal. *Nature Climate Change* 2: 285-288.

Sasaoka, K., S. Chiba and T. Saino. 2011. Climatic forcing and phytoplankton phenology over the subarctic North Pacific from 1998 to 2006, as observed from ocean color data. *Geophysical Research Letters* 38, L15609, doi:10.1029/2011GL048299.

Schroeder, I.D., W.J. Sydeman, N. Sarkar, S.A. Thompson, S.J. Bograd and F.B. Schwing. 2009. Winter pre-conditioning of seabird phenology in the California Current. *Marine Ecology Progress Series* 393: 211-223.

Schwing, F.B. and R. Mendelssohn. 1997. Increased coastal upwelling in the California Current System. *Journal of Geophysical Research* 102(C2): 3421-3438.

Schwing, F.B., N.A. Bond, S.J. Bograd, T. Mitchell, M.A. Alexander and N. Mantua. 2006. Delayed coastal upwelling along the U.S. West Coast in 2005: A historical perspective. *Geophysical Research Letters* 33, L22S01, doi:10.1029/2006GL026911.

Snyder, M.A., L.C. Sloan, N.S. Diffenbaugh and J.L. Bell. 2003. Future climate change and upwelling in the California Current. *Geophysical Research Letters* 30(15), 1823, doi:10.1029/2003GL017647.

Sokal, R. and F.J. Rohlf. 1995. Biometry, 3rd ed .W.H. Freeman and Company, New York, NY. 887 p.

Sparks, T.H., E.P. Jeffree and C.E. Jeffree. 2000. An examination of the relationship between flowering times and temperature at the national scale using long-term phenological records from the UK. *International Journal of Biometeorology* 44: 82-87.

Stenseth, N.C. and A. Mysterud. 2002. Climate, changing phenology, and other life history traits: Nonlinearity and match-mismatch to the environment. *Proceedings of the National Academy of Sciences* 99(21): 13379-13381.

Stewart, R.H. 2004 Introduction to Physical Oceanography. Texas A & M University, College Station, TX. 345 p. Available at http://oceanworld.tamu.edu/resources/ocng_textbook/contents.html. Accessed on February 26, 2013.

Stewart, I.T., D.R. Cayan and M.D. Dettinger. 2005. Changes toward earlier streamflow timing across Western North America. *Journal of Climate* 18: 1136-1155.

Stock, C.A., M.A. Alexander, N.A. Bond, K.M. Brander, W.W.L. Cheung, E.N. Curchitser, T.L. Delworth, J.P. Dunne, S.M. Griffies, M.A. Haltuch, J.A. Hare, A.B. Hollowed, P. Lehodey, S.A. Levin, J.S. Link, K.A. Rose, R.R. Rykaczewski, J.L. Sarmiento, R.J. Stouffer, F.B. Schwing, G.A. Vecchi and F.E. Werner. 2011. On the use of IPCC-class models to assess the impact of climate on Living Marine Resources. *Progress in Oceanography* 88: 1-27.

Sullivan, B.K., J.H. Costello and D. van Keuren. 2007. Seasonality of the copepods *Acartia hudsonica* and *Acartia tonsa* in Narragansett Bay, RI, USA during a period of climate change. *Estuarine, Coastal and Shelf Science* 73: 259-267.

Thackeray, S.J., T.H. Sparks, M. Frederiksen, S. Burthes, P.J. Bacon, J.R. Bell, M.S. Botham, T.M. Brereton, P.W. Bright, L. Carvalho, T. Clutton-Brock, A. Dawson, M. Edwards, J.M. Elliott, R. Harrington, D. Johns, I.D. Jones, J.T. Jones, D.I. Leech, D.B. Roy, A. Scott, M. Smith, R.J. Smithers, I.J. Winfield and S. Wanless. 2010. Trophic level asynchrony in rates of phenological change for marine, freshwater and terrestrial environments. *Global Change Biology* 16: 3304-3313.

Trenberth, K.E., W.G. Large and J.G. Olson. 1989. The effective drag coefficient for evaluating wind stress over the oceans. *Journal of Climate* 2: 1507-1516.

Venegas, R.M., P.T. Strub, E. Beier, R. Letelier, A.C. Thomas, T. Cowles, C. James, L. Soto-Mardones and C. Cabrera. 2008. Satellite-derived variability in chlorophyll, wind stress, sea surface height, and temperature in the northern California Current System. *Journal of Geophysical Research* 113, C03015, doi:10.1029/2007JC004481.

Wang, M., J.E. Overland and N.A. Bond. 2010. Climate projections for selected large marine ecosystems. *Journal of Marine Systems* 79: 258-266.

Ware, D.M. and R.W. Tanasichuk. 1989. Biological basis of maturation and spawning waves in Pacific herring (*Clupea harengus pallasi*). *Canadian Journal of Fisheries and Aquatic Sciences* 46: 1776-1784.

Willis, C.G., B. Ruhfel, R.B. Primack, A.J. Miller-Rushing and C.C. Davis. 2008. Phylogenetic patterns of species loss in Thoreau's woods are driven by climate change. *Proceedings of the National Academy of Sciences* 105(44): 17029-17033.

Wolkovich, E.M., B.I. Cook, J.M. Allen, T.M. Crimmins, J.L. Betancourt, S.E. Travers, S. Pau, J. Regetz, T.J. Davies, N.J.B. Kraft, T.R. Ault, K. Bolmgren, S.J. Mazer, G.J. McCabe, B.J. McGill, C. Parmesan, N. Salamin, MD. Schwartz and E.E. Cleland. 2012. Warming experiments underpredict plant phenological responses to climate change. *Nature* 485: 494-497.

Yoo, S., H.P. Batchelder, W.T. Peterson and W.J. Sydeman. 2008. Seasonal, interannual and event scale variation in North Pacific ecosystems. *Progress in Oceanography* 77: 155-181.

Zwiefel, J.R. and R. Lasker. 1976. Prehatch and posthatch growth of fishes—A general model. *Fishery Bulletin* 74(3): 609-621.

CHAPTER 2. DYNAMIC HEIGHT: A KEY VARIABLE FOR IDENTIFYING THE SPAWNING HABITAT OF SMALL PELAGIC FISHES

Deep-Sea Research I 71 (2013) 79–91

Contents lists available at SciVerse ScienceDirect

Deep-Sea Research I

journal homepage: www.elsevier.com/locate/dsri

Dynamic height: A key variable for identifying the spawning habitat of small pelagic fishes

Rebecca G. Asch*, David M. Checkley Jr.

Scripps Institution of Oceanography, University of California San Diego, 9500 Gilman Drive, La Jolla, CA 92093-0208, USA

ARTICLE INFO

Article history:
Received 16 May 2012
Received in revised form
27 August 2012
Accepted 10 September 2012
Available online 19 September 2012

Keywords:
Dynamic height
Sea surface height
Spawning habitat
Pacific sardine
Northern anchovy
Jack mackerel
California Current

ABSTRACT

Small pelagic fishes off southern California exhibit interannual variations in the regions they occupy. An enhanced understanding of these fluctuations could improve fisheries management and predictions of fish's responses to climate change. We investigated dynamic height as a variable for identifying the spawning habitat of northern anchovy (*Engraulis mordax*), Pacific sardine (*Sardinops sagax*), and jack mackerel (*Trachurus symmetricus*). During cruises between 1998 and 2004, dynamic height was calculated from temperature and salinity profiles, while fish egg concentration was measured with obliquely towed bongo nets and the Continuous, Underway Fish Egg Sampler. Dynamic height ranged between 68 and 108 cm, with values increasing offshore. The greatest probability of encountering anchovy, sardine, and jack mackerel eggs occurred at dynamic heights of 79–83 cm, 84–89 cm, and 89–99 cm, respectively. Four mechanisms were proposed to explain how dynamic height affects egg distribution: (1) dynamic height is a proxy for upper water column temperature and salinity, which are known to influence spawning habitat. (2) Low dynamic heights are indicative of coastal upwelling, which increases primary and secondary productivity. (3) Egg concentration is greater at dynamic heights coincident with geostrophic currents that transport larvae to favorable habitats. (4) Eddies delineated by dynamic height contours retain eggs in productive habitats. To evaluate these mechanisms, a generalized linear model was constructed using dynamic height, temperature, salinity, chlorophyll, zooplankton volume, geostrophic currents, and eddies as independent variables. Dynamic height explained more variance than any other variable in models of sardine and anchovy spawning habitat. Together temperature, salinity, and chlorophyll accounted for 80–95% of the dynamic height effect, emphasizing the importance of the first two mechanisms. However, dynamic height remained statistically significant in the models of anchovy and jack mackerel spawning habitat after considering the effects of all other variables. Dynamic height shows promise as an ecological indicator of spawning habitat, because it integrates the effects of multiple oceanic variables, can be remotely sensed, and is predicted by ocean circulation models.

1. Introduction

Populations of Pacific sardine (*Sardinops sagax*) and northern anchovy (*Engraulis mordax*) exhibit decadal-scale fluctuations in abundance related to low-frequency climate oscillations (Schwartzlose et al., 1999; Chavez et al., 2003; Alheit et al., 2009). In the California Current Ecosystem (CCE), these changes in stock size have been accompanied by shifts in the geographic extent of the habitat occupied by these species (MacCall, 1990; Rodríguez-Sánchez et al., 2002). Examining spawning habitat may be propitious for gaining an understanding of how oceanic conditions influence these changes in fish distribution, since the early life history stages of fishes have a narrower tolerance to many environmental conditions than adults (Pörtner and Farrell, 2008).

Temperature has long been identified as a factor affecting sardine spawning habitat. Tibby (1937) first noted that Pacific sardine spawning was limited to temperatures $>13\,^{\circ}C$. While temperature can have a profound impact on fish physiology, several researchers have suggested that temperature may be a proxy for other environmental cues that more directly affect sardine (Fiedler, 1983; Jacobson and MacCall, 1995; Rodríguez-Sánchez et al., 2002). Consequently, recent research on spawning habitat of small pelagic fishes has focused on combinations of oceanic variables. Lluch-Belda et al. (1991) found sardines spawn across an array of temperatures, but their eggs only occur within a narrow range of upwelling. In contrast, the spawning habitat of anchovy corresponds to a narrower temperature range, but

* Corresponding author. Tel.: +1 617 697 8375; fax: +1 858 822 0562.
E-mail address: rgasch@ucsd.edu (R.G. Asch).

0967-0637/$ - see front matter © 2012 Elsevier Ltd. All rights reserved.
http://dx.doi.org/10.1016/j.dsr.2012.08.006

spawning occurs at both high and low upwelling. Checkley et al. (2000) observed that sardine and anchovy eggs are found in water masses with distinct temperatures and salinities. Weber and McClatchie (2010) modeled the relationship between sardine and anchovy eggs and a suite of biological and physical variables, including temperature, salinity, geostrophic flow, mean chlorophyll concentration, and depth of the chlorophyll maximum. Reiss et al. (2008) and Zwolinski et al. (2011) developed models using satellite observations of sea surface temperature (SST), ocean color, and gradients of sea surface height anomalies (SSHa) that accurately predicted seasonal and inter-annual changes in sardine and anchovy spawning area. Similarly, the boundaries of spawning habitat can be delineated by a combination of SST and zooplankton concentration for sardine (Lynn, 2003) and SST and chlorophyll concentration for anchovy (Fiedler, 1983).

One environmental variable related directly or indirectly to almost all of these predictors of spawning habitat is dynamic height. Dynamic height refers to hydrographically based measurements of sea surface height (SSH). Dynamic height is calculated from vertical profiles of temperature, salinity, and pressure that are integrated over the upper water column above a reference depth. In this manuscript, we will use the term dynamic height to specifically refer to these hydrographic measurements, whereas SSH will be used in a more general sense that includes observations from tide gauges and satellite altimetry. Since dynamic height and integrated water column density are inversely proportional (Pond and Pickard, 1995), areas with fresh, warm seawater correspond to high dynamic heights, whereas locations with salty, cool seawater have low dynamic heights. Gradients in dynamic height are also proportional to geostrophic current velocity. As a result, contours of dynamic height can be used to identify eddies and meanders (Soto-Mardones et al., 2004; Stegmann and Schwing, 2007). Seasonal patterns of dynamic height in the CCE are controlled by a combination of heating, cooling, and changes in current direction, with the first two processes exerting a greater influence in offshore areas and the effect of currents dominating in the coastal zone (Lynn and Simpson, 1987).

In the CCE, chlorophyll concentration is negatively correlated with SSH across both seasonal and interannual scales (Henson and Thomas, 2007; Venegas et al., 2008). Meandering SSH contours indicating the position of the California Current correspond to a boundary between eutrophic inshore waters with high chlorophyll and offshore waters that are more oligotrophic (Strub and James, 2000). Through bottom-up forcing, this relationship between phytoplankton biomass and SSH can exert an influence on zooplankton abundance (Chelton et al., 1982). Several mechanistic processes can explain these relationships. First, SSH is low where the thermocline shoals, bringing denser water closer to the surface. Since the thermocline and nutricline are frequently co-located, this is a mechanism through which surface nutrient flux can increase phytoplankton concentration in areas with low SSH (Wilson and Adamec, 2002). For example, areas with low SSH often demarcate coastal upwelling in the CCE (Kruse and Huyer, 1983). A second mechanism connecting biological productivity and SSH is transport of nutrients and organisms by currents. Strengthening of the California Current leads to increased zooplankton volume (Chelton et al., 1982) and a concurrent decrease in SSH due to the influx of cooler water (Logerwell et al., 2003). Third, eddies whose boundaries can be delineated by SSH contours are often characterized by increased primary production due to upwelling near their center. Closed circulation in eddies can retain and concentrate plankton (Mackas et al., 2005) and advect gradients in chlorophyll to new areas (Chelton et al., 2011).

The relationship between dynamic height and the spawning habitat of small pelagic fishes in the CCE has not been previously studied, although a few authors have examined the influence of closely related variables, such as indices of geostrophic flow (Weber and McClatchie, 2010; Zwolinski et al., 2011). Small pelagic species may exhibit different associations with dynamic height and geostrophic currents because spatial patterns differ between absolute values of SSH and gradients of this variable. Similarly, SSH and SSHa may display different geographic patterns and distinct relationships with fish spawning habitat, because spatial information is removed when subtracting mean values to calculate anomalies.

We hypothesize that the environmental conditions represented by dynamic height can account for spatial patterns in the spawning habitat of small pelagic fishes in the southern CCE. Secondly, we hypothesize that temporal variations in dynamic height explain interannual variability in the location and extent of spawning habitat. In addition to sardine and anchovy, we also examine the spawning habitat of jack mackerel (*Trachurus symmetricus*), which is an abundant, but poorly studied, species in the family Carangidae. Larvae of jack mackerel were the eighth most abundant ichthyoplankton species found between 1951 and 1998 in the southern CCE (Moser et al., 2001). The geographic distribution of jack mackerel spawning habitat has been previously studied (Farris, 1961; Ahlstrom, 1969; Ahlstrom and Stevens, 1976), but no research has explored linkages between environmental variables and their spawning habitat.

Since SSH typically varies by no more than ± 1 m globally (Stewart, 2008), it is unlikely that fishes can directly sense small differences in dynamic height across the $\sim$100-km scale of their spawning habitat. Instead, any dynamic height effect on spawning habitat could be due to dynamic height's role as an ecological indicator that incorporates the influence of multiple oceanic variables. In the second half of this manuscript, we assess the relative importance of four mechanisms that potentially explain how dynamic height affects spawning habitat:

- Mechanism 1: dynamic height is a proxy for integrated, upper water column temperature and salinity, factors known to influence the spawning habitat of small pelagic fishes.
- Mechanism 2: since low dynamic height is indicative of coastal upwelling in the CCE, increases in fish eggs at particular dynamic heights reflect an elevated concentration of planktonic prey for adult fish or early life history stages following upwelling.
- Mechanism 3: given that gradients of dynamic height influence the speed and direction of geostrophic flow, increases in fish eggs at particular dynamic heights reflect spawning in currents that transport larvae to favorable habitats.
- Mechanism 4: eddies delineated by dynamic height contours affect spawning habitat by retaining fish eggs in biologically productive areas.

2. Methods

2.1. Datasets

Fish eggs and hydrographic data were collected during April cruises between 1998 and 2004. All cruises were conducted by the California Cooperative Oceanic Fisheries Investigations (CalCOFI). Data from April were used because eggs of all three fish species were frequently observed this month (Moser et al., 2001). A subset of the CalCOFI time series from 1998 to 2004 was used because two independent measures of fish egg abundance (i.e., bongo net samples and the Continuous, Underway Fish Egg Sampler [CUFES]) were available these years. This period was sufficient for capturing interannual variability in egg distribution,

including extreme events observed during El Niño and La Niña. The area sampled included six CalCOFI transects (i.e., lines 76.7, 80.0, 83.3, 86.7, 90.0, and 93.3) in southern California, which extended offshore of the coastline between San Diego (33.0°N) and north of Point Conception (35.1°N; Fig. 1). During a limited number of years (i.e., 1998, 2003, and 2004), data were also available from CalCOFI transects 60.0–73.3, which encompassed the area in central California north of Morro Bay (35.6°N) to San Francisco Bay (37.8°N; Supplemental information, Section S1). Transects were separated by 72 km. Along transects, stations were spaced 36 km apart inshore of the continental slope and 72 km apart offshore.

The 3-m long bongo net used to collect fish eggs has two openings with a 0.71-m diameter and a mesh size of 505 μm (McGowan and Brown, 1966). This net was towed obliquely at a 45° angle to a depth of 210 m. Tow speed was ~0.5–1.0 m s^{-1} for a duration of ~20 min (Kramer et al., 1972). During 2004, only one station sampled with the bongo net was positive for sardine eggs. This reflects the fact that sardine spawning occurred principally in the central CCE during 2004 (Lo et al., 2010). Since measurements of habitat electivity would not be meaningful during a year when sardine eggs were nearly absent from our study region, bongo net data from 2004 were excluded from our investigation of sardine spawning habitat. This decision did not have a significant effect on the distribution of sardine eggs observed over the full period between 1998 and 2004 (Kolmogorov–Smirnov test: $D=0.008$, $p=1.000$). Also, patterns of dynamic height usage by sardine spawning in central California during this year closely resembled those typically observed in southern California (Supplemental information, Section S1).

CUFES collected fish eggs along CalCOFI transects while the research vessel was underway by pumping seawater through an intake at 3 m depth (Checkley et al., 1997). Seawater flowed through CUFES at ~0.5–1.0 m^3 min^{-1}. Fish eggs were concentrated and filtered through a 505-μm mesh. The sampling interval of CUFES was adjusted opportunistically depending on the abundance of fish eggs, but typically varied between 5 and 30 min (Checkley et al., 2000). The jack mackerel time series from CUFES starts in 1999,

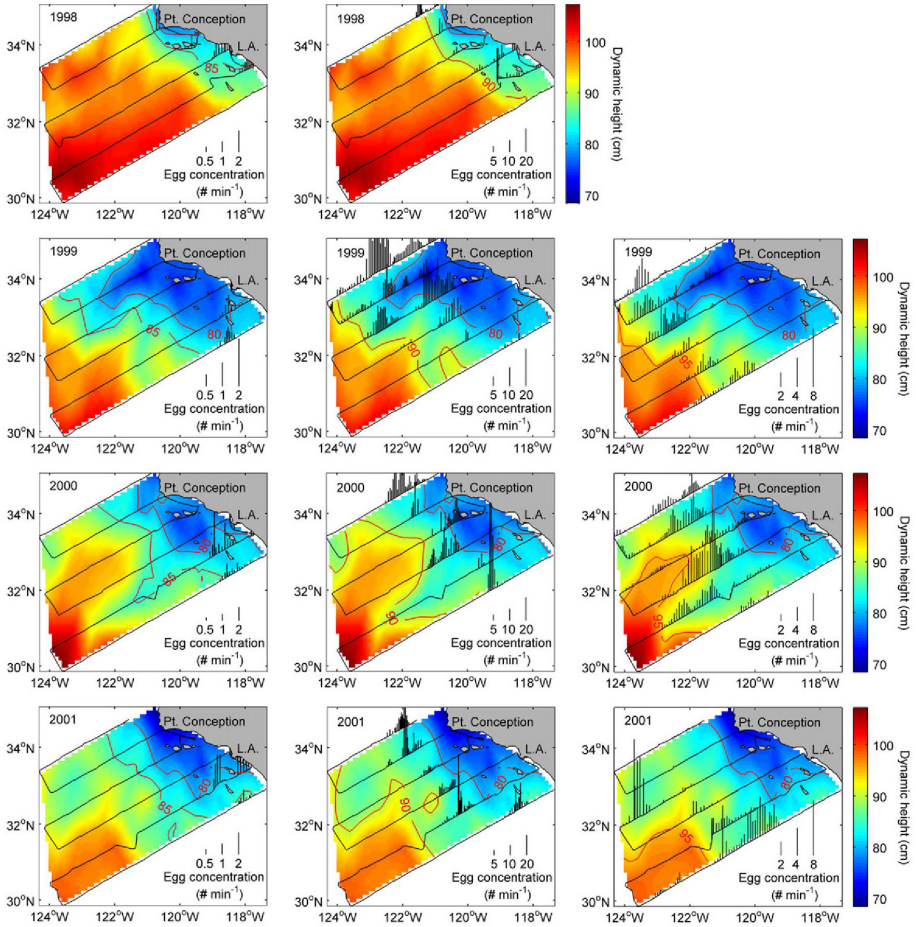

Fig. 1. Maps of the concentration of eggs of northern anchovy (left column), Pacific sardine (middle column), and jack mackerel (right column) between 1998 and 2001. Fish egg data are from spring Continuous, Underway Fish Egg Sampler (CUFES) surveys. The scale of egg concentration varies between years. Interpolated measurements of dynamic height are shown in the background of each map. Black lines show the research cruise track, while red lines indicate the range of dynamic height across which fish eggs of each species was most frequently observed. These ranges are 80–85 cm for anchovy, 80–90 cm for sardine, and 80–95 cm for jack mackerel.

because this species' eggs were not identified when CUFES surveys first began. Comparisons between CUFES and plankton nets have consistently demonstrated significant correlations between sampling methods (Checkley et al., 1997; Lo et al., 2001; Curtis, 2004; Planque et al., 2007). On average CUFES samples were collected every 5.3 km. Due to concerns about autocorrelation at this spatial scale (Supplemental information, Section S2), all statistical tests were performed on bongo net data. CUFES data were used solely for mapping egg distribution.

While eggs <1 day old provide the closest proxy for the distribution of spawning fishes, we used all egg data available from CUFES and bongo net tows to identify the location of spawning habitat for the following reasons: (1) while sardine eggs were aged during some CalCOFI cruises, ages were not recorded for anchovy and jack mackerel eggs (Kramer et al., 1972); (2) due to their extremely patchy distribution, early stages of sardine eggs tended to be under-sampled relative to later stages (Lo et al., 1996); (3) since fish eggs passively drifted in currents, they were advected along with water masses with approximately the same physical characteristics as where they were spawned, and; (4) studies of diffusion have indicated
that this process only disperses sardine and anchovy eggs hundreds to thousands of meters (Smith, 1973; Smith and Hewitt, 1985), a negligible distance relative to the scale of the CalCOFI grid.

Hydrographic data were collected concurrently at stations where the bongo net was deployed. Dynamic height of the surface, relative to 500 m, was derived from water samples obtained from a Niskin rosette, which recorded temperature and salinity to 500 m depth. Using the equation of state, seawater density and specific volume anomalies were calculated. Dynamic height was then computed by numerically integrating specific volume anomalies across pressures found between 0 and 500 m (Pond and Pickard, 1995). At stations with depths <500 m, linear extrapolation from adjacent sites was used to calculate the dynamic height relative to the 500 m reference level. For display purposes, data presented in maps of dynamic height were linearly interpolated to a 0.1° grid using MATLAB (The Mathworks, Inc., Natick, MA, USA).

Other environmental covariates examined to determine their relative influence on spawning habitat include temperature, salinity, chlorophyll concentration, zooplankton displacement volume, speed and direction of geostrophic currents, and the presence/absence of eddies. Data on temperature, salinity, and chlorophyll concentration were acquired from CalCOFI seawater samples from the Niskin rosette. Observations of temperature, salinity, and chlorophyll taken at 10-m intervals from the upper 50 m of the water column were averaged, because sardine and anchovy generally spawn at depths <50 m (Weber and McClatchie, 2010). The bongo net was deployed to obtain zooplankton displacement volume. We used zooplankton displacement volumes where gelatinous organisms with biovolumes $>5\ \mathrm{cm}^3$ were removed (Kramer et al., 1972). Chlorophyll concentration and zooplankton volume were $\log_{10}$ transformed prior to statistical analyses.

Geostrophic flow and the location of eddies were derived directly from calculated values of dynamic height from hydrographic measurements. Geostrophic velocity was calculated with the formulas $u=(-g/f)*(\partial H/\partial y)$ and $v=(g/f)*(\partial H/\partial x)$, where u and v are geostrophic flows in the x and y directions, respectively; g is the gravitational acceleration; f is the Coriolis parameter, and; H is the dynamic height (Stewart, 2008). Gradients of dynamic height were obtained by taking the difference between dynamic heights at adjacent stations along transects. The direction of geostrophic currents was described with a polar coordinate system in which 0° indicates eastward flow, 90° northward flow, 180° westward flow, and 270° (or -90°) southward flow.

We identified eddies with a method modified from Stegmann and Schwing (2007). Locations of eddies were delineated from closed contours of dynamic height separated by 2-cm intervals of dynamic height. If a potential eddy's boundaries extended beyond the edge of our study area, it was categorized as an eddy only if its dynamic height contour enclosed at least two-thirds of a circle. The extent of each eddy was defined based on the minimum and maximum latitude and longitude of closed dynamic height contours. Due to the spatial resolution of the CalCOFI grid, only mesoscale eddies could be reliably detected. Closed contours whose longest dimension was <42 km were not counted as eddies. This size limit corresponded to the smallest diameter of eddies identified in the CCE by Stegmann and Schwing (2007). Eddies were classified as cyclonic (counterclockwise) or anti-cyclonic (clockwise) depending on whether the dynamic height in their center was depressed or elevated, respectively. We identified 17 eddies during spring months between 1998 and 2004. Of these eddies, eight flowed in a cyclonic direction, while nine were anticyclonic.

2.2. Habitat electivity

Over the space and time domain of this study, dynamic height ranged from 68 to 108 cm. Quotient curves were constructed to assess whether eggs were observed at certain dynamic heights more frequently than expected if fishes spawned randomly (Drapeau, 2005). Data were binned into 2-cm dynamic height intervals. To ensure a minimum sample size per bin, any bin containing <8 observations was merged with a neighboring bin. A quotient was calculated by dividing the percent of total egg abundance in a bin by the percent of stations in the bin. To prevent artifacts due to sites with extremely high egg abundance, a three-point running mean was used to smooth quotient curves (Drapeau, 2005). Since offshore sites (CalCOFI station numbers ≥ 70) were principally outside the range where anchovy spawned (Fig. 1), they were excluded from analyses of habitat electivity for anchovy. Quotient curves were developed on a year-by-year basis and for the 7-year time series mean. If a quotient was >1, this indicated positive habitat electivity within a dynamic height interval. Positive electivity can reflect either active habitat selection by spawners or increased survival of eggs in an area. Conversely, quotients <1 suggested avoidance by spawning fish, high mortality of eggs, or recent hatching of eggs. Since there was some overlap between areas where each species exhibited positive electivity, we used Kolmogorov–Smirnov tests to detect significant differences between species in terms of the dynamic heights used. Empirical cumulative distribution functions (CDFs) for each species were graphed to visually portray these differences.

2.3. Generalized linear models

A generalized linear model (GLM) framework was employed to compare the relative influence of oceanic variables on spawning habitat and assess the merit of the four mechanisms proposed to explain why dynamic height affects fish egg distribution. This modeling approach was selected because quotient curves from this study and Lluch-Belda et al. (1991) showed that the frequency of fish egg occurrence often peaked across a distinct range of environmental variables that could be modeled as a quadratic function incorporated into a GLM. We used the presence/absence of eggs as the dependent variable in GLMs in order to model the full extent of areas where spawning occurred. Similar results were also obtained when GLMs were constructed with data on egg concentration (Supplemental information, Section S3). Independent variables in GLMs were selected to correspond to the four mechanisms hypothesized to explain

Table 1
Correlations between oceanographic variables measured during spring cruises between 1998 and 2004. $n=435$.

	Temperature	Salinity	Chlorophyll	Zooplankton volume	Geostrophic current speed	Geostrophic current direction
Dynamic height	0.87***	−0.51***	−0.85***	−0.77***	−0.18***	0.13**
Temperature		−0.34***	−0.82***	−0.77***	−0.19***	0.08
Salinity			0.42***	−0.30***	0.02	0.00
Chlorophyll				0.68***	0.19***	−0.05
Zooplankton volume					0.13**	−0.08
Geostrophic current speed						−0.06

The significance of the Pearson correlation coefficients is indicated as follows:
* $p<0.05$.
** $p<0.01$.
*** $p<0.001$.

how dynamic height influences spawning habitat. These independent variables included dynamic height, temperature (Mechanism 1), salinity (Mechanism 1), chlorophyll (Mechanism 2), zooplankton volume (Mechanism 2), speed and direction of geostrophic currents (Mechanism 3), and presence/absence of eddies (Mechanism 4). Prior to constructing GLMs, we examined the covariance structure between these variables using Pearson correlation coefficients. Both linear and quadratic terms were incorporated into GLMs. Eddies were the one exception to this, since they were treated as a categorical variable. Each bongo net sample was classified as originating from either an area with no eddies, a cyclonic eddy, or an anticyclonic eddy. The form of GLMs was effectively a logistic regression with a binomial distribution and logit link (McCullagh and Nelder, 1989). All GLMs were fit within the R programming environment, version 2.11.1 (R Foundation for Statistical Computing, Wien, Austria).

GLMs were varied in three ways to investigate distinct scientific questions. First, oceanic variables were examined in models individually to evaluate each variable's relative effect on the probability of encountering fish eggs. The peak probability of encountering fish eggs across the range of each variable was defined based on the area where the GLM exceeded 90% of its maximum value. Analysis of deviance tables were used to assess which variable(s) provided the best fit to egg presence/absence data (McCullagh and Nelder, 1989; Bolker, 2008). Significance of linear and quadratic terms in GLMs was examined with likelihood ratio tests (Bolker, 2008).

Second, a full model including all statistically significant oceanic variables and two-way interaction terms was developed to determine whether the effect of dynamic height on egg distribution remained significant after the influence of other variables was taken into account. Recognizing the fact that many oceanic variables covary spatially, we added the dynamic height term last to these GLMs. This was done because analysis of deviance evaluates the deviance of each term sequentially so that a deviance estimate indicates the variation accounted for by a corresponding variable after having eliminated the effects of all terms previously added to the GLM (McCullagh and Nelder, 1989). Any remaining deviance attributed to dynamic height represented the component of the dynamic height effect that could not be explained by other oceanic variables.

A forward, stepwise process was used to develop a third set of GLMs. These GLMs were employed to assess the mechanisms proposed to explain how dynamic height influences the spatial distribution of fish eggs. Again, dynamic height was added to the model last. After the addition of each term to the GLM, the percent reduction in the deviance attributed to dynamic height was calculated to determine how much each environmental variable contributed to the dynamic height effect. The stepwise addition of terms was ended when new terms no longer resulted in a decrease in the deviance of dynamic height or when there were no new statistically significant terms to add. Linear, quadratic, and two-way interaction terms were included in these GLMs. In addition, Section S4 of the Supplemental information presents results from forward, stepwise GLMs where the order in which variables were added to the model was varied to maximize the explanatory capacity of GLMs. However, due to the fact that many of the variables considered here spatially covary (Table 1), the predictive ability of the GLMs in Section S4 may be limited.

Dynamic height observations and bongo net samples of fish eggs from spring CalCOFI cruises during 2005–2008 were used to assess the predictive skill of GLMs that included only dynamic height. The observed percentage of bongo net tows from 2005 to 2008 containing eggs of sardine, anchovy, and jack mackerel was estimated in six dynamic height bins: <78.0 cm, 78.0–82.9 cm, 83.0–87.9 cm, 88.0–92.9 cm, 93.0–97.9 cm, and ≥ 98.0 cm. These intervals were selected so that each bin contained a minimum of 20 observations, resulting in a precision of at least 5% for estimates of the observed probability of fish eggs. A mean prediction was generated using the dynamic height GLM to estimate the probability of encountering eggs at the center of each bin. 95% confidence intervals for predictions were developed from the 2.5th and 97.5th percentiles of GLM predictions at the upper and lower edges of each bin. Prediction skill was assessed by performing a linear regression that compared the observed and predicted probabilities of encountering eggs between 2005 and 2008 (Zagaglia et al., 2004). Separate linear regressions were initially performed for each species. Since the slope and intercept of regressions did not significantly differ between species, we combined the regressions for all three species to increase sample size.

3. Results

3.1. Habitat electivity

Spring observations of dynamic height in the southern CCE ranged between 68 and 108 cm. Reflecting the equatorward flow along the California coast, low dynamic heights (75–80 cm) were usually observed nearshore, while high dynamic heights (95–105 cm) occurred offshore (Fig. 1). More specifically, cruise-wide minima and maxima of dynamic height were typically found around Point Conception and the southwestern extent of our study area, respectively. This likely reflected upwelling of cool, saline water off Point Conception and an influx of warm, subtropical water at the southwestern edge of the CalCOFI region. While a general onshore-offshore gradient in dynamic height was observed, the area was also characterized by meanders and eddies that altered this gradient. The location of the transition zone

between nearshore and offshore values of dynamic height varied substantially between years, as was exemplified by the 1998–1999 alternation between El Niño and La Niña. During the 1998 El Niño, the region with dynamic heights >95 cm expanded shoreward, whereas there was a large region with dynamic heights <80 cm in 1999 (Fig. 1).

We examined data from 449 bongo net samples from cruises between 1998 and 2004. Anchovy, sardine, and jack mackerel eggs were found in 22.3%, 22.9%, and 47.9% of samples, respectively. When egg distribution was overlaid on maps of dynamic height, it was evident that eggs of each species were most frequently observed in water masses characterized by particular dynamic heights (Fig. 1). 64.1% of sardine eggs were distributed throughout waters with dynamic heights between 80 and 90 cm. When dynamic heights within this range contracted shoreward in 1998 and 2003, sardine eggs were found closer to the coast. During years when dynamic heights between 80 and 90 cm covered an extensive offshore area (1999 and 2002), the distribution of sardine eggs also expanded offshore. Compared to sardine, anchovy eggs were less abundant, distributed closer to shore, and most frequently observed within the southern CalCOFI area. 47.0% of anchovy eggs originated from dynamic heights between 80 and 85 cm. During 1999, 2000, and 2001, areas with peak concentrations of anchovy eggs roughly tracked the 80-cm dynamic height contour (Fig. 1). Jack mackerel eggs were located farther offshore than other species. 63.7% of jack mackerel eggs occurred within water with dynamic heights between 80 and 95 cm (Fig. 1). During several years (1999, 2000, and 2002), the inshore or offshore distribution of jack mackerel eggs traced the path of meandering currents indicated by dynamic height contours.

Quotient curves were used to examine whether spawning fishes inhabited certain dynamic heights at a disproportionately high frequency. When data from all cruises were analyzed jointly, quotient curves indicated that anchovy, sardine, and jack mackerel displayed positive spawning habitat electivity at dynamic heights of 78–86 cm, 79–88 cm, and 84–99 cm, respectively. During most years, the quotient curve for sardine eggs peaked at intermediate dynamic heights in between the maximum of the quotient curves for anchovy and jack mackerel eggs (Fig. 2). Exceptions to this pattern occurred in 2000 and 2003 when there was a high degree of overlap between the anchovy and sardine quotient curves. Also, peaks in spawning habitat electivity for sardine and jack mackerel were observed at similar dynamic heights in 2002.

Since there was a large overlap between dynamic heights used by anchovy and sardine when spawning, a Kolmogorov–Smirnov test was performed to detect differences in the CDFs of these species with respect to dynamic height. These tests found significant differences between the CDFs of all species (anchovy-sardine comparison: $D=0.38$, $p<0.001$; sardine-jack mackerel comparison: $D=0.32$, $p<0.001$; anchovy-jack mackerel comparison: $D=0.59$, $p<0.001$). Empirical CDFs in Fig. 3 show that anchovy favored slightly lower dynamic heights than sardine during spawning, while jack mackerel eggs were found at higher dynamic heights. Similar preferred ranges of dynamic height were observed amongst sardine and jack mackerel spawning in central California (Table S1; Fig. S1a).

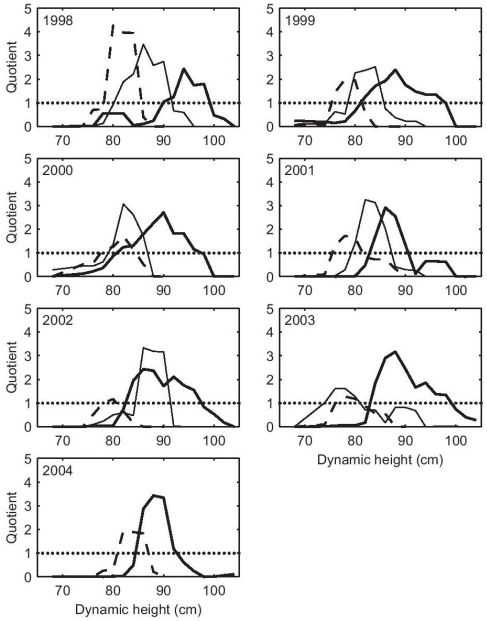

Fig. 2. Annual quotient curves showing the range of dynamic height that northern anchovy (dashed line), Pacific sardine (solid line), and jack mackerel (thick, solid line) prefer to inhabit during spawning. Quotient curves are based on the three-point running mean of quotients calculated for 2-cm intervals of dynamic height. The dotted line in each subplot denotes a quotient of 1. Quotients above 1 represent dynamic heights where there is a higher concentration of eggs than would be expected if egg distribution were random. Quotients less than 1 are either areas avoided by fishes when spawning, areas with low survival of eggs, or areas where eggs recently hatched. Due to the near absence of sardine eggs from the study area in 2004, a quotient curve was not calculated for sardine in this year.

3.2. Generalized linear models

Prior to constructing GLMs, we examined correlations between dynamic height, temperature, salinity, chlorophyll, zooplankton volume, and geostrophic currents to better understand the relationship between these variables. All correlations were significant at $p<0.05$, with the exception of those between salinity and geostrophic current speed, and between geostrophic current direction and temperature, salinity, chlorophyll, zooplankton volume, and geostrophic current speed (Table 1). To correct for the accumulation of type I error due to performing multiple tests, we also evaluated correlations between variables using the Bonferroni method to lower the α at which tests would be

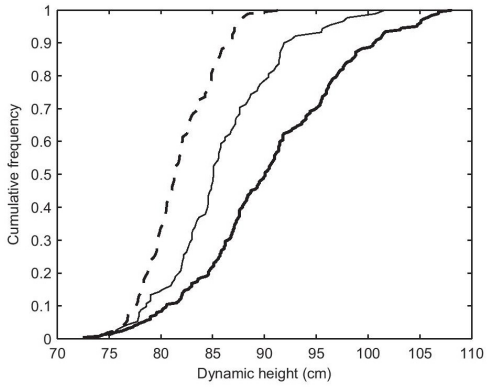

Fig. 3. Empirical cumulative distribution functions (CDFs) of the dynamic heights across which the eggs of northern anchovy, Pacific sardine, and jack mackerel were observed. Lines representing each species are the same as in Fig. 2. Kolmogorov–Smirnov tests indicate that all empirical CDFs were significantly different from each other ($D\geq 0.32$, $p<0.001$).

considered significant ($n=21$, $\alpha_{Bonferroni}=0.002$; Sokal and Rohlf, 1995). Following this correction, the correlations between geostrophic current speed and zooplankton volume and between geostrophic current direction and dynamic height were no longer significant. In order of the decreasing strength of correlations, elevated dynamic height was associated with warmer temperatures, lower chlorophyll, reduced zooplankton volume, lower salinity, and slower geostrophic currents.

In GLMs where each variable was examined individually, model fit was significant in all cases except for the effects of zooplankton volume on sardine, geostrophic current direction on jack mackerel, geostrophic current speed on sardine and jack mackerel, and eddies on all species (Table 2). The majority of GLMs exhibited significant quadratic terms indicating that the probability of encountering eggs was maximized across a specific range of each variable. GLM results were fairly consistent with quotient curves in terms of identifying dynamic heights where the probability of encountering eggs was maximized. The greatest probabilities of fish eggs occurred at dynamic heights of 79–83 cm, 84–89 cm, and 89–99 cm for anchovy, sardine, and jack mackerel, respectively (Fig. 4; Table S3).

Since many oceanic variables displayed cross-shelf gradients and each species typically spawned at different distances from shore, several relationships between fish eggs and environmental variables could be interpreted in terms of these gradients. For example, the maximum probability of anchovy and sardine eggs occurred at 12.0–13.9 °C due to the influence of cool water associated with coastal upwelling (Fig. 4; Table S3). Jack mackerel eggs located farther offshore peaked at warmer temperatures of 13.5–15.6 °C. Salinities <33.2 were found offshore in the relatively fresh water of the California Current (Checkley et al., 2000), whereas nearshore areas were characterized by higher salinities from subsurface water upwelled along the coast. Jack mackerel tended to spawn within the California Current as demonstrated by their preference for waters with salinity <33.1, while anchovy eggs were most frequently observed in coastal areas with salinities of 33.5–33.75. The presence of sardine eggs was greatest at intermediate salinities of 33.0–33.4. The maximum probability of anchovy, sardine, and jack mackerel eggs occurred at chlorophyll concentrations of 1.2–3.9 mg m^{-3}, 0.6–2.2 mg m^{-3}, and <0.5 mg m^{-3}, respectively. Again, this reflected the lower concentration of chlorophyll in offshore waters occupied by jack mackerel when spawning. Maps of chlorophyll concentration revealed that areas where chlorophyll dropped below 0.3 mg m^{-3} closely coincided with the locations of the 90- or 95-cm contours of dynamic height (Fig. S3). Jack mackerel eggs were most commonly observed in offshore areas with <46 cm^3 of zooplankton per 1000 m^3 of seawater strained. The peak probabilities of anchovy eggs (78–264 cm^3/1000 m^3) coincided with biologically richer waters containing greater concentrations of zooplankton.

The direction of geostrophic currents was largely bi-directional with the vast majority of observations indicative of the southeastward flow of the California Current ($-30°$) and a second, but much smaller, mode indicative of northeastward flow (60°). The probability of sardine eggs was maximal at $<-42°$ (Fig. 4; Table S3), suggesting this species spawns in southerly flow of the California Current. Anchovy eggs occurred most often in currents flowing east or northeast ($-6°$ to 23°). The probability of finding anchovy eggs also peaked in the regions with the fastest geostrophic currents (>80 cm s^{-1}). This preference to spawn in fast-flowing, eastward currents could help maintain anchovy eggs and larvae in coastal areas during planktonic life stages.

The relative influence of each oceanic variable on the presence/absence of fish eggs was evaluated with analysis of deviance (Table 2). Dynamic height explained more deviance than any other environmental variable in models of sardine and anchovy eggs. This result implied that dynamic height was not solely a proxy for another variable, even though it was strongly correlated with several oceanic processes. Dynamic height also exhibited a strong

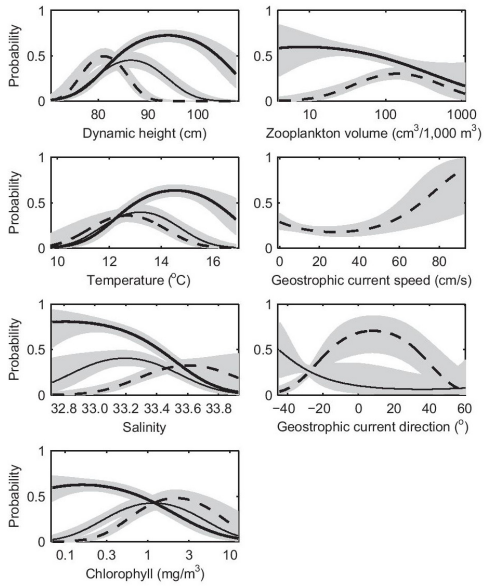

Fig. 4. Probability of encountering fish eggs based on predictions of generalized linear models (GLMs). Each GLM was constructed using a single, independent variable, which is displayed on the *x*-axis of each graph. Lines representing each species are the same as in Fig. 2. 95% confidence intervals are shown in grey. Graphs of GLM results are not included here if neither linear nor quadratic terms were significant at $p<0.05$.

Table 2
Deviance explained by generalized linear models (GLMs) examining the presence/absence of fish eggs. The effect of independent variables was tested individually using quadratic and linear terms. The one exception to this was the "eddies" term, which was incorporated into GLMs as a categorical variable. In the full model, dynamic height was added to the model following the inclusion of all other statistically significant independent variables and interaction terms. Therefore, the deviance explained by dynamic height in the full model is the remaining effect of dynamic height on the presence/absence of fish eggs after accounting for the effects of all other oceanographic factors. Significance levels in GLMs are indicated as follows: $^{*}p<0.05$; $^{**}p<0.01$; $^{***}p<0.001$. The number of asterisks corresponds to the most significant term in a GLM, which could be either linear or quadratic.

Independent variables	Anchovy ($n=435$)	Sardine ($n=378$)	Jack mackerel ($n=435$)
	Deviance		
Dynamic height	119.9^{c***}	48.9^{c***}	82.5^{c***}
Temperature	41.9^{c***}	30.6^{c***}	52.3^{c***}
Salinity	35.4^{c***}	22.9^{c***}	90.5^{c***}
Chlorophyll	81.6^{c***}	36.6^{c***}	54.7^{c***}
Zooplankton volume	19.3^{c**}	4.5	12.9^{a***}
Geostrophic current speed	9.1^{b**}	2.8	0.6
Geostrophic current direction	20.3^{b***}	9.2^{a**}	5.7
Eddies	4.7	0.6	3.7
Dynamic height in full model	33.6^{c***}	1.7	11.8^{b***}

[a] Linear term significant at $p<0.05$.
[b] Quadratic term significant at $p<0.05$.
[c] Linear and quadratic terms significant at $p<0.05$.

influence on the distribution of jack mackerel eggs, but more deviance was explained by salinity for this species. For sardine and anchovy, chlorophyll consistently had the second greatest effect on egg distribution, followed by temperature and salinity. Generally, zooplankton volume, geostrophic current direction and speed, and eddies had weaker effects on egg presence/absence than other variables.

Next, we assessed the deviance explained by dynamic height when it was added last to a GLM including all statistically significant environmental variables and interaction terms. A significant interaction between temperature and chlorophyll was included in this full model GLM for all three species, whereas anchovy and sardine both exhibited significant temperature × salinity and salinity × chlorophyll interactions. In addition, the distribution of anchovy and jack mackerel eggs was affected by significant temperature × zooplankton volume and chlorophyll × zooplankton volume interactions. For anchovy and jack mackerel eggs, the effect of dynamic height remained significant at $p < 0.001$ in the full model, although the deviance it explained was reduced (Table 2). This suggested that the combined effect of environmental variables could only partially explain the impact of dynamic height on egg distribution of these species. In contrast, dynamic height no longer had a significant effect on sardine egg distribution once all other variables were taken into account (Table 2).

Similarly, the forward, stepwise GLMs for anchovy and jack mackerel revealed a decrease in the deviance explained by dynamic height following the addition of model terms, although the overall effect of dynamic height remained significant at $p < 0.01$ (Table 3). By the time the final variable was added to the stepwise GLMs for anchovy and jack mackerel, the deviance explained by dynamic height was reduced by 82–91% of its original value. The influence of dynamic height on sardine egg distribution could be completely accounted for by other oceanic variables in the stepwise GLM, causing dynamic height to become non-significant when added last to this model (Table 3).

Table 3
Stepwise generalized linear models (GLMs) used to evaluate which oceanographic variables accounted for the effect of dynamic height on the spatial distribution of fish eggs. Terms were added to the regression model in a forward, step-wise fashion, such that dynamic height was always added last. Deviance refers to the amount of variability in the model explained by dynamic height. The last column refers to the percentage by which the deviance explained by dynamic height decreased as new terms were added to the regression. Significance of dynamic height in GLMs is indicated as follows: $^{*}p < 0.05$; $^{**}p < 0.01$; $^{***}p < 0.001$. The number of asterisks corresponds to the most significant dynamic height term, which could be either linear or quadratic.

Model step	Variable added	Deviance	%
Anchovy			
1	Dynamic height	119.9[b]***	0.0
2	Chlorophyll	41.7[b]***	65.3
3	Salinity	33.5[a]***	72.1
4	Temperature	27.1[b]***	77.4
5	Chlorophyll × salinity	24.2[b]***	79.8
6	Geostrophic current speed	22.1[b]***	81.6
Sardine			
1	Dynamic height	48.9[b]***	0.0
2	Temperature	24.7[a]***	49.4
3	Salinity	17.4[b]**	64.3
4	Chlorophyll	6.0**	87.7
5	Temperature × salinity	2.5	95.0
6	Geostrophic current direction	2.2	95.5
Jack mackerel			
1	Dynamic height	82.5[b]***	0.0
2	Salinity	14.9[b]**	82.0
3	Temperature	7.3[a]**	91.1

[a] Quadratic effect of dynamic height significant at $p < 0.05$.
[b] Linear and quadratic effects of dynamic height significant at $p < 0.05$.

In models of all species, temperature, salinity, chlorophyll, and their interactions collectively accounted for 80–95% of the dynamic height effect. Geostrophic current speed or direction was included in the stepwise GLMs of anchovy and sardine eggs, but explained little of the deviance ($\leq 1.8\%$) originally attributed to dynamic height. The eddy and zooplankton volume terms were not incorporated into any stepwise GLM.

At the 261 CalCOFI stations sampled between 2005 and 2008, dynamic height ranged between 70 and 106 cm, indicating that there had been little change in this variable since 1998–2004 when its range extended between 68 and 108 cm. However, between 1998–2004 and 2005–2008 the probability of encountering eggs increased from 22.9% to 37.9% for sardine and from 22.3% to 42.5% for anchovy. Concurrently, the probability of jack mackerel eggs dropped from 47.9% to 36.4%. These changes affected the probability of sampling fish eggs in each dynamic height bin, but did not alter the general pattern in which the peak probability of encountering eggs occurred at low dynamic heights for anchovy (78–83 cm), intermediate dynamic heights for sardine (83–88 cm), and elevated dynamic height for jack mackerel (88–93 cm) during 2005–2008 (Fig. 5). Thus, GLMs provided robust predictions of the spatial distribution of eggs in any given year and the dynamic heights favored by spawning fishes, but could not predict interannual variations in the mean probability of encountering eggs. This may reflect differences between realized and potential spawning habitat, where realized spawning habitat is more strongly affected by interannual and seasonal variations in spawning stock biomass (SSB; Planque et al., 2007). Our model predictions correspond to Planque et al.'s definition of potential spawning habitat, while the observations from 2005 to 2008 describe realized spawning habitat.

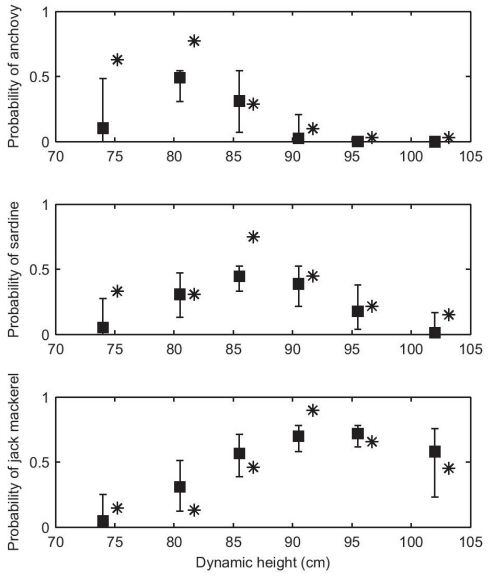

Fig. 5. Predicted probability of encountering fish eggs within binned intervals of dynamic height during the years 2005–2008. Black squares indicate the mean predicted probability of encountering eggs at the center of bins, while error bars denote 95% confidence intervals at the edges of each bin. Predictions are based on generalized linear models originally developed with data from 1998-2004. Asterisks show the observed percent of bongo net samples from 2005 to 2008 that contained fish eggs within each dynamic height bin. In these graphs, the asterisks have been offset by 1.2 cm from the bin centers so that predictions and observations can be viewed at the same time.

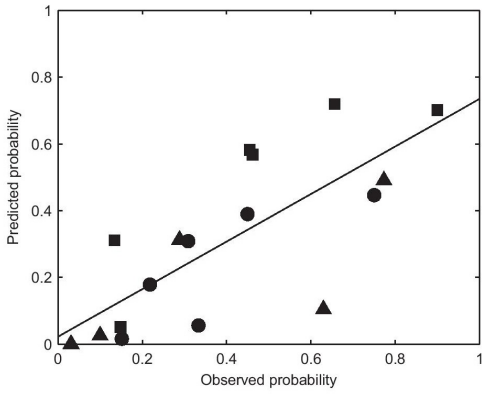

Fig. 6. Linear regression comparing the predicted and observed probability of encountering fish eggs during the spring cruises between 2005 and 2008. Predictions are based on generalized linear models originally developed with data from 1998-2004. Since regression coefficients did not significantly differ between species, data on all three species of fishes have been pooled. Triangles, circles, and squares denote observations of anchovy, sardine, and jack mackerel eggs, respectively. Linear regression formula: $Y=0.0225+0.7119X$, $r^2=0.60$, $p=0.0002$.

Similar results were attained from the linear regression that compared GLM predictions to the observed probability of encountering eggs between 2005 and 2008 (Fig. 6; $r^2=0.60$, $F=23.6$, $n=18$, $p<0.001$). The regression intercept (0.02, 95% confidence interval: -0.12 to 0.17) was not significantly different from zero, while its slope (0.71, 95% confidence interval: 0.40–1.02) did not differ from one. This implied that there was essentially a 1:1 relationship between observed and predicted probabilities. However, the predictions slightly underestimated the probability of encountering eggs due to changes between time periods described above.

4. Discussion

4.1. Influence of dynamic height on spawning habitat

Each species of small pelagic fish in the CCE exhibited positive spawning habitat electivity across a range of dynamic heights where they were sited at a disproportionately high frequency. This range differed among species, with spawning sardine favoring intermediate dynamic heights relative to anchovy and jack mackerel. Our results indicate that dynamic height was the single best oceanic variable for identifying the spawning habitat of anchovy and sardine. SSH has also been linked to variations in the distribution, abundance, or recruitment of fishes, squid, and seabirds in the California Current, Northwest Pacific, and equatorial Atlantic (Logerwell et al., 2003; Zagaglia et al., 2004; Schirripa and Colbert, 2006; Yen et al., 2006; Laidig et al., 2007; Zainuddin et al., 2008; Chen et al., 2009; Wei et al., 2009; Zwolinski et al., 2011). Like our study, several of these papers reported that SSH explained more variability in the distribution, abundance, or survival of species than any other oceanic variable examined (Logerwell et al., 2003; Schirripa and Colbert, 2006; Yen et al., 2006; Zainuddin et al., 2008; Chen et al., 2009). This suggests that the influence of SSH on habitat suitability is widespread.

Across our study area of several 100 km, it is unlikely that fishes can directly sense small gradients in sea level ($\sim$40 cm along CalCOFI transects). Therefore, we proposed four mechanisms to explain how the relationship between dynamic height and other oceanic variables could give rise to the apparent influence of dynamic height on fish egg distribution. These mechanisms are that fishes may preferentially spawn in water masses with a certain temperature or salinity (Mechanism 1), elevated primary and secondary productivity (Mechanism 2), geostrophic currents with a specific direction or speed (Mechanism 3), and eddies that increase retention of ichthyoplankton (Mechanism 4). Evaluation of these mechanisms using GLMs indicated that together the first two mechanisms explained $\geq$80% of the influence of dynamic height on spawning habitat, while $\leq$1.8% could be attributed to the latter two mechanisms (Table 3). This suggests that dynamic height affects egg distribution via a combination of fish spawning in areas with optimal temperatures for their growth and survival and adequate primary production to provide prey for adult fish and/or larvae. In addition to temperature and chlorophyll, spatial variations in dynamic height reflect changes in salinity, which are indicative of distinct water masses that may contain different concentrations of ichthyoplankton. Since no single variable could completely account for the dynamic height effect on spawning habitat, we conclude that dynamic height functions as an ecological indicator that is able to incorporate the influence of multiple oceanic processes. In this way, dynamic height is similar to the Simpson–Hunter stratification parameter, temperature–salinity diagrams, and spiciness, which are all oceanic indices that integrate two or more physical processes and directly or indirectly affect the distribution of fish eggs and larvae (Iles and Sinclair, 1982; Checkley et al., 2000; Sakuma et al., 2007).

Our analysis demonstrates that anchovy, sardine, and jack mackerel spawn in areas characterized by different dynamic heights (Figs. 2 and 3). Use of distinct spawning habitats may be indicative of niche partitioning between these species, where anchovy primarily spawn in coastal waters, jack mackerel reside in the offshore waters of the California Current when spawning, and sardine use the transition zone between these habitats (Fig. 1). Since water mass characteristics (i.e., temperature and salinity) and primary production explained much of the dynamic height effect on spawning habitat, these factors may also contribute to niche differentiation among these species. In waters off Japan, congeners of these three species have distinct niches based on their optimal temperatures for maximizing growth (Takasuka et al., 2007; Takasuka et al., 2008). In addition, the niches of anchovy and sardine can be distinguished based on the size spectrum of their prey. The gill rakers of anchovy are specialized for filter feeding on larger plankters that occur in areas dominated by coastal upwelling. Finer spacing between the gill rakers of sardine allow them to retain smaller plankters found in areas farther offshore where curl-driven upwelling predominates (Rykaczewski and Checkley, 2008). The diet of jack mackerel is also distinct from sardine (Carlisle, 1971). Lastly, these species may possibly use dissimilar spawning habitats to prevent competitive exclusion. However, given their distinct dietary and temperature preferences, competition between these species may be minimal.

While our results from the GLMs highlight the importance of Mechanism 2, it is noteworthy that zooplankton volume was never included in stepwise GLMs where dynamic height was added last (Table 3). This implies that, although low dynamic height is indicative of upwelling and increased primary production, this analysis did not attribute any of the dynamic height effect on egg distribution to spatial variations in secondary production. This was unforeseen since mesozooplankton abundance in the CCE sharply decreases coincident with large gradients of dynamic height (Lynn, 2003). The weak effect of zooplankton volume could reflect the ambiguous ecological role of this indicator. Zooplankton volume is a bulk measure of the abundance of myriad species belonging to diverse functional

groups. Variations in species composition make it difficult to interpret the meaning of changes in zooplankton volume. It is often assumed that high zooplankton volume denotes increased prey for planktivorous fishes (Lynn, 2003), but some authors have identified negative correlations between zooplankton and the egg distribution and recruitment of sardine (Checkley et al., 2000; Agostini et al., 2007). These negative correlations have been attributed to increases in predatory zooplankton that consume fish larvae and eggs. Furthermore, spatial and temporal variations in zooplankton volume do not correspond to fluctuations in the carbon biomass of zooplankton (Lavaniegos and Ohman, 2007). This is because displacement volume is often dominated by gelatinous organisms with low carbon content and little nutritional value.

Based on GLM results, neither geostrophic currents nor eddies explained much of the influence of dynamic height on fish egg distribution. This may reflect the spatial resolution of the CalCOFI grid, since the gradients in dynamic height used to derive geostrophic currents are more precisely measured when observations are spaced over smaller intervals. The relatively coarse scale of the CalCOFI grid is adequate for detecting mean flow in the California Current, nearshore countercurrent flow, large meanders, and mesoscale eddies. However, smaller scale jets and filaments could not be identified. Similarly, only 1–2 bongo net samples were obtained within many eddies due to the spatial resolution of the CalCOFI grid. The scarcity of bongo net samples in eddies may have prevented us from being able to use GLMs to accurately attribute how much of the dynamic height effect was related to fishes spawning in eddies. Nevertheless, an examination of eddy effects using finer resolution CUFES data suggested that sardine, anchovy, and jack mackerel eggs were more abundant in areas outside eddies than within cyclonic eddies, possibly due to high predation within productive eddies. This analysis using CUFES was inevitably affected by autocorrelation, but the fact that neither the bongo net nor CUFES datasets indicated a tendency for fishes to spawn in eddies implies that the results of GLMs were not strongly influenced by spatial scale.

An advantage of using SSH as an indicator of spawning habitat is that it can be remotely sensed by altimetry. Unlike in situ surveys, remote sensing can provide a synoptic view of a region, sample an area more frequently than ships, and provide higher spatial resolution. Despite these advantages of satellite data, there may be greater coherence between fish egg distribution and in situ measurements of dynamic height, because they can be collected concurrently. Contemporaneous sampling is especially important given that the egg stage of small pelagic fishes lasts only 2–4 days at temperatures in the southern CCE (Zweifel and Lasker, 1976), while satellite altimeters record SSH over a 7- to 10-day repeat cycle. The reliability of altimetry data is also reduced within 50 km of land (Martin, 2004), which could constrain the use of altimetry for identifying the habitat of coastal fish. In addition, there are subtle, but important, differences between remotely sensed SSH and SSHa. Remotely sensed sea level anomalies from the Archiving, Validation, and Interpretation of Satellite Oceanographic (AVISO) data project are calculated relative to the mean SSH between 1993 and 1999 observed in a single pixel. Since mean SSH differs between pixels, a spatial component of the altimetry dataset is removed in calculating anomalies. Consequently, certain oceanic features, such as mesoscale eddies, become more apparent in SSHa data than SSH observations (Fig. 7b and c). However, other features, such as onshore-offshore gradients, become obscured in the SSHa dataset (Fig. 7c). While similar circulation patterns can be seen in CalCOFI dynamic height measurements and AVISO SSH (Fig. 7a and b), many of these shared features are not detectable in maps of SSHa. A similar pattern emerged from correlations between dynamic height during April CalCOFI cruises

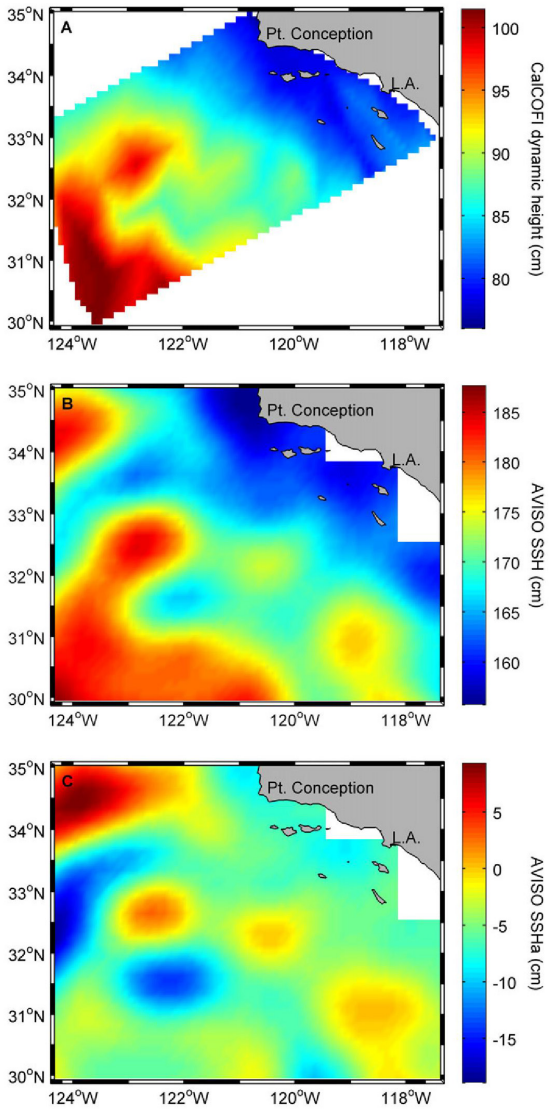

Fig. 7. Maps of (A) dynamic height from California Cooperative Oceanic Fisheries Investigations (CalCOFI), (B) sea surface height (SSH) from the Archiving, Validation, and Interpretation of Satellite Oceanographic (AVISO) data project, and (C) AVISO SSH anomalies (SSHa) from March 27-April 12, 2002. Data have been interpolated onto a 0.1° grid to facilitate comparisons between remotely sensed and in situ observations with different native, spatial resolutions.

from 1998 to 2008 and concurrent AVISO SSH and SSHa observations. Dynamic height and SSH were closely correlated ($r=0.93$, $p<0.001$, d.f.$=658$), while a weaker correlation between dynamic height and SSHa was detected ($r=0.49$, $p<0.001$, d.f.$=658$). Use of dynamic height versus SSHa may explain the differing results of the present study and Zwolinski et al. (2011), who found SSHa gradients to have a relatively weak effect on sardine spawning habitat.

4.2. Interannual variability in spawning habitat

Interannual variability in spawning habitat evident in Figs. 1 and 2 can be attributed to two factors. First, variations in spawning habitat reflect changes in oceanic conditions. During our study, this was exemplified by the El Niño events of 1998 and 2002/2003. Sea level in California is positively correlated with the strength of El Niño with a lag of 3–4 months (Chelton et al., 1982). During El Niño, coastal upwelling is reduced and the thermocline deepens in the CCE (McPhaden et al., 2006). Consequently, coastal waters become warmer and fresher, leading to increased dynamic height. This was evident in 1998 when dynamic heights >95 cm expanded shoreward while the region with dynamic heights <80 cm contracted (Fig. 1). This pattern recurred in 2002/2003, albeit to a much lesser extent since this was a weaker El Niño whose beginning and end roughly coincided with timing of the 2002 and 2003 spring cruises, respectively (NOAA Climate Prediction Center, 2012). These changes reduced the extent of areas with low dynamic height, forcing fishes that favor these habitats to either spawn in other regions, which may be suboptimal, or increase their density in remaining areas. Spawning sardine and jack mackerel responded to the 1998 El Niño via the first strategy since peaks in their quotient curves occurred at slightly higher dynamic heights than normal (Fig. 2). Anchovy utilized the second strategy since they remained in areas with low dynamic heights but exhibited greater spawning habitat electivity than usual in 1998. Song et al. (2012) observed a similar pattern, noting that sardine eggs were more concentrated in recently upwelled waters during El Niño.

Second, the size of a fish stock can influence the extent of its spawning habitat in a given year. As proposed by the basin model (MacCall, 1990), increased stock size may lead to density-dependent declines in habitat quality. In response, fish either occupy new waters that previously displayed lower habitat electivity or the density of fish may increase in areas with the highest electivity. An example of this was observed in 2005–2008 when the frequency of anchovy eggs increased to 42.5% compared to earlier years when eggs occurred at 22.3% of sites. While a stock assessment for anchovy has not been conducted since 1995 (Jacobson et al., 1995), this increased frequency of anchovy eggs is likely due to growth of this species' SSB. This growth was not accompanied by a major change in the dynamic heights used by anchovy when spawning (Fig. 5). Instead, the distribution of anchovy eggs expanded northward, occupying a larger portion of the region with dynamic heights <83 cm. While this finding is in accordance with the basin model, a more definitive test of this model requires data from a larger proportion of anchovy's range (i.e., British Columbia to Baja California).

4.3. Other oceanic variables that affect spawning habitat

The novelty of our study rests in that it is the first to identify in situ measurements of dynamic height as an important variable influencing the spawning habitat of sardine and anchovy. However, we also used to GLMs to model the effect of several other oceanographic variables on the spawning habitat of small pelagic fishes. The ranges of temperature, salinity, chlorophyll concentration, zooplankton volume, and geostrophic currents preferred by spawning anchovy and sardine in our GLMs were generally similar those detected in previous studies (Fiedler, 1983; Lluch-Belda et al., 1991; Checkley et al., 2000; Lynn, 2003; Reiss et al., 2008; Weber and McClatchie, 2010; Zwolinski et al., 2011), although one noteworthy exception is discussed below.

Unique biological communities develop in eddies due to retention of planktonic organisms, upwelling in cyclonic eddies, and transport of coastal species offshore. Anchovy eggs are occasionally found offshore in eddies with similar characteristics to the nearshore habitats where they usually spawn (Fiedler, 1986). Also, abundance and production of late-stage sardine larvae can be extremely high in offshore, cyclonic eddies (Logerwell and Smith, 2001; Logerwell et al., 2001). In contrast to these studies, our results did not detect a significant effect of cyclonic or anticyclonic eddies on the presence/absence of fish eggs. This does not contradict Logerwell and Smith (2001) because our work examines a different life history stage of sardine. Our results suggest that sardine do not preferentially spawn in eddies, but late-stage larvae could still become concentrated in eddies due to retention and/or reduced mortality. Also, uplift of water in the eddy center can concentrate larvae (Nishimoto and Washburn, 2002; Mackas et al., 2005), but the time scale of this process may be too slow to affect the short-lived egg stage. While Fiedler (1986) demonstrates that anchovy eggs may sometimes become concentrated in eddies, this author documented an unusual event that does not occur regularly.

Of the three species examined, jack mackerel has been the least studied, with no prior research identifying how environmental factors affect where it spawns in the CCE. Based on GLMs, jack mackerel spawning habitat includes oceanic regions characterized by high springtime dynamic height (89–99 cm), warm temperatures (13.5–15.6 °C), low salinity (<33.1), and reduced biomass of phytoplankton (<0.5 mg m^{-3} of chlorophyll) and zooplankton (<46 $cm^3/1000$ m^3 strained). Salinity played the largest role in determining which regions were likely to contain jack mackerel eggs (Table 2). The prevalence of jack mackerel eggs in salinities <33.2 suggests that this species spawns in the main California Current, which can be delineated by salinity within this range (Checkley et al., 2000). Chilean jack mackerel (*T. murphyi*), a congener of this species, exhibits similar habitat requirements, spawning in oceanic waters with warm temperatures (Arcos et al., 2001).

5. Conclusions

Dynamic height was the single best oceanic variable for identifying spawning habitat of anchovy and sardine. Each species of small pelagic fish in the CCE exhibited positive spawning habitat electivity across different dynamic heights, indicating that they spawn in distinct portions of the environment, albeit with some partial overlap. In accordance with our initial hypothesis, interannual variability in the extent of each species' preferred range of dynamic height explained year-to-year fluctuations in spawning habitat location. The skill of dynamic height GLMs when making predictions for 2005–2008 demonstrated that spawning habitat preferences remained stable across distinct time periods. The influence of dynamic height on these species' spawning habitat can be largely attributed to the combined effects of temperature, salinity, and chlorophyll on fish egg distribution. Spatial variations in zooplankton volume, geostrophic flow, and eddies accounted for relatively little of the dynamic height effect on spawning habitat.

Spawning habitat models could potentially be used to predict shifts in fish egg distribution due to climate change, assuming the current relationship between spawning habitat and environmental variables remains constant. Climate-induced changes in the latitude and depth inhabited by fishes have been observed in many ecosystems (Beare et al., 2004; Perry et al., 2005; Hsieh et al., 2008, 2009; Nye et al., 2009). These changes are expected to accelerate under future climate change scenarios. One obstacle related to predicting changes in fish distribution is that many models of ocean dynamics, including the widely used Regional Ocean Modeling System (ROMS), are skillful at forecasting physical oceanographic conditions, but are not able to model biological variables with comparable accuracy. In light of this, the relationship between dynamic height and

spawning habitat may be particularly propitious because ROMS and other ocean general circulation models routinely output estimates of SSH.

Improved understanding of the relationship between small pelagic fishes and environmental variables may be useful for transitioning from single species fisheries management to ecosystem-based fisheries management. Sardine is one of the few species whose stock assessment has explicitly considered the effect of environmental variability, since the running mean of SST from the Scripps Pier has been used to determine the fraction of SSB to be harvested (Jacobson and MacCall, 1995; Hill et al., 2011). Recently the reliability of Scripps Pier SST for predicting the recruitment success of sardine has been challenged (McClatchie et al., 2010). Therefore, this may be the right time to examine how other environmental variables could be incorporated into the management of small pelagic fishes. Dynamic height could be useful to consider within this context, because it is linked to a variety of oceanic processes, including fluctuations in temperature, salinity, biological productivity, geostrophic flow, and eddies. Two ways in which dynamic height could be used in fisheries management are: (1) remotely sensed observations of SSH could help identify regions with a potentially high concentration of fish eggs prior to annual egg surveys. Data from these surveys are used as fisheries-independent input to the sardine stock assessment. Knowledge of environmental influences on spawning habitat can increase the efficiency of these surveys by allowing researchers to target areas where eggs are abundant (Fiedler, 1983; Zwolinski et al., 2011). (2) The Magnuson–Stevens Fishery Conservation and Management Act requires that essential fish habitat (EFH) be identified for commercially fished species. Currently, EFH for coastal pelagic species in the CCE is defined based on the 10 °C isotherm (PFMC, 1998). Since dynamic height has a greater influence on the spawning habitat of anchovy and sardine than temperature, this variable may be useful for refining EFH. SSH may also be helpful for delineating fish habitat in regions with a dearth of oceanographic data given that it can be remotely sensed and influences the distribution of a variety of species.

Acknowledgments

This research was funded by a grant from the U.S. Integrated Ocean Observing System (IOOS; No. NA17RJ1231). The NSF IGERT Grant no. 0333444 and the Nancy Foster Scholarship Program supported RGA. We are indebted to the many scientists and crewmembers who collected and processed data from CalCOFI cruises. J. Rodgers-Wolgast provided assistance with calculating the dynamic height relative to 500 m at shallow stations. We appreciate guidance from N. Lo, E. Weber, and J. Zwolinski regarding spatial autocorrelation. M. Kahru offered helpful advice about how to delineate the extent of eddies. Suggestions from D. Cayan, P. Franks, J.A. Koslow, M. Lindegren, S. McClatchie, M. Ohman, M. Priede, R. Rykaczewski, and two anonymous reviewers also improved this manuscript.

Appendix A. Supporting information

Supplementary data associated with this article can be found in the online version at http://dx.doi.org/10.1016/j.dsr.2012.08.006.

References

Agostini, V.N., Bakun, A., Francis, R.C., 2007. Larval stage controls on Pacific sardine recruitment variability: high zooplankton abundance linked to poor reproductive success. Mar. Ecol. Prog. Ser. 345, 237–244.

Ahlstrom, E.H., 1969. Distributional Atlas of Fish Larvae in the California Current Region: Jack Mackerel, *Trachurus symmetricus*, and Pacific Hake, *Merluccius productus*, 1951–1959 CalCOFI Atlas no. 11. Southwest Fisheries Science Center, La Jolla, CA.

Ahlstrom, E.H., Stevens, E., 1976. Report of neuston (surface) collections made on an extended CalCOFI cruise during May 1972. Calif. Coop Ocean. Fish. Invest. Rep. 18, 167–180.

Alheit, J., Roy, C., Kifani, S., 2009. Decadal-scale variability in populations. In: Checkley, D., Alheit, J., Oozeki, Y., Roy, C. (Eds.), Climate Change and Small Pelagic Fish. Cambridge University Press, Cambridge, UK, pp. 281–304.

Arcos, D.F., Cubillos, L.A., Núñez, S.P., 2001. The jack mackerel fishery and El Niño 1997–98 effects off Chile. Prog. Oceanogr. 49, 597–617.

Beare, D.J., Burns, F., Greig, A., Jones, E.G., Peach, K., Kienzle, M., McKenzie, E., Reid, D.G., 2004. Long-term increases in prevalence of North Sea fishes having southern biogeographic affinities. Mar. Ecol. Prog. Ser. 284, 269–278.

Bolker, B.M., 2008. Ecological Models and Data in R. Princeton University Press, Princeton, NJ.

Carlisle Jr., J.G., 1971. Food of the jack mackerel, *Trachurus symmetricus*. Calif. Fish Game 57, 205–208.

Chavez, F.P., Ryan, J., Lluch-Cota, S.E., Ñiquen, M.C., 2003. From anchovies to sardines and back: multidecadal change in the Pacific Ocean. Science 299, 217–221.

Checkley Jr., D.M., Ortner, P.B., Settle, L.R., Cummings, S.R., 1997. A continuous, underway fish egg sampler. Fish. Oceanogr. 6 (2), 58–73.

Checkley Jr., D.M., Dotson, R.C., Griffin, D.A., 2000. Continuous, underway sampling of eggs of Pacific sardine (*Sardinops sagax*) and northern anchovy (*Engraulis mordax*) in spring 1996 and 1997 off southern and central California. Deep-Sea Res. II 47, 1139–1155.

Chelton, D.B., Bernal, P.A., McGowan, J.A., 1982. Large-scale interannual physical and biological interaction in the California Current. J. Mar. Res. 40 (4), 1095–1126.

Chelton, D.B., Gaube, P., Schlax, M.G., Early, J.J., Samuelson, R.M., 2011. The influence of nonlinear mesoscale eddies on near-surface oceanic chlorophyll. Science 334, 328–332.

Chen, X., Li, G., Feng, B., Tian, S., 2009. Habitat suitability index of chub mackerel (*Scomber japonicus*) from July to September in the East China Sea. J. Oceanogr. 65, 93–102.

Curtis, K.A., 2004. Fine scale spatial pattern of Pacific sardine (*Sardinops sagax*) and northern anchovy (*Engraulis mordax*) eggs. Fish. Oceanogr. 13 (4), 239–254.

Drapeau, L., 2005. Introduction to the use of quotient curves for characterizing spawning habitat of small, pelagic fish. In: van der Lingen, C.D., Castro, L., Drapeau, L., Checkley Jr., D. (Eds.), Report of a GLOBEC/SPACC Workshop on Characterizing and Comparing the Spawning Habitat of Small Pelagic Fish, GLOBEC Report no. 21. GLOBEC. International Project Office, Plymouth, UK, pp. 5–6.

Farris, D.A., 1961. Abundance and distribution of eggs and larvae and survival of larvae of jack mackerel (*Trachurus symmetricus*). Fish. Bull. 61, 247–279.

Fiedler, P.C., 1983. Satellite remote sensing of the habitat of spawning anchovy in the Southern California Bight. Calif. Coop. Ocean. Fish. Invest. Rep. 24, 202–209.

Fiedler, P.C., 1986. Offshore entrainment of anchovy spawning habitat, eggs, and larvae by a displaced eddy in 1985. Calif. Coop. Ocean. Fish. Invest. Rep. 27, 144–152.

Henson, S.A., Thomas, A.C., 2007. Phytoplankton scales of variability in the California Current System: 2. Latitudinal variability. J. Geophys. Res. 112, C070818, http://dx.doi.org/10.1029/2006JC004040.

Hill, K.T., Crone, P.R., Lo, N.C.H., Macewicz, B.J., Dorval, E., McDaniel, J.D., Gu, Y., 2011. Assessment of the Pacific Sardine Resource in 2011 for U.S. Management in 2012 NOAA National Marine Fisheries Service. Southwest Fisheries Science Center, La Jolla, CA.

Hsieh, C.-H., Reiss, C.S., Hewitt, R.P., Sugihara, G., 2008. Spatial analysis shows that fishing enhances the climatic sensitivity of marine fishes. Can. J. Fish. Aquat. Sci. 65, 947–961.

Hsieh, C.-H., Kim, H.J., Watson, W., Di Lorenzo, E., Sugihara, G., 2009. Climate-driven changes in abundance and distribution of larvae of oceanic fishes in the southern California region. Global Change Biol. 15, 2137–2152.

Iles, T.D., Sinclair, M., 1982. Atlantic herring: stock discreteness and abundance. Nature 215 (4533), 627–633.

Jacobson, L.D., MacCall, A.D., 1995. Stock-recruitment models for Pacific sardine (*Sardinops sagax*). Can. J. Fish. Aquat. Sci. 52, 566–577.

Jacobson, L.D., Lo, N.C.H., Herrick Jr., S.F., Bishop, T., 1995. Spawning Biomass of the Northern Anchovy in 1995 and Status of the Coastal Pelagic Fishery during 1994. Southwest Fisheries Science Center Administrative Report, LJ-95-12. National Marine Fisheries Service. Southwest Fisheries Science Center, La Jolla, CA.

Kramer, D., Kalin, M.J., Stevens, E.G., Thrailkill, J.R., Zweifel, J.R., 1972. Collecting and Processing Data on Fish Eggs and Larvae in the California Current Region. NOAA Technical Report NMFS CIRC-370. National Oceanic and Atmospheric Administration. National Marine Fisheries Service, Seattle, WA.

Kruse, G.H., Huyer, A., 1983. Relationships among shelf temperatures, coastal sea level, and coastal upwelling index off Newport, Oregon. Can. J. Fish. Aquat. Sci. 40, 238–242.

Laidig, T.E., Chess, J.R., Howard, D.F., 2007. Relationship between abundance of juvenile rockfishes (*Sebastes* spp.) and environmental variables documented off northern California and potential mechanisms for the variation. Fish. Bull. 105, 39–48.

Lavaniegos, B.E., Ohman, M.D., 2007. Coherence of long-term variations of zooplankton in two sectors of the California Current System. Prog. Oceanogr. 75, 42–69.

Lluch-Belda, D., Lluch-Cota, D.B., Hernandez-Vazquez, S., Salinas-Zavala, C.A., Schwartzlose, R.A., 1991. Sardine and anchovy spawning as related to temperature and upwelling in the California current System. Calif. Coop. Ocean. Fish. Invest. Rep. 32, 105–111.

Lo, N.C.H., Green Ruiz, Y.A., Jacob Cervantes, M., Moser, H.G., Lynn, R.J., 1996. Egg production and spawning biomass of Pacific sardine (*Sardinops sagax*) in 1994, determined by the daily egg production method. Calif. Coop. Ocean. Fish. Invest. Rep. 37, 160–174.

Lo, N.C.H., Hunter, J.R., Charter, R., 2001. Use of a continuous egg sampler for ichthyoplankton surveys: application to the estimation of daily egg production of Pacific sardine (*Sardinops sagax*) off California. Fish. Bull. 99, 554–571.

Lo, N.C.H., Macewicz, B.J., Griffith, D.A., 2010. Biomass and reproduction of Pacific sardine (*Sardinops sagax*) off the Pacific northwestern United States, 2003–2005. Fish. Bull. 108 (2), 174–192.

Logerwell, E.A., Smith, P.E., 2001. Mesoscale eddies and survival of late stage Pacific sardine (*Sardinops sagax*) larvae. Fish. Oceanogr. 10 (1), 13–25.

Logerwell, E.A., Lavaniegos, B., Smith, P.E., 2001. Spatially-explicit bioenergetics of Pacific sardine in the Southern California Bight: are mesoscale eddies areas of exceptional prerecruit production? Prog. Oceanogr 49, 391–406.

Logerwell, E.A., Mantua, N., Lawson, P.W., Francis, R.C., Agostini, V.N., 2003. Tracking environmental processes in the coastal zone for understanding and predicting Oregon coho (*Oncorhynchus kisutch*) marine survival. Fish. Oceanogr. 12 (6), 554–568.

Lynn, R., 2003. Variability in the spawning habitat of Pacific sardine (*Sardinops sagax*) off southern and central California. Fish. Oceanogr. 12 (6), 541–553.

Lynn, R.J., Simpson, J.J., 1987. The California Current system: the seasonal variability of its physical characteristics. J. Geophys. Res. 92 (C12), 12,947–12,966.

MacCall, A.D., 1990. Dynamic Geography of Marine Fish Populations. University of Washington Press, Seattle, WA.

Mackas, D.L., Tsurumi, M., Galbraith, M.D., Yelland, D.R., 2005. Zooplankton distribution and dynamics in a North Pacific Eddy of coastal original: II. Mechanisms of eddy colonization by and retention of offshore species. Deep-Sea Res. II 52, 1011–1035.

Martin, S., 2004. An Introduction to Ocean Remote Sensing. Cambridge University Press, Cambridge, UK.

McClatchie, S., Goericke, R., Auad, G., Hill, K., 2010. Re-assessment of the stock-recruit and temperature-recruit relationships for Pacific sardine (*Sardinops sagax*). Can. J. Fish. Aquat. Sci. 67, 1782–1790.

McCullagh, P., Nelder, J.A., 1989. Generalized linear models, second ed.Monographs on Statistics and Applied Probability, vol. 37. Chapman and Hall, New York, NY.

McGowan, J.A., Brown, D.M., 1966. A new opening-closed paired zooplankton net. Bull. Scripps Inst. Oceanogr. 66 (23), 1–56.

McPhaden, M.J., Zebiak, S.E., Glantz, M.H., 2006. ENSO as an integrating concept in earth science. Science 314, 1740–1745.

Moser, H.G., Charter, R.L., Smith, P.E., Ambrose, D.A., Watson, W., Charter, S.R., Sandknop, E.M., 2001. Distributional Atlas of Fish Larvae and Eggs in the Southern California Bight Region: 1951–1998. CalCOFI Atlas no. 34. Southwest Fisheries Science Center, La Jolla, CA..

Nishimoto, M.M., Washburn, L., 2002. Patterns of coastal eddy circulation and abundance of pelagic juvenile fish in the Santa Barbara Channel, California, USA. Mar. Ecol. Prog. Ser. 241, 183–199.

NOAA Climate Prediction Center, 2012. Oceanic Niño Index. NOAA, National Centers for Environmental Prediction, Climate Prediction Center, Camp Springs, MD. Available from: 〈http://www.cpc.ncep.noaa.gov/products/analysis_monitoring/ensostuff/ensoyears.shtml〉. (accessed 22.04.12).

Nye, J.A., Link, J.S., Hare, J.A., Overholtz, W.J., 2009. Changing spatial distribution of fish stocks in relation to climate and population size on the Northeast United States continental shelf. Mar. Ecol. Prog. Ser. 393, 111–129.

Perry, A.L., Low, P.J., Ellis, J.R., Reynolds, J.D., 2005. Climate change and distribution shifts in marine fishes. Science 308, 1912–1915.

PFMC (Pacific Fishery Management Council), 1998. Coastal Pelagic Species Fishery Management Plan. Pacific Fishery Management Council, Portland, OR.

Planque, B., Bellier, E., Lazure, P., 2007. Modelling potential spawning habitat of sardine (*Sardina pilchardus*) and anchovy (*Engraulis encrasicolus*) in the Bay of Biscay. Fish. Oceanogr. 16 (1), 16–30.

Pond, S., Pickard, G.L., 1995. Introductory Dynamic Oceanography, second ed. Butterworth Heinemann, Oxford, UK.

Pörtner, H.O., Farrell, A.P., 2008. Physiology and climate change. Science 322, 690–692.

Reiss, C.S., Checkley Jr., D.M., Bograd, S.J., 2008. Remotely sensed spawning habitat of Pacific sardine (*Sardinops sagax*) and Northern anchovy (*Engraulis mordax*) within the California Current. Fish. Oceanogr. 17 (2), 126–136.

Rodríguez-Sánchez, R., Lluch-Belda, D., Villalobos, H., Ortega-García, S., 2002. Dynamic geography of small pelagic fish populations in the California Current System on the regime time scale (1931–1997). Can. J. Fish. Aquat. Sci. 59, 1980–1988.

Rykaczewski, R.R., Checkley Jr., D.M., 2008. Influence of ocean winds on the pelagic ecosystem in upwelling regions. Proc. Nat. Acad. Sci. USA 105 (6), 1965–1970.

Sakuma, K.M., Ralston, S., Roberts, D.A., 2007. High-frequency patterns in abundance of larval Pacific hake, *Merluccius productus*, and rockfish, *Sebastes* spp., at a single fixed station off central California. Fish. Oceanogr. 16 (4), 383–394.

Schirripa, M.J., Colbert, J.J., 2006. Interannual changes in sablefish (*Anoploma fimbria*) recruitment in relation to oceanographic conditions within the California Current System. Fish. Oceanogr. 15 (1), 25–36.

Schwartzlose, R.A., Alheit, J., Bakun, A., Baumgartner, T.R., Cloete, R., Crawford, R.J.M., Fletcher, W.J., Green-Ruiz, Y., Hagen, E., Kawasaki, T., Lluch-Belda, D., Lluch-Cota, S.E., MacCall, A.D., Matsuura, Y., Nevárez-Martínez, M.O., Parrish, R.H., Roy, C., Serra, R., Shust, K.V., Ward, M.N., Zuzunaga, J.Z., 1999. Worldwide large-scale fluctuations of sardine and anchovy populations. S. Afr. J. Mar. Sci. 21, 289–347.

Smith, P.E., 1973. The mortality and dispersal of sardine eggs and larvae. Rapp. P.-V. Réun. Cons. Int. Explor. Mer. 164, 282–292.

Smith, P.E., Hewitt, R.P., 1985. Anchovy egg dispersal and mortality as inferred from close-interval observations. Calif. Coop. Ocean. Fish. Invest. Rep. 26, 97–110.

Sokal, R., Rohlf, F.J., 1995. Biometry, third ed. W.H. Freeman and Company, New York, NY.

Song, H., Miller, A.J., McClatchie, S., Weber, E.D., Nieto, K.M., Checkley Jr., D.M., 2012. Application of a data-assimilation model to variability of Pacific sardine spawning and survivor habitats with ENSO in the California Current System. J. Geophys. Res. 117, C03009, http://dx.doi.org/10.1029/2011JC007302.

Soto-Mardones, L., Parés-Sierra, A., Garcia, J., Durazo, R., Hormazabal, S., 2004. Analysis of the mesoscale structure in the IMECOCAL region (off Baja California) form hydrographic, ADCP and altimetry data. Deep-Sea Res. II 51, 785–798.

Stegmann, P.M., Schwing, F., 2007. Demographics of mesoscale eddies in the California Current. Geophys. Res. Lett. 34, L14602, http://dx.doi.org/10.1029/2007GL029504.

Stewart, R.H., 2008. Introduction to Physical Oceanography. Texas A & M University, College Station, TX. Available from: 〈http://oceanworld.tamu.edu/resources/ocng_textbook/contents.html〉. (accessed 22.04.12).

Strub, P.T., James, C., 2000. Altimeter-derived variability of surface velocities in the California Current System: 2. Seasonal circulation and eddy statistics. Deep-Sea Res. II 47, 831–870.

Takasuka, A., Oozeki, Y., Aoki, I., 2007. Optimal growth temperature hypothesis: why do anchovy flourish and sardine collapse or vice versa under the same ocean regime? Can J. Fish. Aquat. Sci. 64, 768–776.

Takasuka, A., Oozeki, Y., Kubota, H., 2008. Multi-species regime shifts reflected in spawning temperature optima of small pelagic fish in the western North Pacific. Mar. Ecol. Prog. Ser. 360, 211–217.

Tibby, R.B., 1937. The relation between surface water temperature and the distribution of spawn of the California sardine (*Sardinops caerulea*). Calif. Fish Game 23, 132–137.

Venegas, R.M., Strub, P.T., Beier, E., Letelier, R., Thomas, A.C., Cowles, T., James, C., Soto-Mardones, L., Cabrera, C., 2008. Satellite-derived variability in chlorophyll, wind stress, sea surface height, and temperature in the northern California Current System. J. Geophys. Res. 113, C03015, http://dx.doi.org/10.1029/2007JC004481.

Weber, E.D., McClatchie, S., 2010. Predictive models of northern anchovy *Engraulis mordax* and Pacific sardine *Sardinops sagax* spawning habitat in the California Current. Mar. Ecol. Prog. Ser. 406, 251–263.

Wei, F., Yumei, W., Xuesen, C., 2009. The study on fishing ground of neon flying squid, *Ommastrephes bartrami*, and ocean environment based on remote sensing data in the Northwest Pacific Ocean. Chin. J. Oceanol. Limnol. 27 (2), 408–414.

Wilson, C., Adamec, D., 2002. A global view of bio-physical coupling from SeaWiFS and TOPEX satellite data, 1997–2001. Geophys. Res. Lett. 29 (8), 1257, http://dx.doi.org/10.1029/2001GL014063.

Yen, P.P.W., Sydeman, W.J., Bograd, S.J., Hyrenbach, K.D., 2006. Spring-time distributions of migratory marine birds in the southern California Current: oceanic eddy associations and coastal habitat hotspots over 17 years. Deep-Sea Res. II 53, 399–418.

Zagaglia, C.R., Lorenzzetti, J.A., Stech, J.L., 2004. Remote sensing data and longline catches of yellowfin tuna (*Thunnus albacares*) in the equatorial Atlantic. Remote Sens. Environ. 93, 267–282.

Zainuddin, M., Saitoh, K., Saitoh, S., 2008. Albacore (*Thunnus alalunga*) fishing ground in relation to oceanographic conditions in the western North Pacific Ocean using remotely sensed satellite data. Fish. Oceanogr. 17 (2), 61–73.

Zweifel, J.R., Lasker, R., 1976. Prehatch and posthatch growth of fishes—a general model. Fish. Bull. 74 (3), 609–621.

Zwolinski, J.P., Emmett, R.L., Demer, D.A., 2011. Predicting habitat to optimize sampling of Pacific sardine (*Sardinops sagax*). ICES J. Mar. Sci. 68 (5), 867–879.

Chapter 2, in full, is a reprint of the material as it appears in: Asch, R.G. and D.M. Checkley, Jr. 2013. Dynamic height: A key variable for identifying the spawning habitat of small pelagic fishes. *Deep-Sea Research I* 71: 79-91. The dissertation author was the primary investigator and author of this paper.

CHAPTER 2 APPENDIX:

SUPPLEMENTAL INFORMATION FOR THE MANUSCRIPT *DYNAMIC HEIGHT: A KEY VARIABLE FOR IDENTIFYING THE SPAWNING HABITAT OF SMALL PELAGIC FISHES*

S1. Sampling in the Central California Region

CTD profiles, bongo net tows, and samples from the Continuous, Underway Fish Egg Sampler (CUFES) were available from central California during California Cooperative Oceanic Fisheries Investigations (CalCOFI) cruises in April of 1998, 2003, and 2004. The latter two years surveyed the area between CalCOFI transects 60.0-73.3 [San Francisco Bay (37.8° N) to north of Morro Bay (35.6° N)], whereas only transects 66.7-73.3 [Monterey Bay (36.8° N) to north of Morro Bay] were sampled in 1998. A total of 72 bongo net tows and 82 CTD casts were conducted in this region. With these data, we constructed empirical cumulative distribution functions (CDFs) to examine the range of dynamic heights inhabited by northern anchovy (*Engraulis mordax*), Pacific sardine (*Sardinops sagax*), and jack mackerel (*Trachurus symmetricus*) when spawning in central California. We also used χ^2 goodness-of-fit tests to evaluate the statistical significance of habitat electivity in both southern and central California. Separate tests were performed for each region. For the χ^2 tests, data were binned into four 10-cm intervals of dynamic height. These intervals differed slightly between southern and central California, reflecting the distribution of dynamic height in each region. Expected frequencies for χ^2 tests were calculated assuming that fish spawned randomly across dynamic heights drawn from the observed distribution in each region. Offshore habitats were excluded when computing the expected frequency of anchovy eggs, since these habitats were outside the normal range of spawning anchovy. Similarly, the expected frequencies of eggs used in χ^2 tests for central California excluded dynamic heights from years when a particular species did not occur in this region (i.e., 2003 for anchovy and jack mackerel).

During the years surveyed, dynamic height ranged between 43-97 cm in central California. This lower range of dynamic heights relative to southern California likely reflected both cooler temperatures in these more northerly waters and increased intensity of upwelling. Central and northern California have been characterized as the regions within the California Current Ecosystem (CCE) with maximal upwelling (Parrish *et al*., 1981). As was the case in southern California, sardine eggs were primarily found in regions with intermediate dynamic heights (80-90 cm), while anchovy and jack mackerel eggs occupied areas with lower (70-85 cm) and higher (85-95 cm) dynamic heights, respectively (Fig. S2.1a). Compared to equivalent empirical CDFs from southern California (Fig. 2.3), the tails of the CDFs from central California were shifted towards lower dynamic heights due to the greater availability of these low dynamic height habitats in this region and the scarcity of areas with dynamic heights exceeding 95 cm.

The statistical significance of habitat electivity with respect to dynamic height was evaluated with χ^2 goodness-of-fit tests. These tests were significant at $p < 0.05$ for sardine and jack mackerel in both regions of California (Table S2.1). The χ^2 tests also indicated that each of these species exhibited similar patterns of habitat electivity when spawning in southern and central California. Jack mackerel eggs were observed at a disproportionately high frequency at dynamic heights of 90-100 cm, but this species eschewed areas with low dynamic heights (70-80 cm) when spawning. In both south and central California, the only dynamic height interval across which sardine exhibited positive spawning habitat electivity was 80-90 cm (Table S2.1). In southern California, residuals from χ^2 tests indicated that anchovy eggs also occurred more frequently than expected at dynamic heights between 80-90 cm and less frequently at higher dynamic

heights. In contrast, χ^2 tests for anchovy in central California were not statistically significant. This may reflect the fact that anchovy eggs were relatively rare in central California, occurring in only 11 of the bongo net tows from this region. The scarcity of anchovy eggs may have reduced the statistical power of the χ^2 test.

During April 2004, sardine eggs were largely absent throughout southern California, but were abundant along CalCOFI transects surveyed in central California (Lo *et al*., 2010). Despite this change in geographic distribution, sardine continued to spawn across the same range of dynamic height. Quotient curves constructed for the central California region indicated that sardine displayed positive spawning habitat electivity across dynamic heights of 79-87 cm in 2004. This is very similar to the average range of dynamic heights (79-88 cm) across which sardine eggs exhibited positive electivity in southern California based on quotients curves.

S2. Spatial Scale of Autocorrelation

While the fine-scale resolution of CUFES (mean resolution = 5.3 km) may be advantageous for identifying spatial patterns, it can also lead to autocorrelation between adjacent samples. Due to the lack of independence between autocorrelated observations, most statistical tests will reject a null hypothesis more often than the nominal tolerance value α when data are autocorrelated (Legendre and Legendre, 1998; Ciannelli *et al*., 2007). Previous research on Pacific sardine has shown that autocorrelation of fish egg concentration occurs across spatial scales < 22 km (Lo *et al*., 2001). This indicates that

sardine data collected by CUFES would be autocorrelated, but no autocorrelation would be evident at the larger sampling intervals of the bongo net.

Since no previous information on the maximum spatial extent of autocorrelation exists for northern anchovy and jack mackerel eggs in the CCE, we constructed isotropic variograms of these species using CUFES data from the year 2000. This year was chosen because it was the first year in our time series when spatial patterns were not altered by El Niño or La Niña. To ensure that fish egg data were normally distributed, egg concentration was transformed using the natural logarithm and sites that did not contain eggs were removed from the dataset. The latter step was taken because otherwise an excessive number of zero counts would prevent the data from displaying a Gaussian distribution. Since anchovy eggs were typically absent from offshore regions (i.e., CalCOFI station numbers ≥ 70; Fig. 2.1), these sites were excluded from the variogram constructed for this species. Pairs of CUFES samples separated by a Euclidean distance h were grouped into 5-km bins. The semivariance (γ) of each bin was calculated with the following formula:

$$\gamma(h) = \frac{1}{2|N(h)|}\sum_{N(h)}(z_i - z_j)^2, \quad \text{(S1)}$$

where $N(h)$ is the set of pairwise Euclidean distances h, $|N(h)|$ is the number of pairs in $N(h)$, and z_i and z_j are fish egg concentrations at locations i and j (Kaluzny *et al*., 1998). Only bins containing a minimum of 30 pairs of observations and whose value was less than half of the maximum lag h were used because calculations of $\gamma(h)$ become increasingly variable at large lags and in bins with a small number of observations

(Kaluzny *et al*., 1998). Empirical variograms were produced by graphing lags h against $\gamma(h)$, while theoretical variograms were fitted with a spherical model.

In variograms of anchovy and jack mackerel eggs, the semivariance initially increased as a function of distance between CUFES samples, but eventually reached an asymptote (Fig. S2.2). The distance corresponding to this asymptote is known as the range and is indicative of the maximum spatial scale of autocorrelation. Other parameters estimated to fit a theoretical variogram were the sill and nugget, which refer to the semivariance at the asymptote and at a lag distance of zero, respectively. For anchovy eggs, the range was estimated to be 48 km, while the semivariance of the nugget and sill were 0.33 and 2.49, respectively (Fig. S2.2a). The spherical variogram model for anchovy had an r^2 of 0.47. Based on the range estimated by the theoretical variogram, the scale of autocorrelation for anchovy eggs is much larger than the resolution of the CUFES data (i.e., 5.3 km) and in between the resolution of the nearshore and offshore CalCOFI grid (i.e., 36 and 72 km, respectively). Since anchovy eggs were rarely found offshore, the nearshore CalCOFI grid was the most relevant scale for this species. At this scale, the autocorrelation of anchovy egg concentration had declined by 92% relative to its maximum at the nugget. Therefore, although a small amount of autocorrelation persists, statistical tests are unlikely exhibit major biases when anchovy egg data were analyzed at the scale of the nearshore CalCOFI grid.

For jack mackerel eggs, the range was estimated to be 140 km, while the nugget and sill were 0.25 and 2.30, respectively (Fig. S2.2b). An r^2 of 0.94 indicated an excellent fit between the empirical and theoretical variograms calculated for jack mackerel. The scale of autocorrelation for jack mackerel eggs as denoted by their range is larger than the

spatial resolution of CUFES and both the nearshore and offshore CalCOFI grid. Since jack mackerel eggs predominantly had an offshore distribution (Fig. 2.1), the offshore CalCOFI grid was the most relevant scale for this species. At this scale, the autocorrelation of jack mackerel eggs had decreased by 70% relative to its maximum at the nugget. We have assumed that statistical tests were unlikely to display major biases for jack mackerel at the scale of the offshore CalCOFI grid due to autocorrelation.

S3. Generalized Linear Models (GLMs) of Egg Concentration

To determine if similar oceanic variables influenced both the presence of fish eggs and their concentration, we constructed a generalized linear model (GLM) of egg concentration using the negative binomial distribution. This distribution is appropriate for modeling organisms that display spatially aggregated patterns. Parameters describing the negative binomial distribution of anchovy, sardine, and jack mackerel eggs were estimated with R statistical software (version 2.11.1, R Foundation for Statistical Computing, Wien, Austria). Next, the *U*-statistic goodness-of-fit test was used to evaluate the null hypothesis that fish egg concentration could be described by the negative binomial distribution (Krebs, 1999). In all cases, the null hypothesis could not be rejected at $p < 0.05$, so we proceeded to develop GLMs using the negative binomial distribution. In GLMs, the relationship between egg concentration and oceanic variables was modeled using linear and quadratic terms to allow fishes to exhibit peaks in egg concentration over a range of a given variable. The relative fit of models of each independent variable (i.e., dynamic height, temperature, salinity, chlorophyll concentration, zooplankton volume,

geostrophic current speed and direction, and eddies) was compared with the Akaike Information Criterion (AIC) and analysis of deviance. Since comparisons based on deviance and the AIC produced equivalent results, for conciseness we have opted only to present results from analysis of deviance. The ranges of environmental variables associated with peak egg concentration were identified based on the area where GLM predictions exceeded 90% of their maximum value. Due to extremely high predictions of egg concentration for geostrophic currents flowing in certain directions, GLM outputs were $\log_{10}$ transformed prior to assessing peak egg concentrations for this variable.

Table S2.2 compares the relative explanatory power that different variables have on fish egg concentration based on the negative binomial GLMs. As was the case when examining the presence/absence of eggs, the GLMs investigating variations in egg concentration showed that the largest amounts of residual deviance were explained by dynamic height, chlorophyll, temperature, and/or salinity. Less deviance was explained by zooplankton volume, geostrophic currents, and eddies. For anchovy and jack mackerel, dynamic height accounted for more variability in egg concentration than any other variable (Table S2.2). Chlorophyll concentration and dynamic height explained similar amounts of residual deviance in the negative binomial GLM for sardine. A few variables that contributed significantly to the characterization of areas where fish eggs were present did not explain as much variability in egg concentration. This was the case for geostrophic current speed in the GLM examining anchovy eggs and zooplankton volume in the jack mackerel GLM. In both the models of sardine egg concentration and presence/absence, zooplankton volume had a marginally significant effect ($0.04 < p < 0.06$; Tables 2.2 and S2.2).

The range of oceanic variables across which fishes spawned most frequently is shown in Table S2.3 for models investigating the presence/absence of fish eggs (i.e., logistic regression GLMs) and egg concentration (i.e., negative binomial GLMs). These ranges of environmental variables were generally similar regardless of which type of model was applied. The negative binomial GLMs often predicted slightly narrower ranges of environmental variables. This reflected the fact that eggs may be present over a broader area than just the region where their concentration is maximal. Small differences between predicted ranges from the logistic regressions and negative binomial GLMs may also reflect the influence of a few study sites that contain extremely large numbers of fish eggs. For example, 50% of anchovy eggs sampled between 1998-2004 occurred at five study sites. Oceanic conditions at these sites may have a large influence on the GLMs predicting anchovy egg concentration, but would be unlikely to affect models of the presence/absence of anchovy eggs as strongly.

In addition to model predictions, empirical CDFs also indicated that the dynamic heights used by spawning small pelagic fishes were similar regardless of whether analyses were conducted with egg concentration data or the presence/absence of fish eggs (Figs. 2.3 and S2.1b).

S4. Forward, Stepwise Models of the Presence/Absence of Fish Eggs

Forward, stepwise models using all predictor variables were constructed to evaluate which variables would be included in the optimal model of egg distribution for each species. Models were developed in a similar manner to those described in Section

2.3 of this manuscript. The presence/absence of fish eggs was used as the dependent variable, whereas independent variables were incorporated into each model as linear and quadratic terms. First-order interactions between sets of two independent variables were also included in models. Models were fit with a GLM framework in which a binomial distribution and logit link were used (i.e., logistic regression). During the step-wise fitting process, the contribution of linear and quadratic terms was evaluated jointly. The AIC was used to assess whether the addition of terms improved model fit. The step-wise process of model building was terminated when the inclusion of additional terms no longer reduced the AIC.

These step-wise models differed from those shown in Table 2.3 where the dynamic height term was added last to the model. The latter models were designed to evaluate the contribution of each independent variable towards explaining the dynamic height effect, whereas the models presented here were constructed to find the optimal combination of variables for predicting fish egg distribution. Nevertheless, it should be noted that the predictive capacity of these models may be limited due to collinearity between variables that show similar spatial patterns (Table 2.1). In contrast, collinearity between variables was explicitly incorporated into the design of GLMs in Table 2.3, where the degree of collinearity between variables influenced how of much of the dynamic height effect on fish egg distribution could be attributed to each variable.

Table S2.4 shows the variables incorporated into the optimal predictive models of the distribution of anchovy, sardine, and jack mackerel eggs. Dynamic height was included as the first term in models of anchovy and sardine eggs, where it accounted for 70.5% and 49.8% of the deviance explained by the models, respectively, for each species.

The final step-wise model of anchovy egg distribution also contained the following variables: zooplankton volume, temperature, geostrophic current speed, and eddies. In addition to dynamic height, other terms included in the step-wise model of sardine eggs were chlorophyll, salinity, geostrophic current direction, and interactions between these variables (Table S2.4). Dynamic height was incorporated as the second term in the model of jack mackerel egg distribution, following the addition of salinity to the model. The remaining variables in the step-wise model of jack mackerel eggs were zooplankton volume, chlorophyll concentration, and two interaction terms. Aside from dynamic height, zooplankton volume was the only other variable consistently incorporated into spawning habitat models of all three species. This suggests that, although zooplankton volume by itself does not explain a high degree of variability in fish egg distribution (Table 2.2), it is a secondary factor that becomes important when considered in conjunction with other variables. Since temperature has been frequently used to describe the spawning habitat of these fishes (Fiedler, 1983; Lluch-Belda *et al*., 1991; Checkley *et al*., 2000; Reiss *et al*., 2008; Weber and McClatchie, 2010; Zwolinski *et al*., 2011), it is also noteworthy that temperature was only incorporated into the predictive, step-wise model of one of the three species. This implies that temperature may be a proxy for other environmental factors that more directly influence the distribution of small pelagic fishes (Fiedler, 1983; Jacobson and MacCall, 1995; Rodríguez-Sánchez *et al*., 2002).

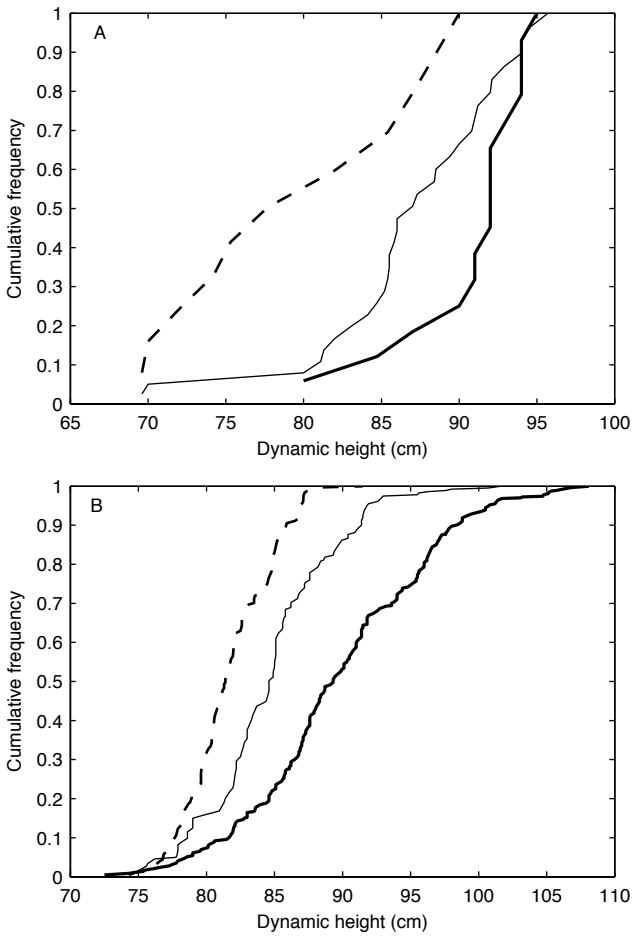

Figure S2.1. Empirical cumulative distribution functions (CDFs) of the dynamic heights across which the eggs of northern anchovy (dashed line), Pacific sardine (solid line), and jack mackerel (thick, solid line) were observed. (A) Presence/absence of eggs in the central California. (B) Egg concentration (# per 10 m^2) at sites where eggs were present in southern California. Egg concentration data were $\log_e$ transformed prior to constructing CDFs in the bottom panel.

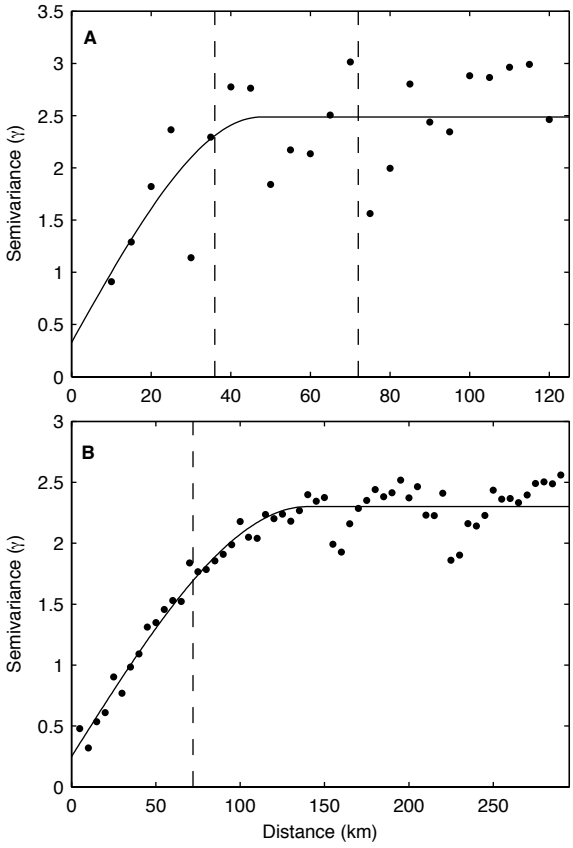

Figure S2.2. Variograms of anchovy (A) and jack mackerel eggs (B) based on Continuous, Underway Fish Egg Sampler (CUFES) data collected during the spring 2000 California Cooperative Oceanic Fisheries Investigations (CalCOFI) cruise. Dots indicate the semivariance of data in 5-km bins, while the solid line is a theoretical variogram fit to an isotropic, spherical model. Dashed lines indicate the spatial scale of the CalCOFI grid at nearshore and offshore sites (i.e., 36 and 72 km, respectively). Only the offshore grid scale is displayed in (B) because jack mackerel eggs do not frequently occur in coastal waters.

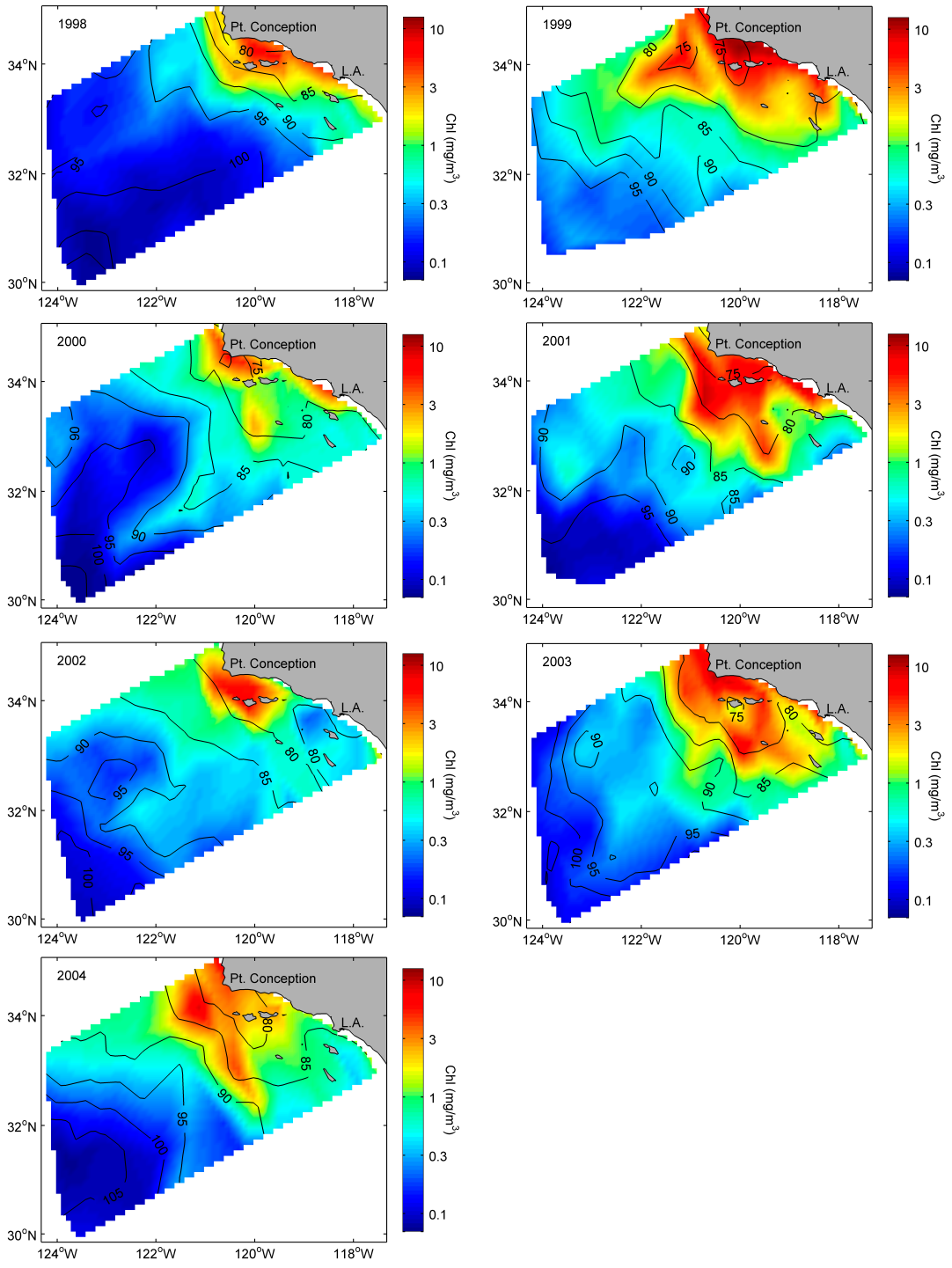

Figure S2.3. Maps of the average chlorophyll concentration over the upper 50 m of the water column during spring cruises between 1998-2004. Similarities in the spatial distribution of chlorophyll and dynamic height are illustrated by the inclusion of dynamic height contours (black lines).

Table S2.1. Contingency table comparing the observed number of samples with fish eggs in dynamic height bins and the number of samples that would be expected if fishes spawned uniformly. Data in the left half of the table are from southern California, while results from central California are shown to the right. Numbers in parentheses are the percentage of eggs in each dynamic height category. Residuals, degrees of freedom (d.f.), and *p*-values are from a Pearson's χ^2 test of goodness of fit. The 'N – 1' modification to this test was used to account for small expected numbers in some dynamic height bins (Campbell, 2007). N/A indicates dynamic heights ≥ 100.0 cm that were not included in the contingency table for anchovy, because spawning anchovies were generally absent from offshore areas where high dynamic heights occurred.

Southern California Anchovy					Central California Anchovy			
Dynamic height (cm)	< 80.0	80.0-89.9	90.0-99.9	≥ 100.0	< 70.0	70.0-79.9	80.0-89.9	≥ 90.0
Observed	35 (35%)	63 (64%)	1 (1%)	N/A	1 (9%)	5 (45%)	4 (36%)	1 (9%)
Expected	41 (41%)	52 (53%)	6 (6%)	N/A	1 (6%)	3 (27%)	4 (39%)	3 (27%)
Residuals	0.9	2.3	4.1	N/A	0.2	1.3	< 0.1	1.3
Test Results: $\chi^2 = 7.3$; d.f. = 2; $p < 0.05$					Test Results: $\chi^2 = 2.6$; d.f. = 3; $p = 0.46$			
Sardine					Sardine			
Dynamic height (cm)	< 80.0	80.0-89.9	90.0-99.9	≥ 100.0	< 70.0	70.0-79.9	80.0-89.9	≥ 90.0
Observed	16 (16%)	66 (65%)	18 (18%)	2 (2%)	1 (3%)	1 (3%)	19 (59%)	11 (34%)
Expected	26 (25%)	42 (41%)	26 (25%)	9 (9%)	2 (6%)	7 (21%)	11 (35%)	12 (38%)
Residuals	3.7	14.4	2.2	5.6	0.4	4.9	5.3	0.1
Test Results: $\chi^2 = 26.0$; d.f. = 3; $p < 0.001$					Test Results: $\chi^2 = 10.4$; d.f. = 3; $p < 0.05$			
Jack mackerel					Jack mackerel			
Dynamic height (cm)	< 80.0	80.0-89.9	90.0-99.9	≥ 100.0	< 70.0	70.0-79.9	80.0-89.9	≥ 90.0
Observed	20 (9%)	93 (43%)	80 (37%)	22 (10%)	0 (0%)	0 (0%)	3 (20%)	12 (80%)
Expected	50 (23%)	91 (42%)	52 (24%)	22 (10%)	1 (5%)	3 (21%)	5 (35%)	6 (40%)
Residuals	18.2	< 0.1	15.5	0.0	0.7	3.1	1.0	6.2
Test Results: $\chi^2 = 33.7$; d.f. = 3; $p < 0.001$					Test Results: $\chi^2 = 10.3$; d.f. = 3; $p < 0.05$			

Table S2.2. Deviance explained by generalized linear models (GLMs) examining the concentration of anchovy, sardine, and jack mackerel eggs. The effect of independent variables was tested individually using quadratic and linear terms. The one exception to this was the "eddies" term, which was incorporated into GLMs as a categorical variable. Significance levels are indicated as follows: * $p < 0.05$; ** $p < 0.01$; *** $p < 0.001$. The number of asterisks corresponds to the most significant term in a GLM, which could be either linear or quadratic.

Independent variables	Anchovy (n = 435) Deviance	Sardine (n = 378)	Jack mackerel (n = 435)
Dynamic height	136.5[c]***	40.8[c]***	43.8[c]***
Temperature	33.2[c]***	25.9[c]***	25.7[c]***
Salinity	11.1[c]***	4.8[c]**	33.4[c]***
Chlorophyll	29.9[c]***	42.8[c]***	28.8[c]***
Zooplankton volume	17.2[c]***	7.7[c]*	3.6
Geostrophic current speed	3.3	0.1	0.2
Geostrophic current direction	7.3[b]***	5.6[c]***	7.6[a]**
Eddies	5.4	1.2	0.3

[a] Linear term significant at $p < 0.05$
[b] Quadratic term significant at $p < 0.05$
[c] Linear and quadratic terms significant at $p < 0.05$

Table S2.3. Comparison of characteristics associated with the spawning habitat of small pelagic fishes based on logistic regressions and negative binomial generalized linear models (GLMs). The range of each oceanic variable indicates the area where logistic regression or negative binomial GLM predictions exceeded 90% of their maximum value. In the case of geostrophic current direction, negative binomial GLM predictions of egg concentration were $\log_{10}$ transformed prior to estimating the range. N/A denotes a variable that did not significantly affect spawning habitat.

Oceanic variable	Logistic regression	Negative binomial GLM
Dynamic height (cm)		
Anchovy	79 – 83	81 - 83
Sardine	84 – 89	82 - 86
Jack mackerel	89 – 99	89 - 95
Temperature (° C)		
Anchovy	12.0 - 13.4	13.0 - 13.6
Sardine	12.5 - 13.9	12.7 - 13.4
Jack mackerel	13.5 - 15.6	13.8 - 14.9
Salinity		
Anchovy	33.5 - 33.7	33.4 - 33.5
Sardine	33.0 - 33.4	33.2 - 33.4
Jack mackerel	< 33.1	33.1 - 33.3
Chlorophyll (mg m^{-3})		
Anchovy	1.2 - 3.9	1.3 - 2.4
Sardine	0.6 - 2.2	1.1 - 1.9
Jack mackerel	< 0.5	0.1 - 0.4
Zooplankton volume (cm^3 1,000 m^{-3})		
Anchovy	78 – 264	163 - 297
Sardine	N/A	129 - 352
Jack mackerel	< 46	N/A
Geostrophic current speed (cm s^{-1})		
Anchovy	> 80	N/A
Sardine	N/A	N/A
Jack mackerel	N/A	N/A
Geostrohic current direction (°)		
Anchovy	-6 – 23	-9 - 7
Sardine	< -42	< -34
Jack mackerel	N/A	< -30

Table S2.4. Model coefficients, deviance explained, and the Akaike Information Criterion (AIC) for variables included in the forward, step-wise models of the presence/absence of fish eggs. In the table, the linear term for each variable is listed first followed by the quadratic term. The significance of each term in the logistic regression models was examined with likelihood ratio tests. * $p < 0.05$; ** $p < 0.01$; *** $p < 0.001$. The number of asterisks corresponds to the most significant term in the regression, which could be either linear or quadratic.

Model step	Variable added	Model coefficients	Deviance	AIC
Anchovy				
1	Intercept	-201.5540		463.7
2	Dynamic height	457.5520		
		-302.2754	119.9[c]***	347.7
3	Zooplankton volume	-13.7238		
		2.6780	26.5[c]***	325.2
4	Temperature	6.5218		
		-0.2240	10.4[a]**	318.8
5	Geostrophic current speed	-6.2928		
		8.4202	7.8[b]**	315.0
6	Eddies	-198.9824		
		-202.9225	5.5	313.5
Sardine				
1	Intercept	-2,814.7882		440.8
2	Dynamic height	29.1149		
		-14.8834	48.9[c]***	395.9
3	Chlorophyll	-22.5160		
		0.1819	18.6[c]**	381.3
4	Salinity	165.4036		
		-2.4312	9.0[a]**	376.3
5	Zooplankton volume	116.7740		
		2.8384	11.2[b]**	369.2
6	Dynamic height x chlorophyll	29.0667	2.5	368.7
7	Salinity x zooplankton volume	-3.8552	2.1	368.6
8	Geostrophic current direction	-0.0308		
		0.0001	5.8[a]*	366.8

[a] Linear effect of dynamic height significant at $p < 0.05$

[b] Quadratic effect of dynamic height significant at $p < 0.05$

[c] Linear and quadratic effects of dynamic height significant at $p < 0.05$

Table S2.4 (continued)

Model step	Variable added	Model coefficients	Deviance	AIC
Jack mackerel				
1	Intercept	-5,829.9103		604.5
2	Salinity	311.3174		
		-4.1722	90.5[c]***	518.0
3	Dynamic height	1,307.0140		
		-115.1607	14.9[c]**	507.2
4	Zooplankton volume	118.7881		
		2.0371	9.1[c]*	502.0
5	Salinity x dynamic height	-32.9709	3.9*	500.2
6	Chlorophyll	-0.9883		
		0.4591	5.9[a]*	498.3
7	Salinity x zooplankton volume	-3.7626	3.0	497.3

[a] Linear effect of dynamic height significant at $p < 0.05$
[b] Quadratic effect of dynamic height significant at $p < 0.05$
[c] Linear and quadratic effects of dynamic height significant at $p < 0.05$

References Cited in Chapter 2 Appendix

Campbell, I. 2007. Chi-squared and Fisher-Irwin tests of two-by-two tables with small sample recommendations. *Statistics in Medicine* 26: 3661-3675.

Checkley, Jr., D.M., R.C. Dotson and D.A. Griffin. 2000. Continuous, underway sampling of eggs of Pacific sardine (*Sardinops sagax*) and northern anchovy (*Engraulis mordax*) in spring 1996 and 1997 off southern and central California. *Deep-Sea Research Part II* 47: 1139-1155.

Ciannelli, L., P. Fauchald, K.S. Chan, V.N. Agonstini and G.E. Dingsør. 2007. Spatial fisheries ecology: Recent progress and future prospects. *Journal of Marine Systems* 71: 223-236.

Fiedler, P.C. 1983. Satellite remote sensing of the habitat of spawning anchovy in the Southern California Bight. *California Cooperative Oceanic Fisheries Investigations Reports* 24: 202-209.

Jacobson, L.D. and A.D. MacCall. 1995. Stock-recruitment models for Pacific sardine (*Sardinops sagax*). *Canadian Journal of Fisheries and Aquatic Sciences* 52: 566-577.

Kaluzny, S.P., S.C. Vega, T.P. Cardoso and A.A. Shelly. 1998. S+ Spatial Stats. User's Manual for Windows and Unix. Springer, New York, NY. 344 p.

Krebs, CJ. 1999. Ecological Methodology, 2nd ed. Addison Wesley Longman, New York, NY. 620 p.

Legendre, P. and L. Legendre. 1998. Numerical Ecology, 2nd ed. Developments in Environmental Modelling 20. Elsevier, New York, NY. 853 p.

Lo, N.C.H., J.R. Hunter, J.R. and R. Charter. 2001. Use of a continuous egg sampler for ichthyoplankton surveys: application to the estimation of daily egg production of Pacific sardine (*Sardinops sagax*) off California. *Fishery Bulletin* 99: 554-571.

Lo, N.C.H., B.J. Macewicz and D.A. Griffith. 2010. Biomass and reproduction of Pacific sardine (*Sardinops sagax*) off the Pacific northwestern United States, 2003-2005. *Fishery Bulletin* 108(2): 174-192.

Lluch-Belda, D., D.B. Lluch-Cota, S. Hernandez-Vazquez, C.A. Salinas-Zavala and R.A. Schwartzlose. 1991. Sardine and anchovy spawning as related to temperature and upwelling in the California current System. *California Cooperative Oceanic Fisheries Investigations Reports* 32: 105-111.

Parrish, R.H., C.S. Nelson and A. Bakun. 1981. Transport mechanisms and reproductive success of fishes in the California Current. *Biological Oceanography* 1(2): 175-203.

Reiss, C.S., D.M. Checkley, Jr. and S.J. Bograd. 2008. Remotely sensed spawning habitat of Pacific sardine (*Sardinops sagax*) and Northern anchovy (*Engraulis mordax*) within the California Current. *Fisheries Oceanography* 17(2): 126-136.

Rodríguez-Sánchez, R., D. Lluch-Belda, H. Villalobos and S. Ortega-García. 2002. Dynamic geography of small pelagic fish populations in the California Current System on the regime time scale (1931-1997). *Canadian Journal of Fisheries and Aquatic Sciences* 59: 1980-1988.

Weber, E.D. and S. McClatchie. 2010. Predictive models of northern anchovy *Engraulis mordax* and Pacific sardine *Sardinops sagax* spawning habitat in the California Current. Marine Ecology Progress Series 406: 251-263.

CHAPTER 3. CHANGES IN PHYTOPLANKTON PHENOLOGY DETECTED WITH THE COMMUNITY EARTH SYSTEM MODEL 1.0 (CESM1): LONG-TERM TRENDS AND THE INFLUENCE OF CLIMATE OSCILLATIONS

Abstract

Changes in the phenology of marine phytoplankton are ecologically important because phytoplankton seasonality can affect total annual primary production, sequestration of CO_2 through the biological pump, and abundance of higher trophic level organisms whose reproduction is timed to coincide with plankton blooms. Most studies of phytoplankton phenology have been too short to evaluate the prevalence of long-term changes due to anthropogenic forcing or decadal-scale climate oscillations. Here phytoplankton phenology in the North Pacific (5°S – 66°N, 151°E – 76°W) was examined between 1961 and 2007 with the ocean component of the Community Earth System Model 1.0 (CESM1) forced with atmospheric observations. Comparisons with SeaWiFS chlorophyll concentration indicated that CESM1 could simulate mean dates of bloom initiation and midpoint with as much skill as it could predict mean bloom magnitude ($r \geq 0.65$). CESM1 exhibited less skill identifying mean dates of bloom termination ($r = 0.51$) and duration ($r = 0.18$). Changes in bloom initiation date at 23-34% of CESM1 grid cells were correlated with the Multivariate ENSO Index (MEI), Pacific Decadal Oscillation, or North Pacific Gyre Oscillation, while 20% of grid cells exhibited long-term trends in bloom initiation. The first principal component for each of five phenological metrics (bloom initiation, midpoint, termination, duration, and magnitude) was either correlated with the MEI or displayed a long-term trend. Climate effects on bloom initiation were more pervasive than effects on bloom midpoint, termination, and duration. Compared to terrestrial ecosystems, the long-term trends in

phytoplankton phenology are noteworthy in terms of their rapid rate of change and greater prevalence of delayed phenology.

1. Introduction

Phenology refers to the study of recurring, biological events and how they are influenced by regional climate and meteorology. Traditionally, most phenological studies examine discrete events, such as the date of first flowering and bud burst among plants or the timing of the reproductive activity and seasonal migration among animals (Greve, 2003). In contrast, studies of phytoplankton phenology track continuous, seasonal changes in the abundance of phytoplankton, typically focusing on variability in the dates of spring and fall blooms. The phenology of phytoplankton has been proposed as an indicator of pelagic ecosystem condition, which could be used to track changes in ocean ecosystem dynamics due to natural and anthropogenic perturbations (Platt *et al*., 2009, 2010).

With regard to understanding how climate change will alter marine ecosystems, investigating long-term changes in phytoplankton phenology will be key since seasonal dynamics influence integrated annual rates of primary and export production. Annual primary production is affected by both the duration and timing of phytoplankton blooms (Yamada and Ishizaka, 2006; Song *et al*., 2011). For example, earlier blooms are correlated with greater annual net primary production in the Northwest Atlantic (Song *et al*., 2011). The seasonal coincidence between phytoplankton blooms, zooplankton grazers, and viruses can influence the efficiency of export production where

anthropogenic CO_2 is sequestered in the deep ocean through the biological pump (Lutz *et al*., 2007; Henson *et al*., 2009; Sapiano *et al*., 2012). Later spring blooms have been associated with greater flux of phytoplankton biomass to the benthos on the Nova Scotian Shelf and in the Gulf of Maine (Song *et al*., 2011), whereas, in the Bering Sea, export production increases in cold years with late sea ice retreat and early ice-associated phytoplankton blooms (Hunt and Stabeno, 2002; Hunt *et al*., 2002). This reflects in part the differential effects of temperature on the metabolism of phytoplankton and grazers, which can in turn influence trophic coupling. Since there is a seasonal succession of phytoplankton species that is difficult to accurately monitor with remote sensing, phenological patterns may also serve as an indicator of changes in phytoplankton community composition (Chiba *et al*., 2012). Lastly, variations in plankton phenology can affect the reproductive success of fishes and other upper trophic level predators who often time sensitive life history stages to coincide with plankton blooms (Cushing, 1974, 1990; Platt *et al*., 2003; Sydeman *et al*., 2006; Koeller *et al*., 2009). Mismatches between these events can result in starvation and reduced growth among planktivorous larval fishes, which can in turn increase their vulnerability to predation and result in poor recruitment to fisheries in subsequent years.

While few studies have investigated the phenological response of marine phytoplankton to climate change (*e.g*., Edwards and Richardson, 2004; Hashioka *et al*., 2009), long-term monitoring has examined climate-related changes in the phenology of primary producers throughout many temperate, terrestrial ecosystems. In terrestrial habitats, the earlier advent of spring conditions due to warming temperatures has stimulated an early start of the growing season among plants. Observational studies

indicate that between 68-94% of plant species have responded to increasing temperatures by advancing their phenology (Menzel *et al*., 2006; Miller-Rushing and Primack, 2008; Cook *et al*., 2012; Wolkovich *et al*., 2012). Similarly, remote sensing of the normalized difference vegetation index (NDVI) suggests that since 1982 advancing phenology has prolonged the photosynthetically active period across 88% of the Arctic and 81% of North Hemisphere boreal habitats (Xu *et al.*, 2013). A smaller percentage (10-18%) of terrestrial primary producers have exhibited delayed phenology due to chilling requirements, where a plant must be exposed to cool temperatures for an extended period before it is able to respond to spring warming (Cook *et al*., 2012). The most rapid rates of terrestrial, phenological changes have been observed among species residing in high latitudes (Root *et al*., 2003; Parmesan, 2007) and those active in early spring (Wolkovich *et al*., 2012).

Compared to terrestrial ecosystems, net primary production in the ocean displays smaller seasonal fluctuations, although intraseasonal and interannual variability in marine primary production can be quite high, reflecting the rapid turnover time of phytoplankton (Field *et al.*, 1998). As a result, seasonal patterns account for < 40% of the variance in time series of chlorophyll across many regions (Venegas *et al*., 2008; Sapiano *et al*., 2012). The equatorial Pacific is one such area with a low-amplitude seasonal cycle, although a small peak in chlorophyll concentration is typically observed in spring (Yoo *et al*., 2008; Racault *et al*., 2012). The eastern equatorial Pacific, which is characterized by enhanced primary productivity due to upwelling, exhibits a seasonal, chlorophyll maximum during the summer or autumn (Racault *et al*., 2012; Sapiano *et al*., 2012). Similarly, the North Pacific subtropical gyre displays a small peak in chlorophyll

between October and December (Sapiano *et al*., 2012). At latitudes > 30° N, there is a gradual progression from late winter phytoplankton blooms to spring and summer blooms at higher latitudes (Racault *et al*., 2012). A secondary fall peak in chlorophyll is also observed in coastal areas poleward of 40° N and across the transition between the subtropical and subpolar gyres (Henson and Thomas, 2007; Yoo *et al*., 2008; Sapiano *et al*., 2012). North of this transition area, the spring bloom becomes progressively later, while the fall bloom becomes earlier until they merge, resulting in a single summer bloom (Yoo *et al*., 2008). The one exception to this latitudinal pattern occurs in high nutrient, low chlorophyll (HNLC) areas, where maximal chlorophyll concentration is detected in September and October (Yoo *et al*., 2008). Compared to the Atlantic Ocean, the North Pacific is characterized by a reduced latitudinal gradient of bloom timing, a larger area with aseasonal variation in phytoplankton abundance, and high interannual variability in phenology (Racault *et al*., 2012; Sapiano *et al.*, 2012). The reduced latitudinal gradient in North Pacific phytoplankton phenology reflects greater control of phytoplankton abundance by efficient grazing (Parsons *et al.*, 1966) and altered seasonality in HNLC regions where phytoplankton growth is limited by iron (Yoo *et al*., 2008).

With a few notable exceptions (*e.g*., Edwards and Richardson, 2004; Wiltshire *et al*., 2008; Kim *et al.*, 2009), most research on phytoplankton phenology has relied on remotely sensed time series, since satellites can synoptically sample the ocean globally on a daily basis. However, the amount of phenological information that can be acquired from remote sensing is limited by gaps in time series due to cloud cover, reduced accuracy of satellite chlorophyll retrievals in coastal areas, a lack of information on

seasonal variations in species composition and subsurface production, and seasonal changes in the chlorophyll-to-carbon ratio of phytoplankton (Martin, 2004). The current utility of remotely sensed data for detecting long-term trends related to climate change is also limited since ocean color has only been continuously monitored by satellites since 1997. While the Coastal Zone Color Scanner (CZCS) collected data on chlorophyll concentration between 1978-1986, comparability between CZCS and recent satellite missions is hindered by differences in calibration techniques, atmospheric correction, and the number of bands sensed in the visible light range (Aiken *et al.*, 1995). Nonetheless, several studies have reported trends in the magnitude, seasonality, and duration of phytoplankton blooms in the Arctic, California Current, Nova Scotian Shelf, and elsewhere over the period since SeaWiFS began monitoring ocean color (Kahru *et al*., 2009, 2011; Vargas *et al*., 2009; Song *et al*., 2011; Racault *et al*., 2012; Sapiano *et al*., 2012). Whether trends in ocean color are connected to anthropogenic warming or interannual-to-decadal variability remains unclear since the launch of SeaWiFS coincided with the strong 1997/1998 El Niño, which had a substantial impact on primary production throughout the Pacific. Since natural climate oscillations can dampen or amplify the signal of global warming, Henson *et al*. (2010) estimated that between 35-41 years of continuous ocean color data are needed in the North Pacific to attribute trends in chlorophyll concentration to climate change with a high degree of certainty.

Given the absence of a sufficiently long ocean color time series to detect climate-related trends, an alternative approach is to examine mechanisms driving variations in phytoplankton phenology with Dynamic Green Ocean Models (DGOMs). DGOMs link nutrient-phytoplankton-zooplankton-detritus (NPZD) models with an ocean general

circulation model (OGCM) to represent interactions between climate and ocean biogeochemistry. In addition to providing forecasts of how pelagic ecosystems will respond to future climate change, DGOMs can be used to hindcast past changes based on simulations in which atmospheric forcing applied to the OGCM is constrained by historical observations (Large and Yeager, 2009). DGOMs can also be used to explore the underlying ocean-ecosystem dynamics responsible for changes in primary production and phytoplankton seasonality (Marinov *et al*., 2010; Hashioka *et al*., 2012), which can be difficult to examine mechanistically during field campaigns.

Compared to climate models used in the fourth Intergovernmental Panel on Climate Change (IPCC) assessment, the most recent generation of DGOMs and OGCMs exhibit improved accuracy in their ability to reproduce spatial and temporal patterns observed *in situ* at regional-to-global scales. One such example is the Community Earth System Model 1.0 (CESM1) and its ocean biogeochemistry (BGC) sub-module, which is the DGOM used in the research described in this manuscript. The fully coupled atmosphere-ocean version of CESM1(BGC) is able to simulate mean annual surface and subsurface temperature, salinity, and macronutrient concentrations such that correlations (r) with empirical observations exceed 0.8 (Moore *et al*., 2013). The coupled version of this model is also able to generate mean concentrations of chlorophyll and iron where $r > 0.6$ when compared to *in situ* and satellite observations. In addition, CESM1(BGC) can accurately reproduce the locations of HNLC regions (Moore *et al*., 2013) and replicate the spatial patterns and temporal evolution of El Niño, La Niña, and lower frequency modes of climate variability (Deser *et al*., 2012). Nevertheless, biases persist in coupled CESM1(BGC) simulations such that oxygen minimum zones (OMZ) in the Indian and

eastern Pacific basins are too large, sea surface temperature (SST) is too warm in coastal upwelling ecosystems, mixed layer depth (MLD) is underestimated in the Southern Ocean, and thermohaline mixing is overestimated in the North Atlantic (Danabasoglu *et al.*, 2012; Moore *et al.*, 2013).

Along with other DGOMs, CESM1(BGC) has been able to accurately capture the mean timing of the chlorophyll maximum in mesotrophic-to-eutrophic regions of the ocean (Hashioka *et al*., 2012). However, DGOMs have difficulty capturing the timing of fall phytoplankton blooms in regions with dual spring and fall blooms (Henson *et al*., 2009; Song *et al*., 2011). This reflects the fact that fall blooms are typically smaller than spring blooms and have more variable phenology. Studies of phytoplankton phenology using DGOMs have indicated that decadal climate oscillations, such as the North Atlantic Oscillation (NAO) and the North Pacific Gyre Oscillation (NPGO), influence the timing of phytoplankton blooms through their influence on regional wind strength. Increased westerly winds during positive NAO conditions deepens MLD leading to delayed phytoplankton phenology in the subpolar North Atlantic (Henson *et al*., 2009). Similarly, the earlier onset of upwelling-favorable winds during the positive NPGO phase results in an earlier start of seasonal phytoplankton population growth in the California Current Ecosystem (CCE) (Chenillat *et al*., 2012). Future changes in phenology have also been examined with the NEMURO model (a DGOM), which predicted that a doubling of atmospheric CO_2 relative to pre-industrial levels will cause phytoplankton to bloom 10-20 days earlier in the Northwest Pacific (Hashioka *et al*., 2009).

Here we describe the use of an ocean-ice hindcast experiment conducted with CESM1(BGC) to investigate variations in phytoplankton phenology across the North

Pacific between 1961-2007. This hindcast used historical atmospheric data to calculate air-sea fluxes of heat, freshwater, and momentum, which in turn drive the physical oceanic component of CESM1(BGC) (Large and Yeager, 2009). Since this simulation was forced with atmospheric observations, the temporal evolution of biological and physical oceanographic variables outputted by CESM1(BGC) can be compared directly to historical observations. This differs from fully coupled atmosphere-ocean simulations, where model output and empirical observations can only be compared in a statistical sense (*i.e*., means and standard deviations are comparable rather than year-to-year variations) (Stock *et al*., 2011).

While a DGOM run in hindcast mode has been employed to examine climate influences on phytoplankton phenology in the North Atlantic (Henson *et al*., 2009), to the best of our knowledge, similar research has not been conducted in the Pacific Ocean. In the North Pacific, there are three modes of climate variability that are likely to affect phytoplankton phenology. One mode is El Niño-Southern Oscillation (ENSO), which is the predominant source of climate variability across periods of 2-7 years (McPhaden *et al.*, 2006). At the decadal scale, the Pacific Decadal Oscillation (PDO) and NPGO, respectively, comprise the first and second modes of variability in North Pacific SST and sea surface height (SSH) (Mantua *et al*., 1997; Di Lorenzo *et al*., 2008).

In addition to examining the effects of interannual-to-decadal climate oscillations, the ocean-ice hindcast will allow us to identify long-term trends in phytoplankton phenology that may be related to anthropogenic climate change. This reflects the fact that the 47-year duration of the ocean-ice simulation exceeds the ~40-year period of continuous data that Henson *et al*. (2010) deemed necessary to detect trends in

chlorophyll concentration due to global warming given prevailing natural variability. Also, the 1961-2007 period of the ocean-ice hindcast includes two reversals of the sign of the PDO, making it feasible to differentiate between a secular warming trend and the 1977 PDO phase shift that resulted in a transition from cool to warm conditions in the eastern Pacific (Stewart *et al.*, 2005; See first data chapter).

Objectives of this research are to: (1) compare estimates of phytoplankton phenology based on CESM1(BGC) and SeaWiFS to validate whether CESM1(BGC) can accurately assess the dates of phytoplankton blooms across the North Pacific; (2) examine interannual variations in phytoplankton phenology during the years between 1961 and 2007; (3) determine how the spatial extent and magnitude of long-term trends in phytoplankton phenology compare to the effects of climate oscillations (*i.e.*, ENSO, PDO, NPGO), and; (4) identify which phenological indicators (*i.e.*, time of bloom initiation, midpoint, termination, duration, and magnitude) are most sensitive to climate perturbations.

2. Methods

2.1. Overview of the CESM1(BGC) Model

CESM1 consists of coupled models that simulate dynamic processes occurring in the atmosphere, ocean, cryosphere, and on land. The ocean physics component of CESM1 is based on version 2 of the Parallel Ocean Program (POP) (Smith *et al*., 2010). In the ocean, CESM1 uses a curvilinear grid with a longitudinal resolution of 1.13° and a

latitudinal resolution varying between 0.27-0.65° (Danabasoglu *et al*., 2012). The finest latitudinal resolution occurs in equatorial areas. Oceanic properties and fluxes are calculated across 60 vertical layers, whose thickness varies between 10-150 m (Moore *et al*., 2013). The thinnest vertical layers are found in the upper 200 m of the water column. Additional details about the most recent generation of the physical oceanic model incorporated in CESM1 can be found in Danabasoglu *et al*. (2012).

For all analyses presented here, historical atmospheric conditions from the years 1960-2007 were forced with the Coordinated Ocean-Ice Reference Experiments (CORE), version 2 described in Large and Yeager (2009). CORE incorporates observations of near surface vector wind, temperature, specific humidity, and atmospheric density from the NCEP reanalysis, but also includes satellite data on radiation, SST, sea-ice concentration, and precipitation during periods when remotely sensed data were available. This historical atmospheric forcing allows the seasonal and interannual evolution of the modeled ocean state to be prescribed in a manner that is directly, rather than solely statistically, comparable to ocean observations.

CESM1(BGC) includes three functional groups of phytoplankton: diatoms, diazotrophs, and a small phytoplankton category, which consists of coccolithophores and nano- and picoplankton (Moore *et al*., 2002). The single zooplankton functional group in CESM1(BGC) has differential grazing rates set for each phytoplankton category based on a Holling type III function (Moore *et al*., 2002). Rates of phytoplankton growth are a function of light intensity, nutrient concentration, and temperature in this model. Diatom growth can be limited by the availability of iron, nitrogen, phosphate, or silicate, while small phytoplankton growth is not affected by silicate. Neither nitrogen nor silicate limit

diazotroph growth. In addition to these nutrients, CESM1(BGC) also tracks variations in dissolved oxygen, alkalinity, air-sea exchange of CO_2 and O_2, dissolved inorganic carbon (DIC), semi-labile dissolved organic matter (DOM), and sinking particulates (Moore *et al*., 2013). Parameterization of CESM1(BGC) varies such that the small phytoplankton functional group has a lower nutrient half-saturation coefficient than diatoms and diazotrophs (Moore *et al*., 2002). The growth functions for diatoms and small phytoplankton are parameterized with a steeper initial slope of their P-I curves than diazotrophs. Q_{10} responses to temperature are parameterized similarly for all three phytoplankton groups. Additional information about the development of the ocean ecosystem and biogeochemistry component of CESM1 is provided in Moore *et al*. (2002, 2004), while Moore *et al*. (2013) and Long *et al*. (2013) describe changes made in the most recent generation of this model.

2.2. Identification of Phenological Events

This study examined variations in phytoplankton phenology across the region of the North Pacific Ocean between 5.2°S – 66.1°N and 150.7°E – 76.1°W. Data from the CESM1(BGC) were initially outputted on a daily basis so that fine temporal resolution changes in phenology could be investigated. Phenological metrics were calculated from surface chlorophyll concentration that was summed across the three functional groups of phytoplankton and then $\log_{10}$ transformed.

Two general classes of methods have been used to identify phenological events in time series of plankton abundance. “Threshold approaches” detect phenological events on

the date when a time series first surpasses a given threshold that can be based on the maximum slope of a time series (White *et al*., 2009), inflection points (Rolinski *et al*., 2007), a percentage of the cumulative, annual sum of plankton abundance (Greve *et al*., 2005), or a percentage of the maximum or median annual abundance (Siegel *et al*., 2002; Fuentes-Yaco *et al*., 2007; Kim *et al*., 2009). "Statistical approaches" entail fitting a probability density function (Yamada and Ishizaka, 2006; Rolinski *et al*., 2007), sigmoidal curve (Zhang *et al*., 2003; Ueyama and Monger, 2005), or a series of harmonic functions (Vargas *et al*., 2009) to a time series and then extracting phenological information from the fitted, statistical model. Statistical approaches often assume that seasonal time series are unimodal, which can present problems when applying this approach to areas with dual spring and fall phytoplankton blooms. On the other hand, threshold approaches are sensitive to brief fluctuations in phytoplankton abundance, which may represent high-frequency variability in response to transient weather events rather than a seasonal pattern of variation in chlorophyll (Rolinski *et* al., 2007; Ji *et al.*, 2010; Racault *et al.*, 2012). As a result, we initially developed one statistical method and one threshold method to detect phenological events.

In each CESM1 grid cell, the 75^{th} quantile of $\log_{10}$-transformed chlorophyll measured over 8-day time steps each year was used as the threshold for defining the initiation and termination of phytoplankton blooms. This threshold was selected for two reasons. First, use of the 75^{th} quantile implied that approximately one-quarter of the data each year would be included as part of a phytoplankton bloom, ensuring that events identified with this method would encompass approximately one season if only a single phytoplankton bloom was detected each year. Second, since this threshold varied

interannually and from pixel-to-pixel, we were able to detect phenological events in both oligotrophic and eutrophic regions and during years when chlorophyll concentration was below average. Bloom initiation was defined as the date when a time series first surpassed this threshold. The one exception to this was if the time series immediately dropped below the 75th quantile and did not rise above it again within any of the next five time steps. This rule helped further safeguard against confounding seasonal patterns and aseasonal, high-frequency fluctuations in chlorophyll concentration. Similarly, bloom termination occurred during the last time step when chlorophyll remained above the 75th quantile, but then decreased below this threshold without exceeding this limit at any point within the next five time steps. If there were less than five time steps separating the beginning and end of blooms in successive years, these blooms were merged and counted as a single phenological event. This approach for identifying phenological events is similar to the local threshold method used in White *et al*. (2009), which is one of the methods where remotely sensed plant phenology best matched *in situ* observations.

The second method used to identify phenological events involved fitting a harmonic curve with annual and semi-annual cycles to the chlorophyll time series from each CESM1 grid cell. Harmonic curves were fit on an annual basis to allow for year-to-year variations in phenology. Bloom initiation was defined as the date when the slope of the harmonic curve reached its maximum. Conversely, bloom termination occurred when a local minimum in the harmonic curve's slope was detected.

In addition to dates of bloom initiation and termination, three other phenological indicators were derived for phytoplankton blooms identified with the harmonic and threshold methods. The duration of a phytoplankton bloom was calculated as the

difference between dates of bloom termination and initiation. The midpoint of a bloom was defined as bloom's start date plus half of its duration. Bloom magnitude was computed as the mean of $\log_{10}$-transformed chlorophyll concentration over the duration of a bloom.

2.3. Model Skill Assessment of Modes of SST Variability and Phytoplankton Phenology

Before investigating interannual-to-decadal changes in phytoplankton phenology with the CESM1(BGC) ocean-ice hindcast, we evaluated the model's skill at detecting variations in oceanographic and phenological processes. Temporal and spatial variations in North Pacific SST from the ocean-ice hindcast were compared to empirical SST data from version 2.5 of the enhanced International Comprehensive Ocean-Atmosphere Data Set (ICOADS). Monthly ICOADS SST with a 1° latitude/longitude resolution was obtained from the NOAA Earth System Research Laboratory (ESRL) (http://icoads.noaa.gov). Daily SST data from CESM1(BGC) were averaged over monthly intervals to ensure that these datasets had the same temporal resolution. The first five modes of SST variability were examined separately for ICOADS and CESM1(BGC) using principal component analysis (PCA). Pixels in ICOADS with data gaps for > 75% of the monthly time steps were removed prior to PCA so that poorly sampled regions would not have an unduly large influence on this analysis. In areas where data were missing from fewer time steps, gaps in ICOADS were filled with the *inpaint_nans* two-dimensional, interpolation tool from the MATLAB Central File Exchange (D'Errico,

2004). Constraints were placed on *inpaint_nans* so that it could not extrapolate beyond the minimum or maximum temperature in ICOADS (*e.g.*, -2.8 - 34° C). PCA was performed on both raw SST data where seasonal patterns were retained and monthly SST anomalies where the seasonal signal was removed to examine interannual-to-decadal variability. During PCA, eigenvectors were calculated from a correlation matrix of the spatial component of SST data or SST anomalies (Emery and Thompson, 2001). Temporal variations in the first five principal components of ICOADS and CESM1(BGC) were inspected using principal component scores a_{it}, which were calculated as follows:

$$a_{it} = \sum_{it} (\psi_{it} - \bar{o_i}) * \phi_{it},$$

where Ψ_{it} is ICOADS or CESM1(BGC) SST (or the monthly SST anomaly) at time t and pixel i, $\bar{o}_i$ is the mean SST (or monthly SST anomaly) at i, and ϕ_{it} is the corresponding eigenvector (Emery and Thompson, 2001). Correlations between the ICOADS and CESM1(BGC) principal component scores were computed to assess whether these datasets exhibited similar modes of variability. Similarities between ICOADS and CESM1(BGC) were also evaluated by mapping the spatial signature of each dataset's first five principal components.

Time series of the SST principal components were compared to the Multivariate ENSO Index (MEI), PDO, and NPGO time series. Monthly anomalies of the MEI index developed by Wolter and Timlin (1998) were obtained from the NOAA ERSL (http://www.esrl.noaa.gov/psd/enso/mei/). The PDO index was acquired from the Joint Institute for the Study of the Atmosphere and Ocean (Mantua *et al*., 1997;

http://jisao.washington.edu/pdo/PDO.latest). The NPGO index was developed and made available by Emanuele Di Lorenzo at the Georgia Institute of Technology (Di Lorenzo *et al*., 2008; http://www.o3d.org/npgo/npgo.php).

To assess the skill of CESM1(BGC) for detecting phenological events, we compared the dates of phenological events identified with CESM1(BGC) and SeaWiFS ocean color data during the 1998-2007 period. SeaWiFS level-3, chlorophyll data with a 9-km resolution were obtained from the NASA Ocean Color Group (http://oceancolor.gsfc.nasa.gov). We averaged SeaWiFS data across the footprint of each CESM1 grid cell, so that the two datasets would have an identical spatial resolution. To reduce the number of days when cloud cover obscured satellite imagery, SeaWiFS and CESM1(BGC) chlorophyll concentration were averaged over 8-day time steps prior to $\log_{10}$ transformation. All phenological metrics were initially calculated with the 8-day time steps and were later multiplied by 8 to convert them to ordinal dates. Following these steps, 7.6% of oceanic pixels in the SeaWiFS dataset were obscured by clouds. In cases where data were missing for two adjacent time steps or less, we used MATLAB (MathWorks, Inc., Natick, MA, USA) to perform a piecewise, shape-preserving, cubic interpolation to fill data gaps. This step further reduced the percentage of cloud-obscured pixels to 3.4%.

One potentially confounding factor when comparing phenological events detected with CESM1(BGC) and SeaWiFS is that SeaWiFS often identified a greater number of blooms per year than CESM1(BGC) (Fig. 3.1). Both SeaWiFS and CESM1(BGC) detected two blooms per year in the Bering Sea, off the coast of British Columbia and Southeast Alaska, in the transition zone between the subtropical and subpolar gyres, and

near the equator. However, the equatorial area where two blooms per year occurred was much more widespread in SeaWiFS imagery than in the CESM1(BGC) ocean-ice hindcast. Similarly, SeaWiFS identified two blooms per year throughout much of the North Pacific subtropical gyre and CCE, whereas CESM1(BGC) typically detected one bloom per year in these regions. Similar results were obtained for both the threshold and harmonic approaches. Many of the additional blooms identified by SeaWiFS may represent short, episodic pulses of increased chlorophyll concentration that have been previously noted in subtropical regions (Racault *et al*., 2012). These episodic and largely aseasonal pulses do not seem to be fully captured by CESM1(BGC). To ensure that the comparison between SeaWiFS and CESM1(BGC) was based on analogous phenological events rather than aseasonal spikes in chlorophyll, we matched the first bloom of the year identified by CESM1(BGC) to the closest phenological event in the SeaWiFS time series. This step was performed separately for bloom initiation and termination to account for the fact that blooms beginning in one year sometimes extended into the next calendar year. For bloom duration, midpoint, and magnitude, we used the same indexing system as was used for bloom initiation when matching phenological events. While bloom matching was necessary to align blooms observed by SeaWiFS and CESM1(BGC) in areas with multiple blooms per year, we acknowledge that a side effect of this step could be to overstate correlations between SeaWiFS and CESM1(BGC). As a result, our comparison between these datasets should be interpreted as a "best case" scenario

Next, we mapped the mean and median dates of phenological events during 1998-2007 to identify regions where phytoplankton phenology differed between SeaWiFS and CESM1(BGC). Medians were considered in addition to means because medians provided

better indicators of winter events that may occur in either December or January during successive years. Mean values of ordinal dates can falsely suggest that such events take place during the middle of the calendar year. Spatial correlations between CESM1(BGC) and SeaWiFS were calculated for each phenological metric to assess model skill. This and all subsequent analyses focused solely on the first bloom identified each year. Since the spatial patterns of phenological events detected with the threshold and harmonic algorithms were generally similar and the threshold method produced higher correlation coefficients when comparing SeaWiFS and CESM1(BGC) for most phenological metrics (*i.e.*, bloom initiation, midpoint, and magnitude), we opted to present only results from the threshold method in this manuscript.

In addition to examining spatial correlations between CESM1(BGC) and SeaWiFS, we also calculated temporal correlations between these datasets reflecting interannual variations in the timing of phenological events that occurred between 1998 and 2007. This was done on a pixel-by-pixel basis and values of the resulting correlation coefficients were mapped over the North Pacific. Similar maps were also produced for correlations between CESM1(BGC) and SeaWiFS calculated based on annual and seasonal anomalies of $\log_{10}$-transformed chlorophyll. Correlation coefficients were averaged across 2° latitudinal bins to assess meridional patterns. Within these bins, we examined the difference between correlations based on annual and seasonal anomalies to evaluate whether there was a degradation in model skill when considering finer-scale, seasonal patterns.

2.4. Detection of Long-term Phenological Trends and Correlations with Climate Indices

Changes in phenological events were assessed using ordinal dates calculated over either a calendar year extending between January and December or an adjusted year spanning from July to June. When an adjusted year was used, an event occurring on July 1st would be assigned an ordinal date of 1, instead of an ordinal date of 182 for the calendar year. Use of the adjusted year was necessary to alleviate discontinuities in ordinal dates in areas where winter phytoplankton blooms may start during either January or December. If the calendar year were used in such areas to calculate rates of phenological change, a switch between bloom initiation in December (days 335-365) to bloom initiation in January (days 1-31) would be marked incorrectly as a large advance in phenology, instead of a smaller delay. Following Racault *et al*. (2012), we used the variance of phenological metrics to pinpoint regions where it was necessary to use the adjusted year. Variance is inflated in regions affected by the December/January discontinuity in ordinal dates. The Levene test of equality of variances was employed to assess whether the variance of bloom initiation, midpoint, or termination was significantly lower when using the adjusted time frame than when variances were calculated with the calendar year (Quinn and Keough, 2002). A second criterion for use of the adjusted year was that median date of a phenological event occurred between November and February. Since measurements of bloom duration and magnitude were unaffected by December/January discontinuities, the calendar year was used in all analyses of these metrics. Figure 3.2 shows that the adjusted year was mainly employed

in oligotrophic regions in the North Pacific subtropical gyre. It should be noted that occasionally phenological changes occurring in opposite directions were observed across adjacent pixels located near the boundary of where the adjusted year was used. In addition to employing the adjusted time frame when investigating long-term changes in CESM1(BGC) phenology, the adjusted time frame was also used when examining temporal correlations between phenological events identified with CESM1(BGC) and SeaWiFS (Section 2.3).

We examined long-term trends in phenological metrics over the years 1961-2007. Data from 1960 (*i.e.*, the first year of the CESM1(BGC) ocean-ice hindcast) were excluded from our analysis due to the fact that blooms beginning in fall/winter 1959 were characterized as having January 1960 start dates. This mischaracterization led to an initial jump in the time series of bloom initiation dates that could confound detection of phenological trends. The five phenological metrics (*i.e.*, bloom initiation, midpoint, termination, duration, and magnitude) from each ocean grid cell were regressed against year to identify long-term, linear changes in phenology. In these regressions and all other statistical tests, $p < 0.05$ was used as the threshold for establishing statistical significance. Given that regressions were performed on a pixel-by-pixel basis, it is possible that multiple testing could have led to accumulation of Type I error, while temporal autocorrelation may have artificially inflated test statistics. Consequently, our interpretation of statistical results primarily focused on identifying qualitative geographical patterns indicative of advancing phenology, delayed phenology, or no change in phenology. These geographical patterns were identified with maps of correlations between phenological metrics and year. In areas with significant negative or

positive correlations, we calculated the mean slope and standard error (SE) from the linear regressions to estimate the rate of change in phytoplankton phenology.

A similar set of analyses was performed to evaluate the relationship between phytoplankton phenology and the MEI, PDO, and NPGO indices. Correlations between the five phenological metrics and these climate indices were calculated across time lags of 0 to 6 months relative to the date of each metric. For bloom duration and magnitude, time lags relative to the midpoint of a particular phytoplankton bloom were employed. Time lags were necessary given that it can take several months for atmospheric teleconnections to propagate across the North Pacific (Schwing *et al*., 2003). Maps were produced displaying geographical areas where phytoplankton phenology was correlated with each climate index. In these maps, only results from the time lag with the lowest *p*-value were shown. We extracted information on the mean phenological change per a 1-unit anomaly in each climate index. These mean rates of change were calculated separately for locations exhibiting significant negative and positive correlations with regard to each climate oscillation.

To develop a better understanding of how climate oscillations may mechanistically affect phytoplankton phenology, we also examined the relationships between the five phenological metrics and three oceanic and atmospheric variables. These variables included NCEP wind speed at 10 m height and modeled SST and MLD from CESM1. Since the NCEP dataset has a native resolution of 1.9° latitude/longitude, linear interpolation was used to transfer wind speed data onto the CESM1 grid. Daily values of these environmental variables were summed over a two-month period of the year whose dates varied between pixels. This “degree days” approach was applied

because previous research has shown that most phenological events are more closely related to degree days than mean annual temperature (Wolkovich *et al*., 2012). The two-month period for calculating degree days (or MLD and wind speed days) included the month of median bloom initiation in a given pixel and the month prior to this event. We then examined correlations between these environmental variables and the five phenological metrics. Correlation strength was averaged zonally across 2° latitudinal bands to assess latitudinal variations in the relationship between phytoplankton phenology, SST, MLD, and wind speed.

We performed a PCA on each phenological metric to verify whether any of the climate oscillations or a long-term, linear trend was the predominant source of temporal variability in North Pacific phytoplankton phenology. Prior to conducting the PCA, any gaps in the time series of a phenological metric were filled with the *inpaint_nans* tool. Since pixels using both the calendar year and adjusted year were included in the PCAs, z-scores were used to standardize data from each grid cell by its mean and standard deviation prior to conducting this analysis (Quinn and Keough, 2002). The last year of data from the ocean-ice hindcast was removed from the PCA performed on bloom duration, because the full duration of some phytoplankton blooms may not have been recorded in this year, resulting in a large discontinuity in the time series of the first principal component of bloom duration between 2006 and 2007. The first five principal components for each phenological indicator were extracted and their correlations with the phenological time series from each ocean grid cell were mapped. We also assessed whether the time series of the first five principal component scores exhibited long-term, linear trends or were correlated with the annually averaged MEI, PDO, or NPGO indices.

When examining correlations with the climate oscillations, both time lags of 0 and 1 year were evaluated.

3. Results

3.1. Comparison between CESM1(BGC) and Empirical Observations

3.1.1. Modes of SST Variability in ICOADS and CESM1

The PCA performed on raw SST data indicated that the first five modes of SST variability explained 80.2% of the variance in ICOADS and 95.2% of the variance in CESM1. 73.4% and 82.6% of the SST variance could be attributed to the first principal component alone in ICOADS and CESM1, respectively. The next four principal components in each dataset accounted for 0.8-8.5% of SST variability. Each principal component from CESM1 was correlated with the equivalent principal component from ICOADS at $r \geq 0.78$ ($n = 576$, $p < 0.0001$, Table 3.1a, Fig. 3.3). In addition to the high degree of temporal correlation between principal components, the spatial patterns exhibited by each principal component were similar when comparing ICOADS and CESM1 (Fig. 3.4). The first principal component of both datasets described the annual seasonal cycle of SST across all latitudes > 10° N. Negative correlations with this principal component were also observed in southern hemisphere near the boundary of our study area (Fig. 3.4). Principal component 2 was related to seasonal variations in SST in the Eastern Tropic Pacific (ETP) (Fig. 3.4). The seasonal cycle in the ETP displayed a

smaller amplitude and greater interannual variability than the seasonal cycle of principal component 1. The third principal component of ICOADS and CESM1 SST revealed a seasonal signal that appeared to be modulated by the inverse of the PDO, since temperatures associated with this principal component dropped following the 1977 transition from negative to positive PDO conditions (Mantua *et al.*, 1997; Fig. 3.3). The principal component 3 time series subsequently increased in 1998 coincident with the return of negative PDO conditions (Chavez *et al*., 2003). High frequency, intraseasonal variability characterized the time series of the fourth and fifth principal components of ICOADS and CESM1 SST (Fig. 3.3).

A second set of PCAs was performed on monthly SST anomalies from ICOADS and CESM1 to determine whether the ocean-ice hindcast could successfully replicate empirical observations of SST variability at the interannual-to-decadal scale once the seasonal signal in these datasets was removed. In this analysis, the first five principal components explained much more variation in SST anomalies in CESM1 (72.4% of variance) than in ICOADS (20.1% of variance). Nevertheless, principal components 1-3 from each of these datasets were positively correlated ($r \geq 0.85$, $n = 576$, $p < 0.0001$) and displayed spatial patterns that resembled each other (Table 3.1b, Figs. 3.5-3.6). The fifth principal component of ICOADS and CESM1 SST anomalies were inversely correlated at $r = -0.62$ ($n = 576$, $p < 0.0001$). Compared to the other principal components, the correlation between principal component 4 from ICOADS and CESM1 was weaker ($r = 0.25$), albeit still statistically significant (Table 3.1b). Principal components 1 and 3 could be clearly interpreted in terms of the predominant climate oscillations in the North Pacific, since these principal components were highly correlated with the MEI (ICOADS:

r = 0.93; CESM1: r = 0.92) and PDO (ICOADS: r = -0.64; CESM1: r = -0.70), respectively. Similarly, the second principal component of monthly SST anomalies was moderately correlated with the NPGO (ICOADS: r = 0.33; CESM1: r = 0.48). Spatially, this principal component highlighted differences in SST variability between the center of the North Pacific subtropical gyre and the currents surrounding this gyre (Fig. 3.6). The fifth principal component of both ICOADS and CESM1 SST anomalies was not closely correlated with any North Pacific climate index. Its spatial pattern emphasized out-of-phase variability in SST anomalies between the eastern and western Pacific at latitudes > 30° N (Fig. 3.6).

In addition to displaying similar modes of variability as evidenced by PCA, CESM1 and ICOADS SST also exhibited similar amplitudes of their seasonal cycles (Fig. S3.1) and similar amplitudes of interannual variability (Fig. S3.2).

3.1.2. Mean and Median Phytoplankton Phenology in SeaWiFS and CESM1(BGC)

Maps of the dates of bloom initiation, midpoint, and termination produced with SeaWiFS and CESM1(BGC) showed similar spatial patterns with distinct phenological regions observed in the Bering Sea, Sea of Okhotsk, subpolar gyre, subtropical gyre, and near the equator (Fig. 3.7). The Bering and Okhotsk Seas were characterized by an initial increase in chlorophyll concentration in May/June, with bloom termination observed during the months of July through September. While these dates were similar in SeaWiFS and CESM1(BGC) imagery, the regions of the Bering and Okhotsk Seas with the latest initiation and termination of phytoplankton blooms differed between these datasets. In

CESM1(BGC), bloom onset and termination occurred later offshore of the southern tip of the Kamchatka Peninsula and around the Aleutian Islands. In contrast, SeaWiFS indicated that bloom initiation and termination occurred latest in the central region of the Bering Sea (Fig. 3.7). Generally, phenological indicators estimated by SeaWiFS and CESM1(BGC) differed by less than one month in this region, with the exception of the area east of the Kamchatka Peninsula where CESM1(BGC) identified blooms with earlier phenology.

In the North Pacific subpolar gyre, CESM1(BGC) also predicted earlier phenology events than those observed by SeaWiFS. Throughout most of this region, CESM1(BGC) indicated that phytoplankton blooms would begin in February and March, whereas SeaWiFS observations displayed greater spatial variability with the mean date of bloom initiation occurring between April and June (Fig. 3.7). A similar pattern also emerged when examining subpolar bloom midpoints and termination. In the SeaWiFS imagery, there was a progression from earlier to later phenology with increasing latitude across the subpolar gyre. This latitudinal gradient was less pronounced in CESM1(BGC). Throughout large areas of the subpolar gyre, the difference between SeaWiFS and CESM1(BGC) phenological indicators exceeded 60 days.

The North Pacific subtropical gyre was characterized by late fall and winter blooms of phytoplankton where chlorophyll concentration typically began to rise between October and December (Figs. 3.7 and S3.3). Since January bloom initiation was also prevalent in the subtropical gyre, the average dates of phenological events in this region were sometimes misleading, implying that bloom initiation occurred in earlier in the fall or summer (Fig. 3.7). Generally, SeaWiFS observations of phytoplankton phenology

were slightly earlier than CESM1(BGC), with greater intra-regional variability in bloom initiation, midpoints, and termination in SeaWiFS. CESM1(BGC) also predicted that the extent of the subtropical gyre would be slightly larger than was observed in SeaWiFS imagery. This difference in gyre size resulted in large discrepancies in phenology (*e.g.*, ≥ 120 days) near the northern and southern boundaries of the subtropical gyre. However, sizeable expanses of the gyre center exhibited differences between CESM1(BGC) and SeaWiFS phenology that were ≤ 30 days.

Maps of phytoplankton phenology in the equatorial Pacific revealed much spatial complexity, reflecting distinct oceanographic features, such as the North Equatorial Current and the equatorial upwelling zone in the ETP (Fig. 3.7). The onset of the seasonal increase in chlorophyll occurred in the early spring in the North Equatorial Current (*e.g.*, ordinal day < 120), while blooms typically ended between ordinal days ~130-180 in this region. In the eastern equatorial region where upwelling is strongest, phytoplankton blooms started during summer months (*e.g.*, June/July) and extended through fall (*e.g.*, September-November). Compared to CESM1(BGC), SeaWiFS phytoplankton blooms occurred later in the North Equatorial Current, but earlier in the ETP. Nevertheless, differences between SeaWiFS and CESM1(BGC) in terms of equatorial phenology were generally small (*e.g.*, ≤ 30 days).

Compared to other phenological metrics, bloom duration exhibited less spatial variability across our study area. In most locations, phytoplankton blooms lasted between 75-100 days (Fig. 3.7). Slightly shorter blooms (*e.g.*, < 60 days) were observed in the subpolar region, especially in SeaWiFS imagery. The longest lasting phytoplankton blooms (*e.g.*, ≥ 120 days) were recorded in the central equatorial region. Across > 60% of

the North Pacific, bloom duration estimated with SeaWiFS and CESM1(BGC) differed by no more than one month. The greatest discrepancies between these datasets in terms of bloom duration (*e.g.,* 50-70 days) occurred in the Bering Sea, where CESM1(BGC) predicted longer blooms.

Geographical variations in bloom magnitude closely resembled gradients in mean annual CESM1(BGC) and SeaWiFS chlorophyll concentration, which have been described by Moore *et al*. (2013). An oligotrophic region with ≤ 0.2 mg m^{-3} of chlorophyll was observed throughout the North Pacific subtropical gyre (Fig. 3.7). Mesotrophic conditions where there were ~0.3-1.0 mg m^{-3} of chlorophyll during phytoplankton blooms occurred throughout most of the subpolar gyre and the equatorial upwelling region. Chlorophyll concentrations exceeding 1 mg m^{-3} were found in the Bering Sea, Sea of Okhotsk, and off the continental shelf of North America in SeaWiFS imagery. However, CESM1(BGC) did not resolve the elevated chlorophyll concentration present during phytoplankton blooms in coastal regions. In addition, the bloom magnitude estimated by CESM1(BGC) was slightly too high in the oligotrophic subtropical gyre, but was biased low in the subpolar gyre.

Spatial correlations between SeaWiFS and CESM1(BGC) indicated that this model had the greatest skill at resolving mean spatial patterns related to bloom initiation ($r = 0.65$), bloom midpoint ($r = 0.67$), and bloom magnitude ($r = 0.65$). When compared to SeaWiFS, CESM1(BGC) exhibited an intermediate ability to reproduce geographic patterns corresponding to bloom termination ($r = 0.51$) and a low capacity to reproduce variations in bloom duration ($r = 0.18$). Spatial correlations between SeaWIFS and CESM1(BGC) based on median values of phenological metrics (Fig. S3.3) were slightly

lower than those obtained from mean values. While these spatial correlations were highly significant for all phenological metrics ($p < 0.0001$) due to the large sample size (n = 15,885), less confidence should be given to trends in CESM1(BGC) phenology for metrics that displayed weaker spatial correlations with SeaWiFS.

3.1.3. Temporal Correlations between SeaWiFS and CESM1(BGC) Phenology

In addition to examining mean and median spatial patterns in SeaWiFS and CESM1(BGC), we also investigated whether the ocean-ice hindcast could reproduce interannual variability in phytoplankton phenology over the 1998-2007 period when SeaWiFS was operational. Temporal correlations between SeaWiFS and CESM1(BGC) were calculated on a pixel-by-pixel basis using year-to-year variations in each phenological metric. During the initiation of phytoplankton blooms, the strongest temporal correlations between SeaWiFS and CESM1(BGC) were observed in the subtropical gyre and the equatorial Pacific (Fig. 3.8a-b). Positive, but weaker correlations, occurred in the eastern Bering Sea, while, in other regions of the subpolar gyre and the North Equatorial Current, the sign of correlations was variable. Overall, temporal correlations between SeaWiFS and CESM1(BGC) bloom initiation dates were positive across 76.2% of pixels and had values of $r > 0.5$ across 37.0% of pixels (Fig. 3.9). Similar patterns were observed for bloom midpoint, although temporal correlations averaged across 2° latitudinal bins were slightly lower than those for bloom initiation (Fig. 3.8d). Unlike bloom initiation and midpoint where the greatest similarities between SeaWiFS and CESM1(BGC) were found at mid-latitudes, the latitudinal band with the

most widespread, positive correlations occurred in the Bering Sea for bloom termination (Fig. 3.8e-f). At other locations, latitudinally averaged, temporal correlations for bloom termination generally varied between $0.18 < r < 0.35$ (Fig. 3.8f). For bloom duration, the only regions where interannual correlations between SeaWiFS and CESM1(BGC) were consistently large and positive occurred at 30° N and in the CCE (Fig. 3.8g-h). While estimates of bloom magnitude based on SeaWiFS and CESM1(BGC) were highly correlated when examining mean spatial patterns, correlations between these datasets were much weaker when considering interannual variations in bloom magnitude (Fig. 3.8i-j). Across most latitudes, interannual correlations for bloom magnitude rarely exceeded $r = 0.2$ as maps of this variable contained sizable areas with both positive and negative correlations. Generally, bloom duration and magnitude contained fewer areas with positive, interannual correlations than did bloom initiation, midpoint and termination (Fig. 3.9).

The supplemental information for this chapter also presents maps of correlations between SeaWiFS and CESM1(BGC) based on annual and seasonal anomalies of log10-transformed chlorophyll (Fig. S3.4). Correlations based on annual and seasonal anomalies were compared to determine whether model skill declined or improved when examining increasingly finer scale, seasonal patterns. At latitudes < 36° N, model skill was generally greater when considering fall anomalies than when examining annual chlorophyll anomalies (Fig. S3.5). At latitudes over 42° N and 50° N, respectively, model skill during winter and spring exceeded the capacity of CESM1(BGC) to predict annual anomalies. Since fall blooms characterized much of the subtropical gyre and late winter/spring blooms occurred across subpolar latitudes, these patterns indicated that

model skill was typically greatest during the season when chlorophyll concentration increased towards its maximal level.

3.2. Changes in Phenology between 1961-2007 based on the Ocean-Ice Hindcast

3.2.1. Long-term, Linear Trends in Phytoplankton Phenology

Between 1961-2007, significant long-term, linear trends in the timing of bloom initiation were observed in 19.5% of the ocean grid cells tracked by CESM1(BGC) (Table 3.2). In Figure 3.10, regions exhibiting delays in phenology are indicated by positive correlations between bloom initiation date and year, while earlier phenological events are denoted by negative correlations. An approximately equal number of grid cells displayed long-term advances (n = 1664) and delays (n = 1432) in bloom initiation. Areas where bloom initiation became earlier during the latter half of the 20th century included the coastal region off Central America and the southwestern extent of our study area (Fig. 3.10a). Later bloom initiation was observed most frequently in the western subpolar gyre and the area located between 120-160° W and 0-20° N. Nevertheless, pixels with significant, long-term trends in bloom initiation dates were largely scattered in small patches throughout much of the study area. A similar spatial pattern was detected when investigating long-term changes in bloom midpoint, although delays in bloom midpoint had a wider spread distribution in the subpolar gyre (Fig. 3.10b).

Long-term trends in bloom termination differed from bloom initiation and midpoint in two notable ways. First, only 13.6% of ocean grid cells exhibited trends in

phenology at the end of phytoplankton blooms (Table 3.2). This percentage was substantially lower than the equivalent percentages for bloom initiation and midpoint. Second, delays in phenology were more common than phenological advances when examining bloom termination (Fig. 3.10c). Delayed phenology was observed in nearly 60% of grid cells with significant changes in the date of bloom termination. Nevertheless, the areas exhibiting delayed phenology at the end of blooms had a similar distribution as areas identified as having delayed bloom initiation and midpoint. In contrast, advancing phenology in tropical and subtropical areas was much more limited in spatial extent when investigating changes in bloom termination (Fig. 3.10c). Similarities between bloom initiation and termination phenology resulted in relatively few areas with changes in bloom duration. Only 10.2% of CESM1 pixels displayed long-term, linear trends in bloom duration (Table 3.2). However, some noteworthy spatial patterns in bloom duration were apparent. In areas with statistically significant changes in bloom duration, blooms tended to become longer in mesotrophic-to-eutrophic regions in the subpolar gyre and ETP, whereas shorter blooms were observed across parts of the oligotrophic subtropical gyre (Fig. 3.10d).

Compared to other phenological metrics, long-term changes in bloom magnitude occurred across a wider geographical area, with significant trends in 48.2% of CESM1 grid cells (Table 3.2). The average concentration of chlorophyll during phytoplankton blooms decreased throughout most of the North Pacific subtropical gyre during the years 1961-2007 (Fig. 3.10e). Scattered areas off the coast of British Columbia and Alaska also exhibited reductions in bloom magnitude, while other subpolar regions experienced

increases in chlorophyll concentration during phytoplankton blooms. Most equatorial areas did not display any trends in bloom magnitude over the 1961-2007 period.

3.2.2. Relationships between Climate Oscillations and Phytoplankton Phenology

Correlations between phenological metrics and climate oscillations were assessed over time lags of 0-6 months to allow for the propagation of climate anomalies across the Pacific basin. For most climate indices and phenological metrics, the percentage of CESM1 grid cells that were significantly correlated with a climate oscillation decreased slightly as time lags increased. However, the spatial patterns associated with climate effects on phenology generally did not change much across time lags. As a result, we have presented results jointly for all time lags.

The PDO and MEI, respectively, exerted a significant influence on the date of bloom initiation across 33.9% and 26.7% of pixels in the North Pacific (Table 3.2). Despite the PDO's slightly more widespread effect, the spatial signature of PDO and MEI correlations with bloom initiation were similar (Fig. 3.11). During positive anomalies of the MEI and PDO indices, warmer than average SST was observed in the northeast Pacific, whereas cool-to-moderate SST predominated in the northwest Pacific (Mantua *et al*., 1997; Wolter and Timlin, 2011). In the subpolar gyre, earlier bloom initiation, indicated by negative correlations with the MEI and PDO, was associated with warm conditions in eastern Pacific, whereas later bloom initiation (*i.e*., positive correlations) occurred during cool conditions in the western Pacific when the MEI and PDO were in their positive phase. The opposite pattern was observed in the subtropical gyre and

equatorial region. At latitudes less than ~30° N, higher SST in the eastern Pacific during positive MEI and PDO anomalies coincided with delayed bloom initiation, while earlier bloom initiation occurred across small patches of pixels in the west. Overall, the similarities between the spatial signatures of the MEI and PDO indicated that phytoplankton phenology reacted similarly to warming whether it occurred at the interannual scale of El Niño/La Niña or the decadal scale of the PDO.

Analogous spatial patterns were observed when examining the effects of the PDO and MEI on bloom midpoint and termination (Figs. S3.6-S3.7). Again, the spatial signature of PDO and MEI effects revealed asynchronous phenological patterns across the east and west Pacific. However, the latitudinal emphasis of PDO and MEI effects on bloom midpoint and termination differed slightly from the pattern observed for bloom initiation. In maps of correlations between these climate indices and bloom midpoint and termination, significant correlations were more prevalent at high latitudes (> 40° N) for the PDO and at lower latitudes (< 40° N) for the MEI (Figs. S3.6-S3.7). Also, compared to bloom initiation, 3-5% fewer pixels were significantly correlated with the PDO and MEI indices (Table 3.2), resulting in decreased spatial coherency in maps of PDO and MEI effects on bloom midpoint and termination.

In contrast to the previously discussed phenological metrics, out-of-phase variations in phenology across the western and eastern Pacific were not evident when assessing the influence of the MEI and PDO on bloom duration (Fig. 3.12). For both of these climate oscillations, positive anomalies led to predominantly to shorter phytoplankton blooms at latitudes below 40° N and longer blooms in the Alaska gyre and other subpolar regions. As was the case with bloom midpoint and termination, MEI

effects on bloom duration were most prevalent in equatorial areas, whereas bloom duration was more closely correlated with the PDO in the subpolar gyre.

When changes in bloom magnitude were assessed, the PDO and MEI effects extended over a larger expanse of the North Pacific than when examining other phenological metrics. Significant correlations between the PDO and bloom magnitude were observed in 52.5% of CESM1 grid cells (Table 3.2). Variations in the MEI affected bloom magnitude over a smaller area (*i.e.*, 40.6% of ocean grid cells, Table 3.2, Fig. 3.13). In > 80% of grid cells with significant effects of these climate oscillations, positive MEI and PDO anomalies resulted in decreases in bloom magnitude. These reductions in chlorophyll concentration occurred throughout the equatorial Pacific, across subtropical latitudes < 30° N, and in the Alaska gyre. The only region where positive MEI and PDO conditions were associated with larger phytoplankton blooms was in the western subpolar region, as well as in the western section of the transition between the subpolar and subtropical gyres (Fig. 3.13). Again, the subpolar expression of this pattern was more pronounced for the PDO index than the MEI. Overall, the effects of the MEI and PDO on bloom magnitude exhibited a similar spatial signature as for long-term, linear trends in bloom magnitude (Fig. 3.10e).

Compared to the PDO and MEI, the NPGO displayed a less extensive effect on phytoplankton phenology. Significant correlations between the NPGO and dates of bloom initiation, midpoint, and termination occurred in 21.0% to 23.7% of CESM1 grid cells (Table 3.2). The NPGO also differed from the PDO and MEI in terms of the spatial signature of its effect on phenology. Bloom initiation was positively correlated with the NPGO in the ETP and Alaska gyre to the south of the Aleutian Islands (Fig. 3.11). These

are both locations where positive NPGO anomalies typically coincide with cooler surface temperatures and lower SSH (Di Lorenzo *et al.*, 2008), implying that these conditions may be associated with the later onset of phytoplankton blooms. Negative correlations between the NPGO and bloom initiation were found to the west of the ETP, the northwest of the Aleutian Islands, and extended farther eastward at mid-latitudes (Fig. 3.13). Similarly, regions with positive correlations between SST, SSH, and the NPGO were mainly found in the western Pacific but expanded eastward at mid-latitudes (Di Lorenzo *et al*., 2008). This indicated that warmer temperatures, high SSH, and an earlier onset of phytoplankton blooms accompanied positive NPGO conditions across this area. The regional response of phytoplankton phenology to variations in the NPGO index was similar regardless of whether bloom initiation, midpoint, or termination was considered (Figs. S3.6-S3.7). Due to the fact that NPGO-related variations in bloom initiation and termination largely tracked each other, relatively few areas of the North Pacific exhibited significant correlations between bloom duration and the NPGO. With a few exceptions, the areas that did have significant correlations with bloom duration were mostly characterized by shorter blooms during the positive phase of the NPGO (Fig. 3.12). Positive NPGO conditions were also associated with larger phytoplankton blooms across sections of the North Pacific subpolar gyre, in the western equatorial zone, and at latitudes between ~20-40° N in the eastern Pacific (Fig. 3.13). The only area were there were negative correlations between bloom magnitude and the NPGO was located in subtropical gyre at 30° N.

3.2.3. Rates of Phenological Change

Figure 3.14 compares the rates of phenological change observed over the 1961-2008 period across climate indices and phenological metrics. Rates of changes in bloom initiation, midpoint, termination, and duration are presented in days per decade when examining long-term, linear trends and in days per unit climate anomaly when investigating the influence of climate oscillations. At sites where significant climate effects were observed, El Niño and La Niña events typically induced larger changes in phytoplankton phenology than did variations in the PDO and NPGO indices. For example, in regions where climate oscillations induced shifts in bloom initiation date, a 1-unit anomaly change in the MEI prompted a mean phenological change of 21.9 ± 0.3 SE days, while a 1-unit anomaly change in the PDO and NPGO resulted in changes of 17.4 ± 0.2 SE days and 17.9 ± 0.3 SE days, respectively. These numbers are based on the absolute value of phenological change, but faster MEI-associated changes were also apparent when advances and delays in phytoplankton phenology were examined separately (Fig. 3.14).

Due to the use of different units, rates of long-term, phenological change cannot be directly compared to the phenological effects of climate oscillations. However, the maximum extent of changes in phenology associated with long-term trends and climate indices can be inferred by multiplying rates of change by the full range of years and climate anomalies examined in our analysis. Annually averaged MEI anomalies ranged between -1.4 and 1.7 during the 47-years of the ocean-ice hindcast, while PDO and NPGO anomalies ranged between -1.3–1.8 and -1.9–2.1, respectively. In the example presented above for changes in bloom initiation date, this translated into a maximum

phenological response to variations in the MEI of 67.9 days (*i.e.*, 21.9 days anomaly^{-1} × Δ3.1 anomalies). Similar calculations yielded maximum responses of 53.9 days for the PDO, 71.6 days for the NPGO, and 69.4 days for regions with long-term trends in the date of bloom initiation. Since similar results were obtained for other phenological metrics, this analysis revealed that long-term trends in phenology currently have effects of a similar size to the dominant sources of natural climate variability in the North Pacific.

When rates of change were compared across phenological metrics, shifts in bloom termination date typically occurred more rapidly than changes in the onset of phytoplankton blooms (Fig. 3.14). For example, in areas where blooms exhibited linear trends towards earlier phenology, bloom termination advanced at a rate of -29.1 ± 0.6 SE days decade^{-1}, which was nearly twice the speed of changes in bloom initiation (*i.e.*, -15.7 ± 0.3 SE days decade^{-1}). Faster changes in bloom termination were more prominent in regions with advancing phenology, although this pattern was also observed in areas with delayed phenology. In most cases, changes in bloom midpoint took place at a rate intermediate between shifts in bloom onset and termination. Since most regions experienced phenological shifts in both bloom initiation and termination in the same direction (Figs. 3.10, 3.11, S3.7), the rate of changes in bloom duration was small compared to other phenological metrics (Fig. 3.14). One final pattern evident in Figure 3.14 is that, even though both advances and delays in phytoplankton phenology were prevalent across the North Pacific, phenological advances occurred more rapidly. This pattern was particularly pronounced for bloom midpoint and termination.

3.2.4. Relationship between Phytoplankton Phenology and Oceanic and Atmospheric Variables

The effect of environmental variables on bloom initiation varied depending on whether latitudes north or south of ~35° N were considered (Fig. 3.15). North of this latitude, years with earlier bloom initiation were associated with weaker wind speed, warmer temperatures, and a shallow MLD. Earlier onset of peaks in chlorophyll concentration to the south of 35° N was correlated with cool temperatures, faster winds, and deeper MLD. The one exception to this latitudinal pattern was that earlier blooms in the ETP coincided with shallow MLD (Fig. 3.15c). This may reflect the fact that upwelling occurs throughout a larger area of the ETP during the fall (Pennington *et al*., 2006), such that blooms occurring later in the year would be associated with a deeper mixed layer. Significant correlations between bloom initiation and MLD were observed over a larger area of the North Pacific than were correlations between bloom initiation, wind speed, and SST (Table 3.2).

Since earlier phytoplankton blooms often have earlier midpoint and termination dates, a similar latitudinal pattern was observed when examining correlations between these phenological metrics, wind speed, and MLD (Figs. S3.8-S3.9). However, significant correlations between these variables and bloom midpoint and termination occurred across a smaller portion of the North Pacific than was the case for bloom initiation (Table 3.2). Unlike wind speed and MLD, there was not a clear difference between subtropical and subpolar areas in terms of relationships between SST, bloom midpoint, and bloom termination.

Similar to our results for bloom midpoint and termination, significant correlations between bloom duration and environmental variables were detected across a relatively sparse area of the North Pacific (Fig. 3.16 and Table 3.2). In regions where significant correlations occurred, there was again a change in the direction of the correlations between areas located approximately south or north of 35° N (Fig. 3.16d). Longer-lasting peaks in chlorophyll concentration were noted north of this latitude when MLD was shallow, wind speed was weak, and SST was warm. This pattern was more evident in Gulf of Alaska than in other regions of the subpolar gyre. To the south, longer peaks in chlorophyll concentration were associated with deep MLD, strong winds, and cool temperatures.

Across most latitudes, larger peaks in bloom magnitude were observed during years with faster wind speeds, cooler than average SST, and a deep mixed layer (Fig. 3.17). Compared to other phenological metrics, statistically significant effects of environmental variables on bloom magnitude were fairly widespread, occurring across 33-46% of CESM1 grid cells (Table 3.2). Another difference between bloom magnitude and other phenological metrics is that SST was the environmental variable with the most prevalent influence on the size of phytoplankton blooms. In contrast, MLD had a slightly more widespread effect on bloom initiation, midpoint, termination, and duration than the other oceanic and atmospheric variables (Table 3.2).

3.2.5. Principal Component Analysis (PCA) Examining Phytoplankton Phenology

Due to the fact that a total of 15,885 CESM1 grid cells were included in the PCA, the first principal component of bloom initiation phenology only accounted for 6.2% of the variance in this dataset (Table 3.3). Nevertheless, this principal component captured variability in phenology across a moderately widespread area, since its time series was significantly correlated with temporal trends in bloom initiation in 25.7% of the pixels tracked by CESM1(BGC). The amount of variance explained by each principal component and the percentage of correlated pixels decreased steadily as successive principal components of bloom initiation were considered, such that the fifth principal component accounted for 3.9% of the variance in this dataset and was correlated with 13.3% of CESM1 grid cells. A similar percentage of phenological variance was explained by the first five principal components from PCAs performed on bloom midpoint, termination, and duration. In contrast, the first principal component of bloom magnitude encompassed 21.8% of the variance in chlorophyll concentration, a much larger percentage than was observed for other phenological metrics. This reflected the fact that there was greater spatial coherency in maps of changes in bloom magnitude than maps of other variables (Figs. 3.10-3.13, S3.6-S3.7).

Since climate oscillations and long-term trends generally affected phytoplankton phenology across one-third or less of the ocean grid cells tracked by CESM1(BGC), we wanted to verify whether these factors were the predominant influences affecting temporal variations in phenology across the North Pacific. To realize this objective, we examined whether the first five principal components of our phenological metrics were correlated with any of the previously discussed climatic factors. Of the 25 principal components considered here (*e.g.*, five principal components per each of five

phenological metrics), 19 were correlated with the MEI, PDO, or NPGO or exhibited a significant long-term, linear trend (Fig. 3.18). Often a particular principal component was correlated with multiple climate indices. In 16 of the 19 cases where significant correlations were detected, the strongest correlation reflected either a long-term, linear trend or the influence of the MEI.

The temporal trends and spatial patterns associated with the first principal component of each phenological metric are shown in Figure 3.19. Figures S3.10-S3.14 contain supplemental information on the time series and regional expression of principal components 2-5, although these are not discussed here. The first principal component of both bloom initiation and midpoint displayed long-term trends, albeit in different directions (Fig. 3.19a-b). For bloom initiation, its first principal component exhibited a continuous decline ($Y = 3{,}487.72 - 1.76\,X$, $r^2 = 0.57$, $n = 46$, $p < 0.0001$), such that sites positively correlated with this principal component were characterized by earlier initiation of phytoplankton blooms in recent years. The spatial signature of the first principal component of bloom initiation was similar to the pattern seen when examining sites with long-term changes in the date of bloom onset (Figs. 3.10a and 3.19f), although correlations with pixels were in opposite directions. Both maps in Figs. 3.10a and 3.19f show advancing phytoplankton phenology in the ETP and southwestern extent of our study area, while delays in bloom initiation were found in the western subpolar gyre and immediately west of the ETP. The slight asynchrony in phenological patterns between the western and eastern Pacific observed in this principal component's regional expression may be due to the fact that this principal component was also correlated with the MEI and PDO (Fig. 3.18).

This zonal asynchrony in phenology was also evident in the first principal component of bloom midpoint (Fig. 3.19g). Since this principal component's time series showed a continual increase ($Y = -2{,}706.73 + 1.36X$, $r^2 = 0.35$, $n = 46$, $p < 0.0001$, Fig. 3.19b), sites in the eastern Pacific that were positively correlated with the first principal component of bloom midpoint can be interpreted as locations where phytoplankton are now blooming later in the year than they were in the early 1960s. Conversely, most areas west of 160° W and south of 40° N were negatively correlated with the first principal component of bloom midpoint and exhibited long-term advances in phenology.

The first principal component of bloom termination was most closely correlated with the MEI (Fig. 3.19c). This correlation had an r of 0.51 and a p-value of 0.0003 (n = 46) when a one-year time lag was used. Since La Niña events typically lag El Niño by about one year, correlations with this principal component can be interpreted in terms of the relationship between La Niña and bloom termination phenology. The spatial signature of this principal component indicated that, during La Niña years, phytoplankton blooms ended earlier than usual in the eastern Pacific, but ended later in the western-to-central Pacific (Fig. 3.19h). This pattern was consistent across all latitudes.

The first principal component of bloom duration could also be interpreted in terms of the effect of La Niña on phenology, since this principal component was inversely correlated with the MEI ($r = -0.45$, $n = 46$, $p = 0.0018$, Fig. 3.19d). Based on the map identifying pixels correlated with this principal component, La Niña most strongly affected bloom duration in the equatorial region, where cool, La Niña conditions coincided with longer lasting phytoplankton blooms (Fig. 3.19i). A similar spatial pattern

was noted in Fig. 3.12 when examining the relationship between bloom duration and the MEI.

Like bloom initiation, the first principal component of bloom magnitude revealed a long-term decline, which indicated a decrease in mean chlorophyll concentration during phytoplankton blooms ($Y = 5{,}922.55 - 2.99X$, $r^2 = 0.48$, $n = 47$, $p < 0.0001$, Fig. 3.19e). However, this time series also showed a minor reversal leading to an increase in bloom magnitude beginning in the late 1990s. The timing of this reversal appears to have coincided with the 1998 change in the sign of the PDO. The PDO and the first principal component of bloom magnitude were indeed significantly correlated, but this correlation explained a smaller percentage of the variance in this principal component time series ($r^2 = 0.41$, $n = 47$, $p < 0.0001$) than the long-term trend (Fig. 3.19). Throughout the North Pacific, interannual variations in bloom magnitude at latitudes < 30° N were positively correlated with this principal component, suggesting bloom magnitude has declined over time in this region (Fig. 3.19j).

4. Discussion

4.1. Detection of Mean Phenological Patterns across the North Pacific

Several recent papers have used the SeaWiFS chlorophyll time series to examine mean phenological patterns across the North Pacific using different methods to detect the onset and termination of phytoplankton blooms (Sasaoka *et al*., 2011; Racault *et al*., 2012; Sapiano *et al*., 2012). A study comparing ten methods of identifying terrestrial

phenological events with remote sensing indicated that differences between methods could bias estimates of phenology by as much as two months (White *et al*., 2009). It is likely that comparably large differences between methods exist when using remote sensing to characterize phytoplankton phenology. As a result, it is useful to compare our findings to other phenological studies to evaluate whether the discrepancies between CESM1(BGC) and SeaWiFS are large relative to differences in mean phytoplankton phenology that emerge due to the application of different phenological methods.

In the North Pacific subpolar gyre, Racault *et al*. (2012) and Sasaoka *et al*. (2011) both identified late April through June as the period of bloom initiation based on SeaWiFS. Our analysis of SeaWiFS produced estimates of bloom initiation consistent with these studies. In contrast, Sapiano *et al*. (2012) detected greater spatial variability of bloom onset across the subpolar gyre, indicating that phytoplankton blooms could begin anywhere between March and July. This wider range of dates begins to encompass the February-March bloom onset detected in this region by CESM1(BGC). Another difference between CESM1(BGC) and SeaWiFS phenology was that all four SeaWiFS-based analyses in the subpolar gyre showed that the gyre center had the latest occurring phytoplankton blooms. CESM1(BGC) identified the Aleutian Islands and the area surrounding the Kamchatka Peninsula as displaying the latest blooms.

Since the subtropical gyre is an oligotrophic region with a low-amplitude seasonal cycle, it is characterized by a reduced signal-to-noise ratio for detecting phenological patterns, which has caused studies utilizing different methods to identify varying dates of bloom onset. Due to the low seasonal signal-to-noise ratio, Sapiano *et al.* (2012) was unable to detect any phenological pattern in the southern sector of the North Pacific

subtropical gyre and declared this to be an aseasonal region. Farther north, Sapiano *et al*. (2012) found that most phytoplankton blooms began in October and December, although February/March bloom onset was common along the northern boundary of this biome. Racault *et al*. (2012) also identified differences between the southern and northern subtropical gyre in terms of phenology. In the northern gyre, Racault *et al*. (2012) obtained similar results to Sapiano *et al*. (2012), detecting a winter onset of phytoplankton blooms that occurred between November and March. However, summer initiation (*e.g*., July-October) of blooms was reported from the southern subtropical gyre by Racault *et al*. (2012). The difference between these studies may stem from the fact that Racault *et al*. (2012) noted that some phytoplankton blooms in the subtropical gyre were the result of episodic, aseasonal mixing events. Since Sapiano *et al.* (2012) identified blooms by fitting seasonal, harmonic functions to the SeaWiFS time series, their method would not have been able to detect episodic blooms that may have been especially common in the southern subtropical gyre. Our results from both CESM1(BGC) and SeaWiFS are broadly consistent with these two studies, since we identified October-January as the median months of bloom onset throughout most of the subtropical gyre, with February/March bloom initiation occurring near the gyre's northern boundary. Like Racault *et al*. (2012), we also detected a few regions of the gyre where the median date of bloom onset occurred during summer. Differences in the seasonal dynamics of the northern and southern halves of the subtropical gyre have also been described in the North Atlantic, where phenology varies out-of-phase across these regions (Ueyama and Monger, 2005).

Of the biogeographical regions examined here, the equatorial zone exhibited the greatest spatial variation in mean phenological patterns. This variability was also evident in a review of primary production in the ETP, where early spring maximum of chlorophyll concentration were identified near Panama, the Peruvian upwelling area, and in the North Equatorial Counter Current; winter peaks in chlorophyll occurred off Tehuantepec and in the North Equatorial Current, and; summer maxima were observed in the equatorial upwelling region, South Equatorial Current, and around the Galapagos (Pennington *et al*., 2006). Much of this phenological diversity can be attributed to the influence of upwelling in the eastern equatorial region. Since the geographic extent of equatorial upwelling is maximal during summer and fall (Pennington *et al*., 2006), chlorophyll concentration in regions affected by upwelling also peaked during these months. This explains why both our study and Racault *et al*. (2012) detected phytoplankton blooms occurring between June-September in the eastern equatorial region. Sapiano *et al*. (2012) identified slightly later onset of phytoplankton blooms (*e.g*., September-December) in this area. Both our study and Sapiano *et al*. (2012) observed a high degree of spatial patchiness in equatorial phytoplankton phenology, as well as an east-west gradient in bloom initiation dates. All three studies showed phytoplankton blooms beginning during December-March in the central-to-western equatorial Pacific. These patterns were evident in analyses performed with both CESM1(BGC) and SeaWiFS. Overall, differences between CESM1(BGC) and SeaWiFS in terms of mean bloom initiation dates were of a similar magnitude to discrepancies between SeaWiFS-based analyses that used different methods to identify phenological transition points.

While relatively consistent geographic patterns were observed across all studies of bloom initiation and termination phenology, this was not the case for bloom duration. Racault *et al*. (2012) and Sasaoka *et al*. (2011) identified short phytoplankton blooms lasting ≤ 100 days in the subpolar and southern subtropical gyres, with longer blooms (*e.g*., 105-150 days) detected in the northern subtropical gyre and around the equator. North of 30° N, Racault *et al*. (2012) also observed a decrease in bloom duration with increasing latitude, although this pattern was more pronounced in the North Atlantic than the North Pacific. In contrast, Sapiano *et al.* (2012) detected longer-lasting phytoplankton blooms (*e.g*., 120-180 days) with uniform bloom duration found across different latitudinal bands. Sapiano *et al*. (2012) did not detect a decrease in bloom duration with increasing latitude. Our results were more consistent with Racault *et al*. (2012) and Sasaoka *et al*. (2011) in terms of the length of phytoplankton blooms, but were similar to Sapiano *et al*. (2012) in that we did not detect a strong latitudinal gradient. Another commonality between our work and Sapiano *et al*. (2012) was that bloom duration was longest in the center of the subpolar gyre compared to surrounding regions. Interestingly, this pattern was more clearly displayed in CESM1(BGC) than SeaWiFS.

Since we initially applied both threshold and statistical approaches for characterizing phytoplankton phenology, our research offered insight into the source of discrepancy in bloom duration identified by Racault *et al*. (2012) and Sapiano *et al*. (2011). When we examined estimates of bloom duration generated from our harmonic algorithm, we found longer-lasting phytoplankton blooms (often 100-200 days) and increased prevalence of zonal banding, similar to Sapiano *et al*. (2012). Since our harmonic algorithm and the algorithm developed by Sapiano *et al*. (2012) differed in

terms of the definition of bloom initiation and termination, parameter optimization technique, and treatment of multiple years of data, these similarities may reflect general properties of the statistical methods used to characterize phytoplankton phenology.

One additional area where it is worthwhile to compare our results with previous studies of North Pacific phytoplankton phenology is the geographic pattern of the mean number of blooms per year. Racault *et al*. (2012) and Sasaoka *et al*. (2011) limited their analysis to the first phytoplankton bloom detected each year, whereas Sapiano *et al*. (2012) mapped areas of the North Pacific exhibiting single and multiple blooms per year. Their map resembled the pattern in Figure 3.1 since both their and our studies detected dual spring and fall phytoplankton blooms in coastal areas north of 40° N and the transition zone between the subpolar and subtropical gyres. Dual blooms were also identified in the eastern equatorial region. Our CESM1(BGC) analysis exhibited greater consistency with Sapiano *et al*. (2012) than our SeaWiFS-based results, which indicated a more widespread extent of dual phytoplankton blooms in the equatorial region. In addition, our analysis of SeaWiFS phenology identified two blooms per year across much of the subtropical gyre, a pattern that was not evident in either CESM1(BGC) or Sapiano *et al.* (2012). The comparable number of blooms per year identified by CESM1(BGC) and Sapiano *et al.* (2012) lends further credence to using this model to investigate historical trends in phenology.

Thus far, the evaluation of CESM1(BGC) model skill discussed in this section has focused solely on mean phenological patterns. A pertinent feature of the CESM1(BGC) ocean-ice hindcast is that, since atmospheric data force the ocean sub-model in this simulation, phenological events from a given year should reflect observed meteorological

conditions. As a result, we examined interannual correlations between SeaWiFS and CESM1(BGC) phenology to further assess model fidelity to biological observations. Compared to mean phenological patterns, model skill was slightly weaker when investigating interannual correlations with SeaWiFS, although correlation strength varied greatly between regions. Bloom duration and bloom magnitude exhibited particularly weak interannual correlations between SeaWiFS and CESM1(BGC). Generally, interannual correlations were strongest for phenological events and seasonal chlorophyll anomalies that coincided with the start of a bloom. Future research should take into account variations in model skill across different phenological metrics and geographic regions, perhaps focusing principally on areas with the greatest fidelity to observations. Nevertheless, here we opted to comprehensively examine all regions of the North Pacific and all phenological metrics to provide a baseline of the utility of CESM1(BGC) for studying phytoplankton phenology. Future versions of CESM1(BGC) will hopefully improve upon this baseline.

4.2. Forcing Mechanisms and the Response of Phytoplankton Phenology to Climate Oscillations

In temperate-to-boreal, oceanic habitats, Sverdrup's critical depth hypothesis has long been invoked to explain the dominant factors determining the timing of the spring bloom. This hypothesis states that net phytoplankton population growth cannot occur if the MLD exceeds a critical depth where depth-integrated primary production is equal to the depth-integrated respiration (Sverdrup, 1953). As winter conditions end, solar

irradiance increases, deepening the critical depth, while the MLD shoals due to the combined effects of warming and freshening of surface waters and decreased mixing from winter storms. Once the critical depth shoals below the MLD, a bloom occurs if phytoplankton growth is not effectively controlled by grazing. While recent studies have proposed alternative explanations for the occurrence of the spring bloom related to the seasonality of turbulent convection and zooplankton grazing (Behrenfeld, 2010; Taylor and Ferrari, 2011), numerous investigations conducted since the advent of remote sensing have continued to provide support for Sverdrup's critical depth hypothesis (Siegel *et al*., 2002; Yamada and Ishizaka, 2006; Henson *et al*., 2009; Platt *et al*., 2010; Song *et al*., 2010).

In subtropical and tropical regions, critical depth rarely exceeds the MLD, so light limitation does not influence bloom timing (Mann and Lazier, 1996). However, the limited vertical mixing of the water column in subtropical areas means that nutrients in surface waters are not routinely replenished by the greater nutrient reserves found at depth. As a result, phytoplankton blooms in subtropical regions mainly occur during winter when water column mixing is maximal, lifting the constraints of nutrient limitation on phytoplankton growth (Yoder *et al*., 1993; Dutkiewicz *et al*., 2001). In addition to these large-scale effects on phytoplankton phenology, bloom timing can also be influenced by local processes, such as storms, mixing by mesoscale eddies, and horizontal advection of distinct water masses (McGillicuddy *et al*., 2007; Greene *et al*., 2012; Mahadevan *et al.*, 2012).

CESM1(BGC) was able to reproduce these different mechanisms that control bloom timing in the subtropical and subpolar gyres of the North Pacific. In accordance

with Sverdrup's critical depth hypothesis, CESM1(BGC) indicated that earlier and longer lasting blooms occurred during years with weak winds, warm SST, and a shallow mixed layer in the subpolar gyre, but the inverse was observed in the subtropical gyre (Figs. 3.15-3.16). These results from CESM1(BGC) were analogous to the relationships between SeaWiFS phenology, wind speed, SST, and water column stratification observed in the North Atlantic and North Pacific subpolar gyres (Ueyama and Monger, 2005; Yamada and Ishizaka, 2006; Sasaoka *et al*., 2011). Although comparably less research has examined interannual variations in bloom timing in subtropical gyres, negative SST anomalies in subtropical and equatorial biomes are correlated with longer peaks in SeaWiFS chlorophyll (Racault *et al*., 2012). Both this study and Racault *et al*. (2012) also detected a change in the direction of correlations between phytoplankton phenology and environmental variables at 35° N. Other studies have placed the boundary as to where Sverdrup's critical depth hypothesis is applicable farther poleward or equatorward at latitudes between 30-45° N (Obata *et al*., 1996; Siegel *et al*., 2002; Henson and Thomas, 2007).

The optimal stability window hypothesis developed by Gargett (1997) provides a potential mechanism that links basin-scale climate oscillations, such as ENSO, PDO, and NPGO, with out-of-phase variations in phenology in subpolar and subtropical regions. In addition to their effect on physical oceanic conditions, the MEI, PDO, and NPGO also exert an influence on atmospheric processes since these indices are associated, respectively, with variations in trade wind strength, the Aleutian Low pressure system, and the gradient in sea level pressure (SLP) between Hawaii and Alaska (Mantua *et al*., 1997; McPhaden, *et al*., 2006; Chhak *et al*., 2009). Due to their connection to

atmospheric pressure fields, these climate oscillations are correlated with changes in wind strength and precipitation, which in turn affect water column stratification. Gargett (1997) proposed that an optimal window of water column stability exists that promotes elevated primary and secondary production in both the subpolar and subtropical gyres. Under mean conditions, the subpolar gyre is characterized by less than optimal stability resulting in light limitation related to vigorous water column mixing. In contrast, under mean conditions, the subtropical gyre experiences higher than optimal stability, which exacerbates nutrient limitation. Thus, a basin-scale increase (decrease) in water column stability, modulated through interannual-to-decadal climate oscillations, will result in elevated (reduced) biological production in the subpolar gyre, but reduced (elevated) production in the subtropical gyre.

While this hypothesis was originally developed to explain out-of-phase variations in mean annual primary and secondary production, it can also be applied to explain why phytoplankton phenology exhibits a differential response to climate indices in the subpolar and subtropical gyres. During warm climate regimes, mixing will be diminished causing earlier phytoplankton blooms in the subpolar gyre due to an earlier easing of light limitation. On the other hand, reduced mixing will delay phytoplankton blooms in the subtropical gyre due to a prolongation of the period when stratification and nutrient limitation persist. This pattern was evident when we examined correlations between bloom initiation phenology, the MEI, and the PDO in the northeast Pacific. When positive anomalies of the MEI and PDO resulted in warmer temperatures and heightened stratification in the northeast Pacific, phytoplankton blooms were largely delayed in low latitude areas likely due to an extended period of seasonal nutrient limitation. In contrast,

the same climate regime led to earlier phytoplankton blooms in the Alaska gyre where light limitation exerts a larger influence on phytoplankton phenology. We observed the opposite pattern in the northwest Pacific reflecting the fact that positive MEI and PDO conditions are associated with cooler temperatures and reduced stratification in this region (Mantua *et al*., 1997; Wolter and Timlin, 2011). The similar spatial signature of MEI and PDO effects on phenology is not surprising given that coupled atmosphere-ocean runs of CESM1 generate similar regional SST anomalies related to these climate oscillations, albeit at different time scales (Deser *et al*., 2012). Sasaoka *et al*. (2011) also noted that positive (warm) anomalies of the Southern Oscillation Index (SOI) are associated with earlier phenological events in eutrophic areas of the subarctic Pacific and later phenology in oligotrophic and HNLC regions. The west-east asynchrony of ENSO effects on phytoplankton phenology has been previously observed by Yoo *et al*. (2008) who reported that El Niño coincided with delays in the seasonal chlorophyll maximum in the CCE and North Equatorial Counter Current, while phytoplankton bloomed earlier during El Niño in the Sea of Japan.

Less support was provided for the optimal stability window hypothesis when examining the effect of the NPGO on bloom initiation phenology. Areas characterized by cool SST during the positive phase of the NPGO typically exhibited delayed phenology, while regions with warm conditions displayed phenological advances. This pattern was consistent regardless of whether a subtropical or subpolar region was considered. An alternative explanation for this phenological pattern is that warming associated with the NPGO had a metabolic effect increasing the growth rate of individual phytoplankters, resulting in more rapidly developing blooms during warm conditions.

Compared to the regional effects of climate oscillations on bloom initiation phenology, less asynchronous variation in bloom duration between the western and eastern Pacific basin was observed. Instead, positive anomalies of the MEI and PDO principally resulted in shorter blooms at latitudes < 40° N and longer blooms in subpolar regions. Relatively few areas exhibited significant correlations between bloom duration and the NPGO. However, in areas where significant NPGO effects were detected, shorter blooms predominated during the positive phase of the NPGO at high latitudes, whereas longer blooms were more common at latitudes < 20° N. These results are consistent with the findings of Racault *et al*. (2012) who determined that, during the SeaWiFS period, the warm phases of the MEI, NAO, and Southern Annular Mode (SAM) were linked to increased phytoplankton bloom duration in subpolar regions and shorter blooms in subtropical and tropical areas. Racault *et al*. (2012) attributed the shorter, subtropical blooms to increased nutrient limitation during warm years and the longer, subpolar blooms to an extended period of summer conditions. Across the North Pacific subarctic, Sasaoka *et al*. (2011) identified a pattern where longer phytoplankton blooms occurred during El Niño in areas characterized by low chlorophyll concentration. While this finding may initially seem to contradict the results of our study and those of Racault *et al*. (2012), these subarctic, low chlorophyll areas may represent part of the transition zone between the subpolar and subtropical gyres. During the warm phase of climate oscillations, the boundaries of the subtropical gyre can expand, such that phytoplankton blooms in the transition zone take on phenological characteristics usually associated with the subtropical gyre (Henson *et al*., 2009). One such characteristic may include the longer duration of phytoplankton blooms that occur in subtropical regions.

Regions with significant correlations between bloom magnitude and the three climate oscillations again resembled maps of correlations between these oscillations and SST anomalies. Warm SST anomalies coincided with a reduced size of blooms, whereas higher chlorophyll concentration during blooms was observed during the cool phase of MEI, PDO, and NPGO regimes. As discussed above, this reflects the connection between cool, oceanic conditions and increased ventilation of surface waters, resulting in elevated concentrations of nutrients used by phytoplankton. Cool conditions were linked to increases in bloom magnitude in both the subtropical and subpolar Pacific. This is likely related to the fact that, even though macronutrients are not depleted in the subpolar gyre, this area forms part of an HNLC region where iron concentration limits phytoplankton growth (Tsuda *et al*., 2003). As has been observed in the North Atlantic (Song *et al*., 2010), it can be inferred here that light limitation has a primary influence on phytoplankton phenology and bloom duration in the subarctic Pacific, but nutrient concentration has a greater effect on bloom magnitude. Observational studies of North Pacific oceanography have documented connections between chlorophyll concentration and the MEI, PDO, and NPGO similar to the ones that we observed with CESM1(BGC) (Di Lorenzo *et al*., 2008; Yoo *et al*., 2008; Martinez *et al*., 2009).

4.3. Long-term, Linear Trends in Phytoplankton Phenology

While changes in terrestrial, plant phenology related to global warming have been documented across a range of ecosystems (Parmesan and Yohe, 2003; Root *et* al., 2003; Parmesan, 2007; Miller-Rushing and Primack, 2008), this represents one of the first

studies to identify long-term trends in phytoplankton phenology during the 20th century across a substantial proportion of an ocean basin. Previous work has detected advances in the timing of the fall bloom in the North Sea (Edwards and Richardson, 2004), earlier phytoplankton blooms in the Arctic Ocean and CCE (Kim *et al*., 2009; Kahru *et al*., 2011), and delayed phytoplankton phenology in the Sea of Japan and off the Nova Scotian Shelf (Yamada and Ishizaka, 2006; Song *et al*., 2011). However, with the exception of Edwards and Richardson (2005), these studies have lasted less than 20 years, making it difficult to confidently attribute trends in phytoplankton phenology to global warming or natural variability. Furthermore, studies comparing global trends in chlorophyll concentration between the CZCS and SeaWiFS eras have obtained contradictory results as to whether changes in phytoplankton seasonality have occurred. Gregg and Conkright (2002) noted that seasonal patterns remained unchanged between the CZCS and SeaWiFS eras, while Antoine *et al*. (2005) identified changes in the timing of the spring bloom across latitudes of 40-50° N, as well as reduced seasonality in the inter-tropical zone. However, the shift from a negative to a positive PDO between the CZCS and SeaWiFS periods, as well as variations in the Atlantic Multidecadal Oscillation (AMO), complicate the interpretation of these seasonal changes (Martinez *et al*., 2009).

It is possible that natural variability has amplified or dampened the long-term, linear trends in phenology that we detected. However, the time series that we analyzed included multiple reversals of both the PDO and NPGO. As a result, neither of these two decadal climate indices displayed a linear trend between 1961-2007 (Fig. S3.10). Linear trends in phytoplankton phenology could also emerge due to the assimilation of satellite

data into the ocean-ice hindcast midway through the time series. However, this seems unlikely to have produced spurious trends given that there was not a step change in the phenological PCA time series that coincided with the addition of satellite data to the hindcast. As a result, the long-term shifts in phenology that we identified are likely, although not conclusively, a signal of anthropogenic climate change. Mechanisms through which climate change could alter phytoplankton phenology include changes in seasonal concentrations of nutrients due to reduced water column mixing at low latitudes, a shorter period of light limitation at subpolar latitudes due to earlier stratification, metabolic effects of warmer temperatures on phytoplankton growth rates, and shifts in the phenology of grazers.

Higher latitudes have been characterized as areas that often display faster and wider spread changes in phenology (Root *et al*., 2003; Parmesan, 2007; Kahru *et al*., 2011; Xu *et al.*, 2013). However, among phytoplankton, we did not detect a more extensive area with long-term, phenological trends in subpolar regions than in lower latitudes. This is similar to the findings of Antoine *et al*. (2005) who also did not observe any changes in phytoplankton seasonality at high latitudes between the CZCS and SeaWiFS eras. Henson *et al*. (2010) noted that, due to less natural variability in equatorial regions, shorter time series of chlorophyll are required to identify trends related to climate change. Conversely, this may partially explain the relative dearth of long-term trends in phenology that we observed at higher latitudes. A second potential explanation is that dinoflagellates have been shown to exhibit larger changes in phenology than diatoms (Edwards and Richardson, 2004). Since diatoms make up a larger portion of the phytoplankton community at high latitudes, this could result in greater phenological

stability. One additional hypothesis explaining the scarcity of high latitude changes in phenology stems from the idea that phenological change may effectively track seasonal isotherms (Burrows *et al*., 2011). Due to the reduced amplitude of the seasonal cycle in tropical areas, organisms residing there may have to undergo larger changes in phenology to ensure that seasonal activities continue to take place at approximately the same temperature.

Areas with long-term trends in bloom duration and magnitude exhibited latitudinal patterns similar to those observed when investigating MEI and PDO effects on bloom duration and bloom size. Increases in bloom duration and magnitude occurred principally in the subpolar gyre, while trends toward shorter and smaller blooms were mainly found at latitudes < 40° N. Antoine *et al*. (2005) also reported increases in chlorophyll concentration at high latitudes and decreases in the oligotrophic, subtropical gyres during recent decades. As discussed in the section on climate oscillations, changes in bloom duration and magnitude likely reflect the fact that warming leads to greater stratification in subtropical region, which subsequently shortens the period when the water column is sufficiently mixed to replenish surface nutrients. This mechanism has a consistent effect on subtropical, bloom duration and magnitude regardless whether interannual (*e.g*., MEI) or decadal (*e.g*., PDO, NPGO, long-term trends) time scales are considered. In the subpolar gyre, the increase in bloom magnitude and duration between 1961-2007 may be due to either: (1) increased stratification prolonging the season when phytoplankton are not mixed below the critical depth, or; (2) warming induced Q_{10} changes in phytoplankton growth rates. When using a DGOM to examine how a doubling of atmospheric CO_2 would affect the spring bloom in the northwest Pacific, Hashioka *et*

al. (2009) concluded that increases in maximum phytoplankton biomass in the Kuroshio extension were tied to a quickening of phytoplankton metabolism under warmer temperatures, lending support to the latter hypothesis. Similarly, model and theoretical predictions developed by Marinov *et al*. (2010) also indicated that future changes in diatom and small phytoplankton growth rates in the subpolar Pacific would be affected more strongly by temperature changes than changes in light and nutrient limitation.

4.4. Sensitivity of Different Phenological Metrics to Climate Variability and Change

Compared to bloom termination, bloom initiation dates displayed greater comparability between SeaWiFS and CESM1(BGC), were correlated with climate oscillations and environmental variables across a larger area of the North Pacific, exhibited greater spatial coherency, and were subject to slower phenological changes. This pattern was consistent across all climate indices, environmental variables, and when examining long-term, linear trends. Typically, the rate of changes in bloom midpoint and the spatial extent of its correlations with climatic and oceanic indices were intermediate between bloom initiation and termination phenology. The less widespread effects of the MEI, PDO, and NPGO on bloom termination may reflect the fact that the end of phytoplankton blooms is often controlled more by biological processes, such as grazing pressure and nutrient depletion (Rolinski *et al*., 2007; Racault *et al*., 2012), than by physical processes. Climate oscillations only indirectly impact these biological processes, but exert a more direct effect on water column stratification, SST, and wind speed, which are factors that had a greater influence on bloom initiation dates than bloom termination

phenology. Another potential explanation for the more widespread influence of climate oscillations on bloom initiation is that the start of a bloom is often more pronounced, occurring more rapidly and synchronously than the end of a bloom (Rolinski *et al*, 2007). This results in a more precise identification of the date of bloom start compared to bloom termination (Leopold and Jones, 1947; Zhang *et al*., 2006; Rolinski *et al*., 2007). Greater phenological precision may increase the statistical likelihood of detecting climatic and oceanic effects on phenology given the existence of such effects. The faster rate of change in bloom termination phenology compared to bloom initiation was more pronounced in areas with advancing phenology. The accelerated rate of change in such locations may reflect a rapid depletion of the nutrient supply at the end of a bloom. Nutrient depletion could occur more quickly under warm oceanic conditions due to both upregulated phytoplankton metabolism and heightened stratification limiting the flux of nutrients from depth.

Despite the differences between bloom initiation and termination phenology, the spatial signatures of these phenological metrics were generally similar, such that regions that experienced earlier bloom onset over a particular period tended to exhibit an earlier end to phytoplankton blooms. Racault *et al*. (2012) also noted a positive correlation between dates of bloom onset and bloom termination when examining global phytoplankton phenology. Synchronous changes in bloom initiation and termination dates led to decreased variability in bloom duration. As a result, changes in bloom duration were slow compared to other phenological metrics and were not affected by climate oscillations across as wide an area. Since climate-related changes in annual primary production are modulated in part by bloom duration, this finding suggests that trends in

phytoplankton phenology are unlikely to contribute much to future changes in primary production per se. However, given the low comparability between SeaWiFS and CESM1(BGC) estimates of bloom duration and the large differences in bloom duration estimated with different phenological methods (Racault *et al*., 2012; Sapiano *et al*., 2012; the current study), additional research is needed to confirm this result.

Bloom magnitude was correlated with climate oscillations and exhibited long-term, linear trends across a larger area of the North Pacific than any other phenological indicator. The spatial "patchiness" of other metrics suggests that mesoscale processes (*e.g*., eddies, meanders of currents) and intraseasonal variations in local weather may have a prominent influence on phytoplankton phenology. Kahru *et al*. (2011) also detected abundant small-scale, spatial variability between areas displaying trends in phytoplankton phenology during the SeaWiFS era. Similarly, in terrestrial ecosystems, there is often as much variability in phenological trends among species living in the same area as there is between different regions (Parmesan, 2007). The spatial patchiness of climate effects on phenology may complicate the interpretation of results from *in situ* monitoring programs, since it is uncertain whether trends detected at a particular location are representative of a larger region.

4.5. Cross-Ecosystem Comparison of Rates of Phenological Change

In locations in the North Pacific where significant, long-trends in phytoplankton phenology were observed, 46.3% of changes indicated delayed onset of blooms. Similarly, the midpoint and termination of blooms were delayed, respectively, in 54.5%

and 58.7% of the CESM1 grid cells where long-term changes were detected. Previous studies have also identified delays in phytoplankton phenology in the North Atlantic, Sea of Japan, and Nova Scotian Shelf over recent years (Yamada and Ishizaka, 2006; Kahru *et al*., 2011; Song *et al*., 2011). Compared to terrestrial studies of 20th century changes in phenology, the high percentage of phenological delays that we observed in pelagic ecosystems appears to be unique. Field-based, multi-species studies of trends in terrestrial phenology have typically identified delayed phenology among ~20% or fewer of the species examined (Parmesan and Yohe, 2003; Root *et al*., 2003; Menzel *et al*., 2006; Cook *et al*., 2012). The one exception is a study by White *et al*. (2009) that used remote sensing to investigate areas of North America that exhibited trends in spring vegetation phenology between 1982-2006. White *et al*. (2009) detected shifts towards earlier phenology across 7% of their study area and delayed phenology across 5%. This difference between our study and research conducted in terrestrial ecosystems may partially reflect the fact that we examined phenological changes that occur during all months of the year, whereas many terrestrial studies focused solely on spring events (Parmesan and Yohe, 2003; Root *et al*., 2003; Parmesan, 2007). Terrestrial research investigating fall phenology has produced mixed results, with some studies reporting earlier occurrence of phenological events and others reporting delays (Cleland, 2007). Nevertheless, the prevalence of delayed phenological events likely represents a real difference in how marine and terrestrial ecosystems are affected by climate, since this phenomenon can be explained by increased stratification leading to a later onset of fall and winter mixing of the water column in subtropical areas.

A second difference between marine and terrestrial ecosystems is related to the very fast rates of long-term, phenological changes that we detected among North Pacific phytoplankton. Between 1961 and 2007, bloom initiation dates advanced at a mean rate of -15.7 ± 0.3 SE days decade^{-1} in areas with significantly earlier blooms, while mean delays of 14.4 ± 0.3 SE days decade^{-1} were observed in other regions (Fig. 3.14). In contrast, a meta-analysis that examined phenological changes among predominantly terrestrial organisms obtained a mean rate of phenological advance of 2.8 ± 0.4 SE days decade^{-1} (Parmesan, 2007). Similarly, changes in phytoplankton phenology from the CESM1(BGC) hindcast occurred at a faster rate than long-term changes in holo- and merozooplankton phenology in the North Sea (-2.3 to -10.7 days decade^{-1}; Edwards and Richardson, 2004) and larval fish phenology in the CCE (mean advance: -6.4 days decade^{-1}; mean delay: 5.1 days decade^{-1}; see first data chapter).

Several factors may explain these differing rates of phenological change. First, we presented mean rates of change separately for regions with earlier and later phenological trends, so that the large changes in opposite directions would not cancel each other out. We also calculated mean rates of change that only included regions where a significant, long-term trend in phenology was observed. If mean rates of change had been calculated jointly for both phenological advances and delays and had included all CESM1 grid cells, we would have inevitably computed a much slower rate of change, but this would have also misleadingly obscured the rapid changes detected in some regions. Similarly, Parmesan (2007) found that discrepancies between two earlier meta-analyses examining phenological changes (*e.g.*, Parmesan and Yohe, 2003; Root *et al.*, 2003) could be

explained mainly by the decision whether to include data on species that were unresponsive to climate change.

Second, Burrows *et al*. (2011) developed a hypothesis that might serve to explain why we detected more rapidly changing phenology among marine phytoplankton than has been observed among terrestrial primary producers. They hypothesized that phenological changes should track seasonal isotherms so that critical events in an organism's life history will continue to occur at an optimal temperature even as the climate changes. Since seasonal temperature gradients in the ocean are less pronounced than on land, organisms will need to undergo more rapid shifts to maintain phenological events at the same isotherm. While this hypothesis is likely relevant to many marine organisms, its applicability to phytoplankton is questionable given the fact that nutrient and light limitation, in addition to temperature, play large roles in determining phenological rates of change.

A more compelling hypothesis to explain the rapid phenological changes among phytoplankton is that their extremely brief life cycle allows them to track seasonal changes in the environment more closely than longer-lived organisms (Richardson and Poloczanska, 2008). This hypothesis serves to explain why phytoplankton exhibited faster shifts in phenology than both longer-lived terrestrial plants and marine organisms in higher trophic levels. One example of this is that pelagic fishes and invertebrates, which usually have short life cycles, have been shown to respond to climate change by undergoing range shifts at a faster rate than higher trophic level predators and benthic species, which are typically longer lived (Murawski, 1993; Cheung *et al*., 2009).

The differing rates of phenological change among phytoplankton and higher trophic level organisms could potentially alter marine food web structure, since many fishes and benthic invertebrates that produce planktotrophic larvae time their reproduction to coincide with plankton blooms. Mismatches between blooms and larval production can result in starvation or reduced growth rates, which can in turn increase the vulnerability of larvae to predation. Reduced survival of larvae can potentially result in poor recruitment to fisheries in subsequent years and declines in population size (Murphy, 1968; Cushing, 1990; Durant *et al*., 2007). Examples where phenological mismatches have led to substantial deccreases in recruitment include North Sea cod (Beaugrand *et al*., 2003), Nova Scotia haddock (Platt *et al*., 2003), and mussels and barnacles in the northern California Current (Barth *et al.*, 2007). In some extreme cases, phenological matches can even lead to local extinctions (Burkle *et al*., 2013). However, it is also important to note that some species have developed evolutionary adaptions to manage the risk of phenological mismatches. These include developing a generalist diet and spreading out reproductive activity over a series of weeks to months as a "bet hedging" strategy (Cushing, 1990; Durant *et al*., 2007). Similarly, density dependence at the juvenile stage can compensate for low survival of earlier life history stages due to phenological mismatches (Reed *et al*., 2013). An interesting question is how the high geographic variability in rates of phenological change among plankton will impact migratory species. Such species may be resilient to phenological mismatches, since they are able to travel to more productive feeding grounds. However, cues used to time seasonal migrations between feeding and breeding grounds are often related to local

climate conditions that may no longer be representative of phenological changes taking place at the other end of the species' migratory range (Durant *et al*., 2007).

4.6. Conclusions

Use of a hindcast simulation with forced atmospheric conditions allowed us to apply CESM1(BGC) to examine historical variations in phytoplankton phenology during the late 20th century. In accordance with Sverdrup's critical depth hypothesis, earlier phytoplankton blooms in subpolar ecosystems were correlated with weak winds, warm SST, and a shallow mixed layer, while the inverse pattern was observed in subtropical and equatorial biomes. The onset of phytoplankton blooms exhibited long-term, phenological trends across 20% of the North Pacific, while interannual-to-decadal climate oscillations were correlated with bloom initiation phenology across 23-34% of this region. Long-term trends in phenology resulted in changes in bloom onset dates that were of a similar magnitude to the effect of climate oscillations. Between 1961 and 2007, delays and advances in phytoplankton phenology were equally prevalent across the North Pacific. The MEI and PDO affected phytoplankton phenology across a similar subset of CESM1 grid cells. The influence of the MEI and PDO could be largely interpreted in terms of the effects of surface warming on water column stratification that results in increased nutrient limitation in the subtropical gyre and decreased light limitation in the subpolar gyre. Compared to interannual variations in bloom magnitude, climate oscillations were correlated with phytoplankton phenology across a smaller portion of the North Pacific and showed finer scale spatial variability that may be indicative of local,

oceanic influences on phenology. Variations in bloom initiation, midpoint, and termination dates exhibited a similar spatial signature, resulting in relatively few changes in bloom duration. Long-term changes in phytoplankton phenology are occurring at a rapid rate compared to similar changes observed among terrestrial primary producers and higher trophic level marine organisms. This asynchronous rate of phenological change could result in seasonal mismatches between phytoplankton blooms and planktivorous organisms.

5. Acknowledgments

The NOAA Nancy Foster Scholar Program, California Sea Grant Project R/FISH-210, and the San Diego ARCS Foundation funded research conducted by R.G.A. The methods used to identify phenological transition points were developed as part of a Nancy Foster Scholar research collaboration with the Environmental Research Division (ERD) of the NOAA's Southwest Fisheries Science Center (SWFSC). Discussions with S. Bograd, F. Schwing, I. Schroeder, and R. Lemos provided many helpful suggestions and insights during this research collaboration. D. Checkley, D. Cayan, M. Ohman, S. McClatchie, and J.A. Koslow reviewed an earlier draft of this manuscript and provided a number of helpful suggestions.

This chapter, in part, is currently being prepared for submission for publication of the material. The dissertation author was the primary investigator and author of this material. Matthew C. Long will be a co-author of this publication.

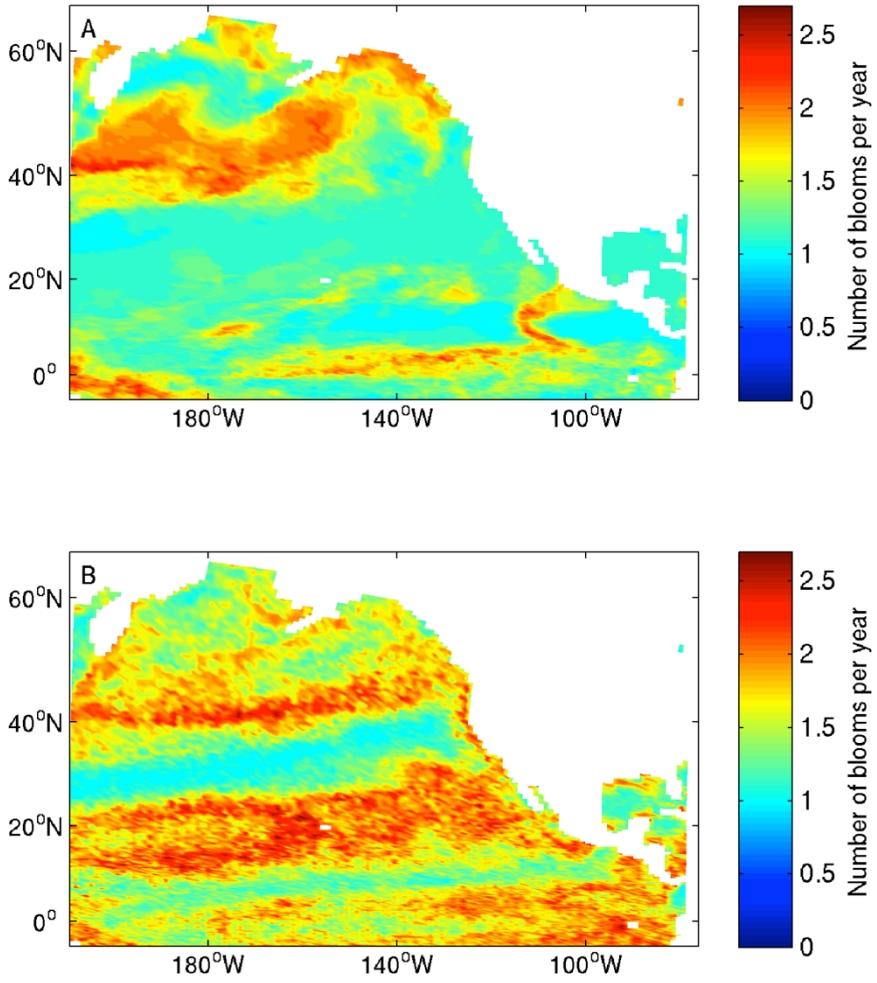

Figure 3.1. Mean number of peaks in chlorophyll concentration identified each year from CESM1(BGC) (A) and SeaWiFS (B) during the years 1998-2007.

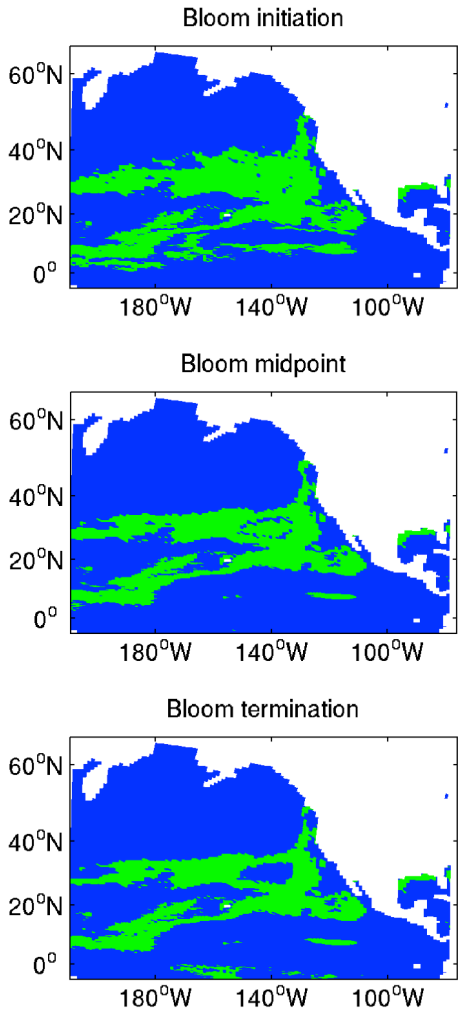

Figure 3.2. Maps showing the areas over which the calendar year (January-December; blue) and the adjusted year (July-June; green) were used to calculate changes in phytoplankton phenology.

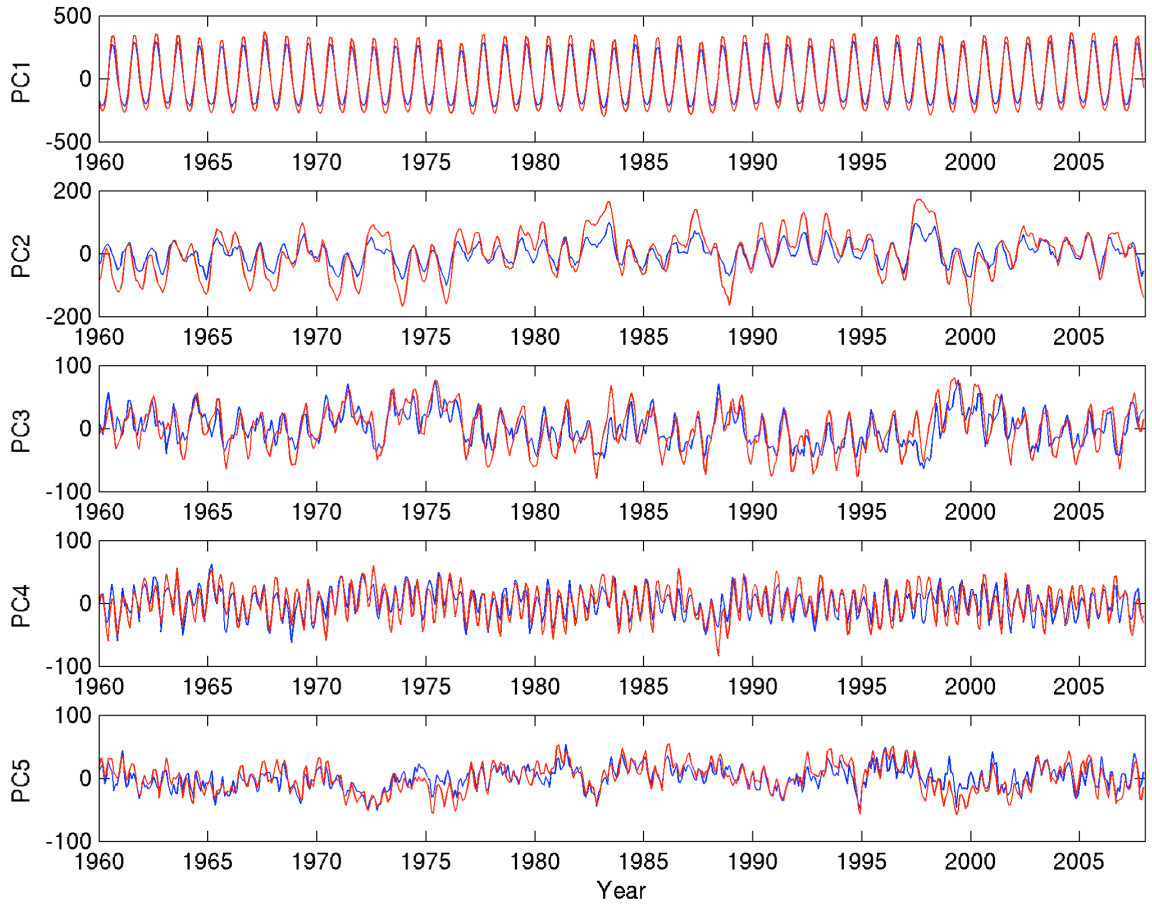

Figure 3.3. Time series of the first five principal component (PC) scores of monthly sea surface temperature (SST) from ICOADS (blue) and CESM1 (red). Raw SST data, which included seasonal signals, were used as the input for this principal component analysis (PCA).

Figure 3.4. Spatial signature of the first five principal components (PCs) of sea surface temperature (SST) from ICOADS (upper row) and CESM1 (lower row). These maps show the correlation between each PC time series and the SST time series from each ocean grid cell. White areas represent either land or regions where observations were available for ≤ 75% of the monthly time steps between 1960-2007.

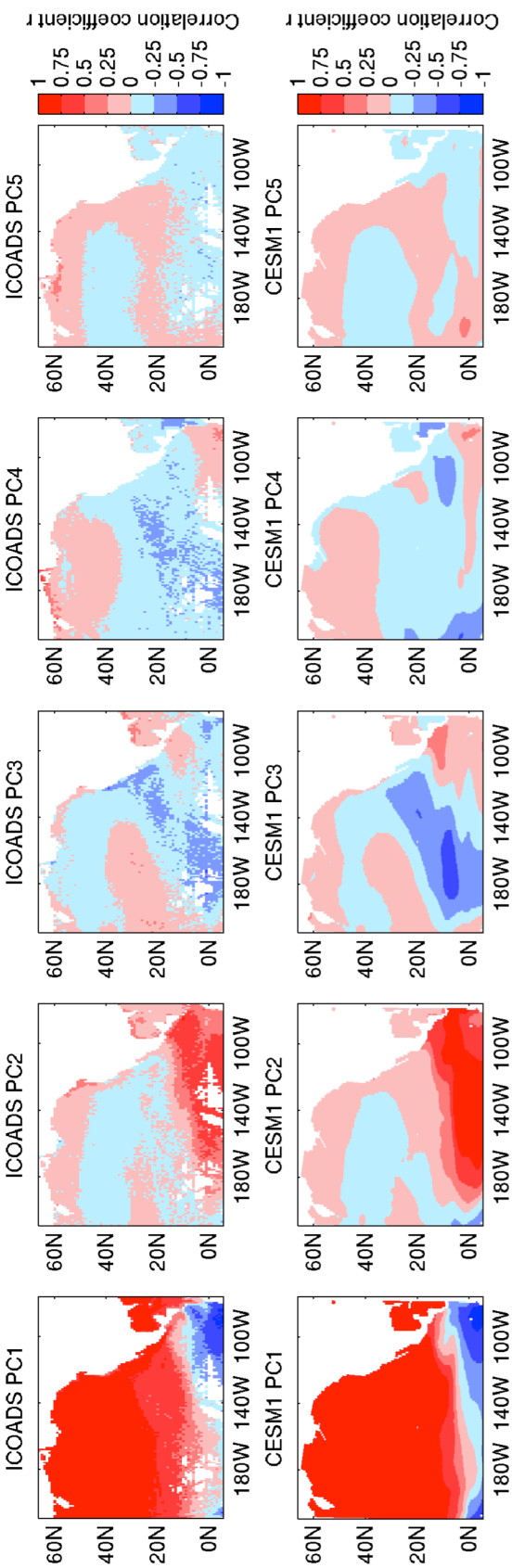
ICOADS PC1
ICOADS PC2
ICOADS PC3
ICOADS PC4
ICOADS PC5
CESM1 PC1
CESM1 PC2
CESM1 PC3
CESM1 PC4
CESM1 PC5
60N
40N
20N
0N
180W 140W 100W
Correlation coefficient r
1
0.75
0.5
0.25
0
-0.25
-0.5
-0.75
-1

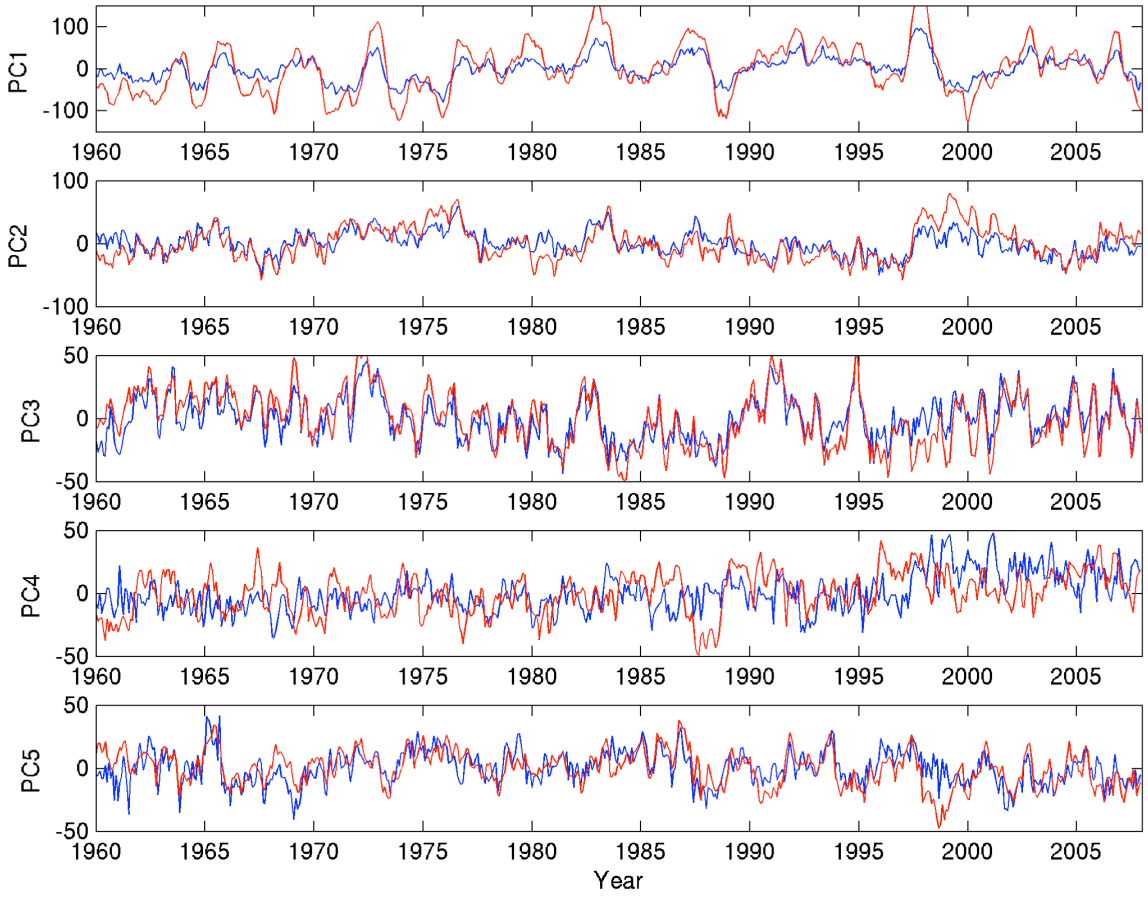

Figure 3.5. Time series of the first five principal component (PC) scores of monthly sea surface temperature (SST) anomalies from ICOADS (blue) and CESM1 (red). This principal component analysis (PCA) was performed on monthly anomalies in order to remove seasonal patterns and highlight interannual and decadal variability. Note that the inverse of the fifth principal component of CESM1 is shown in the bottom panel.

Figure 3.6. Spatial signature of the first five principal components (PCs) of monthly sea surface temperature (SST) anomalies from ICOADS (upper row) and CESM1 (lower row). Figure details are the same as in Figure 3.4, but monthly anomalies are shown to highlight spatial patterns associated with interannual and decadal SST variability. The inverse of the fifth principal component of CESM1 is mapped.

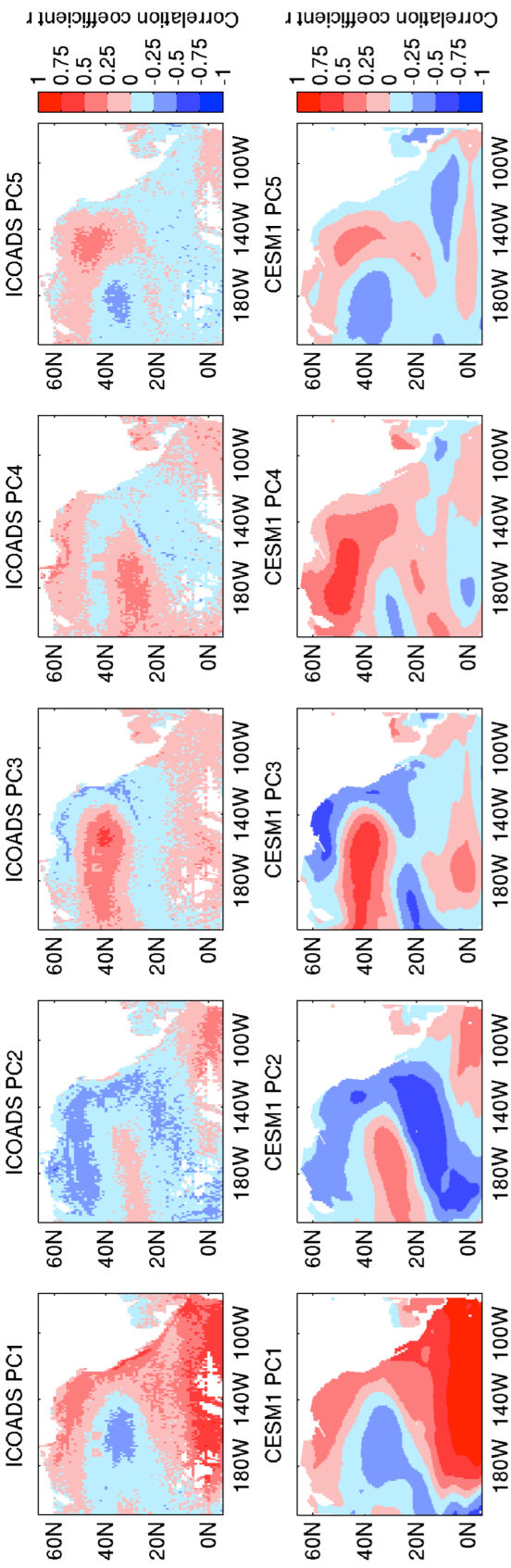
ICOADS PC1
ICOADS PC2
ICOADS PC3
ICOADS PC4
ICOADS PC5
CESM1 PC1
CESM1 PC2
CESM1 PC3
CESM1 PC4
CESM1 PC5
60N
40N
20N
0N
180W 140W 100W
Correlation coefficient r
1
0.75
0.5
0.25
0
-0.25
-0.5
-0.75
-1

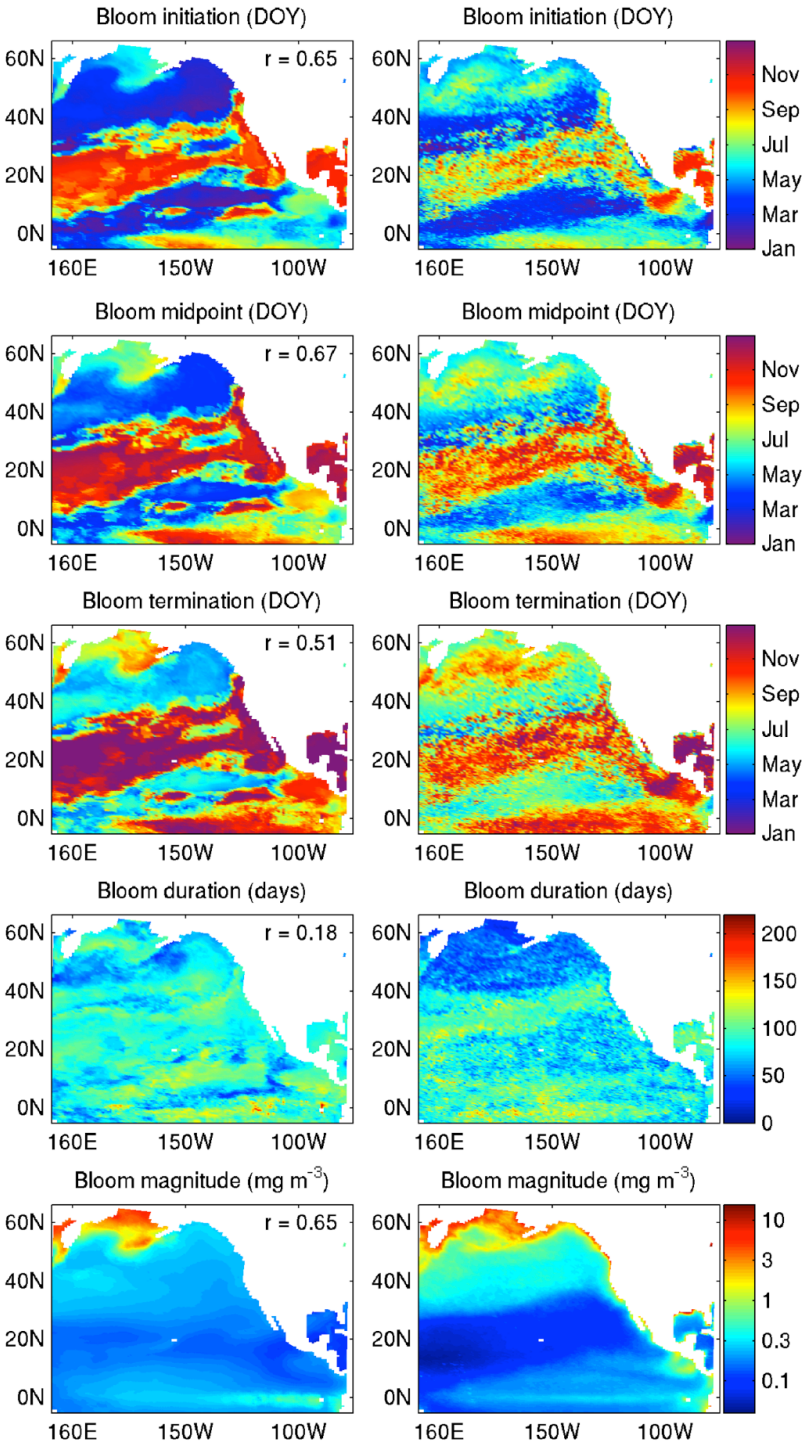

Figure 3.7. Mean day of year (DOY) of bloom initiation, midpoint, and termination during the years 1998-2007. The mean duration and magnitude of these phenological events are also shown. Maps in the left column are derived from CESM1(BGC), while maps on the right are based on remotely sensed chlorophyll from SeaWiFS. Correlation coefficients *r* indicate the strength of spatial correlations between CESM1(BGC) and SeaWiFS for each phenological metric.

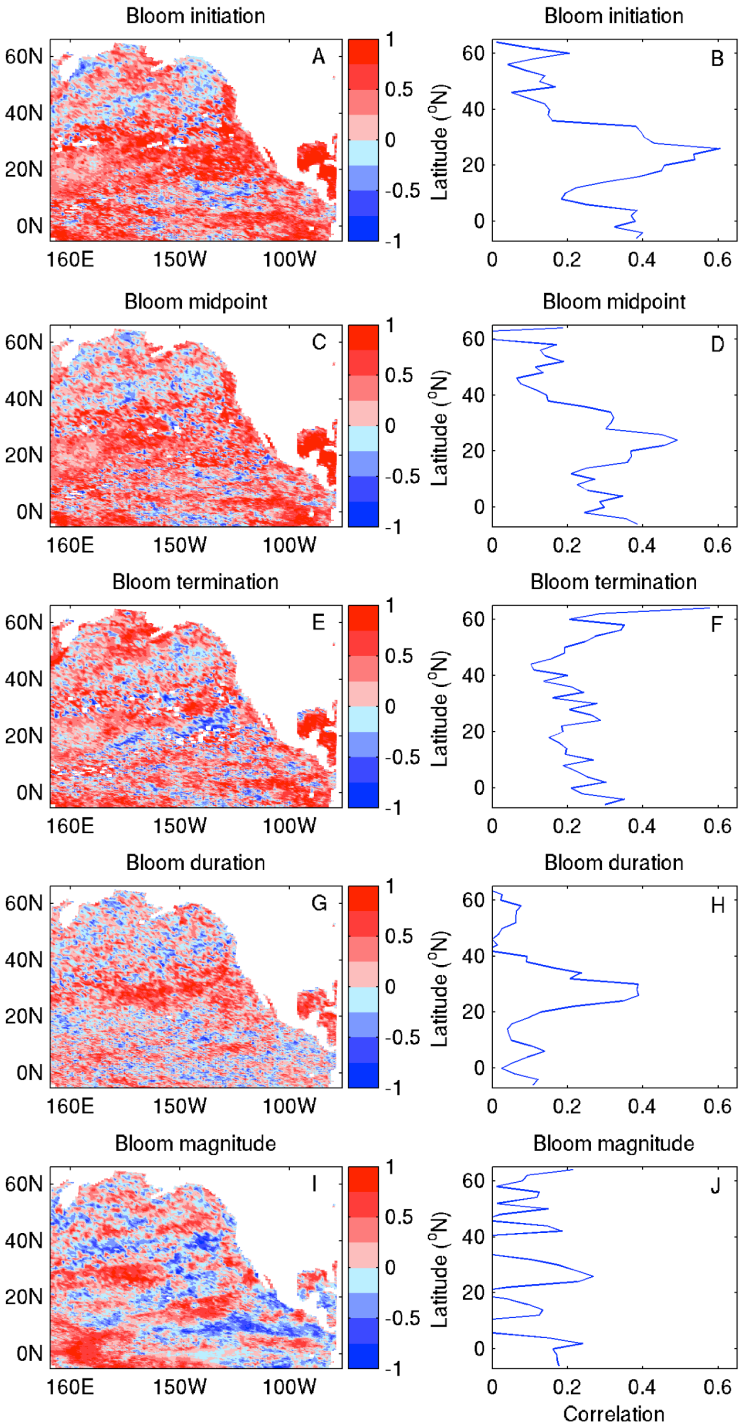

Figure 3.8. Temporal correlations between SeaWiFS and CESM1(BGC) calculated based on interannual variations in the date of bloom initiation, midpoint, termination, duration, and magnitude during the 1998-2007 period. The left column displays maps of these correlations calculated on a pixel-by-pixel basis. Color bars indicate values of the correlation coefficients *r*. The right column shows latitudinal patterns where correlation coefficients have been averaged across 2° bins.

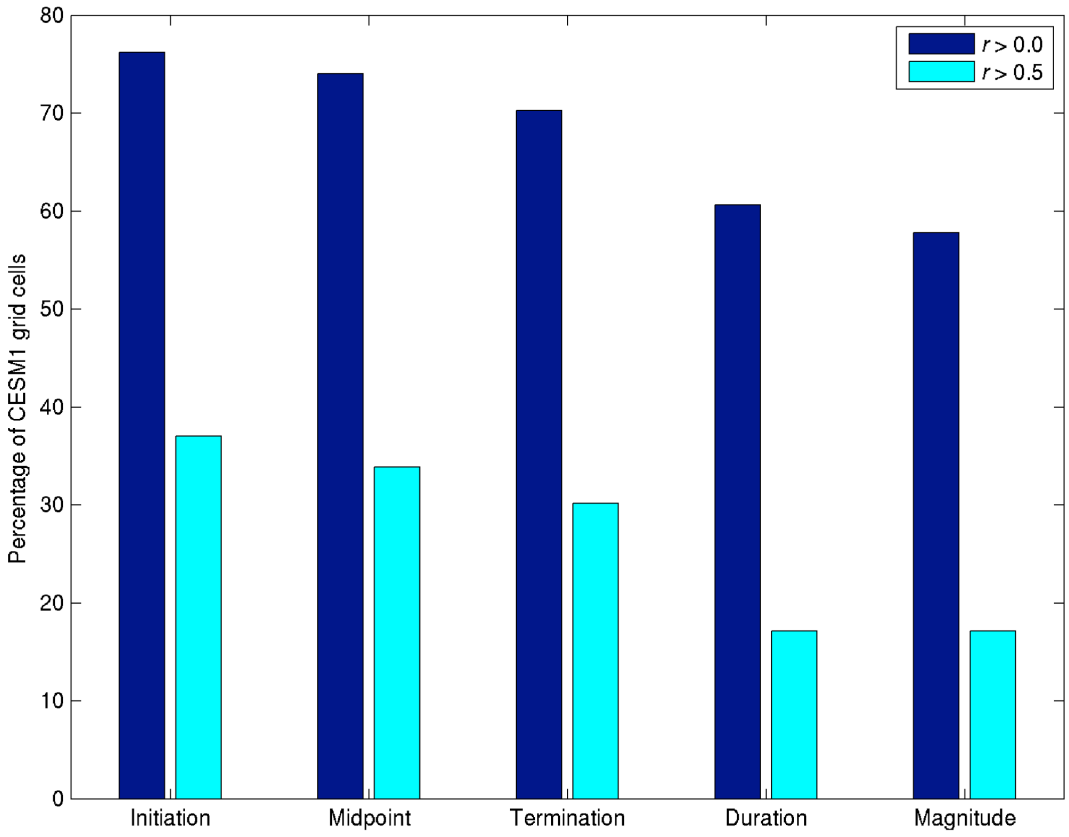

Figure 3.9. Percentage of CESM1 grid cells where temporal correlations between SeaWiFS and CESM1(BGC) were positive ($r > 0.0$) and exceeded $r > 0.5$ for each phenological metric.

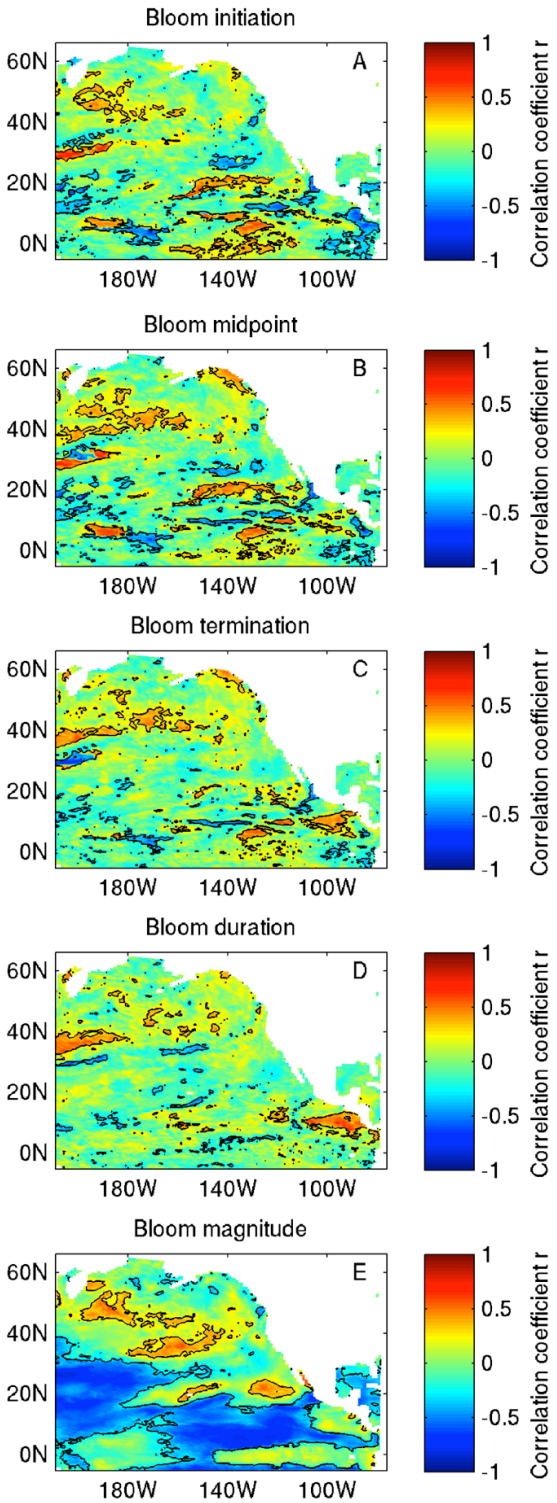

Figure 3.10. Maps of correlations between phenological metrics and year. Colors indicate the value of the Pearson correlation coefficients *r*, whereas black contour lines show grid cells that had significant correlations ($p < 0.05$) indicative of long-term, linear trends in phenology.

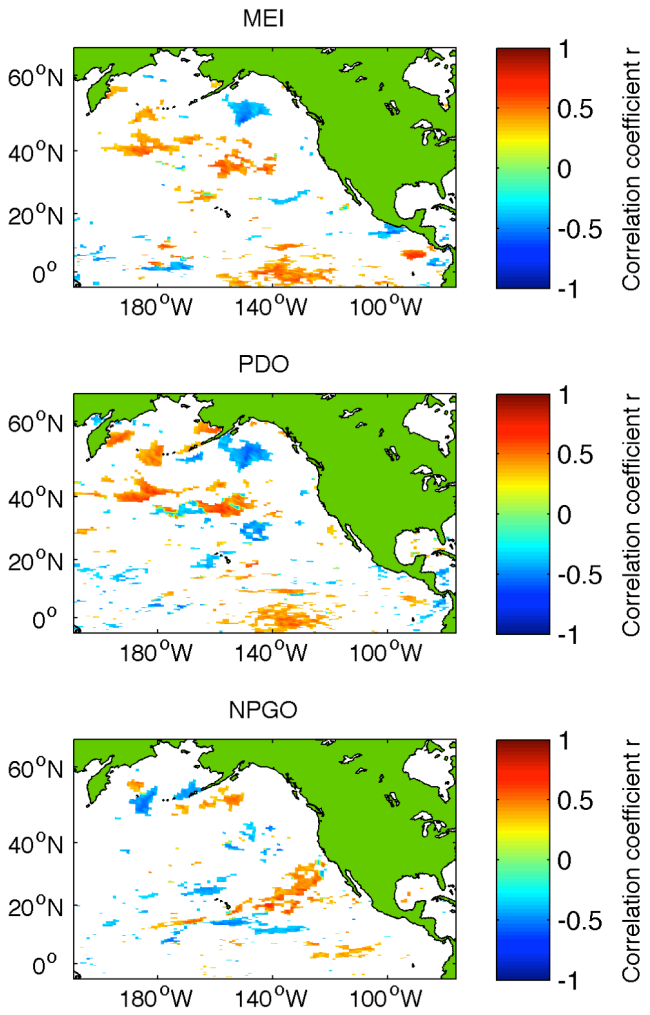

Figure 3.11. Maps of correlations between the date of bloom initiation and three climate indices: the Multivariate ENSO Index (MEI), the Pacific Decadal Oscillation (PDO), and the North Pacific Gyre Oscillation (NPGO). Only grid cells with correlations significant at $p < 0.05$ are shown. In cases where there are two or more time lags of a climate index that were significantly correlated with bloom initiation, the correlation with the lowest p value is displayed.

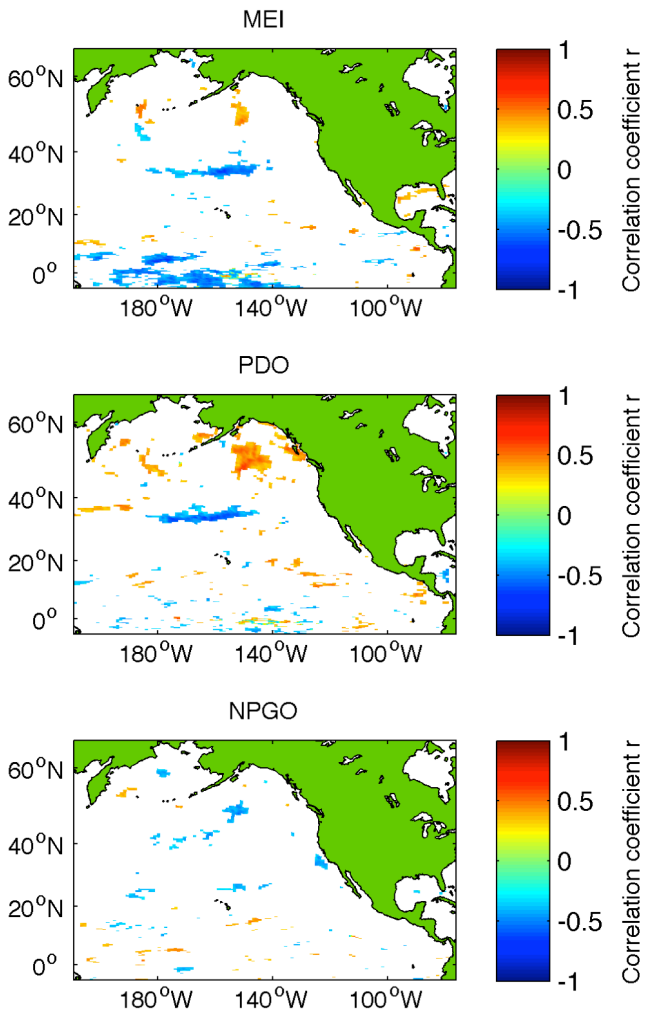

Figure 3.12. Maps of correlations between bloom duration and three climate indices: the Multivariate ENSO Index (MEI), the Pacific Decadal Oscillation (PDO), and the North Pacific Gyre Oscillation (NPGO). Features of this figure are the same as in Figure 3.11.

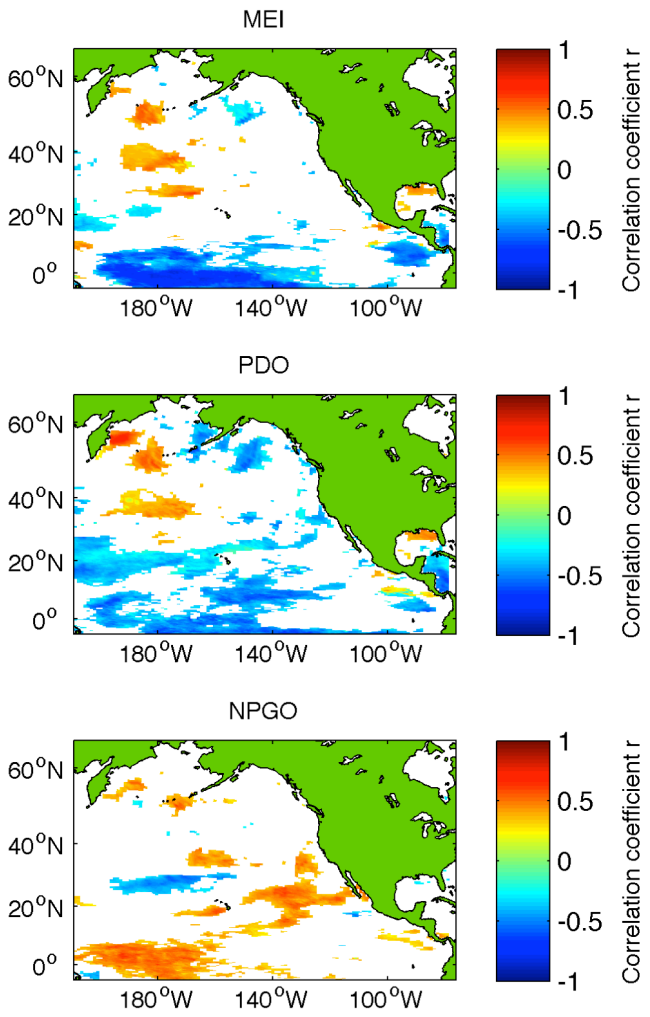

Figure 3.13. Maps of correlations between bloom magnitude and three climate indices: the Multivariate ENSO Index (MEI), the Pacific Decadal Oscillation (PDO), and the North Pacific Gyre Oscillation (NPGO). Features of this figure are the same as in Figure 3.11.

Figure 3.14. Phenological sensitivity of phytoplankton to long-term, linear trends (LTLT), the Multivariate ENSO Index (MEI), the Pacific Decadal Oscillation (PDO), and the North Pacific Gyre Oscillation (NPGO). Means rates of phenological change and their 95% confidence intervals are shown separately for regions that had significant positive or negative correlations with each climate index or that exhibited a long-term trend. Positive (negative) correlations indicate delayed (earlier) phenology, longer (shorter) bloom duration, or larger (smaller) bloom magnitude either when a climate index was in its positive (negative) phase or as part of a long-term trend. Phenological changes (changes in bloom magnitude) are standardized by days decade^{-1} (mg m^{-3} decade^{-1}) when examining long-term trends and by days per unit climate anomaly (mg m^{-3} anomaly^{-1}) for the MEI, PDO, and NPGO. Numbers underneath each mean indicate the sample size.

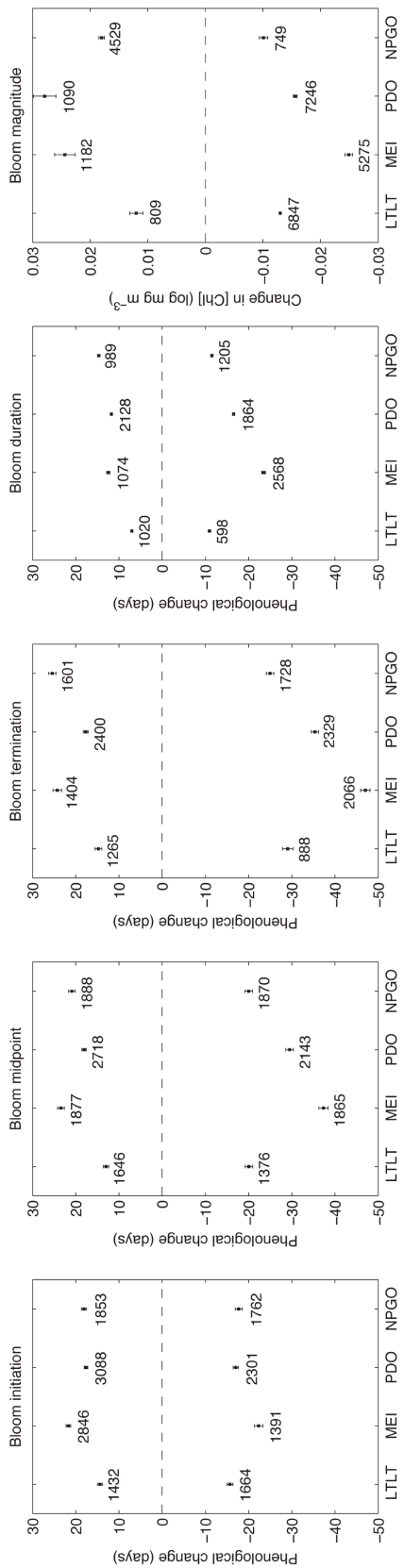
Bloom initiation
Bloom midpoint
Bloom termination
Bloom duration
Bloom magnitude
Phenological change (days)
Change in [Chl] (log mg m−3)
LTLT MEI PDO NPGO
1432 2846 3088 1853
1664 1391 2301 1762
1646 1877 2718 1888
1376 1865 2143 1870
1265 1404 2400 1601
888 2066 2329 1728
1020 1074 2128 989
598 2568 1864 1205
809 1182 1090 4529
6847 5275 7246 749

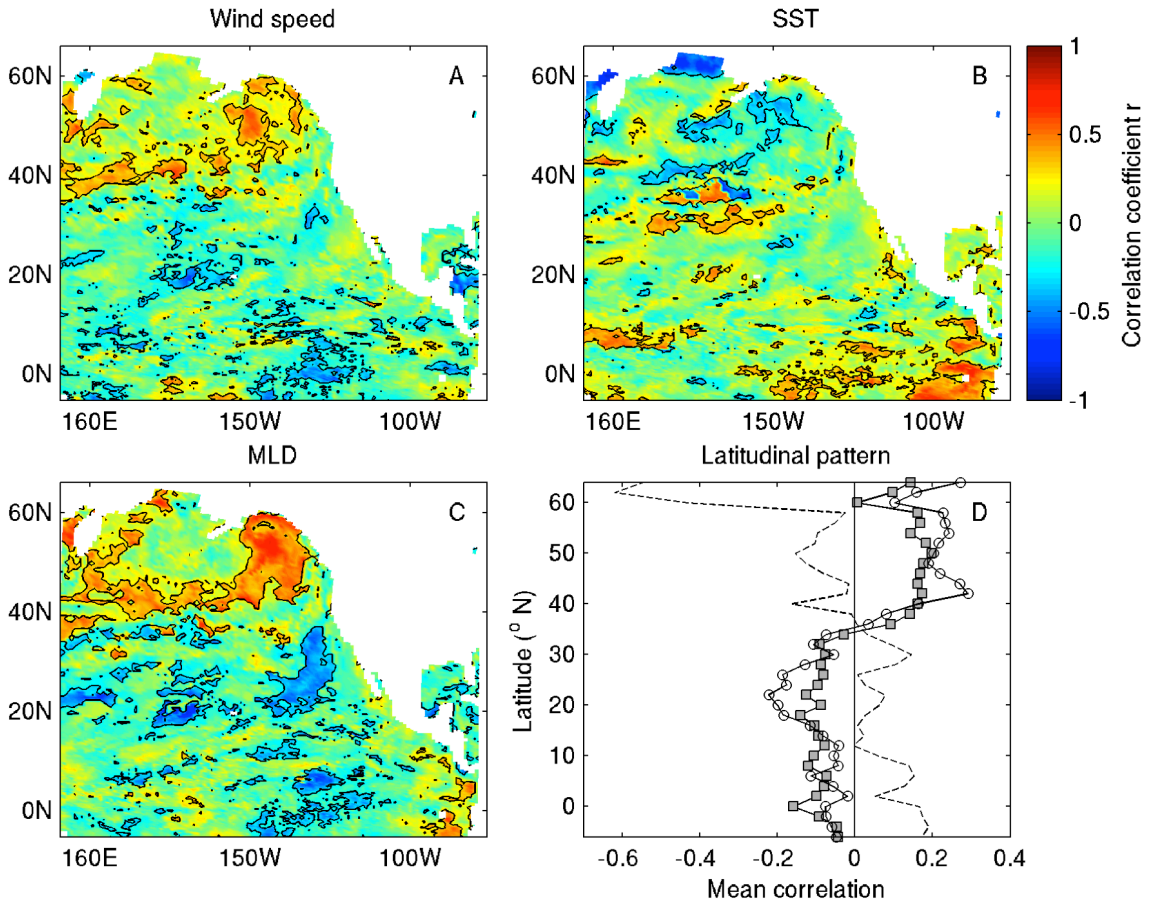

Figure 3.15. Temporal correlations between bloom initiation date and three environmental variables: wind speed at 10 m height, sea surface temperature (SST), and mixed layer depth (MLD). (A-C): Maps of correlation strength for each environmental variable. Black contour lines indicate regions where correlations were significant at $p < 0.05$. (D): Zonally averaged correlation strength across 2° latitudinal bins for wind speed (line with grey squares), SST (dashed line), and MLD (line with white circles).

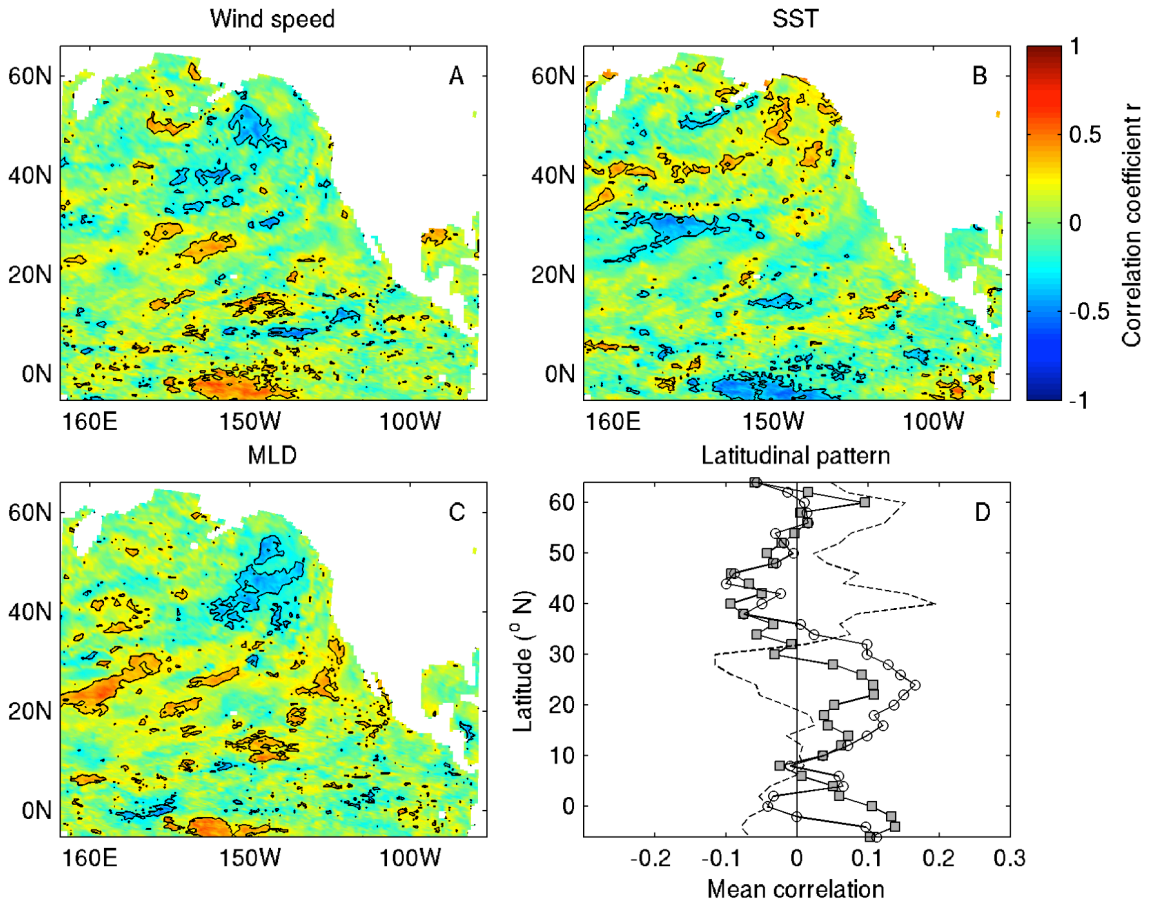

Figure 3.16. Temporal correlations between bloom duration and three environmental variables: wind speed at 10 m height, sea surface temperature (SST), and mixed layer depth (MLD). Features of this figure are the same as in Figure 3.15.

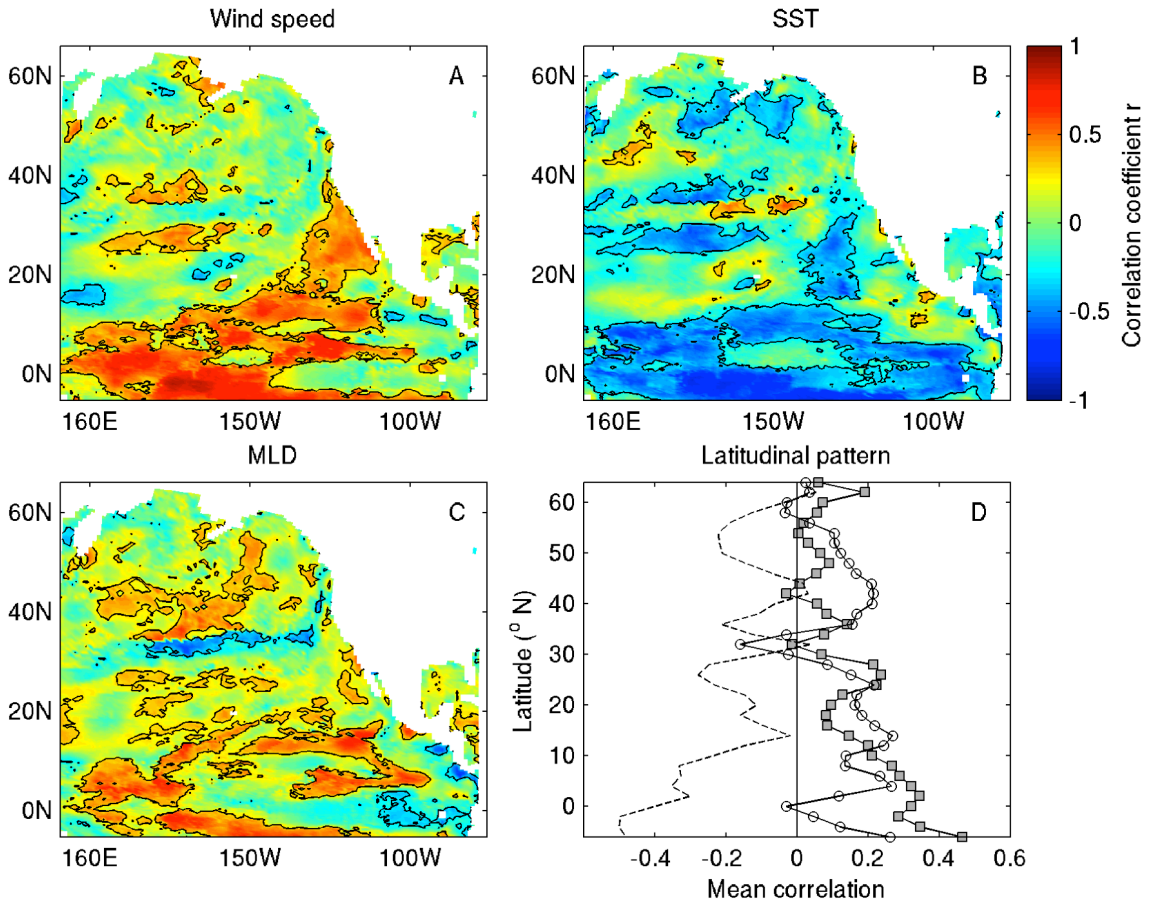

Figure 3.17. Temporal correlations between bloom magnitude and three environmental variables: wind speed at 10 m height, sea surface temperature (SST), and mixed layer depth (MLD). Features of this figure are the same as in Figure 3.15.

Figure 3.18. Correlations between the first five principal component (PC) time series of phenological metrics, year, and three climate indices: the Multivariate ENSO Index (MEI), the Pacific Decadal Oscillation (PDO), and the North Pacific Gyre Oscillation (NPGO). Significant correlations between year and each principal component are labeled as long-term, linear trends (LTLT). Bars indicate the magnitude and direction of significant correlations, whereas non-significant correlations are marked with N/S and no bars are shown. For the three climate indices, correlations are based on annually averaged data with either no time lag or a 1-year time lag. The number 1 indicates cases where a 1-year time lag resulted in a larger absolute value of *r* than the use of no time lag.

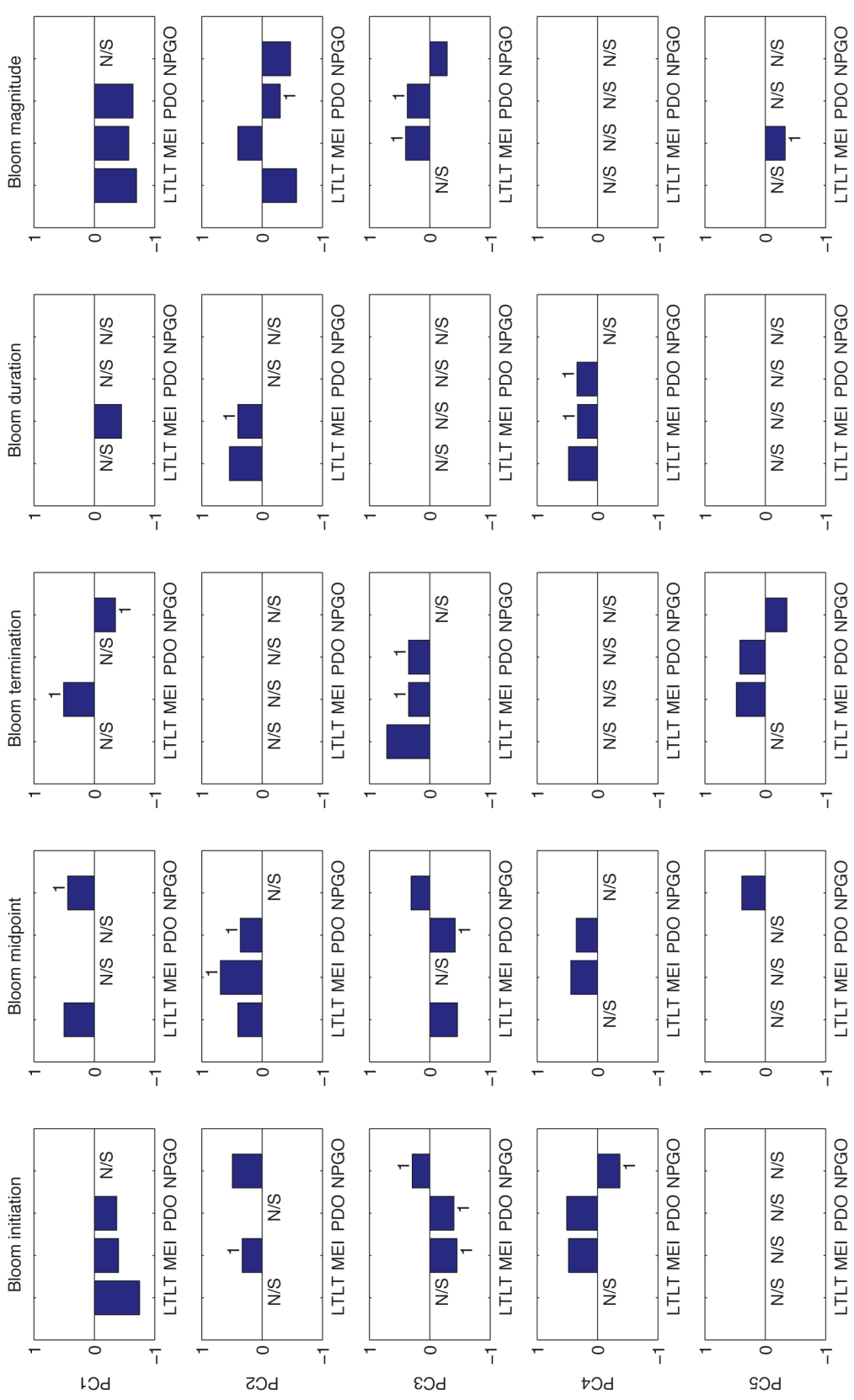
Bloom initiation
Bloom midpoint
Bloom termination
Bloom duration
Bloom magnitude
PC1
PC2
PC3
PC4
PC5
1
0
−1
N/S
LTLT MEI PDO NPGO

Figure 3.19. Time series and spatial patterns associated with the first principal component (PC1) of bloom initiation (A, F), midpoint (B, G), termination (C, H), duration (D, I), and magnitude (E, J). Upper row: The time series of PC scores are shown as black lines. For bloom initiation, midpoint, and termination, negative anomalies indicate earlier phenology, while positive anomalies denote later phenology. For bloom duration and magnitude, negative anomalies reveal shorter blooms with a lower mean concentration of chlorophyll, whereas positive anomalies indicate longer and larger blooms. Also shown is the time series of the climate index that was most closely correlated with each PC time series. The Multivariate ENSO Index (MEI) is indicated by a green line. The MEI time series lagged by one year is plotted in (C), while the inverse of the MEI is shown in (D). The MEI time series was also multiplied by 50, so that it could be displayed on the same y-axis as the PC time series. If the PC time series was more closely correlated with year than any climate index, then a blue line indicates the long-term trend based on linear regression. Lower row: Maps showing the correlation between each PC time series and the time series from each ocean grid cell. Colors indicate the strength and direction of correlation coefficients based on the same scale used in Figure 3.10. Black contour lines denote grid cells that were significantly correlated with a given PC.

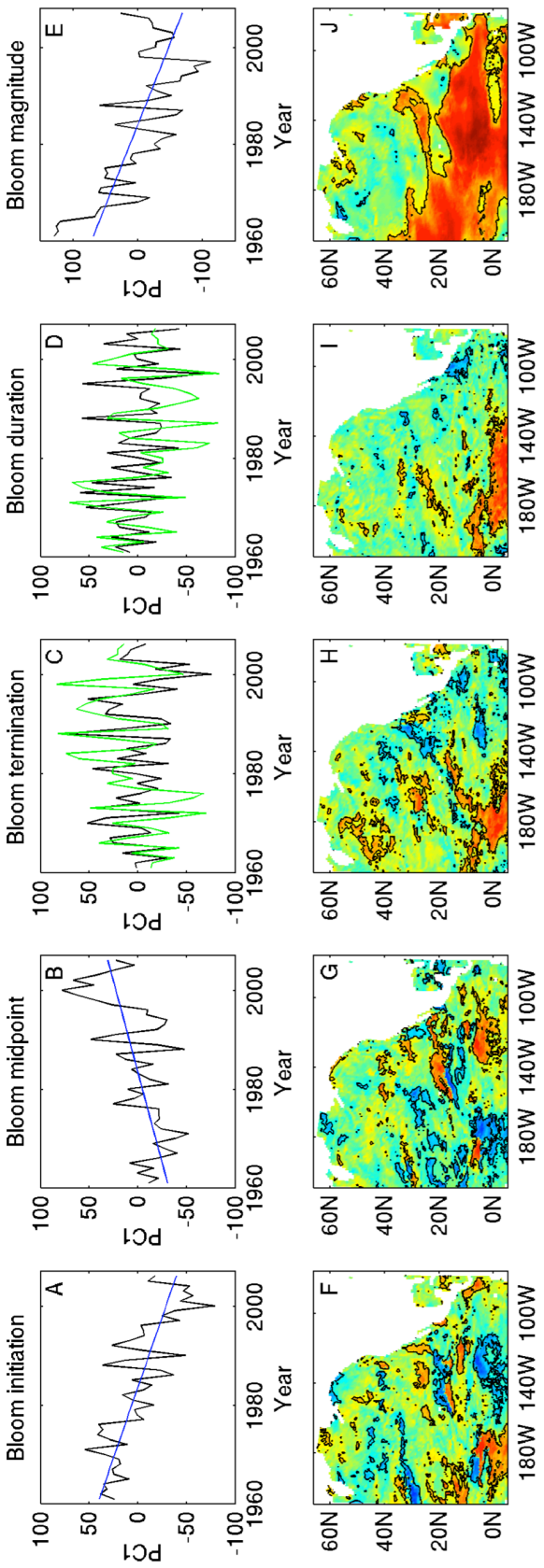
Bloom initiation
A
Bloom midpoint
B
Bloom termination
C
Bloom duration
D
Bloom magnitude
E
PC1
Year
1960
1980
2000
100
50
0
-50
-100
F
G
H
I
J
60N
40N
20N
0N
180W 140W 100W

Table 3.1. Correlations between the first five principal components (PCs) of sea surface temperature (SST) from ICOADS and CESM1. Principal component analysis (PCA) was performed separately on datasets consisting raw SST data (A) and monthly SST anomalies (B). All correlation coefficients $r \geq |0.082|$ were statistically significant at $p < 0.05$ based on two-tailed probability tests. Gray areas indicate the correlation for each CESM1 principal component that exhibited the largest absolute value.

(A) Raw SST data

		CESM1 monthly SST				
		PC1	PC2	PC3	PC4	PC5
ICOADS monthly SST	PC1	0.998	0.021	0.036	0.015	0.000
	PC2	-0.030	0.909	0.267	-0.055	0.143
	PC3	-0.014	-0.218	0.777	-0.473	-0.174
	PC4	-0.029	-0.091	0.456	0.796	0.047
	PC5	-0.001	-0.109	0.116	-0.128	0.797

(B) Monthly SST anomalies

		CESM1 monthly SST				
		PC1	PC2	PC3	PC4	PC5
ICOADS monthly SST	PC1	0.919	-0.185	-0.139	0.049	-0.043
	PC2	0.159	0.729	0.102	-0.468	-0.156
	PC3	0.104	0.102	0.847	0.310	0.108
	PC4	-0.003	0.430	-0.245	0.246	0.242
	PC5	0.002	0.121	-0.118	0.413	-0.618

Table 3.2. Percentage of ocean grid cells where phytoplankton phenology was significantly correlated with climate indices, environmental variables, or exhibited a significant long-term trend. Environmental variables include wind speed, sea surface temperature (SST), and mixed layer depth (MLD). Climate indices include the Multivariate ENSO Index (MEI), Pacific Decadal Oscillation (PDO), or North Pacific Gyre Oscillation (NPGO). For the three climate indices, percentages of ocean grid cells were summed across time lags of 0-6 months. The numbers in parentheses indicate the range of percentages obtained from individual time lags.

Phenological metric	Long-term linear trend	MEI	PDO	NPGO
Initiation	19.5	26.7 (14.6-16.7)	33.9 (9.2-15.1)	22.8 (8.6-10.4)
Midpoint	19.0	23.6 (11.9-13.1)	30.6 (9.0-12.3)	23.7 (9.1-10.8)
Termination	13.6	21.8 (10.6-12.2)	29.8 (8.3-11.5)	21.0 (6.4-9.9)
Duration	10.2	22.9 (8.2-15.5)	25.1 (6.4-9.9)	13.8 (3.9-5.0)
Magnitude	48.2	40.6 (18.7-31.5)	52.5 (18.8-34.0)	33.2 (14.5-19.4)

Phenological metric	Wind speed	SST	MLD
Initiation	17.2	19.1	22.7
Midpoint	12.3	14.1	16.0
Termination	8.6	11.2	11.6
Duration	11.9	11.9	12.4
Magnitude	38.6	45.5	32.5

Table 3.3. Percentage of variation in phytoplankton phenology (% var) explained by each principal component (PC) and the percentage of ocean grid cells (% grid) whose time series was correlated with each PC.

	PC 1		PC 2		PC 3		PC 4	
Phenological metric	% var	% grid	% var	% grid	% var	% grid	% var	% grid
Initiation	6.2	25.7	5.0	20.4	4.8	19.9	4.3	16.0
Midpoint	6.0	24.8	5.4	20.8	4.8	18.4	4.2	14.6
Termination	5.8	22.8	4.7	18.5	4.4	16.9	4.0	14.3
Duration	5.4	18.3	4.4	16.6	4.0	13.8	3.6	13.2
Magnitude	21.8	58.0	9.2	36.6	7.1	29.3	4.6	15.2

	PC 5	
Phenological metric	% var	% grid
Initiation	3.9	13.3
Midpoint	3.8	13.1
Termination	4.0	14.0
Duration	3.5	11.9
Magnitude	3.9	14.2

CHAPTER 3 APPENDIX:

SUPPLEMENTAL INFORMATION FOR THE MANUSCRIPT *CHANGES IN PHYTOPLANKTON PHENOLOGY DETECTED WITH THE COMMUNITY EARTH SYSTEM MODEL 1.0 (CESM1): LONG-TERM TRENDS AND THE INFLUENCE OF CLIMATE OSCILLATIONS*

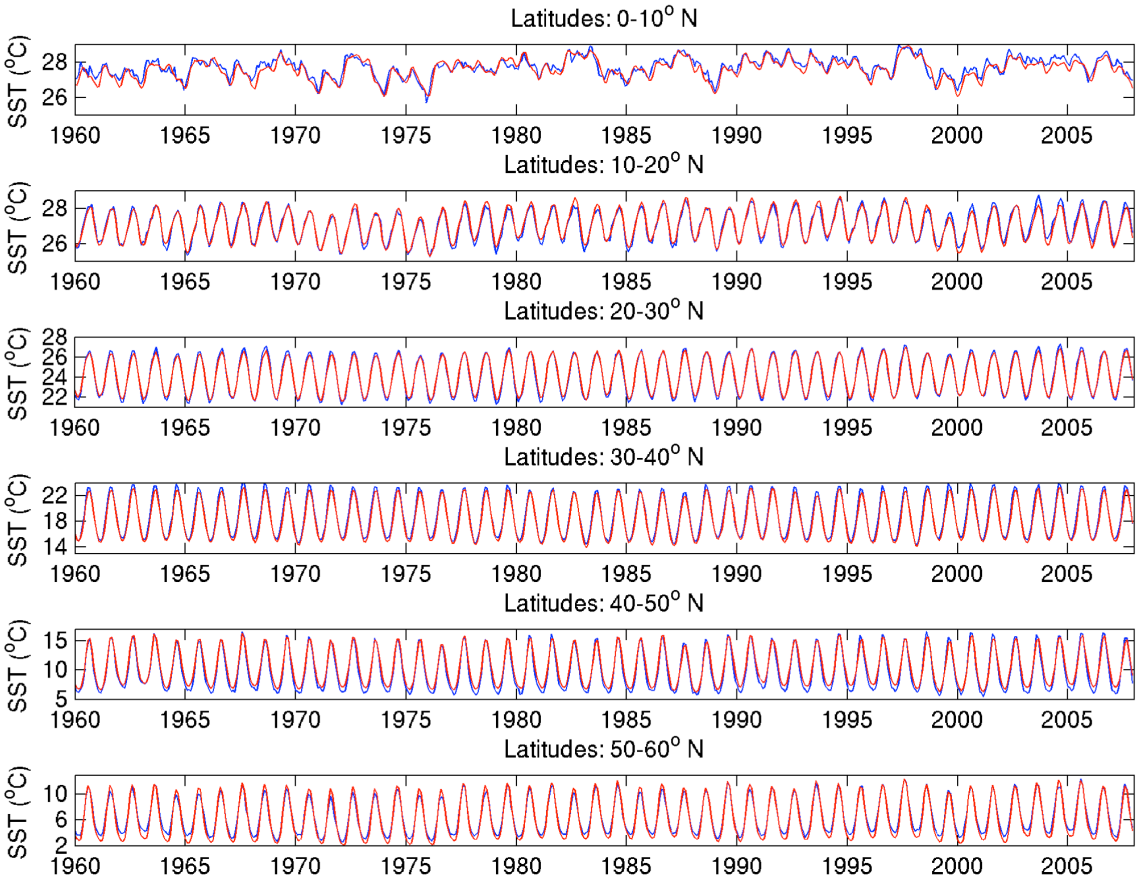

Figure S3.1. Time series of monthly sea surface temperature (SST) from ICOADS (blue) and CESM1 (red) that have been averaged across six 10° latitudinal bands.

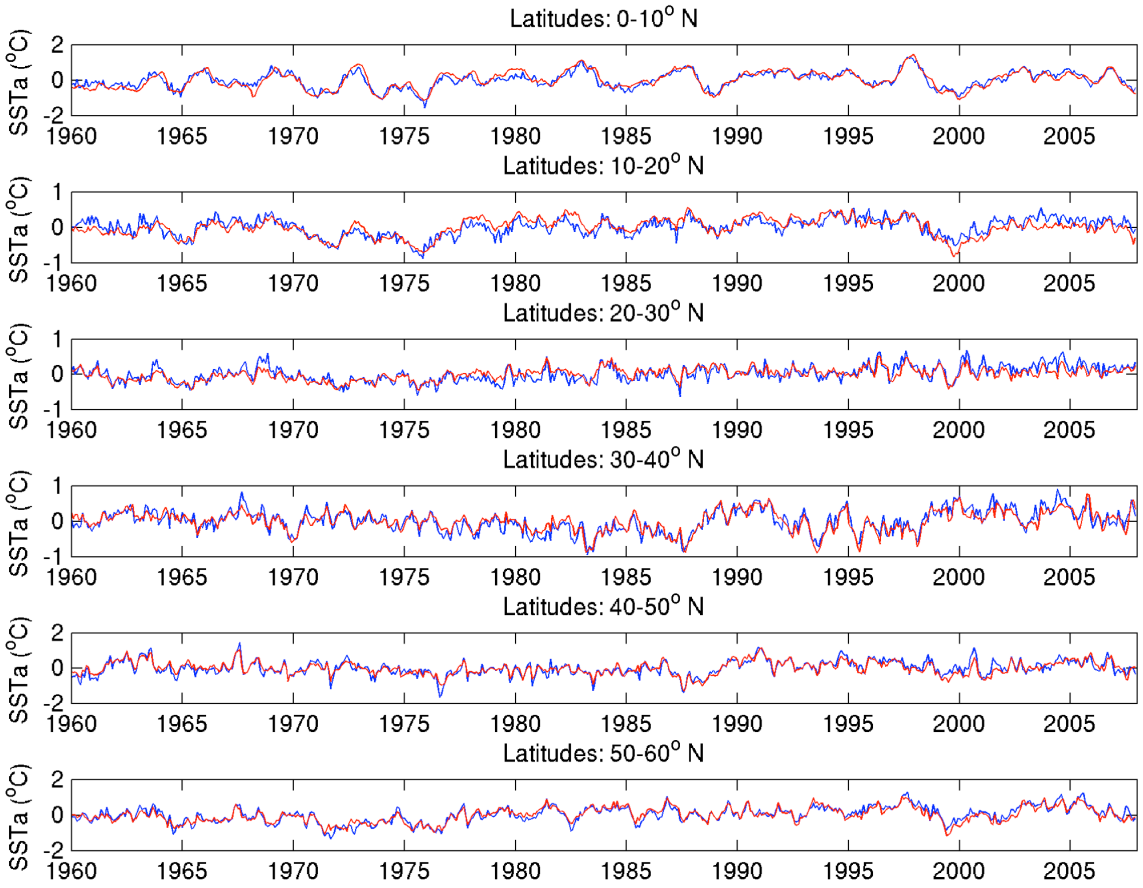

Figure S3.2. Time series of monthly sea surface temperature anomalies (SSTa) from ICOADS (blue) and CESM1 (red) that have been averaged across six 10° latitudinal bands.

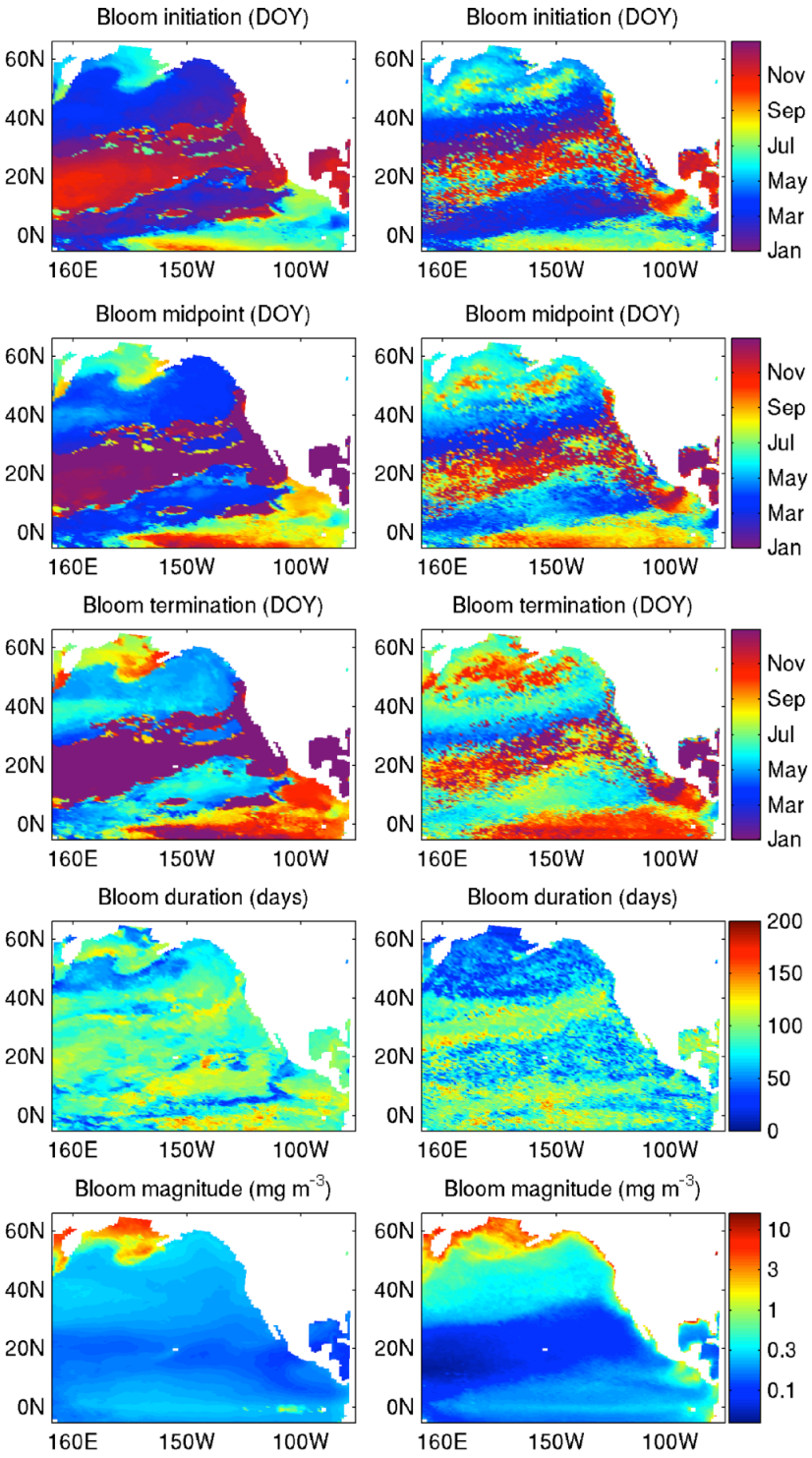

Figure S3.3. Median day of year (DOY) of the initiation, midpoint, and termination of peaks in chlorophyll concentration during the years 1998-2007. The median duration and magnitude of these phenological events are also shown. Maps in the left column are derived from CESM1(BGC), while maps on the right are based on remotely sensed chlorophyll from SeaWiFS.

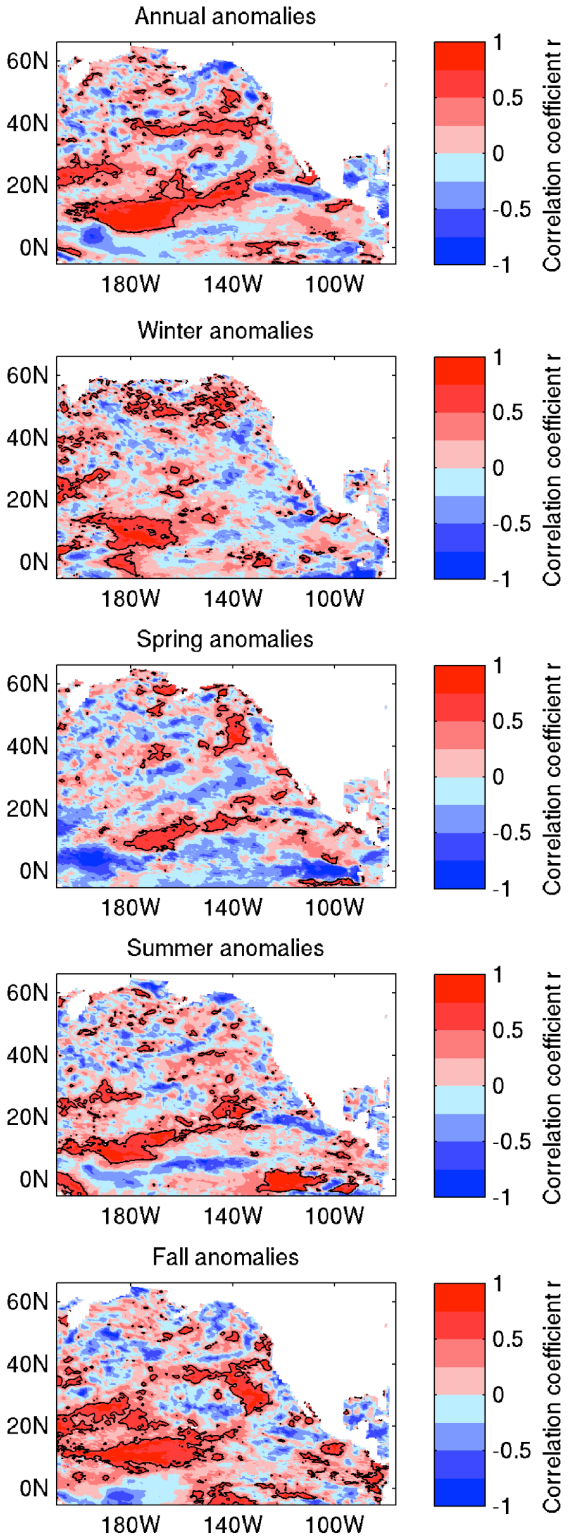

Figure S3.4. Maps of correlations between SeaWiFS and CESM1(BGC) calculated based on annual and seasonal anomalies of log-transformed chlorophyll from the 1998-2007 period. Black contour lines indicate locations where correlations exceed $r > 0.5$.

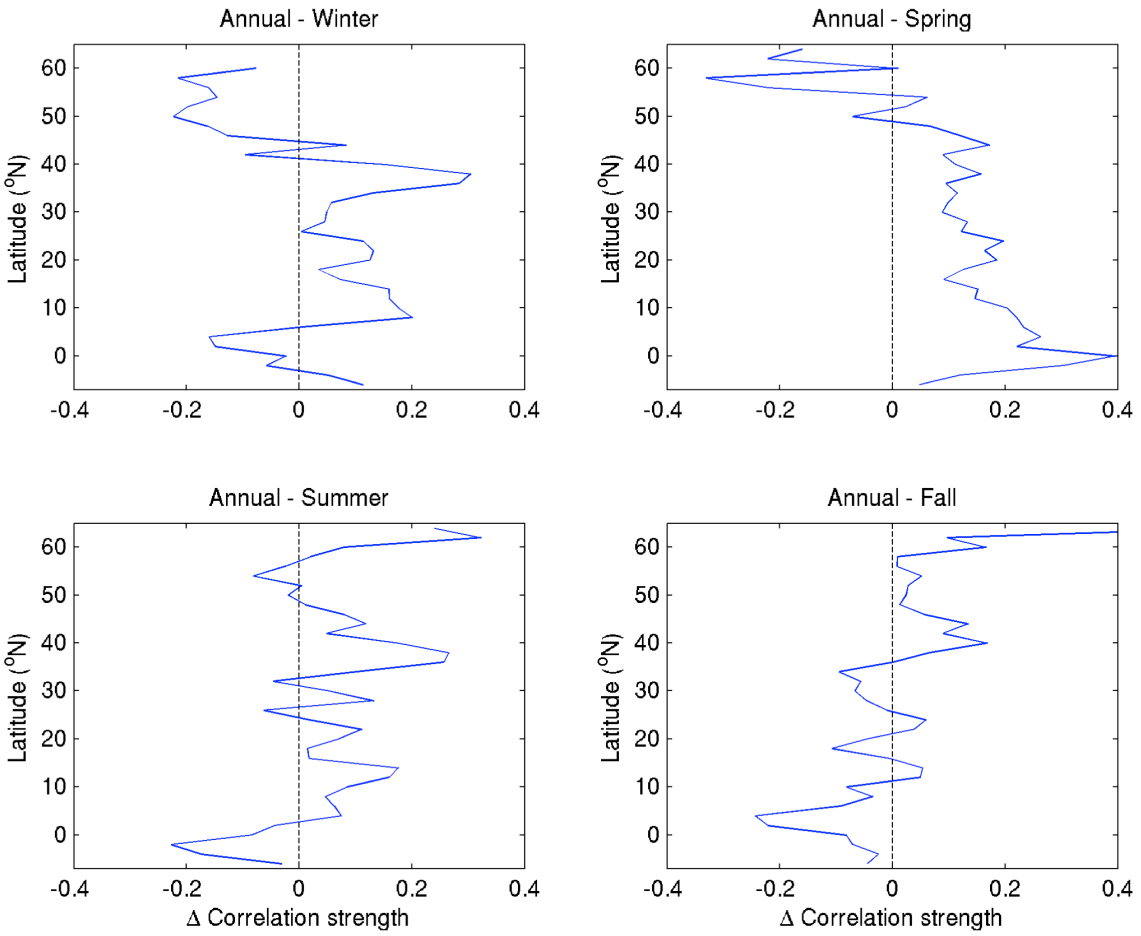

Figure S3.5. Difference between correlations between SeaWiFS and CESM1(BGC) when the correlations were calculated based on either annual or seasonal anomalies of log-transformed chlorophyll. The latitudinal average of correlations in 2° bins is graphed against the difference between annual and seasonal correlation strength. Positive numbers indicate that similarities between SeaWiFS and CESM1(BGC) were greater when considering the annual time scale, whereas negative numbers indicate that correlation strength was greater when considering the seasonal time scale.

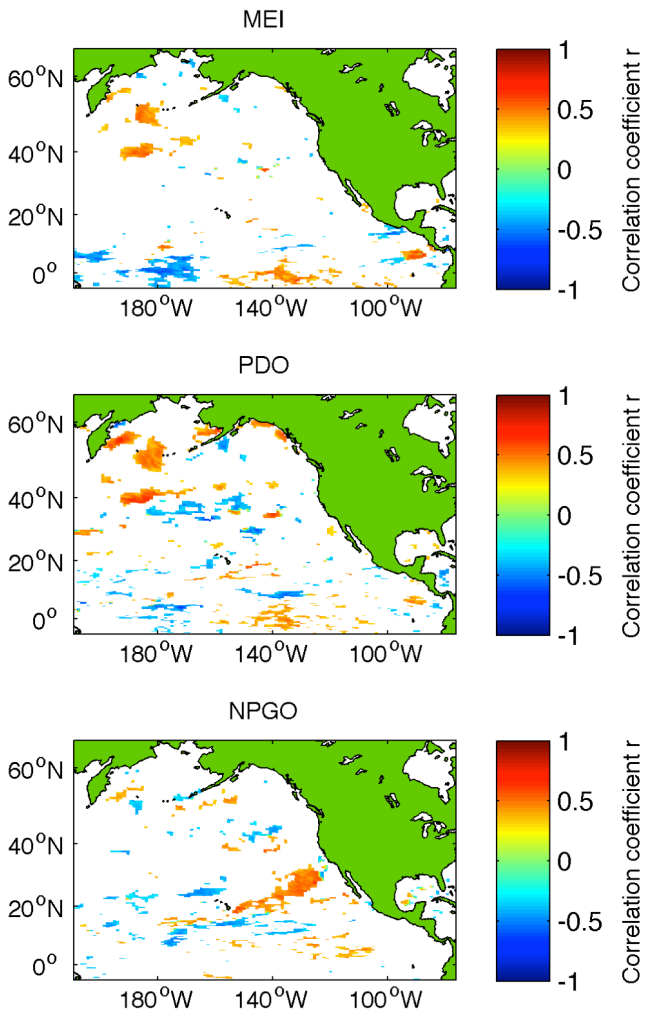

Figure S3.6. Maps of correlations between the date of the bloom midpoint and three climate indices: the Multivariate ENSO Index (MEI), the Pacific Decadal Oscillation (PDO), and the North Pacific Gyre Oscillation (NPGO). Features of this figure are the same as in Figure 3.11.

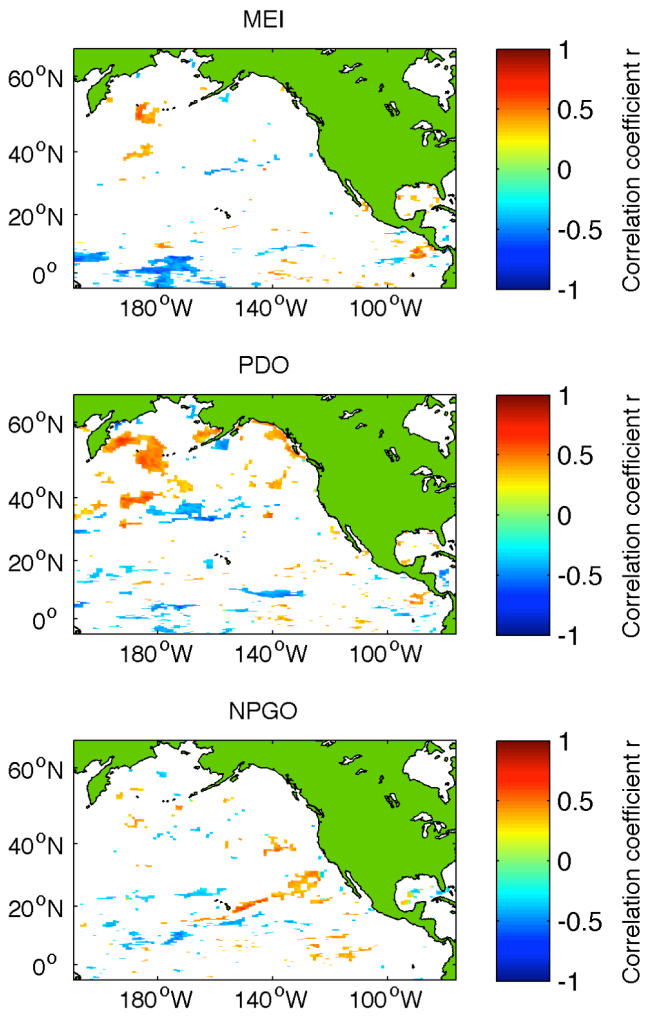

Figure S3.7. Maps of correlations between the date of bloom termination and three climate indices: the Multivariate ENSO Index (MEI), the Pacific Decadal Oscillation (PDO), and the North Pacific Gyre Oscillation (NPGO). Features of this figure are the same as in Figure 3.11.

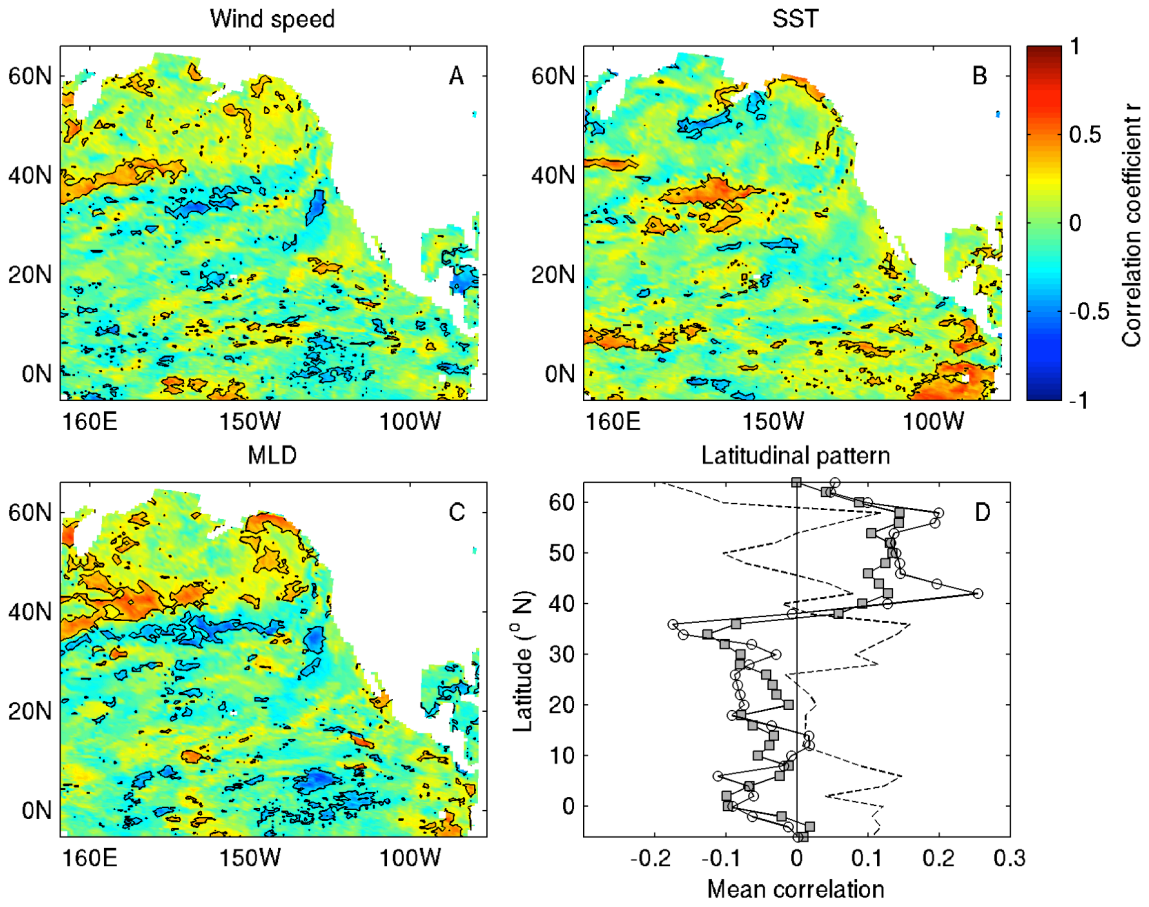

Figure S3.8. Temporal correlations between the date of bloom midpoint and three environmental variables: wind speed at 10 m height, sea surface temperature (SST), and mixed layer depth (MLD). Features of this figure are the same as in Figure 3.15.

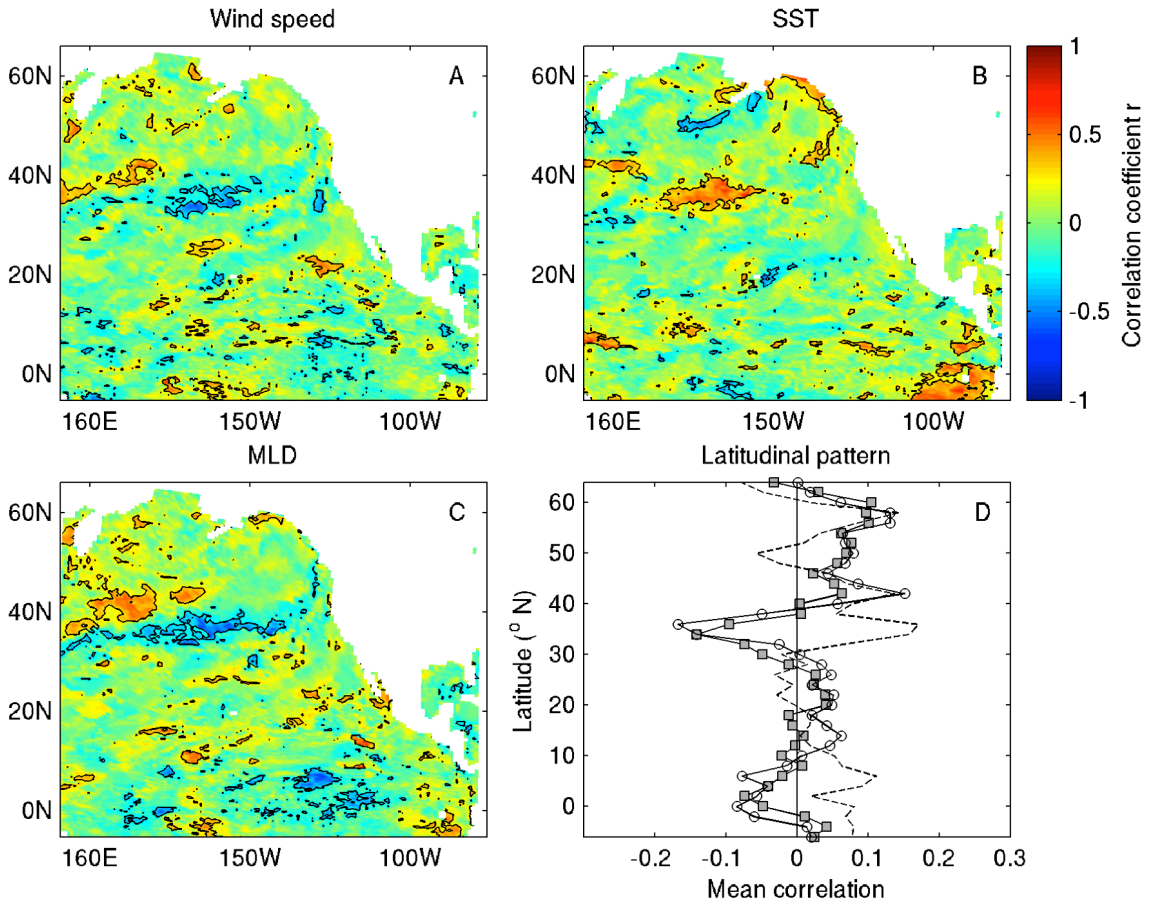

Figure S3.9. Temporal correlations between the date of bloom termination and three environmental variables: wind speed at 10 m height, sea surface temperature (SST), and mixed layer depth (MLD). Features of this figure are the same as in Figure 3.15.

Figure S3.10. Time series and spatial patterns associated with the first five principal components (PC1-5) of bloom initiation. Upper row: The time series of PC scores are shown as black lines. Negative anomalies of the PC time series indicate earlier phenology, while positive anomalies denote later phenology. Also shown is the time series of the climate index that was most closely correlated with each PC time series, where the Multivariate ENSO Index (MEI) is indicated by a green line, the Pacific Decadal Oscillation (PDO) by a pink line, and the North Pacific Gyre Oscillation (NPGO) by a red line. Climate indices were multiplied by 50, so that they could be displayed on the same y-axis as the PC time series. The inverse of the MEI time series lagged by one year is plotted in (C). If the PC time series was more closely correlated with year than any climate index, then a blue line indicates the long-term trend based on a linear regression. No climate indices or linear trends were associated with PC5 (E). Lower row: Maps showing the correlation between each PC time series and the time series from each ocean grid cell. Colors indicate the strength and direction of correlation coefficients based on the same scale used in Figure 3.10. Black contour lines denote grid cells that were significantly correlated with a given PC.

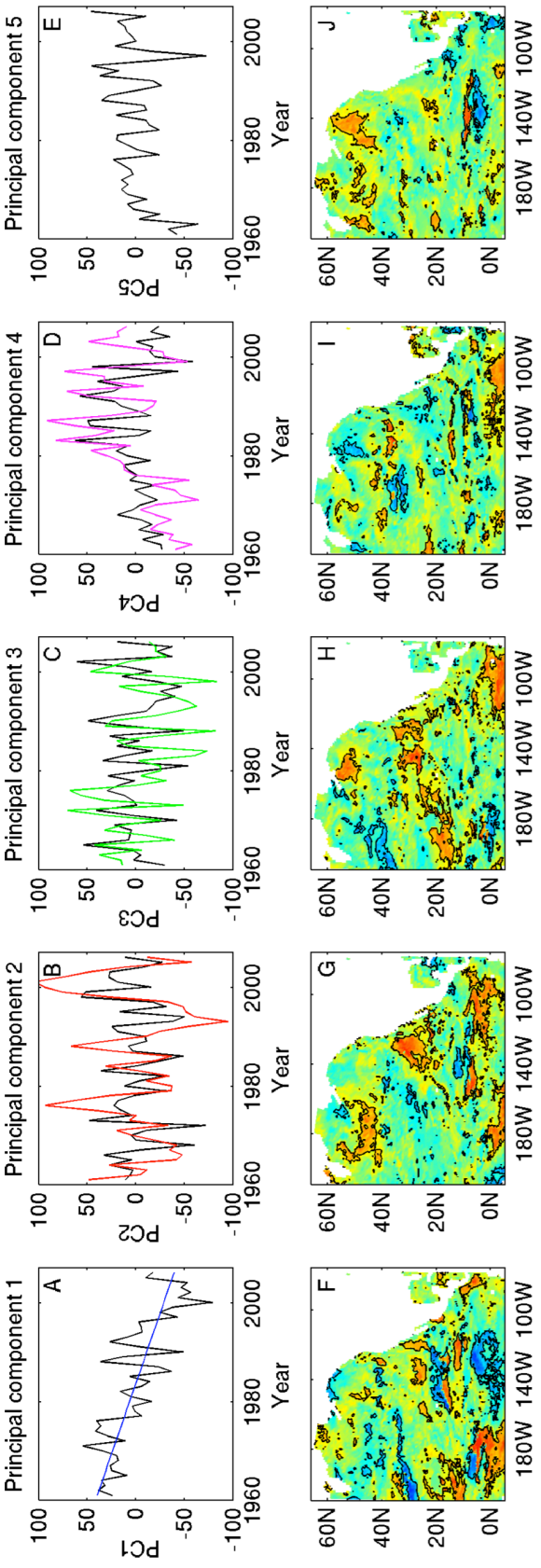
Principal component 1
A
PC1
Year
Principal component 2
B
PC2
Year
Principal component 3
C
PC3
Year
Principal component 4
D
PC4
Year
Principal component 5
E
PC5
Year
F
G
H
I
J
60N
40N
20N
0N
180W 140W 100W

Figure S3.11. Time series and spatial patterns associated with the first five principal components (PC1-5) of bloom midpoint. Negative anomalies of the PC time series indicate earlier phenology, while positive anomalies denote later phenology. Features of this figure are the same as those in Figure S3.10, with the following exception: the Multivariate ENSO Index (MEI) is lagged by one year in (B).

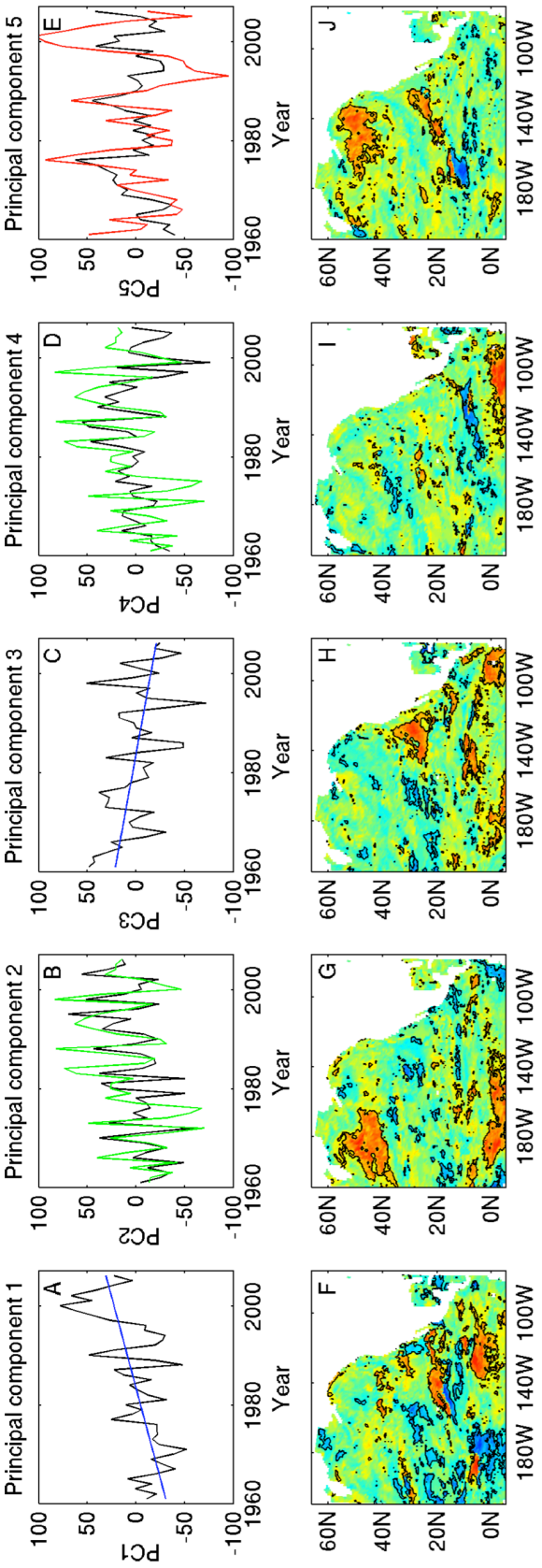
Principal component 1
Principal component 2
Principal component 3
Principal component 4
Principal component 5
PC1
PC2
PC3
PC4
PC5
Year
A
B
C
D
E
F
G
H
I
J
60N
40N
20N
0N
180W 140W 100W

Figure S3.12. Time series and spatial patterns associated with the first five principal components (PC1-5) of bloom termination. Negative anomalies of the PC time series indicate earlier phenology, while positive anomalies denote later phenology. Features of this figure are the same as those in Figure S3.10, with the following exceptions: (1) the Multivariate ENSO Index (MEI) is lagged by one-year in (A); (2) PC2 and PC4 were not correlated with any climate index and did not display long-term, linear trends.

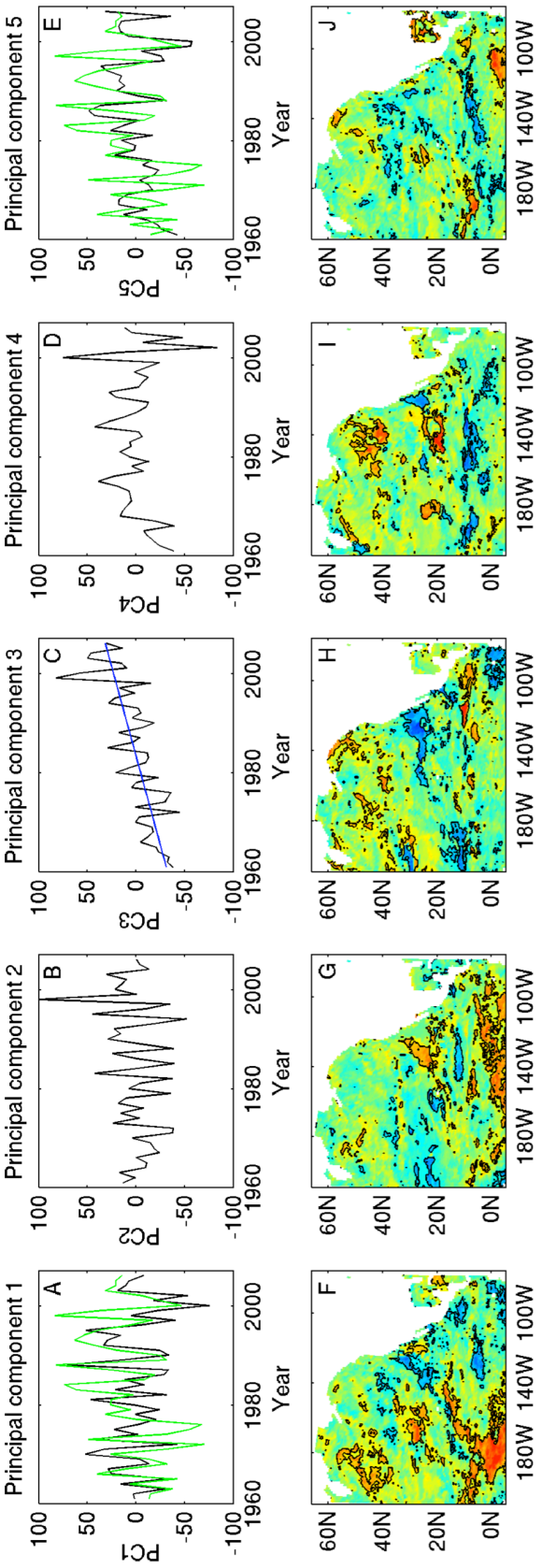
Principal component 1
Principal component 2
Principal component 3
Principal component 4
Principal component 5
PC1
PC2
PC3
PC4
PC5
Year
A
B
C
D
E
F
G
H
I
J
60N
40N
20N
0N
180W 140W 100W

Figure S3.13. Time series and spatial patterns associated with the first five principal components (PC1-5) of bloom duration. Negative anomalies of the PC time series indicate shorter phytoplankton blooms, while positive anomalies denote longer blooms. Features of this figure are the same as those in Figure S3.10, with the following exceptions: (1) the inverse of the Multivariate ENSO Index (MEI) is plotted in (A); (2) PC3 and PC5 were not correlated with any climate index and did not display long-term, linear trends.

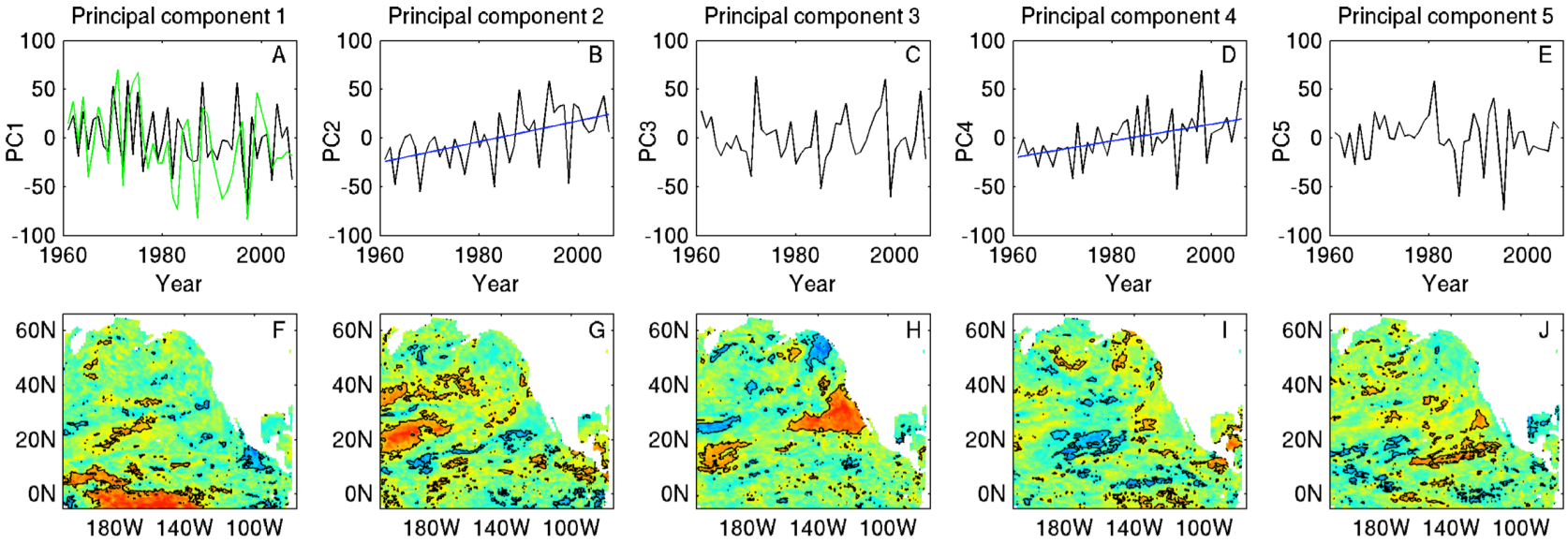
Principal component 1
Principal component 2
Principal component 3
Principal component 4
Principal component 5
A
B
C
D
E
PC1
PC2
PC3
PC4
PC5
100
50
0
-50
-100
1960
1980
2000
Year
F
G
H
I
J
60N
40N
20N
0N
180W
140W
100W

Figure S3.14. Time series and spatial patterns associated with the first five principal components (PC1-5) of bloom magnitude. Negative anomalies of the PC time series indicate blooms with a lower mean chlorophyll concentration, while positive anomalies denote larger blooms. Features of this figure are the same as those in Figure S3.10, with the following exceptions: (1) the Multivariate ENSO Index (MEI) is lagged by one year in (C); (2) the inverse of the MEI lagged by one year is plotted in (E); (3) PC4 was not correlated with any climate index and did not display a long-term, linear trend.

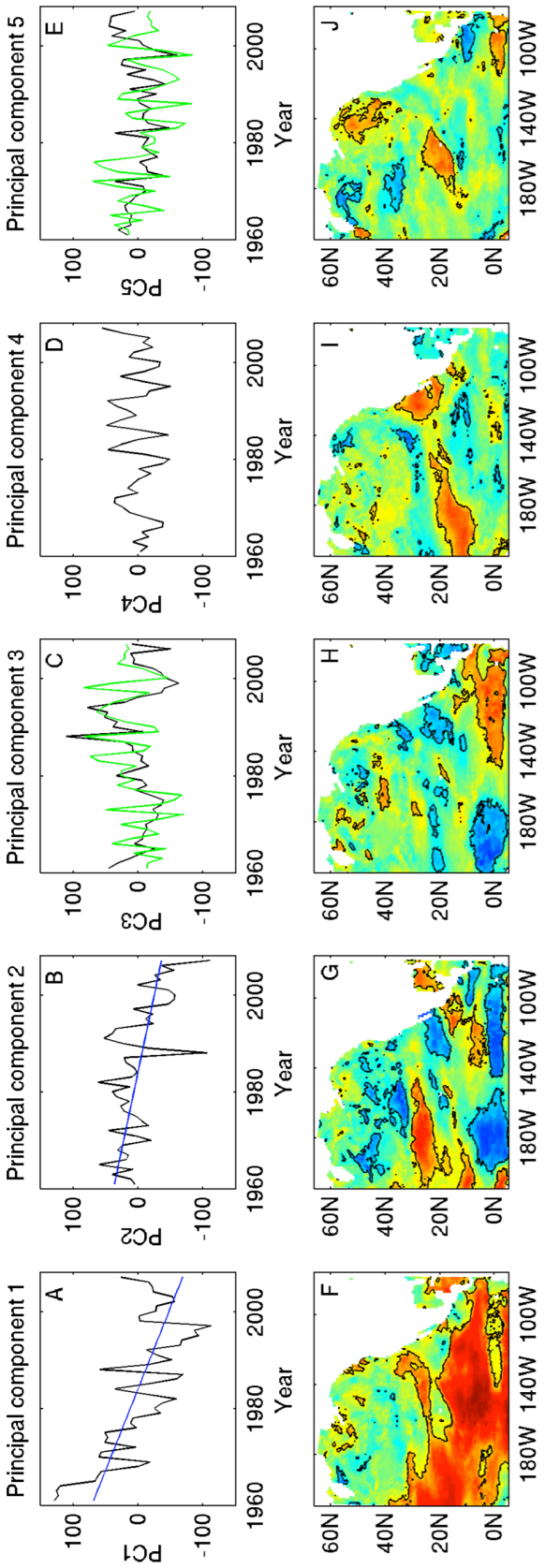
Principal component 1
A
PC1
100
0
-100
1960
1980
2000
Year
Principal component 2
B
PC2
Principal component 3
C
PC3
Principal component 4
D
PC4
Principal component 5
E
PC5
F
G
H
I
J
60N
40N
20N
0N
180W 140W 100W

References

Aiken, J., G.F. Moore, C.C. Trees, S.B. Hooker and D.K. Clark. 1995. The SeaWiFS CZCS-Type Pigment Algorithm. S.B. Hooker and E.R. Firestone (eds.). SeaWiFS Technical Series. Vol. 29. NASA Technical Memorandum 104566. National Aeronautics and Space Administration, Goddard Space Flight Center, Greenbelt, MD. 34 p.

Antoine, D., A. Morel, H.R. Gordon, V.F. Banzon and R.H. Evans. 2005. Bridging ocean color observations of the 1980s and 2000s in search of long-term trends. *Journal of Geophysical Research* 110, C06009, doi:10.1029/2004JC002620.

Barth, J.A., B.A. Menge, J. Lubchenco, F. Chan, J.M. Bane, A.R. Kirincich, M.A. McManus, K.J. Nielsen, S. D. Pierce and L. Washburn. 2007. Delayed upwelling alters nearshore coastal ocean ecosystems in the northern California current. *Proceedings of the National Academy of Sciences* 104(10): 3719-3724.

Behrenfeld, M.J. 2010. Abandoning Sverdrup's critical depth hypothesis on phytoplankton blooms. *Ecology* 91(4): 977-989.

Beaugrand, G., K.M. Brander, J.A. Lindley, S. Souissi and P.C. Reid. 2003. Plankton effect on cod recruitment in the North Sea. *Nature* 426: 661-664.

Burkle, L.A., J.C. Marlin, and T.M. Knight. 2013. Plant-pollinator interactions over 120 years: loss of species, co-occurrence, and function. *Science* 339: 1611-1615.

Burrows, M.T., D.S. Schoeman, L.B. Buckley, P. Moore, E.S. Poloczanska, K.M. Brander, C. Brown, J.F. Bruno, C.M. Duarte, B.S. Halpern, J. Holding, C.V. Kappel, W. Kiessling, M.I. O'Connor, J.M. Pandolfi, C. Parmesan, F.B. Schwing, W.J. Sydeman and A.J. Richardson. 2011. The pace of shifting climate in marine and terrestrial ecosystems. *Science* 234: 652-655.

Chavez, F.P., J. Ryan, S.E. Lluch-Cota and M. Ñiquen C. 2003. From anchovies to sardines and back: multidecadal changes in the Pacific Ocean. *Science* 299: 217-221.

Chenillat, F., P. Rivière, X. Capet, E. Di Lorenzo and B. Blanke. 2012. North Pacific Gyre Oscillation modulates seasonal timing and ecosystem functioning in the California Current upwelling system. *Geophysical Research Letters* 39, L01606, doi:10.1029/2011GL049966.

Cheung, W.W. L., V.W.Y. Lam, J.L. Sarmiento, K. Kearney, R. Watson and D. Pauly. 2009. Projecting global marine biodiversity impacts under climate change scenarios. *Fish and Fisheries* 10: 235-251.

Chhak, K.C., E. Di Lorenzo, N. Schneider and P.F. Cummins. 2009. Forcing of low-frequency ocean variability in the Northeast Pacific. *Journal of Climate* 22: 1255-1276.

Chiba, S., S. Batten, K. Sasaoka, Y. Sasai and H. Sugisaki. 2012. Influence of Pacific Decadal Oscillation on phytoplankton phenology and community structure in the western North Pacific. *Geophysical Research Letters* 39, L15603, doi:10.1029.2012GL052912.

Cleland, E.E., I. Chuine, A. Menzel, H.A. Mooney and M.D. Schwartz. 2007. Shifting plant phenology in response to global change. *Trends in Ecology and Evolution* 22(7): 357-365.

Cook, B.I., E.M. Wolkovich and C. Parmesan. 2012. Divergent responses to spring and winter warming drive community level flowering trends. *Proceedings of the National Academy of Sciences* 109(23): 9000-9005.

Cushing, D.H. 1974. The natural regulation of fish populations. p. 399-412. In Sea Fisheries Research. F.R.H. Jones (ed). John Wiley & Sons, New York, NY.

Cushing, D.H. 1990. Plankton production and year-class strength in fish populations: an update of the match/mismatch hypothesis. *Advances in Marine Biology* 26: 249-293.

Danabasoglu, G., S.C. Bates, B.P. Briegleb, S.R. Jayne, M. Jochum, W.G. Large, S. Peacock and S.G. Yeager. 2012. The CCSM4 Ocean Component. *Journal of Climate* 25: 1361-1389.

D'Errico, J. 2004. Inpaint_nans. MATLAB Central File Exchange. Available at http://www.mathworks.com/matlabcentral/fileexchange/4551. Accessed on June 1, 2013.

Deser, C., A.S. Phillips, R.A. Tomas, Y.M. Okumura, M.A. Alexander, A. Capotondi, J.D. Scott, Y.-O. Kwon and M. Ohba. 2012. ENSO and Pacific Decadal Variability in the Community Climate System Model Version 4. *Journal of Climate* 25: 2622-2651.

Di Lorenzo, E., N. Schneider, K.M. Cobb, P.J.S. Franks, K. Chhak, A.J. Miller, J.C. McWilliams, S.J. Bograd, H. Arango, E. Curchitser, T.M. Powell and P. Rivière. 2008. North Pacific Gyre Oscillation links ocean climate and ecosystem change. *Geophysical Research Letters*, 35, L08607, doi:10.1029/2007GL032838.

Durant, J.M., D.O. Hjermann, G. Ottersen and N.C. Stenseth. 2007. Climate and the match or mismatch between predator requirements and resource availability. *Climate Research* 33: 271-283.

Dutkiewicz, S., M. Follows, J. Marshall and W.W. Gregg. 2001. Interannual variability of phytoplankton abundances in the North Atlantic. *Deep-Sea Research II* 48: 2323-2344.

Emery, W.J. and R.E. Thompson. 2001. Data Analysis and Methods in Physical Oceanography, 2nd ed. Elsevier, Amsterdam, the Netherlands. 638 p.

Edwards, M. and A.J. Richardson. 2004. Impact of climate change on marine pelagic phenology and trophic mismatch. *Nature* 430: 881-884.

Field, C.B, M.J. Behrenfeld, J.T. Randerson and P. Falkowski. 1998. Primary production of the biosphere: integrating terrestrial and oceanic components. *Science* 281: 237-240.

Fuentes-Yaco, C., P.A. Koeller, S. Sathyendranath, and T. Platt. 2007. Shrimp (*Pandalus borealis*) growth and timing of the spring phytoplankton bloom on the Newfoundland-Labrador Shelf. *Fisheries Oceanography* 16(2): 116-129.

Gargett, A.E. 1997. Physics to fish: interactions between physics and biology on a variety of scales. *Oceanography* 10(3): 128-131.

Greene, C.H., B.C. Monger, L.P. McGarry, M.D. Connelly, N.R. Schnepf, A.J. Pershing, I.M. Belkin, P.S. Fratantoni, D.G. Mountain, R.S. Pickart, R. Ji, J.J. Bisagni, C. Chen, S.M.A. Hakkinen, D.B. Haidvogel, J. Wang, E. Head, P. Smith and A. Conversi. 2012. Recent Arctic climate change and its remote forcing of Northwest Atlantic shelf ecosystems. *Oceanography* 25(3): 208-213.

Gregg, W.W. and M.E. Conkright. 2002. Decadal changes in global ocean chlorophyll. *Geophysical Research Letters* 29(15), 1730, doi:10.1029/2002GL014689.

Greve, W. 2003. Aquatic plants and animals. p. 285-403. In Phenology: An Integrative Environmental Science. M.D. Schwartz (ed.). Kluwer Academic Publishers, Boston, MA.

Greve, W., S. Prinage, H. Zidowitz, J. Nast and F. Reiners. 2005. On the phenology of North Sea ichthyoplankton. *ICES Journal of Marine Science* 62: 1216-1223.

Hashioka, T., T.T. Sakamoto and Y. Yamanaka. 2009. Potential impact of global warming on North Pacific spring blooms projected by an eddy-permitting 3-D ocean ecosystem model. *Geophysical Research Letters* 36, L20604 doi:10.1029/2009GL038912.

Hashioka, T., M. Vogt, Y. Yamanaka, C. Le Quéré, E.T. Buitenhuis, M.N. Aita, S. Alvain, L. Bopp, T. Hirata, I. Lima, S. Sailley and S.C. Doney. 2012. Phytoplankton

competition during the spring bloom in four Plankton Functional Type Models. *Biogeosciences Discussions* 9: 18083-18129.

Henson, S.A. and A.C. Thomas. 2007. Interannual variability in timing of bloom initiation in the California Current System. *Journal of Geophysical Research* 112, C08007, doi:/10.1029/2006JC003960.

Henson, S.A., J.P. Dunne and J. L. Sarmiento. 2009. Decadal variability in North Atlantic phytoplankton bloom. *Journal of Geophysical Research* 114, C04013, doi:10.1029/2008JC005139.

Henson, S.A., J.L. Sarmiento, J.P. Dunne, L. Bopp, I. Lima, S.C. Doney, J. John and C. Beaulieu. 2010. Detection of anthropogenic climate change in satellite records of ocean chlorophyll and productivity. *Biogeosciences* 7: 621-640.

Hunt, G.L., Jr. and P.J. Stabeno. 2002. Climate change and the control of energy flow in the southeastern Bering Sea. *Progress in Oceanography* 55: 5-22.

Hunt, G.L., Jr., P. Stabeno, G. Walters, E. Sinclair, R.D. Brodeur, J.M. Napp and N.A. Bond. 2002. Climate change and control of the southeastern Bering Sea pelagic ecosystem *Deep-Sea Research II* 49: 5821-5853.

Ji, R., M. Edwards, D.L. Mackas, J.A. Runge and A.C. Thomas. 2010. Marine plankton phenology and life history in a changing climate: current research and future directions. *Journal of Plankton Research* 32(10): 1355-1368.

Kahru, M., Raphael Kudela, M. Manzano-Sarabia and B.G. Mitchell. 2009. Trends in primary production in the California Current detected with satellite data. *Journal of Geophysical Research*, 114, C02004, doi:10.1029/2008JC004979.

Kahru, M., V. Brotas, M. Manzano-Sarabia and B.G. Mitchell. 2011. Are phytoplankton blooms occurring earlier in the Arctic? *Global Change Biology* 17: 1733-1739.

Kim, H.-J., A.J. Miller, J. McGowan and M.L. Carter. 2009. Coastal phytoplankton blooms in the Southern California Bight. *Progress in Oceanography* 82: 137-147.

Koeller, P., C. Fuentes-Yaco, S. Sathyendranath, A. Richards, P. Ouellet, D. Orr, U. Skúladóttir, K. Wieland, L. Savard and M. Aschan. 2009. Basin-scale coherence in phenology of shrimps and phytoplankton in the North Atlantic Ocean. *Science* 324: 791-793.

Large, W.G. and S.G. Yeager. 2009. The global climatology of an interannually varying air-sea flux data set. *Climate Dynamics* 33: 341-364.

Leopold, A. and S.E. Jones. 1947. A phenological record for Sauk and Dane Counties, Wisconsin, 1935-1945. *Ecological Monographs* 17(1): 81-122.

Long, M.C., K. Lindsay, S. Peacock, J.K. Moore and S.C. Doney. 2013. Twentieth-century ocean carbon uptake and storage in CESM1(BGC). *Journal of Climate* doi:10.1175/JCLI-D-12-00184.1, (in press).

Lutz, M.J., K. Caldeira, R.B. Dunbar and M.J. Behrenfeld. 2007. Seasonal rhythms of net primary production and particulate organic carbon flux to depth describe the efficiency of biological pump in the global ocean. *Journal of Geophysical Research* 112, C10011, doi:10.1029/2006JC003706.

Mahadevan, A., E. D'Asaro, C. Lee and M.J. Perry. 2012. Eddy-driven stratification initiates North Atlantic spring phytoplankton blooms. *Science* 337: 54-58.

Mann, K.H. and J.R.N. Lazier. 1996. Dynamics of Marine Ecosystems. Biological-Physical Interactions in the Oceans, 2nd ed. Blackwell Science, Malden, MA. 394 p.

Mantua N.J., S.R. Hare, Y. Zhang, J.M. Wallace and R.C. Francis. 1997. A Pacific decadal climate oscillation with impacts on salmon. *Bulletin of the American Meteorological Society* 78: 1069-1079.

Marinov, I., S.C. Doney and I.D. Lima. 2010. Response of ocean phytoplankton community structure to climate change over the 21st century: partitioning the effects of nutrients, temperature and light. *Biogeosciences* 7: 3941-3959.

Martin, S. 2004. An Introduction to Ocean Remote Sensing. Cambridge University Press, Cambridge, UK. 426 p.

Martinez, E., D. Antoine, F. D'Ortenzio and B. Gentili. 2009. Climate-driven basin-scale decadal oscillations of oceanic phytoplankton. *Science* 236: 1253-1256.

McGillicuddy, D.J., Jr., L.A. Anderson, N.R. Bates, T. Bibby, K.O. Buesseler, C.A. Carlson, C.S. Davis, C. Ewart, P.G. Falkowski, S.A. Goldthwait, D.A. Hansell, W.J. Jenkins, R. Johnson, V.K. Kosnyrev, J.R. Ledwell, Q.P. Li, D.A. Siegel and D.K. Steinberg. 2007. Eddy/wind interactions stimulate extraordinary mid-ocean plankton blooms. *Science* 316: 1021-1026.

McPhaden, M.J., S.E. Zebiak and M.H. Glantz. 2006. ENSO as an integrating concept in earth science. *Science* 314: 1740-1745.

Menzel, A., T.H. Sparks, N. Estrella, E. Koch, A. Aasa, R. Ahas, K. Alm-Kübler, P. Bissolli, O. Braslavská, A. Briede, F.M. Chmielewski, Z. Crepinsek, Y. Curnel, A. Dahl, C. Defila, A. Donnelly, Y. Filella, K. Jatczak, F. Måge, A. Mestre, O. Nordli, J. Peñuelas, P. Pirinen, V. Remišová, H. Scheifinger, M. Striz, A. Susnik, A.J.H. van

Vliet, F.-E. Wielgolaski, S. Zach and A. Zust. 2006. European phenological response to climate change matches the warming pattern. *Global Change Biology* 12: 1969-1976.

Miller-Rushing, A.J. and R.B. Primack. 2008. Global warming and flowering times in Thoreau's Concord: a community perspective. *Ecology* 89(2): 332-341.

Moore, J.K., S.C. Doney, J.C. Kleypas, D.M. Glover and I.Y. Fung. 2002. An intermediate complexity marine ecosystem model for the global domain. *Deep-Sea Research Part II* 49: 403–462.

Moore, J.K., S.C. Doney and K. Lindsay. 2004. Upper ocean ecosystem dynamics and iron cycling in a global three-dimensional model. *Global Biogeochemical Cycles* 18(4), GB4028, doi:10.1029/2004GB002220.

Moore, J.K., K. Lindsay, S.C. Doney, M.C. Long and K. Misumi. 2013. Marine ecosystem dynamics and biogeochemical cycling in the Community Earth System Model (CESM1(BGC)). *Journal of Climate*, (in press).

Murawski, S.A. 1993. Climate change and marine fish distributions: forecasting from historical analogy. *Transactions of the American Fisheries Society* 122(5): 647-658.

Murphy, G.I. 1968. Pattern in life history and the environment. *American Naturalist* 102(927): 391-403.

Obata, A., J. Ishizaka and M. Endoh. 1996. Global verification of critical depth theory for phytoplankton bloom with climatological in situ temperature and satellite ocean color data. *Journal of Geophysical Research* 101, C9: 20,657-20,667.

Parmesan, C. 2007. Influences of species, latitudes and methodologies on estimates of phenological response to global warming. *Global Change Biology* 13: 1860-1872.

Parmesan, C. and G. Yohe. 2003. A globally coherent fingerprint of climate change impacts across natural systems. *Nature* 421: 37-42.

Parsons, T.R., L.F. Giovando and R.J. LeBrasseur. 1966. The advent of the spring bloom in the eastern subarctic Pacific Ocean. *Journal of the Fish Research Board Canada* 23(4): 539-546.

Pennington, J.T., K.L. Mahoney, V.S. Kuwahara, D.D. Kolber, R. Calienes and F.P. Chavez. 2006. Primary production in the eastern tropical Pacific: a review. *Progress in Oceanography* 69: 285-317.

Platt, T., C. Fuentes-Yaco and K.T. Frank. 2003. Spring algal bloom and larval fish survival. *Nature* 423:398-399.

Platt, T., G.N. White III, L. Zhai, S. Sathyendranath and S. Roy. 2009. The phenology of phytoplankton blooms: ecosystem indicators from remote sensing. *Ecosystem Modelling* 220: 3057-3069.

Platt, T., S. Sathyendranath, G.N. White III, C. Fuentes-Yaco, L. Zhai, E. Devred and C. Tang. 2010. Diagnostic properties of phytoplankton time series from remote sensing. *Estuaries and Coasts* 33: 428-439.

Quinn, G.P. and M.J. Keough. 2002. Experimental Design and Data Analysis for Biologists. Cambridge University Press, Cambridge, UK. 537 p.

Racault, M.-F., C. Le Quéré, E. Buitenhuis, S. Sathyendranath and T. Platt. 2012. Phytoplankton phenology in the global ocean. *Ecological Indicators* 14: 152-163.

Reed, T.E., V. Grøtan, S. Jenouvrier, B.-E. Saether and M.E. Visser. 2013. Population growth in a wild bird is buffered against phenological mismatch. *Science* 340: 488-491.

Richardson, A.J. and E.S. Poloczanska. 2008. Under-resourced, under threat. *Science* 320: 1294-1295.

Rolinski, S., H. Horn, T. Petzoldt and L. Paul. 2007. Identifying cardinal dates in phytoplankton time series to enable the analysis of long-term trends. *Oecologia* 153: 997-1008.

Root, T.L., J.T. Price, K.R. Hall, S.H. Schneider, C. Rosenweig and J.A. Pounds. 2003. Fingerprints of global warming on wild animals and plants. *Nature* 421(2): 57-60.

Sapiano, M.R.P., C.W. Brown, S. Schollaert Uz and M. Vargas. 2012. Establishing a global climatology of marine phytoplankton phenological characteristics. *Journal of Geophysical Research* 117, C08026, doi:10.1029/2012JC007958.

Sasaoka, K., S. Chiba and T. Saino. 2011. Climatic forcing and phytoplankton phenology over the subarctic North Pacific from 1998 to 2006, as observed from ocean color data. *Geophysical Research Letters* 38, L15609, doi:10.1029/2011GL048299.

Schwing, F.B., J. Jiang and R. Mendelssohn. 2003. Coherency of multi-scale abrupt changes between the NAO, NPI and PDO. *Geophysical Research Letters* 30(7), 1406, doi: 10.1029/2002/GL016535.

Siegel, D.A., S.C. Doney and J.A. Yoder. 2002. The North Atlantic spring phytoplankton bloom and Sverdrup's critical depth hypothesis. *Science* 296: 730-733.

Smith, R., P. Jones, B. Briegleb, F. Bryan, G. Danabasoglu, J. Dennis, J. Dukowicz, C. Eden, B. Fox-Kemper, P. Gent, M. Hecht, S. Jayne, M. Jochum, W. Large, K. Lindsay, M. Maltrud, N. Norton, S. Peacock, M. Vertenstein and S. Yeager. 2010. The Parallel Ocean Program (POP) Reference Manual. Ocean Component of the Community Climate System Model (CCSM) and Community Earth System Model (CESM). Los Alamos National Laboratory Technical Report, LAUR-10-01853, Los Alamos, NM. 141 p. Available at http://www.cesm.ucar.edu/models/cesm1.0/pop2/doc/sci/POPRefManual.pdf. Accessed on June 7, 2013.

Song, H., R. Ji, C. Stock and Z. Wang. 2010. Phenology of phytoplankton blooms in the Nova Scotian Shelf-Gulf of Maine region: remote sensing and modeling analysis. *Journal of Plankton Research* 32(11): 1485-1499.

Song, H., R. Ji, C. Stock, K. Kearney and Z. Wang. 2011. Interannual variability in phytoplankton blooms and plankton productivity over the Nova Scotian Shelf and in the Gulf of Maine. *Marine Ecology Progress Series* 426: 105-118.

Stewart, I.T., D.R. Cayan and M.D. Dettinger. 2005. Changes toward earlier streamflow timing across Western North America. *Journal of Climate* 18: 1136-1155.

Stock, C.A., M.A. Alexander, N.A. Bond, K.M. Brander, W.W.L. Cheung, E.N. Curchitser, T.L. Delworth, J.P. Dunne, S.M. Griffies, M.A. Haltuch, J.A. Hare, A.B. Hollowed, P. Lehodey, S.A. Levin, J.S. Link, K.A. Rose, R.R. Rykaczewski, J.L. Sarmiento, R.J. Stouffer, F.B. Schwing, G.A. Vecchi and F.E. Werner. 2011. On the use of IPCC-class models to assess the impact of climate on Living Marine Resources. *Progress in Oceanography* 88: 1-27.

Sverdrup, H.U. 1953. On conditions for the vernal blooming of phytoplankton. *Journal du Conseil International pour l'Exploration de la Mer* 18: 287-295.

Sydeman, W.J., R.W. Bradley, P. Warzybok, C.L. Abraham, J. Jahncke, K.D. Hyrenbach, V. Kousky, J.M. Hipfner and M.D. Ohman. 2006. Planktivorous auklet *Ptychoramphus aleuticus* responses to ocean climate, 2005: unusual atmospheric blocking? *Geophysical Research Letters* 33, L22S09, doi:10.1029/2006GL026736.

Taylor, J.R. and R. Ferrari. 2011. Shutdown of turbulent convection as a new criterion for the onset of spring phytoplankton blooms. *Limnology and Oceanography* 56(6): 2293-2307.

Tsuda, A., S. Takeda, H. Saito, J. Nishioka, Y. Nojiri, I. Kudo, H. Kiyosawa, A. Shiomoto, K. Imai, T. Ono, A. Shimamoto, D. Tsumune, T. Yoshimura, T. Ano, A. Hinuma, M. Kinugasa, K. Suzuki, Y. Sohrin, Y. Noiri, H. Tani, Y. Deguchi, N. Tsurushima, H. Ogawa, K. Fukami, K. Kuma and T. Saino. 2003. A mesoscale iron enrichment in the western subarctic Pacific induces a large centric diatom bloom. *Science* 300: 958-961.

Ueyama, R. and B.C. Monger. 2005. Wind-induced modulation of seasonal phytoplankton blooms in the North Atlantic derived from satellite observations. *Limnology and Oceanography* 50(6): 1820-1829.

Vargas, M., C.W. Brown and M.R.P. Sapiano. 2009. Phenology of marine phytoplankton from satellite ocean color measurements. *Geophysical Research Letters* 36, L01608, doi:10.1029/2008GL036006.

Venegas, R.M., P.T. Strub, E. Beier, R. Letelier, A.C. Thomas, T. Cowles, C. James, L. Soto-Mardones and C. Cabrera. 2008. Satellite-derived variability in chlorophyll, wind stress, sea surface height, and temperature in the northern California Current System. *Journal of Geophysical Research* 113, C03015, doi: 10.1029/2007JC004481.

White, M.A., K.M. de Beurs, K. Didan, D.W. Inouye, A.D. Richardson, O.P. Jensen, J. O'Keefe, G. Zhang, R.R. Nemani, W.J.D. van Leeuwen, J.F. Brown, A. de Wit, M. Schaepman, X. Lin, M. Dettinger, A.S. Bailey, J. Kimball, M.D. Schwartz, D.D. Baldocchi, J.T. Lee and W.K. Lauenroth. 2009. Intercomparison, interpretation, and assessment of spring phenology in North American estimated from remote sensing for 1982-2006. *Global Change Biology* 15: 2335-2359.

Wiltshire, K.H., A.M. Malzahn, K. Wirtz, W. Greve, S. Janisch, P. Mangelsdorf, B.F.J. Manly and M. Boersma. 2008. Resilience of North Sea phytoplankton spring bloom dynamics: an analysis of long-term data at Helgoland Roads. *Limnology and Oceanography* 53(4): 1294-1302.

Wolkovich, E.M., B.I. Cook, J.M. Allen, T.M. Crimmins, J.L. Betancourt, S.E. Travers, S. Pau, J. Regetz, T.J. Davies, N.J.B. Kraft, T.R. Ault, K. Bolmgren, S.J. Mazer, G.J. McCabe, B.J. McGill, C. Parmesan, N. Salamin, MD. Schwartz and E.E. Cleland. 2012. Warming experiments underpredict plant phenological responses to climate change. *Nature* 485: 494-497.

Wolter, K. and M.S. Timlin. 1998. Measuring the strength of ENSO events – how does 1997/98 rank? *Weather* 53: 315-324.

Wolter, K. and M.S. Timlin. 2011. El Niño/Southern Oscillation behavior since 1871 as diagnosed in an extended multivariate ENSO index (MEI.ext). *International Journal of Climatology* 31: 1074-1087.

Xu, L., R.B. Myneni, F.S. Chapin III, T.V. Callaghan, J.E. Pinzon, C.J. Tucker, Z. Zhu, J. Bi, P. Ciais, H. Tømmervik, E.S. Euskirchen, B.C. Forbes, S.L. Piao, B.T. Anderson, S. Ganguly, R.R. Nemani, S.J. Goetz, P.S.A. Beck, A.G. Bunn, C. Cao and J.C. Stroeve. 2013. Temperature and vegetation seasonality diminishment over northern lands. *Natural Climate Change* doi:10.1038/nclimate1836.

Yamada, K. and J. Ishizaka. 2006. Estimation of interdecadal change of spring bloom timing, in the case of the Japan Sea. *Geophysical Research Letters* 33, L02608, doi:10.1029/2005GL024792.

Yoder, J.A., C.R. McClain, G.C. Feldman and W.E. Esaias. 1993. Annual cycles of phytoplankton chlorophyll concentrations in the global ocean: a satellite view. *Global Biogeochemical Cycles* 7(1): 181-193.

Yoo, S., H.P. Batchelder, W.T. Peterson and W.J. Sydeman. 2008. Seasonal, interannual and event scale variation in North Pacific ecosystems. *Progress in Oceanography* 77: 155-181.

Zhang, Z., M.A. Friedl, C.B. Schaaf, A.H. Strahler, J.C.F. Hodges, F. Gao, B.C. Reed and A. Huete. 2003. Monitoring vegetation phenology using MODIS. *Remote Sensing of Environment* 84: 471-475.

Zhang, X. M.A. Friedl and C.B. Schaaf. 2006. Global vegetation phenology from Moderate Resolution Imaging Spectroradiometer (MODIS): evaluation of global patterns and comparison with in situ measurements. *Journal of Geophysical Research* 111, G04017, doi:10.1029/2006JG000217.

CONCLUSIONS AND FUTURE RESEARCH DIRECTIONS

Among the 51 phenophases of fishes examined in the southern California Current Ecosystem (CCE) in Chapter 1, 39% have shifted their spawning time since the 1950s so that their larvae are appearing in the water column earlier in the year, while 18% of phenophases have exhibited a trend towards delayed occurrence of larvae. At the interannual time scale, El Niño events have prompted an earlier larval occurrence among the fish assemblage with a decadal trend towards earlier spawning. This demonstrates that fishes in this phenology group reacted similarly to warming temperatures regardless of whether the warming was associated with interannual climate variability or decadal temperature trends. In contrast, species in the other two phenology groups exhibited delays in larval occurrence during El Niño, possibly reflecting the delayed onset of coastal upwelling during El Niño years. The Pacific Decadal Oscillation (PDO) and North Pacific Gyre Oscillation (NPGO) did not have a major effect on fish phenology when examined at the assemblage level. However, it remains possible that these modes of climate variation may have a larger influence of the phenology of individual species. Sea surface temperature (SST) was the only oceanic variable significantly correlated with phenological variability among the fishes with advancing phenology, whereas species in the delayed phenology group were influenced by fluctuations in both SST and coastal upwelling. This may reflect the fact that fishes in the delayed phenology group commonly resided in coastal areas where seasonal upwelling and associated offshore transport influence whether larvae are maintained in the coastal zone. In contrast, epipelagic fishes that reside in coastal-oceanic habitats were most frequently members of

the advancing phenology group. Relative to the 1950s, species with no long-term, linear trend in phenology exhibited a contraction in the duration of their period of maximal larval abundance, potentially reflecting reduced temporal overlap between their spawning time and optimal environmental conditions.

The long-term delay in phenology among coastal fishes in the CCE is intriguing because, in most ecosystems, climate change has been associated with the earlier arrival of phenological events. Future research following up on this result from Chapter 1 could investigate whether a consistent pattern of phenological delays is observed when examining alternate datasets that monitor the abundance of coastal fishes. At a minimum, three such datasets monitoring the concentration of coastal fish larvae exist in the Southern California Bight. These datasets include:

- A monitoring program conducted at the San Onofre Nuclear Generating Station between 1978-1986 that surveyed larval abundance on a weekly to quarterly basis.
- Bight-wide surveys of larval fishes conducted on a monthly-to-bimonthly basis between 1978-1985. The Los Angeles County Museum serves as the repository for data from these cruises.
- A series of surveys monitoring the larval fish community around several southern California power plants. These surveys were conducted on an approximately monthly basis between 1997-2006.

The advantage of examining phenological patterns with these datasets is that they have a higher frequency temporal resolution than California Cooperative Oceanic

Fisheries Investigations (CalCOFI). However, variations between monitoring programs in terms of the depths and sites sampled, as well as questions about the comparability of survey methods, may complicate the interpretation of any changes in phenology observed between the 1978-1986 and 1997-2006 periods of these surveys.

A second question arising from the results of Chapter 1 relates to the fact that no changes in upwelling seasonality were observed in the CalCOFI region. In contrast, regional climate models have predicted delays in seasonal upwelling in the northern CCE under a scenario where the atmospheric CO_2 concentration doubled (Snyder *et al*., 2003; Diffenbaugh *et al*., 2004). This raises the question of whether seasonal oceanic conditions will change synchronously across both the southern and northern CCE under climate change. If seasonal upwelling becomes later in the northern CCE while remaining unchanged in the southern CCE, this could potentially alter the migratory behavior of fishes that breed in the southern CCE, but feed seasonally in the northern CCE. Examples of such species include Pacific sardine (*Sardinops sagax*) and Pacific hake (*Merluccius productus*). Delayed upwelling would likely lead to seasonal delays in primary and secondary production in the northern CCE. As a result, fishes feeding in this area may stay longer and migrate to their spawning grounds in the southern CCE later. One way to potentially evaluate whether seasonal conditions and fish phenology are changing in different ways across the CCE would be to compare the results presented in Chapter 1 with variations in phenology observed along the Newport Line. The Newport Line is the site of an ongoing monitoring program in central Oregon where ichthyoplankton have been sampled with methods comparable to CalCOFI on a biweekly-to-monthly basis during the years 1971-1972, 1977-1978, 1983, and 1996-Present (Auth *et al.*, 2011). This

would present an ideal location to evaluate the hypothesis that seasonal oceanographic conditions in the northern CCE may influence the timing when sardine and Pacific hake arrive at their spawning grounds in the southern CCE.

In Chapter 2, an examination of the influence of dynamic height on fish spawning habitat identified waters with dynamic heights between 79-83 cm as the preferred spawning grounds of anchovy, whereas jack mackerel typically spawned at dynamic heights between 89-99 cm. Pacific sardine eggs were observed most frequently at intermediate dynamic heights (*i.e.*, 84-89 cm). During years when El Niño or La Niña led to an expansion or contraction, respectively, of offshore waters with high dynamic heights (*i.e.*, > 95 cm), fish egg distribution changed in synchrony with these changes in physical oceanography. Generalized linear models (GLMs) that individually examined the effects of eight environmental variables found that dynamic height was the single variable that best explained fluctuations in the spawning habitat of sardine and anchovy. For jack mackerel, salinity explained slightly more variance in egg distribution than dynamic height. Results from this chapter suggest that the influence of dynamic height on fish egg distribution is mediated primarily through the relationship between dynamic height, temperature, salinity, and chlorophyll concentration. Dynamic height is calculated from depth-integrated specific volume anomalies, which are, in turn, derived from variations in temperature and salinity throughout the upper water column. As a result, dynamic height may serve as a proxy for fluctuations in temperature and salinity, factors known to influence the spawning habitat of small pelagic fishes (Lluch-Belda *et al*., 1991; Checkley *et al*., 2000). A second mechanism through which dynamic height appears to affect fish habitat is related to the fact that low dynamic heights are indicative

of coastal upwelling in the CCE. Consequently, increases in fish eggs at particular dynamic heights may reflect an elevated concentration of planktonic prey for adult or larval fishes in areas characterized by upwelling. While the relationship between spawning habitat and dynamic height was only evaluated over a 7-year period, similar habitat preferences were observed in 2005-2008 when the realized and available spawning habitat of sardine, anchovy, and jack mackerel were compared with of out-of-sample prediction.

Spawning habitat models developed for sardine have been used to track the monthly timing of the seasonal migration of this species between the southern and northern CCE (Reiss *et al.*, 2008; Zwolinski *et al.*, 2011). This suggests that spawning habitat models, such as those developed in Chapter 2, could be potentially used to assess interannual variations in fish phenology. Most of the variables included in the spawning habitat models of sardine, anchovy, and jack mackerel are monitored by remote sensing on a daily-to-weekly basis. As a result, the phenology of spawning habitat availability could be examined at a weekly resolution by using remotely sensed data as independent variables to be inputted into a spawning habitat model. Since several spawning habitat models for Pacific sardine have been produced in the southern CCE (*e.g.*, Weber and McClathcie, 2010; Zwolinski *et al.*, 2011; GLMs developed in Chapter 2), a multi-model ensemble could be developed, which would help better assess the reliability of predictions of available spawning habitat derived from these models.

In Chapter 3, the biogeochemistry (BGC) sub-module of the Community Earth System Model 1.0 was run in hindcast mode where the ocean component of this model was forced with atmospheric observations from 1961-2007. Five metrics describing the

phenology of North Pacific phytoplankton were calculated based on this CESM1(BGC) simulation. When phenological metrics from CESM1(BGC) were compared to equivalent metrics from SeaWiFS chlorophyll data, the mean dates of bloom initiation, bloom midpoint, and bloom magnitude showed high comparability between these two datasets ($r \geq 0.65$). Mean dates of bloom termination and bloom duration from CESM1(BGC) were less comparable to those from SeaWiFS.

In the North Pacific subpolar gyre, CESM1(BGC) indicated that earlier blooms occurred during years with weak winds, warm temperatures, and a shallow mixed layer, whereas in subtropical and equatorial regions earlier blooms were associated with the opposite conditions. Long-term trends in bloom initiation were detected in 20% of CESM1 grid cells, whereas the Multivariate ENSO Index (MEI), PDO, and NPGO were correlated with bloom initiation phenology in 27%, 34%, and 23% of CESM1 grid cells, respectively. Both positive and negative correlations with the climate indices were prevalent. Similarly, long-term advances and delays in phenology were detected with a similar frequency throughout the North Pacific. Since variations in bloom midpoint and termination phenology had a similar regional expression to fluctuations in bloom initiation dates, there were comparatively few pixels with changes in bloom duration. This was especially true when examining NPGO effects and detecting long-term trends in bloom duration. A principal component analysis (PCA) indicated that the first principal component of each phenological metric was either correlated with the MEI or displayed a long-term, linear trend. Compared to both terrestrial primary producers and marine organisms in higher trophic levels, the long-term trends identified in Chapter 3 suggested that phytoplankton phenology is changing at a quicker pace. In areas with long-term

advances in bloom initiation date, the mean rate of change was -15.7 ± 0.3 SE days decade^{-1}, while areas with delayed bloom initiation experienced changes at a mean rate of 14.4 ± 0.3 SE days decade^{-1}. This rapid rate of phenological change among marine primary producers could potentially increase the frequency of mismatches between the timing of phytoplankton blooms and the seasonal abundance of planktivores.

Several future steps can be taken to further explore variations in plankton phenology with CESM1(BGC). I have undertaken preliminary research to use this model to examine changes in phytoplankton phenology between 1985-2005 and 2080-2100 with the RCP 8.5 emissions scenario. This scenario assumes that anthropogenic climate change will lead to a radiative forcing of 8.5 W m^{-2} at the top of the atmosphere by the year 2100. In addition, mechanisms underlying changes in phytoplankton phenology can be explored with earth system models in greater depth than can often be done with field campaigns. Four main mechanisms are included in CESM1(BGC) that could lead to changes in phytoplankton phenology: (1) seasonal variations in nutrient concentration; (2) light limitation; (3) direct effects of temperature on phytoplankton growth and metabolism, and; (3) changes in the abundance or phenology of zooplankton grazing. Marinov *et al*. (2010) used Taylor series expansion to determine the relative importance of the first three processes on changes in phytoplankton species composition under global warming. A similar analysis could be performed to compare the relative influence of light limitation, nutrients, grazing, and direct temperature effects on phytoplankton phenology. A third potential line of future research using CESM1(BGC) would be to apply this model to develop predictions about whether mismatches between larval fishes and phytoplankton blooms will become more frequent under climate change. The spawning

phenology of several fish species (*e.g.*, Pacific herring, Atlantic cod, dab) has been modeled as a function of cumulative degree days, since temperature has a physiological effect on the rate of gonadal maturation in many fishes (Ware and Tanasichuk, 1989; Hutchings and Myers, 1994; Lange and Greve, 1997). Changes in cumulative degree days can be calculated with CESM1(BGC) over relevant regions of the ocean in order to develop predictions of future fish spawning phenology under climate change scenarios. This could then be compared with predicted changes in phytoplankton phenology to assess the likelihood of mismatches.

Lastly, despite the examination of different trophic levels, datasets, and spatial scales, several similarities emerge when comparing the results of Chapters 1 and 3. First, compared to the mean rate of phenological change among terrestrial organisms (2.8 days decade^{-1}; Parmesan, 2007), both phytoplankton and larval fish phenology show rapid changes over the latter half of the 20th century. Burrows *et al*. (2011) has suggested that these rapid changes may reflect a less pronounced seasonal gradient of ocean temperatures compared to land. As a result, organisms may need to undergo larger shifts in phenology to ensure that seasonal life history activities continue to occur at a constant temperature. A second similarity between phytoplankton phenology studied in Chapter 3 and fish phenology examined in Chapter 1 is that long-term delays in phenology were commonly observed. This differs notably from the relatively rare occurrence of phenological delays detected in terrestrial ecosystems (Root *et al*., 2003; Cook *et al*., 2012). Third, both phytoplankton phenology across the North Pacific and larval fish phenology in the CCE were strongly influenced by El Niño, in addition to exhibiting long-term, linear trends. Fourth, both analyses indicated that phenological changes can be

quite variable across sub-regional spatial scales. This pattern was evident in many of the maps of phenological metrics shown in Chapter 3. Similarly, different phenological patterns were observed in the southern CCE among coastal fishes and fishes with an offshore distribution. This spatial variability suggests that mesoscale phenomena (*e.g.*, eddies, fronts, meanders in current flow) and intra-seasonal variations in weather may have a large effect on phytoplankton and fish phenology. Fine-scale variability also poses a challenge for programs monitoring phenological changes because it suggests that trends found at one site may not be representative of changes occurring across a larger region.

References

Auth, T.D., R.D. Brodeur, H.L. Soulen, L. Ciannelli and W.T. Peterson. 2011. The response of fish larvae to decadal changes in environmental forcing factors off the Oregon coast. *Fisheries Oceanography* 20(4): 314-328.

Burrows, M.T., D.S. Schoeman, L.B. Buckley, P. Moore, E.S. Poloczanska, K.M. Brander, C. Brown, J.F. Bruno, C.M. Duarte, B.S. Halpern, J. Holding, C.V. Kappel, W. Kiessling, M.I. O'Connor, J.M. Pandolfi, C. Parmesan, F.B. Schwing, W.J. Sydeman and A.J. Richardson. 2011. The pace of shifting climate in marine and terrestrial ecosystems. *Science* 234: 652-655.

Checkley, D.M., Jr., R.C. Dotson, and D.A. Griffith. 2000. Continuous, underway sampling of eggs of Pacific sardine (*Sardinops sagax*) and northern anchovy (*Engraulis mordax*) in spring 1996 and 1997 off southern and central California. *Deep-Sea Research II* 47: 1139-1155.

Cook, B.I., E.M. Wolkovich and C. Parmesan. 2012. Divergent responses to spring and winter warming drive community level flowering trends. *Proceedings of the National Academy of Sciences* 109(23): 9000-9005.

Diffenbaugh, N.S., M.A. Snyder and L.C. Sloan. 2004. Could CO_2-induced land-cover feedbacks alter near-shore upwelling regimes? *Proceedings of the National Academy of Sciences* 101(1): 27-32.

Hutchings, J.A. and R.A. Myers. 1994. Timing of cod reproduction: interannual variability and the influence of temperature. *Marine Ecology Progress Series* 108: 21-31.

Lange, U. and W. Greve. 1997. Does temperature influence the spawning time, recruitment and distribution of flatfish via its influence on the rate of gonadal maturation? *Deutsche Hydrographische Zeitschrift* 49(2): 251-263.

Lluch-Belda, D., D.B. Lluch-Cota, S. Hernandez-Vazquez, C.A. Salinas-Zavala and R.A. Schwartlose. 1991. Sardine and anchovy spawning as related to temperature and upwelling in the California current System. *California Cooperative Oceanic Fisheries Investigations Reports* 32: 105-111.

Marinov, I., S.C. Doney and I.D. Lima. 2010. Response of ocean phytoplankton community structure to climate change over the 21st century: partitioning the effects of nutrients, temperature and light. *Biogeosciences* 7: 3941-3959.

Parmesan, C. 2007. Influences of species, latitudes and methodologies on estimates of phenological response to global warming. *Global Change Biology* 13: 1860-1872.

Reiss, C.S., D.M. Checkley, Jr and S.J. Bograd. 2008. Remotely sensed spawning habitat of Pacific sardine (*Sardinops sagax*) and Northern anchovy (*Engraulis mordax*) within the California Current. *Fisheries Oceanography* 17(2): 126-136.

Root, T.L., J.T. Price, K.R. Hall, S.H. Schneider, C. Rosenweig and J.A. Pounds. 2003. Fingerprints of global warming on wild animals and plants. *Nature* 421(2): 57-60.

Snyder, M.A., L.C. Sloan, N.S. Diffenbaugh and J.L. Bell. 2003. Future climate change and upwelling in the California Current. *Geophysical Research Letters* 30(15), 1823, doi:10.1029/2003GL017647.

Ware, D.M. and R.W. Tanasichuk. 1989. Biological basis of maturation and spawning waves in Pacific herring (*Clupea harengus pallasi*). *Canadian Journal of Fisheries and Aquatic Sciences* 46: 1776-1784.

Weber, E.D. and S. McClatchie. 2010. Predictive models of northern anchovy *Engraulis mordax* and Pacific sardine *Sardinops sagax* spawning habitat in the California Current. *Marine Ecology Progress Series* 406: 251-263.

Zwolinski, J.P., R.L. Emmett and D.A. Demer. 2011. Predicting habitat to optimize sampling of Pacific sardine (*Sardinops sagax*). *ICES Journal of Marine Science* 68(5): 867-879.